

應用 GYC 部分區域穩定理論於 Froude-van der Pol 系統之廣義同步與控制, 以 Legendre 函數為參數的 Lorenz 系統之超渾沌, 歷史 Chen 系統渾沌的技巧性控制及藉實用漸進穩定理論的陰-陽適應渾沌同步

學生:張育銘

指導教授:戈正銘



本篇論文以 GYC 部分區域穩定理論來研究新渾沌 Froude-van der Pol 系統其廣義同步及渾沌控制。藉由 GYC 部分區域穩定理論, Lyapunov 函數及控制器皆較傳統系統設計簡單, 且因為系統階數低於傳統系統, 所以可得到較小的模擬誤差。本篇以相圖、Lyapunov 指數、分歧圖、參數圖等數值模擬方法, 研究帶有 Legendre 函數為參數的 Lorenz 系統其超渾沌現象。此外本篇首次研究歷史 Chen 系統的渾沌行為, 當代 Chen 系統皆以被詳盡研究, 但至今尚未有文章對歷史 Chen 系統深入著墨, 因此, 接下來研究討論 Chen 系統中“陰”參數其歷史渾沌行為。本篇藉由線性耦合的方式, 選取一合適的耦合參數, 來探討“陽”和“陰” Chen 系統其廣義同步渾沌現象, 並藉由實用漸進穩定理論, 其原理是兩實用適應同步渾沌系統, 方程式中參數將其一設為不確定的, 其餘設為估測的參數, 加以利用實用漸進穩定理論來研究 “陰-陽” 適應渾沌同步。

**Chaos, Chaos Generalized Synchronization and
Control of a New Froude-van der Pol System by GYC
Partial Region Stability Theory and Hyperchaos of
Lorenz System with Legendre Function Parameters,
Historical Chaos and Yin-Yang Synchronization for
Chaotic Chen Systems with Well Designed Active
Control, Pragmatical Generalized Yin-Yang
Synchronization for Chaotic Chen System by Adaptive**

Student: Yu-Ming Chang



Advisor: Zheng-Ming Ge

Abstract

In this thesis, a new chaotic Froude-van der Pol system is studied. A new strategy of achieving chaos generalized synchronization and chaos control by GYC partial region stability is proposed. Using the GYC partial region stability theory, the Lyapunov function used becomes a simple linear homogeneous function of error states and the controllers are simpler than traditional controllers, and give less simulation error because they are in lower order than that of traditional controllers. The chaotic behaviors of a Lorenz system with Legendre function parameters is firstly studied numerically by time histories of states, phase portraits, Poincaré maps, bifurcation

diagram, Lyapunov exponents and parameter diagrams. Abundance of hyperchaos and of chaos is found, which offers the potential for many applications. In this thesis, the behavior of historical Chen system is firstly studied. To our best knowledge, most of contemporary Chen system are researched in detail, but there are no articles in investigating a thorough inquiry about the history of Chen system so far. Therefore, the historical chaos of Chen system with “*Yin* parameters” is introduced. In this thesis, we employ an applicable coupling parameters by linear coupling strategy to complete the goal of generalized synchronization of *Yin* and *Yang* Chen systems and take advantage of using an adaptive *Yin-Yang* chaos synchronization of *Yin* and *Yang* Chen system by pragmatical asymptotically stability theorem. This pragmatical adaptive synchronization of two chaotic systems of which one has uncertain parameters the another has estimated parameters, is achieved by pragmatical asymptotically stability theorem.



誌謝

本篇碩士論文能夠順利的完成，首先要感謝的人，便是不斷給予耐心指導及諄諄教誨，我的指導教授戈正銘老師。老師在我求學的過程中，在研究上，給予我研究方向及專業領域的知識，遇到困難時，讓我學習如何克服及解決難題。感謝老師不厭其煩的修改論文，才讓本篇論文得以完整。私底下，與老師的相處，藉由老師深厚的文學素養，了解古今中外文史的發展，頓時對過去的史事有更深一層的領悟。從老師的詩詞創作裡，感受到對詩詞欣賞的意境，對文學上有進一步的認知。最後，誠摯感謝老師過去兩年辛苦的教導，對於未來的路，讓我有新的啟發及目標。

兩年的碩士研究生涯中，感謝博士班楊振雄、張晉銘、李仕宇學長細心指導，碩士班李彥賢、何俊諺、許凱銘、江峻宇、陳聰文學長，在研究的過程中，給予我珍貴的意見及鼓勵。同時要感謝同學徐瑜韓、陳志銘在課業上的幫忙，在過去的兩年中互相扶持成長，留下許多記憶猶新的記憶。另外還要感謝學弟李泳厚、蔡尚恩、江振賓、王翔平幫忙處理研究室的大小雜事，讓我們能心無旁騖致力於論文研究。

最終感謝我的家人，當我兩年前仍對未來一片迷惘時，你們在精神上大力的支持，讓我有更多的動力繼續走下去。也感謝姪女芯語及外甥承翰的誕生，在這兩年求學過程中，每當步履蹣跚拖著疲累的身體回到家，看到你們無邪天真的笑容，疲累感瞬時消逝，讓我感到無比的溫馨。最後，感謝你們的支持，我會勇敢堅持下去，朝理想邁進。

Contents

Chinese Abstract	i
Abstract	ii
Acknowledgement	iv
Contents	v
List of Figures	vii
Chapter 1 Introduction	1
Chapter 2 Chaos Generalized Synchronization of a New Froude- van der Pol System by GYC Partial Region Stability Theory	5
2.1 Preliminaries.....	5
2.2 Chaos Generalized Synchronization Strategy	5
2.3 A New Froude-van der Pol System	6
2.4 Numerical Simulations	7
2.5 Summary.....	13
Chapter 3 Chaos Control of a New Froude-van der Pol System by GYC Partial Region Stability Theory	24
3.1 Preliminaries.....	24
3.2 Chaos Control Scheme	24
3.3 Chaos of a new Froude-van der Pol system	25
3.4 Numerical Simulations	26
3.5 Summary.....	31
Chapter 4 Hyperchaos of a Lorenz System with Legendre Function Parameters	39
4.1 Preliminaries.....	39
4.2 Classical Lorenz System and a Lorenz system with Legendre Function Parameters	39
4.3 Numerical Simulations	40
4.4 Summary.....	43
Chapter 5 Historical Chaos for Chen System	54
5.1 Preliminaries.....	54
5.2 Yang Chen system	54
5.3 Yin Chen system.....	54
5.4 Numerical Simulations	55
5.5 Summary.....	57
Chapter 6 Historical Chaos and Yin-Yang Synchronization for Chaotic Chen Systems with Well Designed Active Control	73
6.1 Preliminaries.....	73
6.2 Generalized Yin-Yang Synchronization Strategy	73

6.3 The Yang and Yin Chen systems	74
6.4 Numerical Simulations	75
6.5 Summary.....	79
Chapter 7 Pragmatical Generalized Yin-Yang Synchronization for Chaotic Chen System by Adaptive Control.....	90
7.1 Preliminaries.....	90
7.2 Pragmatical generalized Yin-Yang synchronization scheme by adaptive control	90
7.3 The chaotic behavior of Yang and Yin Chen systems.....	92
7.4 Numerical simulations of generalized Yin-Yang synchronization	93
7.5 Summary.....	101
Chapter 8 Conclusions	110
Appendix A GYC Partial Region Stability Theory.....	111
Appendix B Systems of Positive States	119
Appendix C Pragmatical Asymptotical Stability Theory	123
References.....	126



List of Figures

Fig. 2.1 Phase portrait of a new Froude-van der Pol system.	14
Fig. 2.2 Time histories of a new Froude-van der Pol system.	14
Fig. 2.3 Bifurcation diagram of a new Froude-van der Pol system.	15
Fig. 2.4 Lyapunov exponents of a new Froude-van der Pol system.	15
Fig. 2.5 Phase portraits of errors dynamics for <i>Case I</i> .	16
Fig. 2.6 Time histories of errors for <i>Case I</i> .	17
Fig. 2.7 Time histories of $x_i + 20, y_i$ for <i>Case I</i> .	17
Fig. 2.8 Phase portraits of error dynamics for <i>Case II</i> .	18
Fig. 2.9 Time histories of errors for <i>Case II</i> .	19
Fig. 2.10 Time histories of $x_i - y_i + 20$ and $-m \sin \omega t$ for <i>Case II</i> .	19
Fig. 2.11 Phase portraits of error dynamics for <i>Case III</i> .	20
Fig. 2.12 Time histories of errors for <i>Case III</i> .	21
Fig. 2.13 Time histories of $\frac{1}{4}x_i^4 + 100$ and y_i for <i>Case III</i> .	21
Fig. 2.14 Phase portraits of error dynamics for <i>Case IV</i> .	22
Fig. 2.15 Time histories of errors for <i>Case IV</i> .	23
Fig. 2.16 Time histories of $x_i(t-5) - y_i + 50$ and $-z_i^2$ for <i>Case IV</i> .	23
Fig. 3.1 Chaotic phase portraits for new Froude-van der Pol system in the first quadrant.	32
Fig. 3.2 Phase portraits of error dynamics for <i>Case I</i> .	33
Fig. 3.3 Time histories of errors for <i>Case I</i> .	34
Fig. 3.4 Phase portrait of error dynamics (e1&e2) for <i>Case II</i> .	34
Fig. 3.5 Phase portrait of error dynamics (e3&e4) for <i>Case II</i> .	35
Fig. 3.6 Time histories of errors for <i>Case II</i> .	35

Fig. 3.7 Time histories of x_1, x_2, x_3, x_4 <i>Case II</i> .	36
Fig. 3.8 Phase portrait of error dynamics (e_1 & e_2) for <i>Case III</i> .	36
Fig. 3.9 Phase portrait of error dynamics (e_3 & e_4) for <i>Case III</i> .	37
Fig. 3.10 Time histories of errors for <i>Case III</i> .	37
Fig. 3.11 Time histories of x_1, x_2, x_3 for <i>Case III</i> .	38
Fig. 4.1 Phase portrait, Poincaré maps of x_1, x_2 states for classical Lorenz system.	44
Fig. 4.2 Time histories of L_1 and L_2 .	44
Fig. 4.3 Phase portrait and Poincaré maps for Lorenz system with Legendre function parameters when $c_1 = 27.43, k=2.25$.	45
Fig. 4.4 Time histories of three states for Lorenz system with Legendre function parameters when $c_1 = 27.43, k=2.25$.	45
Fig. 4.5 The bifurcation diagram for Lorenz system with Legendre function parameters, where $c_1 = 27.43$.	46
Fig. 4.6 The enlarged bifurcation diagram for Lorenz system with Legendre function parameters, where $c_1 = 27.43$.	46
Fig. 4.7 The Lyapunov exponent for Lorenz system with Legendre function parameters.	47
Fig. 4.8 The parameter diagram for Lorenz system with Legendre function parameters.	47
Fig. 4.9 The parameter diagram for modified Lorenz system between $k=0.35\sim 0.352$.	48
Fig. 4.10 The parameter diagram for modified Lorenz system between $k=2.05\sim 2.35$.	48
Fig. 4.11 Phase portrait for Lorenz system with Legendre function parameters when $c_1 = 27.43, \varepsilon = 1.2, \omega = 0.8$ and $k=2.175$ (period1).	49

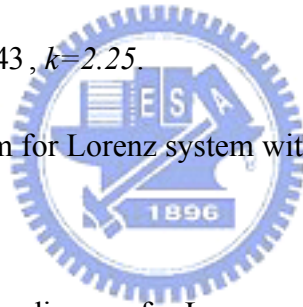


Fig. 4.12 Time histories for Lorenz system with Legendre function parameters when $c_1 = 27.43$, $\varepsilon = 1.2$, $\omega = 0.8$ and $k=2.175$ (period1).	49
Fig. 4.13 Phase portrait for Lorenz system with Legendre function parameters when $c_1 = 27.43$, $\varepsilon = 1.2$, $\omega = 0.8$ and $k=2.1$ (period2).	50
Fig. 4.14 Time histories for Lorenz system with Legendre function parameters when $c_1 = 27.43$, $\varepsilon = 1.2$, $\omega = 0.8$ and $k=2.1$ (period2).	50
Fig. 4.15 Phase portraits for Lorenz system with Legendre function parameters when $k=0.35$ (hyperchaos).	51
Fig. 4.16 Time histories for Lorenz system with Legendre function parameters when $k=0.35$ (hyperchaos).	51
Fig. 4.17 The Lyapunov exponent for Lorenz system with Legendre function parameters when $\varepsilon = 0 \sim 10$.	52
Fig. 4.18 The Lyapunov exponent for Lorenz system with Legendre function parameters when $\omega = 0 \sim 10$.	52
Fig. 4.19 Enlarged figure for Lorenz system with Legendre function parameters when $\omega = 0 \sim 10$.	53
Fig. 5.1 Phase portraits of <i>Yang Chen</i> system with $a = 35$, $b = 3$ and $c = 27.2$.	58
Fig. 5.2 Time histories of three states for <i>Yang Chen</i> system with parameters $a = 35$, $b = 3$ and $c = 27.2$.	59
Fig. 5.3 Period1 of phase portraits for <i>Yang Chen</i> system with parameters $a = 35$, $b = 3$ and $c=30$.	59
Fig. 5.4 Period2 of phase portraits for <i>Yang Chen</i> system with parameters $a = 35$, $b = 3$ and $c=28.8$.	60
Fig. 5.5 Period4 of phase portraits for <i>Yang Chen</i> system with parameters $a = 35$, $b = 3$ and $c=28.63$.	60

Fig. 5.6 Period8 of phase portraits for <i>Yang</i> Chen system with parameters $a = 35$, $b = 3$ and $c = 28.609$.	61
Fig. 5.7 Phase portrait of <i>Yin</i> Chen system with $a = -35$, $b = -3$ and $c = -27.2$.	61
Fig. 5.8 Phase portrait of <i>Yin</i> Chen system with $a = -35$, $b = -3$ and $c = -27.2$.	62
Fig. 5.9 Time histories of three states for <i>Yin</i> Chen system with $a = -35$, $b = -3$ and $c = -27.2$.	62
Fig. 5.10 Period1 of phase portraits for <i>Yin</i> Chen system with parameters $a = -35$, $b = -3$ and $c = -30$.	63
Fig. 5.11 Period2 of phase portraits for <i>Yin</i> Chen system with parameters $a = -35$, $b = -3$ and $c = -28.8$.	63
Fig. 5.12 Period4 of phase portraits for <i>Yin</i> Chen system with parameters $a = -35$, $b = -3$ and $c = -28.63$.	64
Fig. 5.13 Period8 of phase portraits for <i>Yin</i> Chen system with parameters $a = -35$, $b = -3$ and $c = -28.609$.	64
Fig. 5.14 Bifurcation diagram of chaotic <i>Yang</i> Chen system with $a = 35$ and $b = 3$.	65
Fig. 5.15 Lyapunov exponents of chaotic <i>Yang</i> Chen system with $a = 35$ and $b = 3$.	65
Fig. 5.16 Bifurcation diagram of chaotic <i>Yin</i> Chen system with $a = -35$ and $b = -3$.	66
Fig. 5.17 Lyapunov exponents of chaotic <i>Yin</i> Chen system with $a = -35$ and $b = -3$.	66
Fig. 5.18 Bifurcation diagram of chaotic <i>Yang</i> Chen system with $a = 35$ and $c = 27.2$.	67
Fig. 5.19 Lyapunov exponents of chaotic <i>Yang</i> Chen system with $a = 35$ and $c = 27.2$.	67
Fig. 5.20 Bifurcation diagram of chaotic <i>Yin</i> Chen system with $a = -35$ and $c = -27.2$.	68
Fig. 5.21 Lyapunov exponents of chaotic <i>Yin</i> Chen system with $a = -35$ and $c = -27.2$.	68

Fig. 5.22 Bifurcation diagram of chaotic <i>Yang</i> Chen system with $b = 3$ and $c = 27.2$.	69
Fig. 5.23 Lyapunov exponents of chaotic <i>Yang</i> Chen system with $b = 3$ and $c = 27.2$.	69
Fig. 5.24 Bifurcation diagram of chaotic <i>Yin</i> Chen system with $b = -3$ and $c = -27.2$.	70
Fig. 5.25 Lyapunov exponents of chaotic <i>Yin</i> Chen system with $b = -3$ and $c = -27.2$.	70
Fig. 6.1 Phase portrait of <i>Yang</i> Chen system with $a=35$, $b=3$, and $c=28$.	80
Fig. 6.2 Phase portrait of <i>Yin</i> Chen system with $a_1 = -35$, $b_1 = -3$ and $c_1 = -28$.	80
Fig. 6.3 Phase portrait of three errors dynamics with $k = 3200$ for <i>Case I</i> .	81
Fig. 6.4 Phase portrait of errors dynamics (e1&e2) with $k = 3200$ for <i>Case I</i> .	81
Fig. 6.5 Phase portrait of errors dynamics (e1&e3) with $k = 3200$ for <i>Case I</i> .	82
Fig. 6.6 Time histories of errors with $k = 3200$ for <i>Case I</i> .	82
Fig. 6.7 Time histories of x_i versus y_i with $k = 3200$ for <i>Case I</i> .	83
Fig. 6.8 Phase portrait of three errors dynamics with $k = 3100$ for <i>Case II</i> .	83
Fig. 6.9 Phase portrait of errors dynamics (e1&e2) with $k = 3100$ for <i>Case II</i> .	84
Fig. 6.10 Phase portrait of errors dynamics (e1&e3) with $k = 3100$ for <i>Case II</i> .	84
Fig. 6.11 Time histories of errors with $k = 3100$ for <i>Case II</i> .	85
Fig. 6.12 Time histories of x_i versus y_i with $k = 3100$ for <i>Case II</i> .	85
Fig. 6.13 Phase portrait of three errors dynamics with $k = 2700$ for <i>Case III</i> .	86
Fig. 6.14 Phase portraits of errors dynamics (e1&e2) with $k = 2700$ for <i>Case III</i> .	86
Fig. 6.15 Phase portraits of errors dynamics (e1&e3) with $k = 2700$ for <i>Case III</i> .	87
Fig. 6.16 Time histories of errors with $k = 2700$ for <i>Case III</i> .	87
Fig. 6.17 Time histories of x_i versus y_i with $k = 2700$ for <i>Case III</i> .	88
Fig. 6.18 Phase portraits of three errors dynamics with $k = 2900$ for <i>Case IV</i> .	88
Fig. 6.19 Time histories of errors with $k = 2900$ for <i>Case IV</i> .	89

Fig. 6.20 Time histories of x_i versus y_i with $k = 2900$ for <i>Case IV</i> .	89
Fig. 7.1 Phase portrait of <i>Yin</i> and <i>Yang</i> chaotic systems for <i>Case I</i> .	103
Fig. 7.2 Time histories of errors for <i>Yin</i> and <i>Yang</i> Chen chaotic systems for <i>Case I</i> .	103
Fig. 7.3 Time histories of parametric errors for <i>Yin</i> and <i>Yang</i> Chen chaotic systems for <i>Case I</i> .	104
Fig. 7.4 Time histories of states of <i>Yin</i> and <i>Yang</i> Chen chaotic systems for <i>Case I</i> .	104
Fig. 7.5 Phase portrait of Ikeda-Lorenz system.	105
Fig. 7.6 Phase portrait of <i>Yin</i> and <i>Yang</i> chaotic systems with Ikeda-Lorenz system as goal system for <i>Case II</i> .	105
Fig. 7.7 Time histories of errors for <i>Yin</i> and <i>Yang</i> Chen chaotic systems for <i>Case II</i> .	106
Fig. 7.8 Time histories of parametric errors for <i>Yin</i> and <i>Yang</i> Chen chaotic systems for <i>Case II</i> .	106
Fig. 7.9 Time histories of states of <i>Yin</i> and <i>Yang</i> Chen chaotic systems for <i>Case II</i> .	107
Fig. 7.10 Phase portrait of Rössler system.	107
Fig. 7.11 Phase portrait of <i>Yin</i> and <i>Yang</i> chaotic systems with Rössler system as goal system for <i>Case III</i> .	108
Fig. 7.12 Time histories of errors for <i>Yin</i> and <i>Yang</i> Chen chaotic systems for <i>Case III</i> .	108
Fig. 7.13 Time histories of parametric errors for <i>Yin</i> and <i>Yang</i> Chen chaotic systems for <i>Case III</i> .	109
Fig. 7.14 Time histories of states of <i>Yin</i> & <i>Yang</i> Chen chaotic systems for <i>Case III</i> .	109

Chapter 1

Introduction

Chaos has been found in nonlinear systems of various physical field and intensively investigated. We know that chaotic system has extremely sensitive dependence on initial conditions. So, Dynamics behaviors of chaotic system is studied extensively.

Synchronization of two chaotic systems was first introduced by Pecora and Corroll [1] in 1990, and has been widely applied in science and engineering. There are many control techniques to synchronize chaotic systems, such as adaptive control method, active control approach, invariant manifold method, and linear error feedback control [2-8], etc.

The generalized synchronization [9-14] is investigated among many kinds of synchronizations. It means that there exists a given functional relationship between the states of the master and that of the slave.

Since the famous OGY control method is given by Ott et al. [15] in 1990, numerous control methods have been widely applied in controlling chaos. For example, the adaptive control, the method of chaos control based on sampled data , the inverse optimal control, the active control and linear error feedback control [16-23], etc.

A new stability theory, GYC partial region stability theory, has been proposed [24-26]. By using the GYC partial region stability theory, generalized synchronization and chaos control can be obtained, the new Lyapunov function becomes a simple linear homogeneous function of error states and reduces the simulation error due to lower order of the controllers than that of traditional controllers.

Hyperchaos and chaos are desirable in some systems such as communications,

convective heat transfer, chemical reactions, and liquid mixing. When a chaotic system has more than one positive Lyapunov exponent, the dynamics of the system is expanded in more than one direction, giving rise to a more complex attractor. Generally, this type is called hyperchaotic system. Hyperchaos was first introduced by Rössler [27] and received great attention because of its potential in various engineering systems [28-31]. In this thesis, the constant parameters of the classical Lorenz system is replaced with Legendre functions of time. The hyperchaos is found for this system, which gives potential in many applications.

In general, nonlinear dynamics is called the chaos theory, which has been widely studied over several decades before. It changes the scientific way of looking at the dynamics of natural systems. Since the original research of an three-dimensional nonlinear system given by mathematical meteorologist E. N. Lorenz in 1963 [32], and he found out chaotic in a simple system of three autonomous ordinary differential equations to describe the simplified Rayleigh-Benard problem, chaos has been extensively investigated in many physical fields, such as power converters, chemical reactions, information processing, biological systems, secure communications [33], etc.

There are many articles in studying contemporary Chen system [34-39]. Although the contemporary Chen system has been discussed in detail, but no article was published in looking for the history of Chen system. As a result, there are abundant dynamics behavior in the historical Chen system found in this thesis.

In conventional Chinese philosophy[40-42], *Yin* is the negative, historical or feminine principle in nature, while *Yang* is the positive, contemporary or masculine principle in nature. *Yin* and *Yang* are two basic opposites respectively in Chinese philosophy. We call the positive parameters as *Yang* parameters for the contemporary Chen system, and negative parameters as *Yin* parameters for the historical Chen system to analyze the following simulation results. In this thesis, the historical Chen system is

introduced and the historical chaotic behavior with *Yin* parameters is studied by phase portraits, Poincaré maps, bifurcation diagram, Lyapunov exponents.

Historical chaos and generalized *Yin-Yang* synchronization are investigated for chaotic Chen system with well designed active control via four numerical simulation examples in this thesis.

All of the synchronization phenomena have a clear feature that the trajectories of the drive and response systems can not identically withstand to start from different initial conditions. However, a little bit of errors from initial conditions will lead to completely different trajectories for chaotic systems. For this reason, how to control two chaotic systems to be synchronized is a current objective. Generally, most of them are based on the exact knowledge of structure and parameters of the system. But in practice, some or all of the system parameters are uncertain. In this thesis, an adaptive *Yin-Yang* synchronization of historical and contemporary Chen chaos by pragmatical asymptotically stability theorem was investigated via three numerical simulations.

This thesis is organized as follows. In Chapter 2, in Section 2.1, preliminaries are presented. In Section 2.2, chaos generalized synchronization strategy by GYC partial region stability theory is proposed. In Section 2.3, a new Froude-van der Pol system is presented. In Section 2.4, four simulation examples are given. In Section 2.5, summary is given. The partial region stability theory is enclosed in Appendix A.

In Chapter 3, in Section 3.1, preliminaries are presented. In Section 3.2, chaos control scheme by GYC partial region stability theory is proposed. In Section 3.3, a new Froude-van der Pol system is presented. In Section 3.4, three simulation examples are given. In Section 3.5, summary is given. The partial region stability theory is enclosed in Appendix A.

In Chapter 4, in Section 4.1, preliminaries are presented. In Section 4.2, a brief description of a classical Lorenz system and of a Lorenz system with Legendre function

parameters are introduced. In Section 4.3, time histories of states, phase portraits, Poincaré maps, bifurcation diagram, Lyapunov exponents and parameter diagrams are presented. In Section 4.4, summary is given.

In Chapter 5, in Section 5.1, preliminaries are presented. In Section 5.2, the *Yang* Chen system is presented. In Section 5.3, the *Yin* Chen system is introduced. In Section 5.4, three simulation cases of *Yin* and *Yang* Chen system are given for analyzing and comparing. In Section 5.5, summary is given.

In Chapter 6, in Section 6.1, preliminaries are presented. In Section 6.2, generalized *Yin-Yang* synchronization strategy is presented. In Section 6.3, the *Yang* and *Yin* Chen systems are introduced. In Section 6.4, four simulation cases are given for analyzing. In Section 6.5, summary is given.

In Chapter 7, in Section 7.1, preliminaries are presented. In Section 7.2, pragmatical generalized *Yin-Yang* synchronization scheme by adaptive control is given. In Section 7.3, the chaotic behavior of *Yang* and *Yin* Chen systems are introduced. In Section 7.4, numerical simulations of generalized *Yin-Yang* synchronization are given for analyzing. In Section 7.5, summary is given. Pragmatical asymptotical stability theory is enclosed in Appendix C.

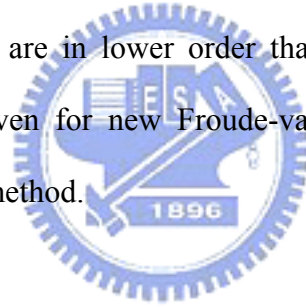
In Chapter 8, conclusions are given.

Chapter 2

Chaos Generalized Synchronization of a New Froude- van der Pol System by GYC Partial Region Stability Theory

2.1 Preliminaries

In this Chapter, a new strategy of achieving chaos generalized synchronization by GYC partial region stability is proposed. Using the GYC partial region stability theory, the Lyapunov function used becomes a simple linear homogeneous function of error states and the controllers are simpler than traditional controllers, and give less simulation error because they are in lower order than that of traditional controllers. Numerical simulations are given for new Froude-van der Pol system to verify the effectiveness of the proposed method.



2.2 Chaos Generalized Synchronization Strategy

Consider the following unidirectional coupled chaotic systems

$$\begin{cases} \dot{\mathbf{x}} = \mathbf{f}(t, \mathbf{x}) \\ \dot{\mathbf{y}} = \mathbf{h}(t, \mathbf{y}) + \mathbf{u} \end{cases} \quad (2.1)$$

where $\mathbf{x} = [x_1, x_2, \dots, x_n]^T \in R^n$, $\mathbf{y} = [y_1, y_2, \dots, y_n]^T \in R^n$ denote the master state vector and slave state vector respectively, \mathbf{f} and \mathbf{h} are nonlinear vector functions, and $\mathbf{u} = [u_1, u_2, \dots, u_n]^T \in R^n$ is a control input vector.

The generalized synchronization can be accomplished when $t \rightarrow \infty$, the limit of the error vector $\mathbf{e} = [e_1, e_2, \dots, e_n]^T$ approaches zero:

$$\lim_{t \rightarrow \infty} \mathbf{e} = 0 \quad (2.2)$$

where

$$\mathbf{e} = \mathbf{G}(\mathbf{x}) - \mathbf{y} \quad (2.3)$$

$\mathbf{G}(\mathbf{x})$ is a given function of \mathbf{x} .

By using the partial region stability theory, the linear homogeneous function of entries of \mathbf{e} can be used to construct a positive definite Lyapunov function. The controllers can be designed in lower order than that of traditional controllers and introduce less simulation error.

2.3 A New Froude-van der Pol System

Froude system and van der Pol system[43] are two typical nonlinear nonautonomous systems:

$$\begin{cases} \frac{d}{dt} x_1 = x_2 \\ \frac{d}{dt} x_2 = (a - bx_2^2)x_2 + c \sin x_1 + d \cos \omega t \end{cases} \quad (2.4)$$

$$\begin{cases} \frac{d}{dt} x_3 = x_4 \\ \frac{d}{dt} x_4 = -fx_3 + g(x_3^2 - 1)x_4 - h \sin \omega t \end{cases} \quad (2.5)$$

Changing $d \cos \omega t$ term in Eq.(2.4) by dx_3 and $h \sin \omega t$ term in Eq.(2.5) by

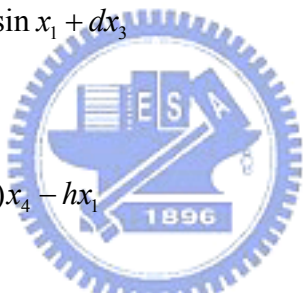
hx_1 , respectively, we obtain a new autonomous Froude-van der Pol system:

$$\begin{cases} \frac{d}{dt} x_1 = x_2 \\ \frac{d}{dt} x_2 = (a - bx_2^2)x_2 + c \sin x_1 + dx_3 \\ \frac{d}{dt} x_3 = x_4 \\ \frac{d}{dt} x_4 = -fx_3 + g(x_3^2 - 1)x_4 - hx_1 \end{cases} \quad (2.6)$$

where x_1, x_2, x_3, x_4 are state variables, and a, b, c, d, f, g, h are parameters. When $a = 0.35, b = 0.1, c = 1.0, d = -1, f = 1, g = -0.1, h = -0.1$, and the initial states of system are $x_1(0) = 0.2, x_2(0) = 0.35, x_3(0) = 0.2, x_4(0) = 0.35$. Its chaotic phase portrait, time histories of states, bifurcation diagram, and Lyapunov exponent are shown in Figs. 2.1-4.

2.4 Numerical Simulations

A master Froude-van der Pol system and a slave one with the unidirectional coupling are given:

$$\begin{cases} \frac{d}{dt}x_1 = x_2 \\ \frac{d}{dt}x_2 = (a - bx_2^2)x_2 + c \sin x_1 + dx_3 \\ \frac{d}{dt}x_3 = x_4 \\ \frac{d}{dt}x_4 = -fx_3 + g(x_3^2 - 1)x_4 - hx_1 \end{cases} \quad (2.7)$$


$$\begin{cases} \frac{d}{dt}y_1 = y_2 + u_1 \\ \frac{d}{dt}y_2 = (a - by_2^2)y_2 + c \sin y_1 + dy_3 + u_2 \\ \frac{d}{dt}y_3 = y_4 + u_3 \\ \frac{d}{dt}y_4 = -fy_3 + g(y_3^2 - 1)y_4 - hy_1 + u_4 \end{cases} \quad (2.8)$$

CASE I. The generalized synchronization error function is $e_i = x_i - y_i + k (i = 1, 2, 3, 4)$:

$$\begin{cases} e_1 = x_1 - y_1 + k \\ e_2 = x_2 - y_2 + k \\ e_3 = x_3 - y_3 + k \\ e_4 = x_4 - y_4 + k \end{cases} \quad (2.9)$$

where k is positive constant, we choose $k=20$, in order that the error dynamics

always happens in first quadrant. Our goal is $y_i = x_i + k$, i.e.

$$\lim_{t \rightarrow \infty} e_i = \lim_{t \rightarrow \infty} (x_i - y_i + k) = 0, (i = 1, 2, 3, 4) \quad (2.10)$$

The error dynamics becomes

$$\begin{cases} \dot{e}_1 = x_2 - y_2 - u_1 \\ \dot{e}_2 = (a - bx_2^2)x_2 + c \sin x_1 + dx_3 \\ \quad - ((a - by_2^2)y_2 + c \sin y_1 + dy_3) - u_2 \\ \dot{e}_3 = x_4 - y_4 - u_3 \\ \dot{e}_4 = -fx_3 + g(x_3^2 - 1)x_4 - hx_1 - (-fy_3 + g(y_3^2 - 1)y_4 - hy_1) - u_4 \end{cases} \quad (2.11)$$

where

$$\dot{e}_i = \dot{x}_i - \dot{y}_i, (i = 1, 2, 3, 4) \quad (2.12)$$

Let initial states be $(x_1, x_2, x_3, x_4) = (0.2, 0.35, 0.2, 0.35)$, $(y_1, y_2, y_3, y_4) = (1, 2, 2.2,$

1.5), we find that the error dynamics always exists in first quadrant as shown in Fig. 2.5.

By GYC partial region asymptotical stability theorem, one can choose a Lyapunov function in the form of a positive definite function in first quadrant:

$$V = e_1 + e_2 + e_3 + e_4 \quad (2.13)$$

Its time derivative is

$$\begin{aligned} \dot{V} &= \dot{e}_1 + \dot{e}_2 + \dot{e}_3 + \dot{e}_4 \\ &= (x_2 - y_2 - u_1) \\ &\quad + ((a - bx_2^2)x_2 + c \sin x_1 + dx_3 \\ &\quad - ((a - by_2^2)y_2 + c \sin y_1 + dy_3) - u_2) \\ &\quad + (x_4 - y_4 - u_3) \\ &\quad + (-fx_3 + g(x_3^2 - 1)x_4 - hx_1 - (-fy_3 + g(y_3^2 - 1)y_4 - hy_1) - u_4) \end{aligned} \quad (2.14)$$

Choose

$$\begin{aligned}
u_1 &= x_2 - y_2 + e_1 \\
u_2 &= (a - bx_2^2)x_2 + c \sin x_1 + dx_3 \\
&\quad - ((a - by_2^2)y_2 + c \sin y_1 + dy_3) + e_2 \\
u_3 &= x_4 - y_4 + e_3 \\
u_4 &= -fx_3 + g(x_3^2 - 1)x_4 - hx_1 - (-fy_3 + g(y_3^2 - 1)y_4 - hy_1) + e_4
\end{aligned} \tag{2.15}$$

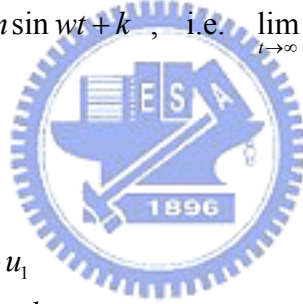
We obtain

$$\dot{V} = -e_1 - e_2 - e_3 - e_4 < 0 \tag{2.16}$$

which is a negative definite function in first quadrant. Four error states versus time and time histories of states are shown in Figs. 2.6-7.

CASE II. The generalized synchronization error function is $e_i = x_i - y_i + m \sin wt + k$, $(i = 1, 2, 3, 4)$.

Our goal is $y_i = x_i + m \sin wt + k$, i.e. $\lim_{t \rightarrow \infty} e_i = \lim_{t \rightarrow \infty} (x_i - y_i + m \sin wt + k) = 0$, $(i = 1, 2, 3, 4)$



The error dynamics become

$$\begin{cases}
\dot{e}_1 = x_2 - y_2 + mw \cos wt - u_1 \\
\dot{e}_2 = (a - bx_2^2)x_2 + c \sin x_1 + dx_3 \\
\quad - ((a - by_2^2)y_2 + c \sin y_1 + dy_3) + mw \cos wt - u_2 \\
\dot{e}_3 = x_4 - y_4 + mw \cos wt - u_3 \\
\dot{e}_4 = -fx_3 + g(x_3^2 - 1)x_4 - hx_1 - (-fy_3 + g(y_3^2 - 1)y_4 - hy_1) \\
\quad + mw \cos wt - u_4
\end{cases} \tag{2.17}$$

where

$$\dot{e}_i = \dot{x}_i + mw \cos wt - \dot{y}_i, \quad (i = 1, 2, 3, 4) \tag{2.18}$$

Let initial states be $(x_1, x_2, x_3, x_4) = (0.2, 0.35, 0.2, 0.35)$, $(y_1, y_2, y_3, y_4) = (1, 2, 2.2, 1.5)$, and $w=1, m=2, k=20$, we find that the error dynamic always exists in first quadrant as shown in Fig. 2.8. By GYC partial region asymptoical stability theorem, one can choose a Lyapunov function in the form of a positive definite function in first

quadrant:

$$V = e_1 + e_2 + e_3 + e_4 \quad (2.19)$$

Its time derivative is

$$\begin{aligned} \dot{V} = & (x_2 - y_2 - u_1 + m\omega \cos \omega t) \\ & + ((a - bx_2^2)x_2 + c \sin x_1 + dx_3 - ((a - by_2^2)y_2 + c \sin y_1 + dy_3 + u_2) \\ & + m\omega \cos \omega t) + (x_4 - y_4 - u_3 + m\omega \cos \omega t) \\ & + (-fx_3 + g(x_3^2 - 1)x_4 - hx_1 - (-fy_3 + g(y_3^2 - 1)y_4 - hy_1 + u_4) + m\omega \cos \omega t) \end{aligned} \quad (2.20)$$

Choose

$$\begin{aligned} u_1 &= x_2 - y_2 + m\omega \cos \omega t + e_1 \\ u_2 &= (a - bx_2^2)x_2 + c \sin x_1 + dx_3 - ((a - by_2^2)y_2 + c \sin y_1 + dy_3) \\ &+ m\omega \cos \omega t + e_2 \\ u_3 &= x_4 - y_4 + m\omega \cos \omega t + e_3 \\ u_4 &= -fx_3 + g(x_3^2 - 1)x_4 - hx_1 - (-fy_3 + g(y_3^2 - 1)y_4 - hy_1) + m\omega \cos \omega t + e_4 \end{aligned} \quad (2.21)$$

We obtain

$$\dot{V} = -e_1 - e_2 - e_3 - e_4 < 0 \quad (2.22)$$

which is a negative definite function in first quadrant. Four state errors versus time and time histories of $x_i - y_i + k$, $-m \sin \omega t$ are shown in Figs. 2.9-10.

CASE III. The generalized synchronization error function is $e_i = \frac{1}{4}x_i^4 - y_i + k$, $(i=1,2,3,4)$ where $k=100$.

Our goal is $y_i = \frac{1}{4}x_i^4 + k$, i.e. $\lim_{t \rightarrow \infty} e = \lim_{t \rightarrow \infty} (\frac{1}{4}x_i^4 - y_i + k) = 0$, $(i=1,2,3,4)$

The error dynamics becomes

$$\begin{cases} \dot{e}_1 = x_1^3 x_2 - y_2 - u_1 \\ \dot{e}_2 = x_2^3 ((a - bx_2^2)x_2 + c \sin x_1 + dx_3) \\ \quad - ((a - by_2^2)y_2 + c \sin y_1 + dy_3) - u_2 \\ \dot{e}_3 = x_3^3 x_4 - y_4 - u_3 \\ \dot{e}_4 = x_4^3 (-fx_3 + g(x_3^2 - 1)x_4 - hx_1) - (-fy_3 + g(y_3^2 - 1)y_4 \\ \quad - hy_1) - u_4 \end{cases} \quad (2.23)$$

where

$$\dot{e}_i = x_i^3 \dot{x}_i - \dot{y}_i, \quad (i = 1, 2, 3, 4) \quad (2.24)$$

Let initial states be $(x_1, x_2, x_3, x_4) = (0.2, 0.35, 0.2, 0.35)$, $(y_1, y_2, y_3, y_4) = (1, 2, 2.2, 1.5)$, and we find that the error dynamics always exists in first quadrant as shown in Fig. 2.11. By GYC partial region asymptotical stability theorem, one can choose a Lyapunov function in the form of a positive definite function in first quadrant:

$$V = e_1 + e_2 + e_3 + e_4 \quad (2.25)$$

Its time derivative is

$$\begin{aligned} \dot{V} &= \dot{e}_1 + \dot{e}_2 + \dot{e}_3 + \dot{e}_4 \\ &= (x_1^3 x_2 - y_2 - u_1) + (x_2^3 ((a - bx_2^2)x_2 + c \sin x_1 + dx_3) \\ &\quad - ((a - by_2^2)y_2 + c \sin y_1 + dy_3) - u_2) + (x_3^3 x_4 - y_4 - u_3) \\ &\quad + (x_4^3 (-fx_3 + g(x_3^2 - 1)x_4 - hx_1) - (-fy_3 + g(y_3^2 - 1)y_4 \\ &\quad - hy_1) - u_4) \end{aligned} \quad (2.26)$$

Choose

$$\begin{aligned} u_1 &= x_1^3 x_2 - y_2 + e_1 \\ u_2 &= x_2^3 ((a - bx_2^2)x_2 + c \sin x_1 + dx_3) \\ &\quad - ((a - by_2^2)y_2 + c \sin y_1 + dy_3) + e_2 \\ u_3 &= x_3^3 x_4 - y_4 + e_3 \\ u_4 &= x_4^3 (-fx_3 + g(x_3^2 - 1)x_4 - hx_1) - (-fy_3 + g(y_3^2 - 1)y_4 \\ &\quad - hy_1) + e_4 \end{aligned} \quad (2.27)$$

We obtain

$$\dot{V} = -e_1 - e_2 - e_3 - e_4 < 0 \quad (2.28)$$

which is a negative definite function in first quadrant. Four state errors versus time and time histories of $\frac{x_i^4}{4} + 100, y_i$ are shown in Figs. 2.12-13.

CASE IV. The generalized synchronization error function is $e_i = x_i(t - \tau) - y_i + z_i^2 + k$,

z_i is the state of hyperchaotic Lü system [44].

The goal system for synchronization is hyperchaotic Lü system and initial states are $(5, 8, -1, -3)$, delay time $\tau = 5$, system parameters $a_1 = 36$, $b_1 = 3$, $c_1 = 20$, $r_1 = -0.35$.

$$\begin{cases} \frac{d}{dt} z_1 = a_1(z_2 - z_1) + z_4 \\ \frac{d}{dt} z_2 = -z_1 z_3 + c_1 z_2 \\ \frac{d}{dt} z_3 = z_1 z_2 - b_1 z_3 \\ \frac{d}{dt} z_4 = z_1 z_3 + r_1 z_4 \end{cases} \quad (2.29)$$

We have $\lim_{t \rightarrow \infty} e_i = \lim_{t \rightarrow \infty} (x_i(t - \tau) - y_i + z_i^2 + k) = 0$, $(i = 1, 2, 3, 4)$, where $k = 50$.

The error dynamics becomes

$$\begin{cases} \dot{e}_1 = x_2 - y_2 + a_1(z_2 - z_1) + z_4 - u_1 \\ \dot{e}_2 = (a - bx_2^2)x_2 + c \sin x_1 + dx_3 - ((a - by_2^2)y_2 + c \sin y_1 \\ \quad + dy_3) + (-z_1 z_3 + c_1 z_2) - u_2 \\ \dot{e}_3 = x_4 - y_4 + z_1 z_2 - b_1 z_3 - u_3 \\ \dot{e}_4 = (-fx_3 + g(x_3^2 - 1)x_4 - hx_1) - (-fy_3 + g(y_3^2 - 1)y_4 - hy_1) \\ \quad + (z_1 z_3 + r_1 z_4) - u_4 \end{cases} \quad (2.30)$$

Let initial states be $(x_1, x_2, x_3, x_4) = (0.2, 0.35, 0.2, 0.35)$, $(y_1, y_2, y_3, y_4) = (1, 2, 2.2, 1.5)$, and we find that the error dynamics always exists in first quadrant as shown in Fig. 2.14. By GYC partial region asymptotical stability theorem, one can choose a Lyapunov function in the form of a positive definite function in first quadrant:

$$V = e_1 + e_2 + e_3 + e_4 \quad (2.31)$$

By Eqs. (2.30),(2.31),

$$\begin{aligned} \dot{V} = & (x_2 - y_2 + a_1(z_2 - z_1) + z_4 - u_1) + ((a - bx_2^2)x_2 + c \sin x_1 + dx_3 \\ & - ((a - by_2^2)y_2 + c \sin y_1 + dy_3) + (-z_1 z_3 + c_1 z_2) - u_2) \\ & + (x_4 - y_4 + z_1 z_2 - b_1 z_3 - u_3) + ((-fx_3 + g(x_3^2 - 1)x_4 - hx_1) \\ & - (-fy_3 + g(y_3^2 - 1)y_4 - hy_1) + (z_1 z_3 + r_1 z_4) - u_4) \end{aligned} \quad (2.32)$$

Choose

$$\begin{aligned}
u_1 &= x_2 - y_2 + a_1(z_2 - z_1) + z_4 + e_1 \\
u_2 &= (a - bx_2^2)x_2 + c \sin x_1 + dx_3 - ((a - by_2^2)y_2 + c \sin y_1 \\
&\quad + dy_3) + (-z_1z_3 + c_1z_2) + e_2 \\
u_3 &= x_4 - y_4 + z_1z_2 - b_1z_3 + e_3 \\
u_4 &= (-fx_3 + g(x_3^2 - 1)x_4 - hx_1) - (-fy_3 + g(y_3^2 - 1)y_4 - hy_1) \\
&\quad + (z_1z_3 + r_1z_4) + e_4
\end{aligned} \tag{2.33}$$

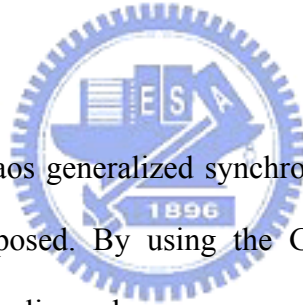
We obtain

$$\dot{V} = -e_1 - e_2 - e_3 - e_4 < 0 \tag{2.34}$$

which is a negative definite function in first quadrant. Four state errors versus time and time histories of $x_i(t - \tau) - y_i + 50$ are shown in Figs. 2.15-16.

2.5 Summary

In this Chapter, a new chaos generalized synchronization method by GYC partial region stability theory is proposed. By using the GYC partial region stability the Lyapunov function is a simple linear homogeneous function of error states and the controllers are simpler. As a result, less simulation error is introduced. The new Froude-van der Pol system and hyperchaotic Lü system are used as one of four simulation examples which prove the effectiveness of the proposed method.



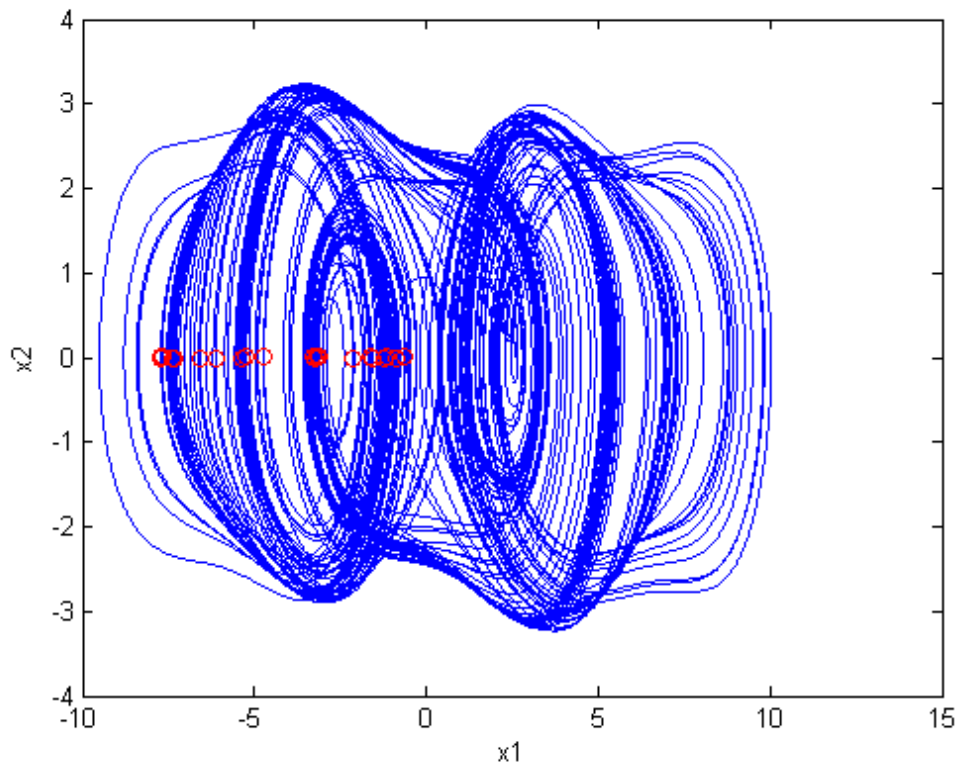


Fig. 2.1 Phase portrait of a new Froude-van der Pol system.

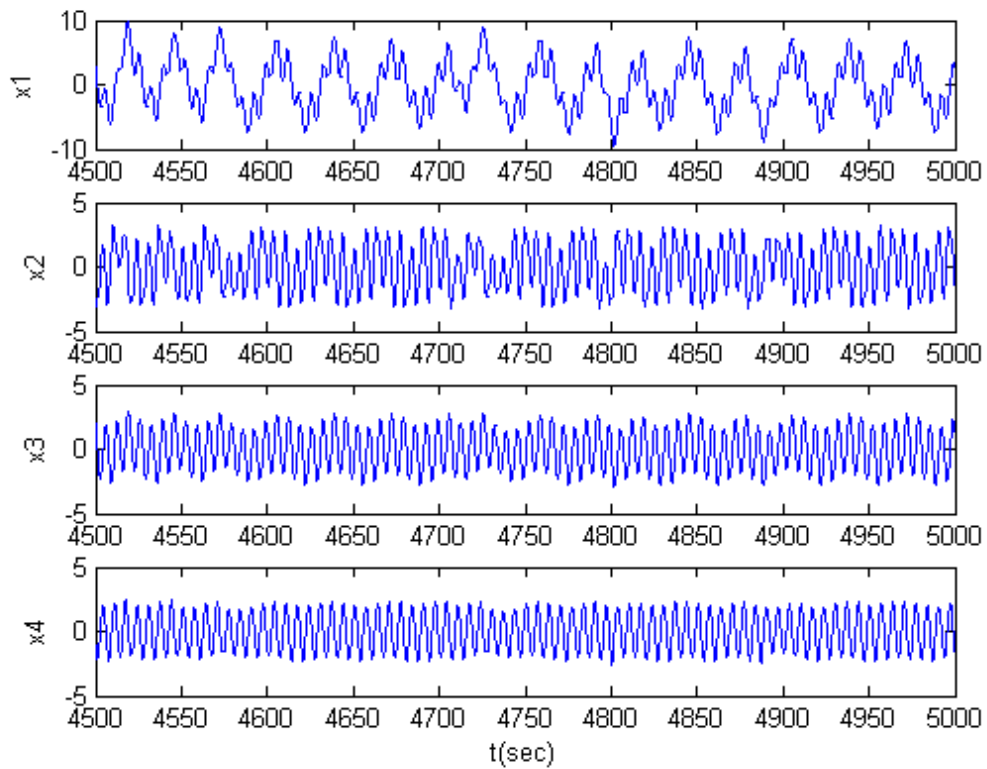


Fig. 2.2 Time histories of a new Froude-van der Pol system.

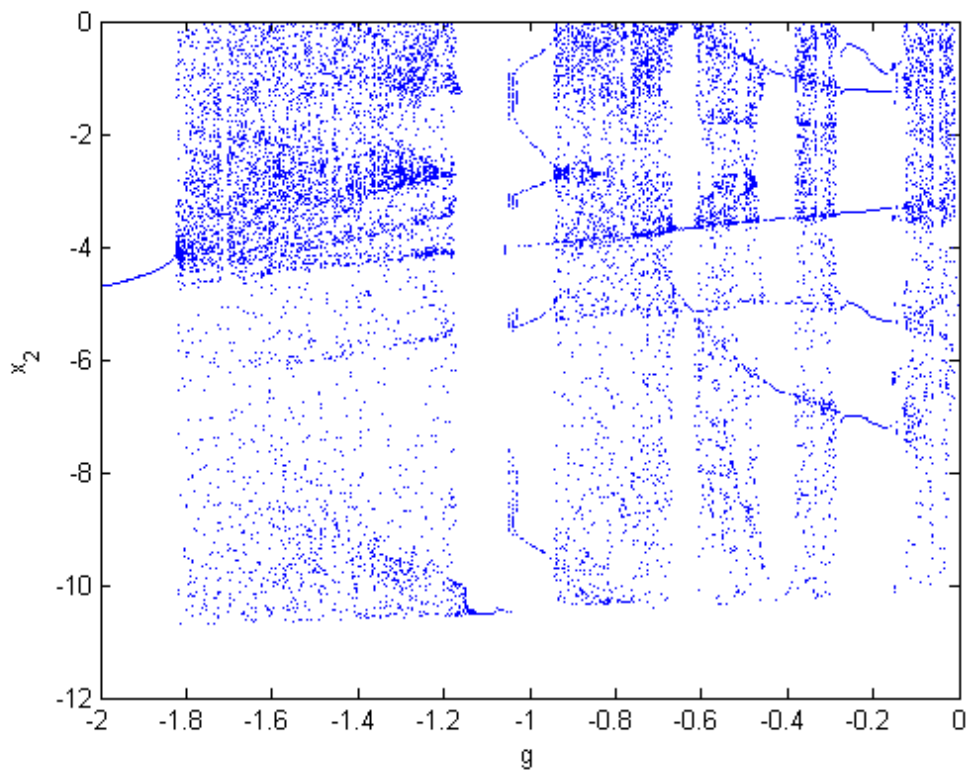


Fig. 2.3 Bifurcation diagram of a new Froude-van der Pol system.

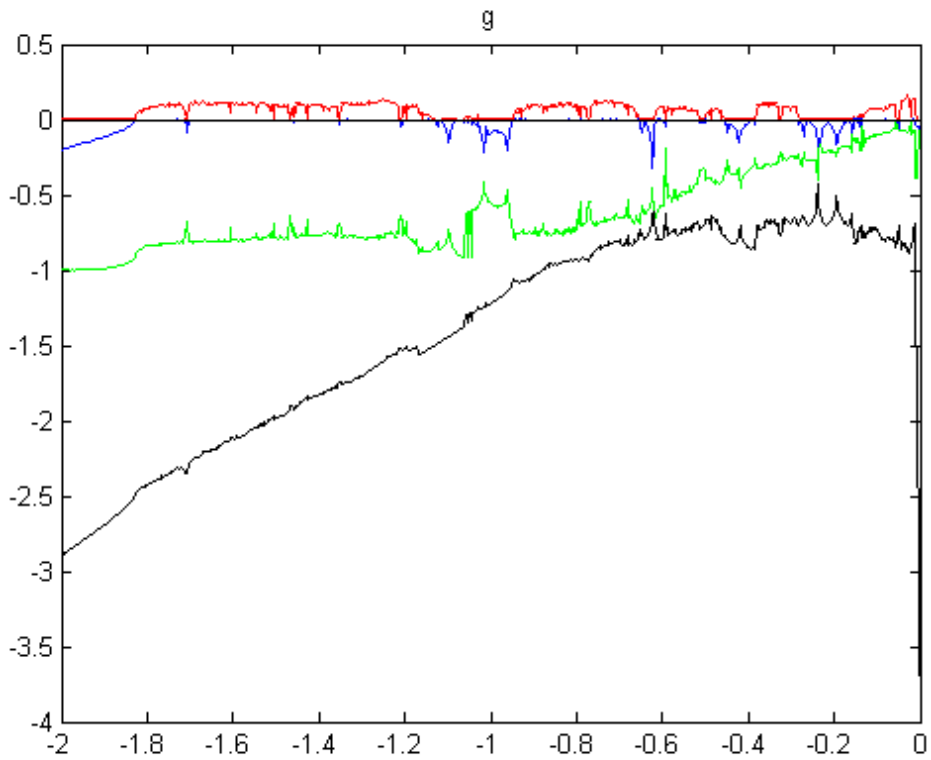


Fig. 2.4 Lyapunov exponents of a new Froude-van der Pol system.

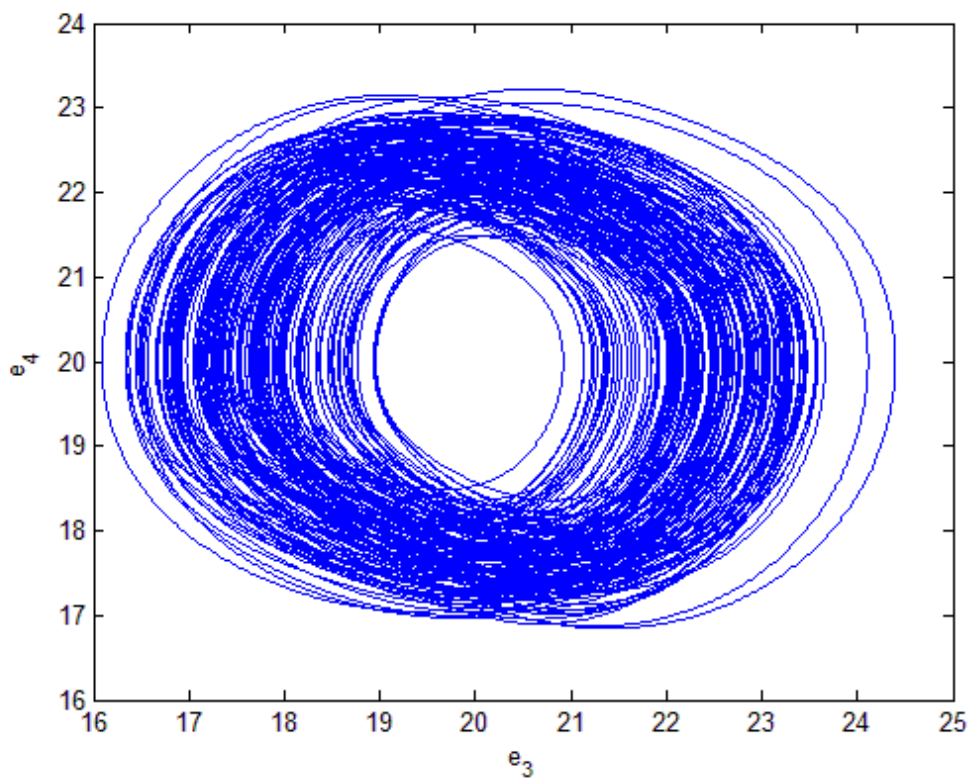
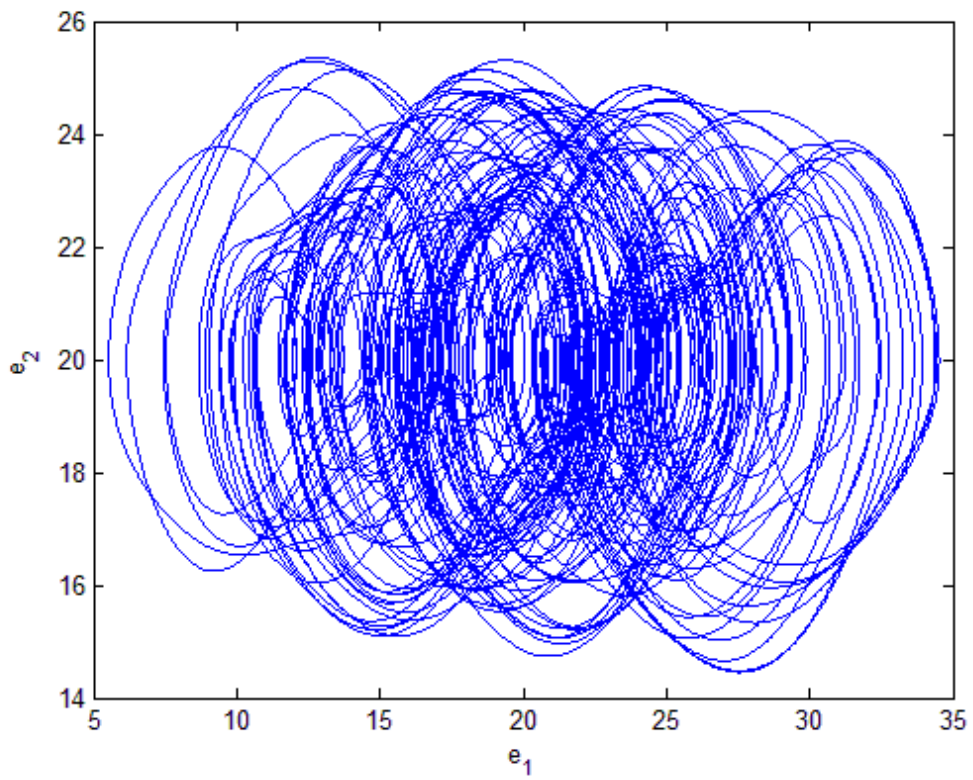


Fig. 2.5 Phase portraits of errors dynamics for *Case I*.

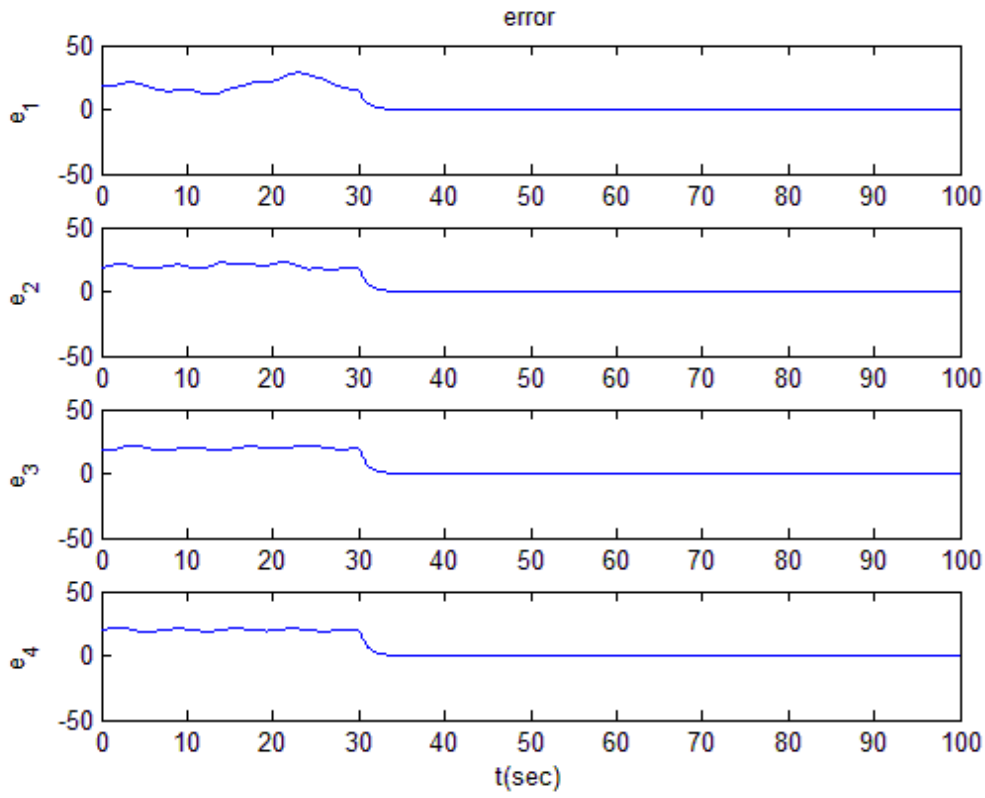


Fig. 2.6 Time histories of errors for Case I.

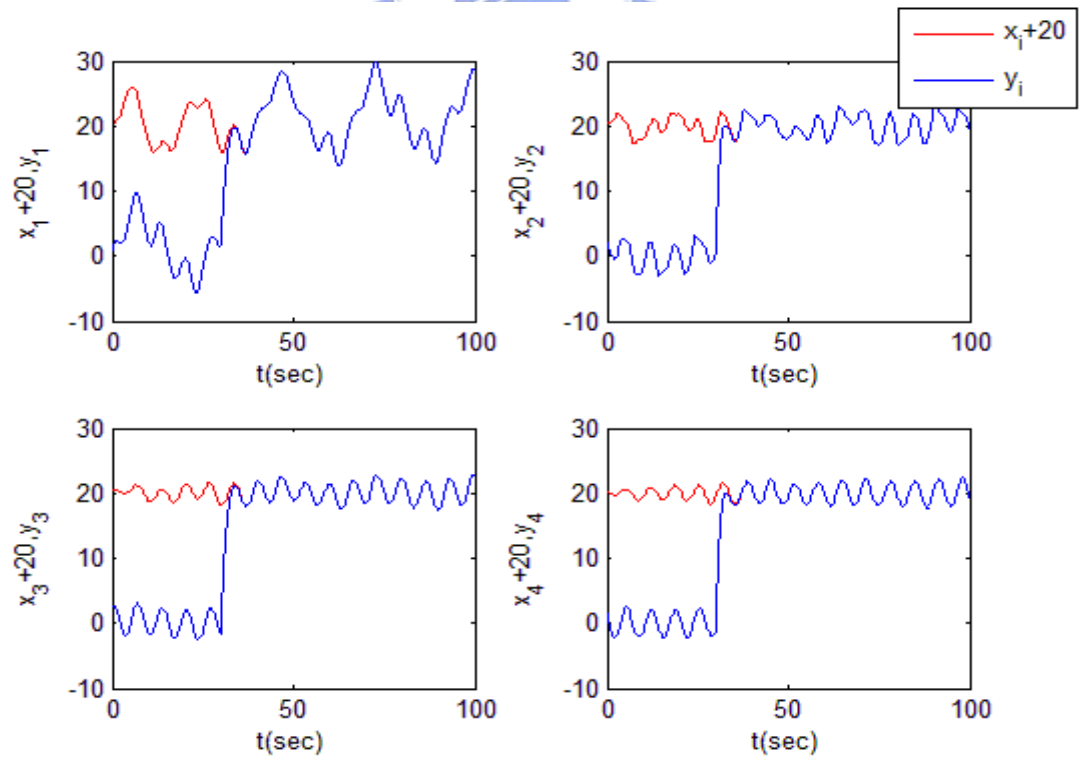


Fig. 2.7 Time histories of $x_i + 20, y_i$ for Case I.

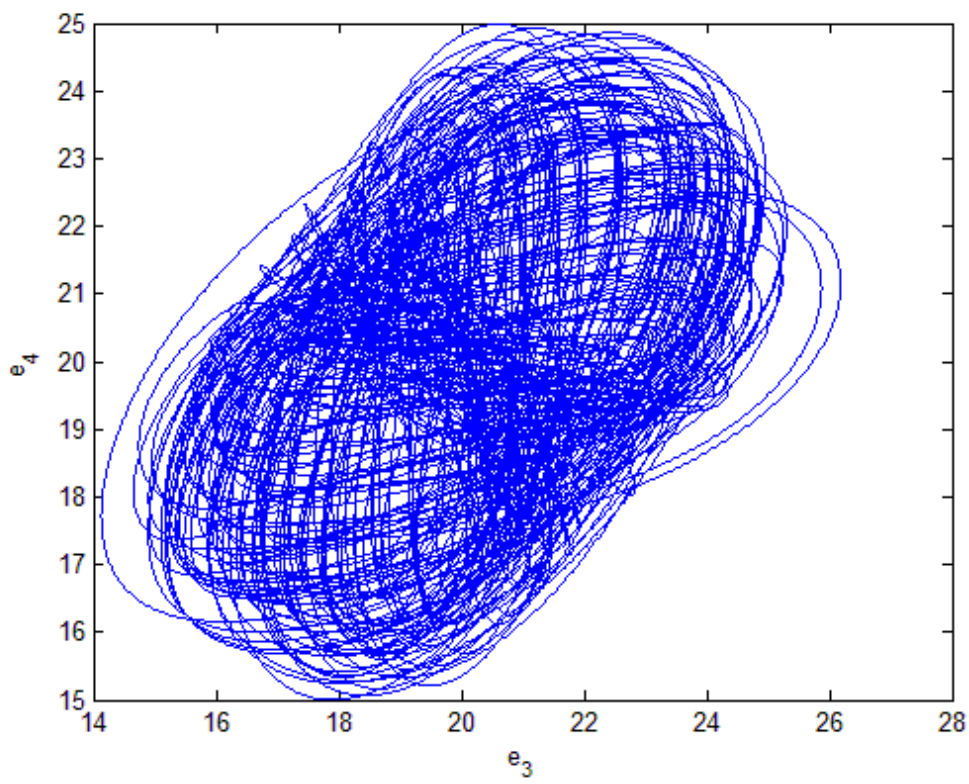
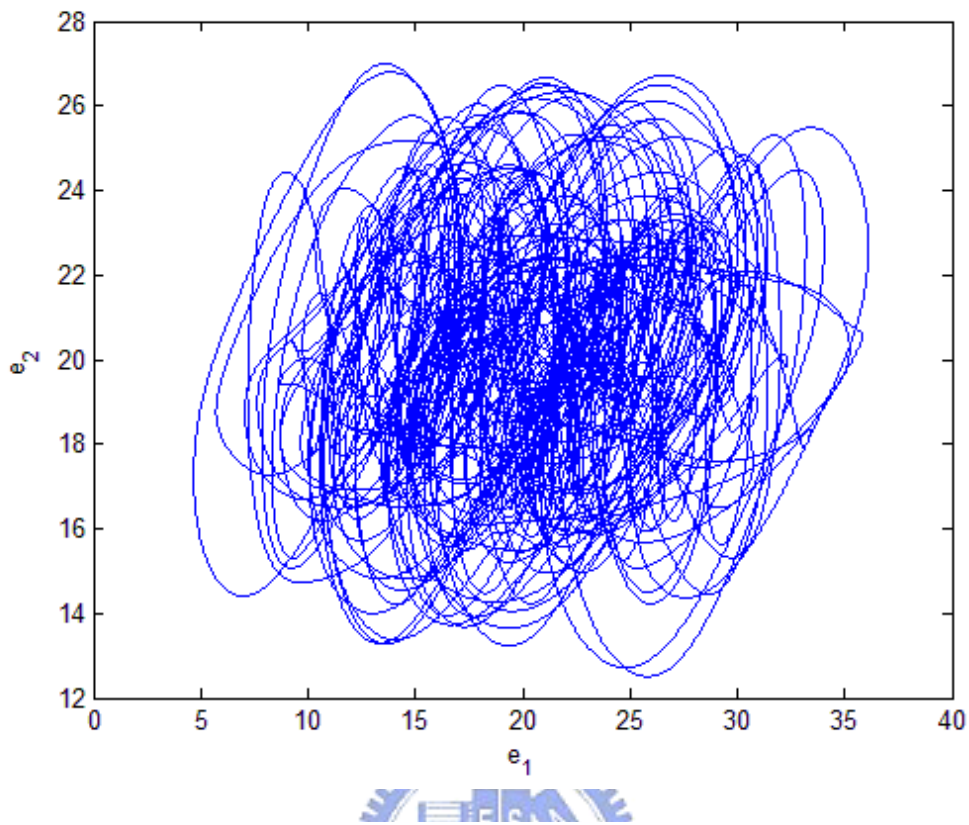


Fig. 2.8 Phase portraits of error dynamics for *Case II*.

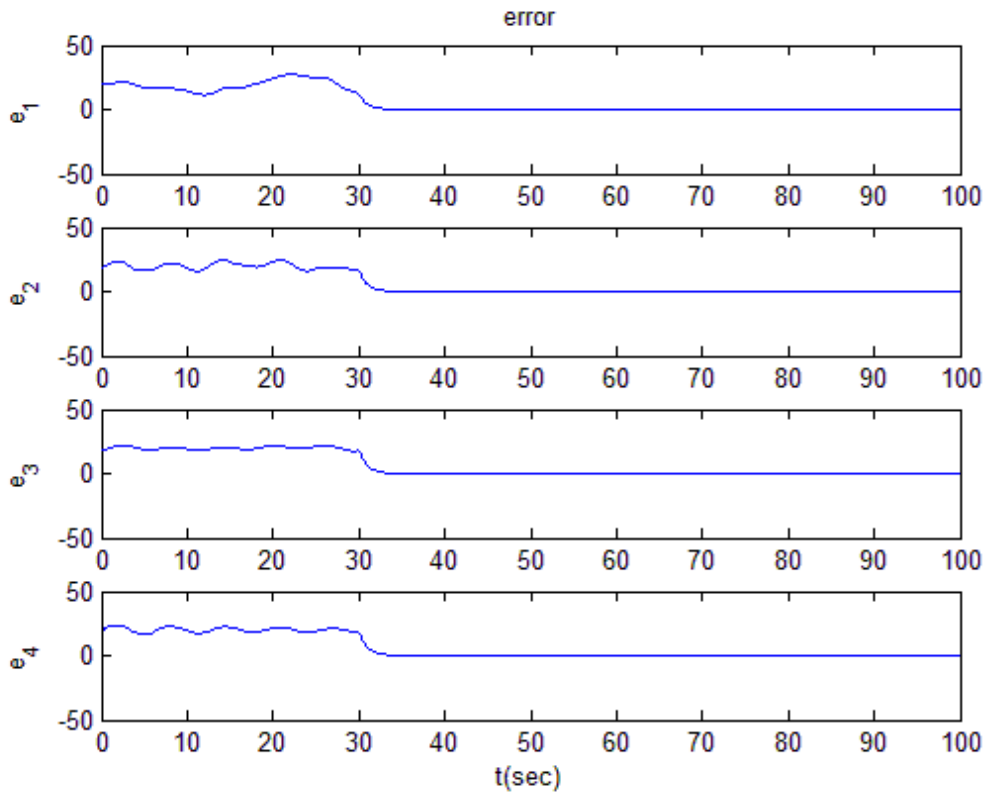


Fig. 2.9 Time histories of errors for Case II.

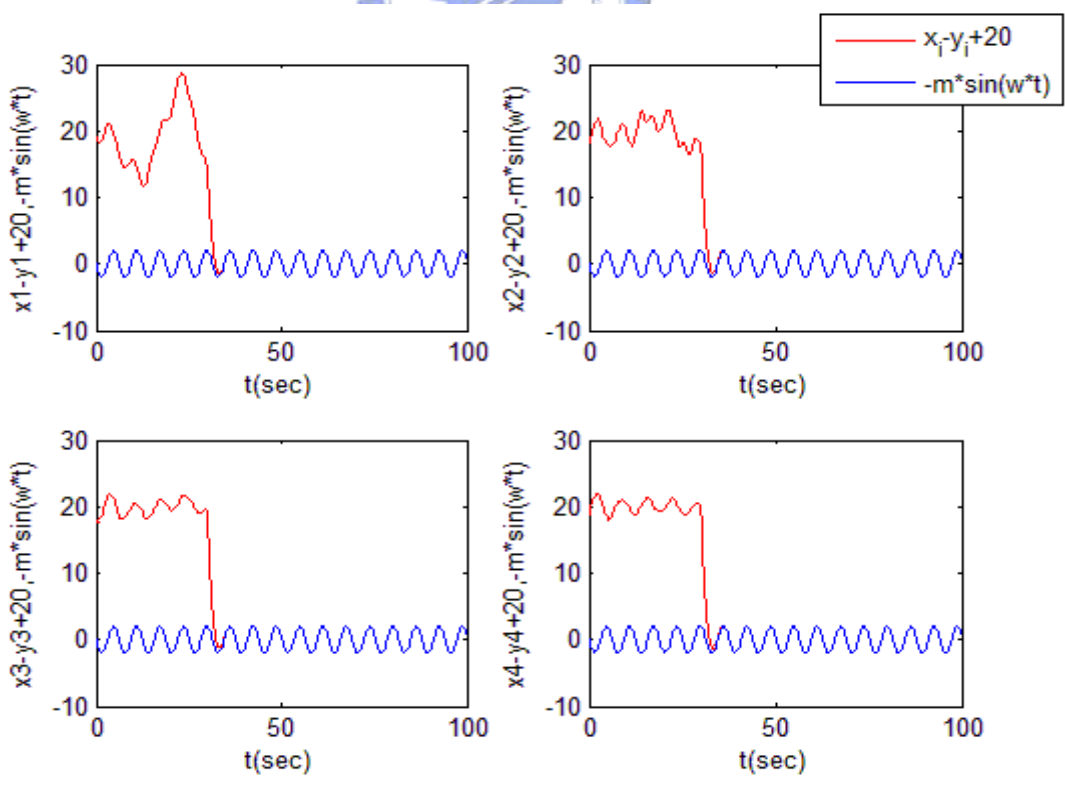


Fig. 2.10 Time histories of $x_i - y_i + 20$ and $-m \sin \omega t$ for Case II.

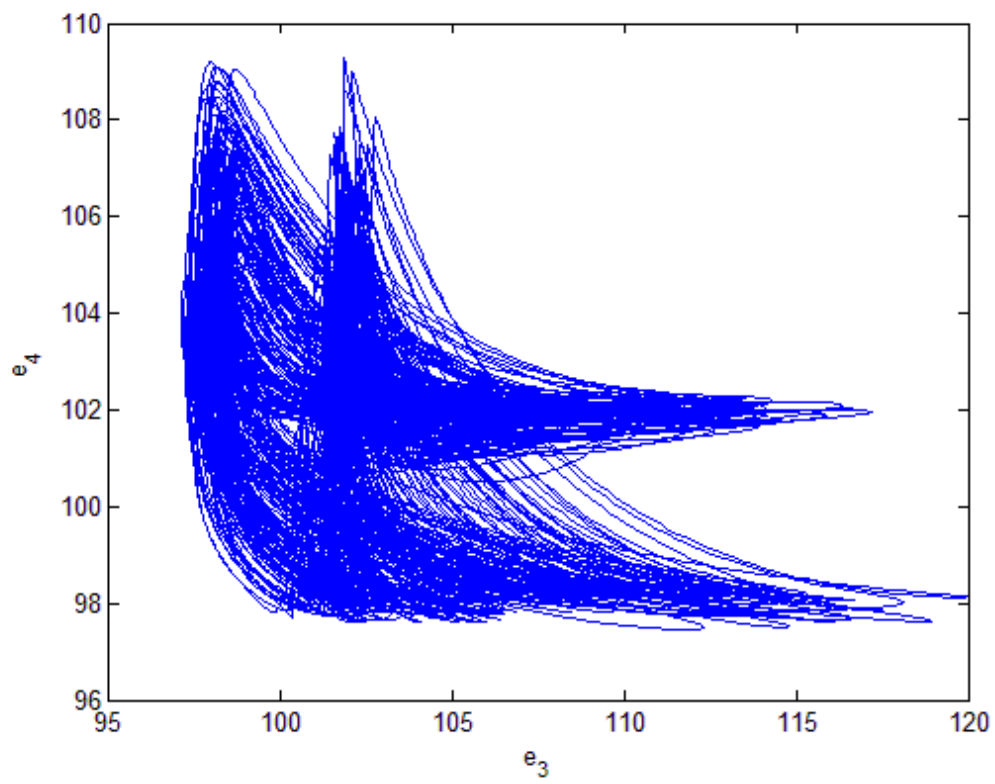
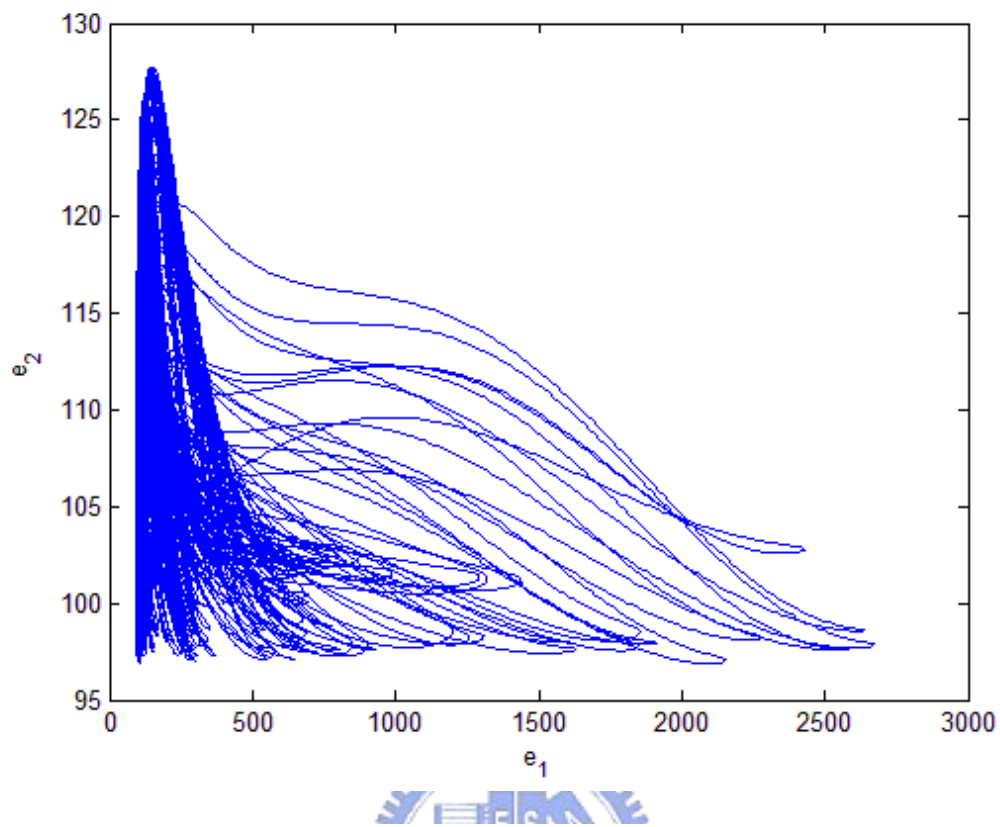


Fig. 2.11 Phase portraits of error dynamics for *Case III*.

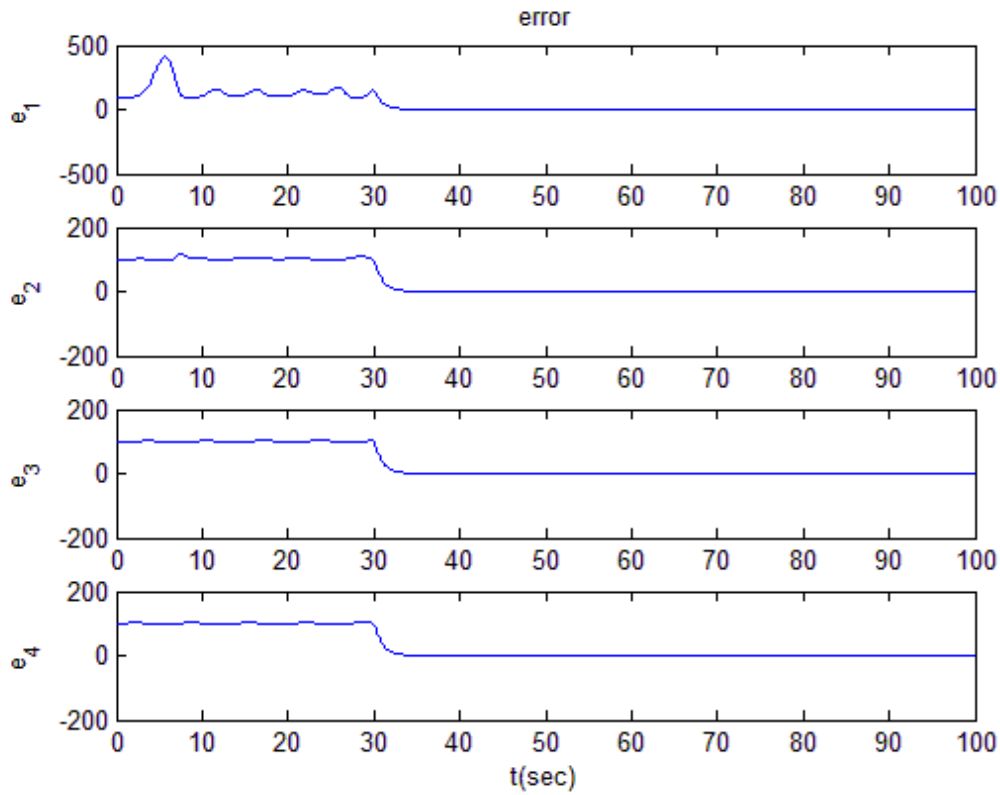


Fig. 2.12 Time histories of errors for *Case III*.

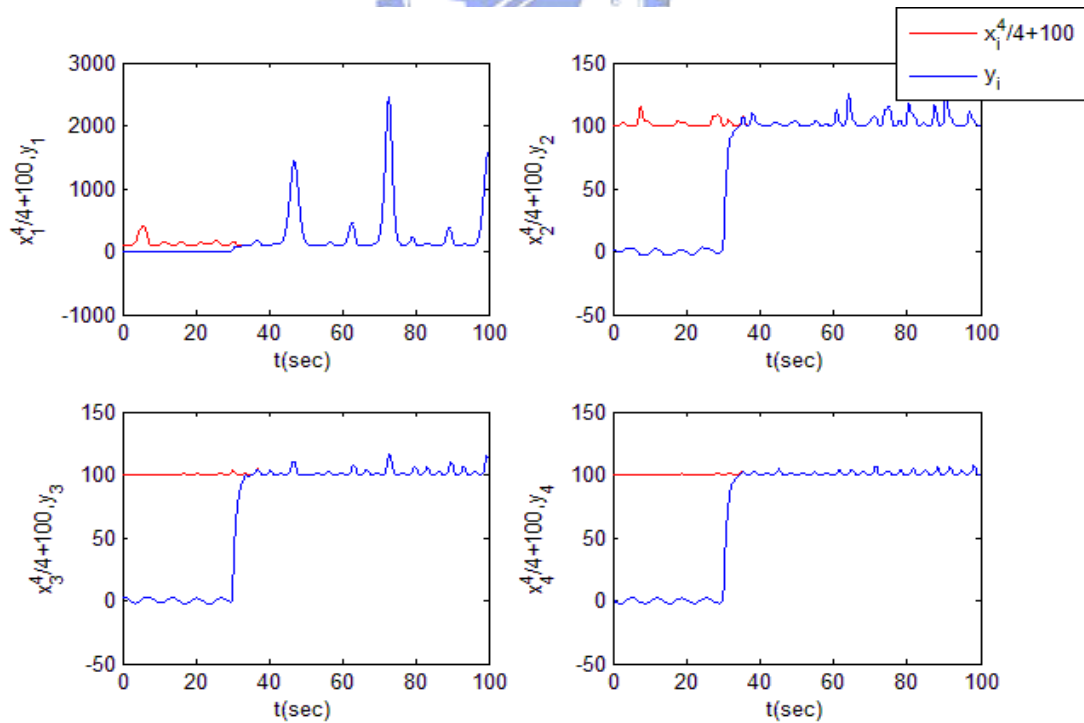


Fig. 2.13 Time histories of $\frac{1}{4}x_i^4 + 100$ and y_i for *Case III*.

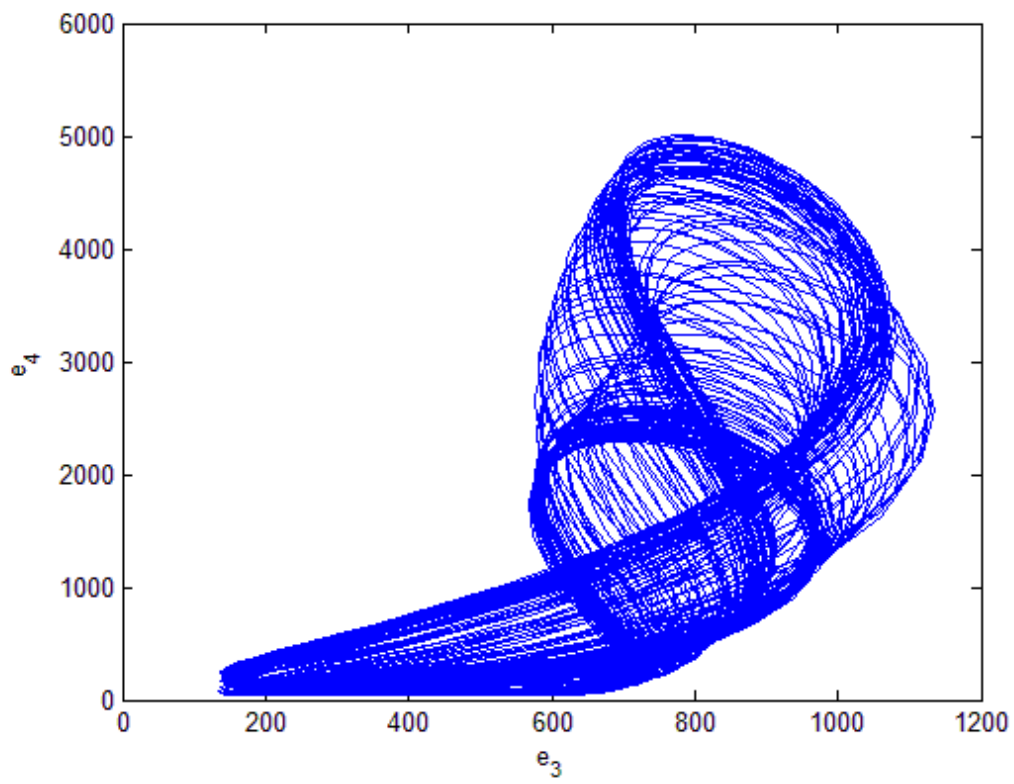
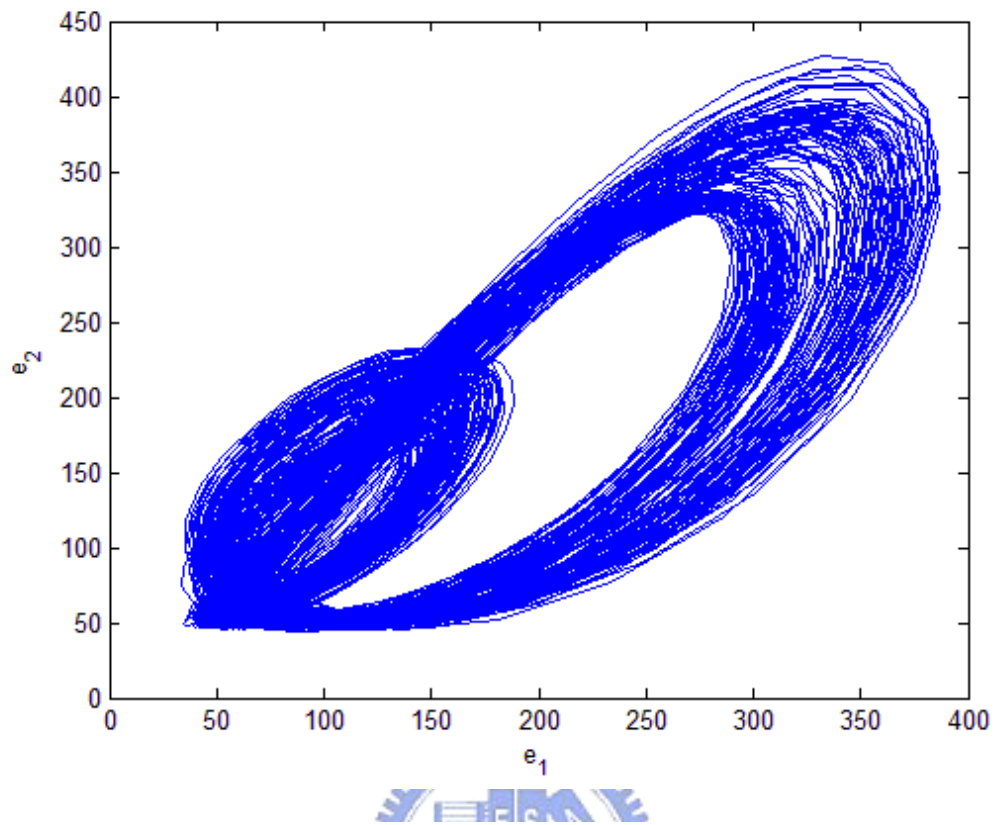


Fig. 2.14 Phase portraits of error dynamics for *Case IV*.

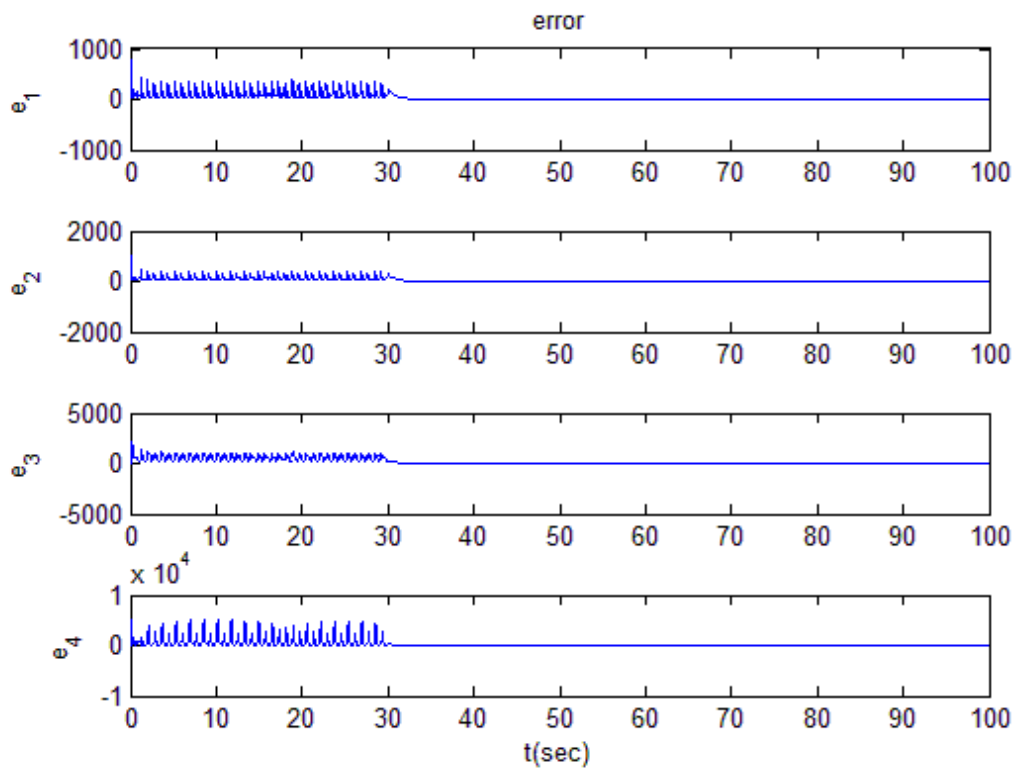


Fig. 2.15 Time histories of errors for *Case IV*.

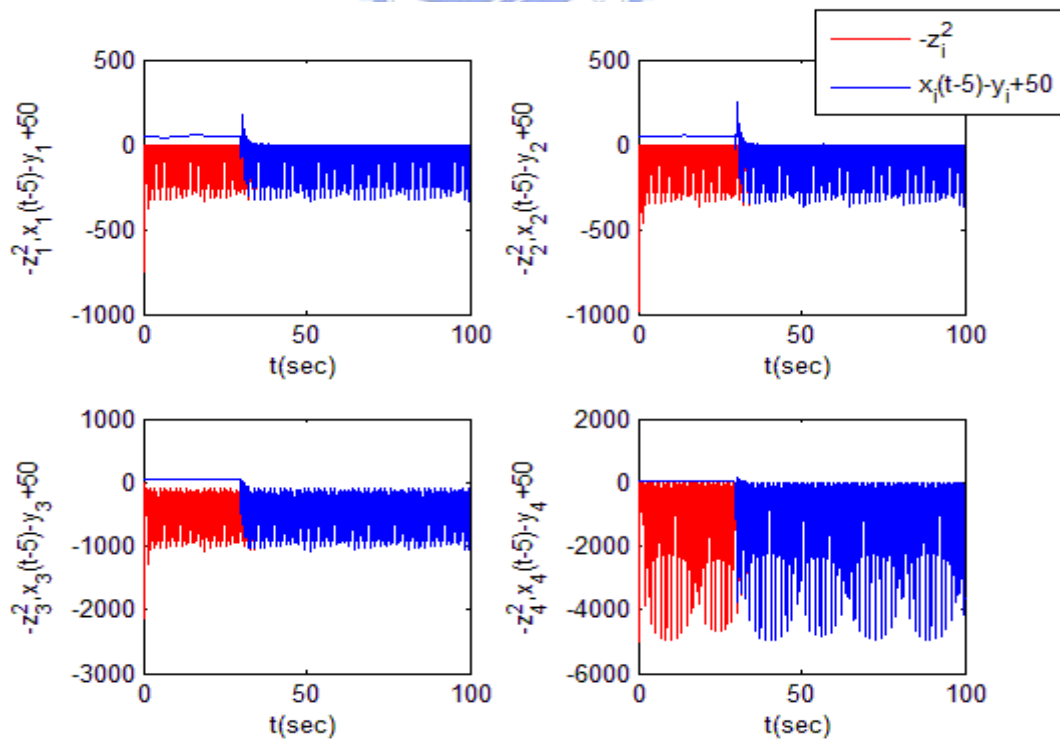


Fig. 2.16 Time histories of $x_i(t-5) - y_i + 50$ and $-z_i^2$ for *Case IV*.

Chapter 3

Chaos Control of a New Froude-van der Pol System by GYC

Partial Region Stability Theory

3.1 Preliminaries

In this Chapter, a new strategy by using GYC partial region stability theory [24-26] is proposed to achieve chaos control for a new Froude-van der Pol system. The new Lyapunov function used is a simple linear homogeneous function of error states and the lower degree controllers are simpler and introduce less simulation error. Three numerical simulations are given to show the effectiveness of the proposed strategy.

3.2 Chaos Control Scheme

Consider the following chaotic system

$$\dot{\mathbf{x}} = \mathbf{f}(t, \mathbf{x}) \quad (3.1)$$

where $\mathbf{x} = [x_1, x_2, \dots, x_n]^T \in R^n$ is a the state vector, $\mathbf{f} : R_+ \times R^n \rightarrow R^n$ is a vector function.

The goal system which can be either chaotic or regular, is

$$\dot{\mathbf{y}} = \mathbf{g}(t, \mathbf{y}) \quad (3.2)$$

where $\mathbf{y} = [y_1, y_2, \dots, y_n]^T \in R^n$ is a state vector, $\mathbf{g} : R_+ \times R^n \rightarrow R^n$ is a vector function.

In order to make the chaos state \mathbf{x} approaching the goal state \mathbf{y} , define $\mathbf{e} = \mathbf{x} - \mathbf{y}$ as the state error. The chaos control is accomplished in the sense that:

$$\lim_{t \rightarrow \infty} \mathbf{e} = \lim_{t \rightarrow \infty} (\mathbf{x} - \mathbf{y}) = 0 \quad (3.3)$$

In this Chapter, we will use examples in which the error dynamics always happens in the first quadrant of coordinate system and use GYC partial region stability theory

which is enclosed in Appendix A. The Lyapunov function is a simple linear homogeneous function of error states and the controllers are simpler because they are of lower degree than that of traditional controllers and introduce less simulation error.

3.3 Chaos of a new Froude-van der Pol system

Froude system and van der Pol system[43] are two typical nonlinear nonautonomous systems:

$$\begin{cases} \frac{d}{dt}x_1 = x_2 \\ \frac{d}{dt}x_2 = (a - bx_2^2)x_2 + c \sin x_1 + d \cos \omega t \end{cases} \quad (3.4)$$

$$\begin{cases} \frac{d}{dt}x_3 = x_4 \\ \frac{d}{dt}x_4 = -fx_3 + g(x_3^2 - 1)x_4 - h \sin \omega t \end{cases} \quad (3.5)$$

Changing $d \cos \omega t$ term in Eq.(3.4) by dx_3 and $h \sin \omega t$ term in Eq.(3.5) by

hx_1 , respectively, we obtain a new autonomous Froude-van der Pol system:

$$\begin{cases} \frac{d}{dt}x_1 = x_2 \\ \frac{d}{dt}x_2 = (a - bx_2^2)x_2 + c \sin x_1 + dx_3 \\ \frac{d}{dt}x_3 = x_4 \\ \frac{d}{dt}x_4 = -fx_3 + g(x_3^2 - 1)x_4 - hx_1 \end{cases} \quad (3.6)$$

where x_1, x_2, x_3, x_4 are state variables, and a, b, c, d, f, g, h are parameters, where $a = 0.35$, $b = 0.1$, $c = 1.0$, $d = -1$, $f = 1$, $g = -0.1$, $h = -0.1$, and the initial states of system are $x_1(0) = 0.2, x_2(0) = 0.35, x_3(0) = 0.2, x_4(0) = 0.35$. Its chaotic phase portrait, time histories of states, bifurcation diagram, and Lyapunov exponent are shown in Figs. 2.1-4.

3.4 Numerical Simulations

The following chaotic system is the new Froude-van der Pol system of which the old origin is translated to $(x_1, x_2, x_3, x_4) = (k, k, k, k)$, where k is a positive constant, and the chaotic motion always happens in the first quadrant of coordinate system (x_1, x_2, x_3, x_4) . Taking $k = 10$, this translated new Froude-Van der Pol system

$$\begin{cases} \frac{dx_1}{dt} = x_2 - 10 \\ \frac{dx_2}{dt} = (a - b(x_2 - 10)^2)(x_2 - 10) + c \sin(x_1 - 10) + d(x_3 - 10) \\ \frac{dx_3}{dt} = x_4 - 10 \\ \frac{dx_4}{dt} = -f(x_3 - 10) + g((x_3 - 10)^2 - 1)(x_4 - 10) - h(x_1 - 10) \end{cases} \quad (3.7)$$

is presented as simulated examples where the initial states of system are $x_1(0) = 0.2, x_2(0) = 0.35, x_3(0) = 0.2, x_4(0) = 0.35$ and the parameters of system are, $a = 0.35, b = 0.1, c = 1, d = -2, f = 4.9, g = -0.1, h = -1.76$. The chaotic motion is shown in Fig. 3.1.

In order to lead (x_1, x_2, x_3, x_4) to the goal, we add control terms u_1, u_2, u_3, u_4 to each equation of Eq. (3.7), respectively.

$$\begin{cases} \frac{dx_1}{dt} = x_2 - k + u_1 \\ \frac{dx_2}{dt} = (a - b(x_2 - k)^2)(x_2 - k) + c \sin(x_1 - k) + d(x_3 - k) + u_2 \\ \frac{dx_3}{dt} = x_4 - k + u_3 \\ \frac{dx_4}{dt} = -f(x_3 - k) + g((x_3 - k)^2 - 1)(x_4 - k) - h(x_1 - k) + u_4 \end{cases} \quad (3.8)$$

CASE I. Control the chaotic motion to zero.

In this case we will control the chaotic motion of the new Froude-van der Pol system (3.7) to zero. The goal is $y = 0$. The state error is $e_i = x_i - y_i = x_i$, ($i=1, 2, 3, 4$)

and error dynamics becomes

$$\begin{cases} \dot{e}_1 = \dot{x}_1 = x_2 - 10 + u_1 \\ \dot{e}_2 = \dot{x}_2 = (a - b(x_2 - 10)^2)(x_2 - 10) + c \sin(x_1 - 10) + d(x_3 - 10) + u_2 \\ \dot{e}_3 = \dot{x}_3 = x_4 - 10 + u_3 \\ \dot{e}_4 = \dot{x}_4 = -f(x_3 - 10) + g((x_3 - 10)^2 - 1)(x_4 - 10) - h(x_1 - 10) + u_4 \end{cases} \quad (3.9)$$

In Fig. 3.2, we see that the error dynamics always exists in first quadrant.

By GYC partial region stability, one can easily choose a Lyapunov function in the form of a positive definite function in first quadrant as:

$$V = e_1 + e_2 + e_3 + e_4 \quad (3.10)$$

Its time derivative through error dynamics (3.9) is

$$\begin{aligned} \dot{V} &= \dot{e}_1 + \dot{e}_2 + \dot{e}_3 + \dot{e}_4 \\ &= (x_2 - 10 + u_1) + [(a - b(x_2 - 10)^2)(x_2 - 10) + c \sin(x_1 - 10) \\ &\quad + d(x_3 - 10) + u_2] + (x_4 - 10 + u_3) \\ &\quad + [-f(x_3 - 10) + g((x_3 - 10)^2 - 1)(x_4 - 10) - h(x_1 - 10) + u_4] \end{aligned} \quad (3.11)$$

Choose

$$\begin{cases} u_1 = -x_2 + 10 - e_1 \\ u_2 = -(a - b(x_2 - 10)^2)(x_2 - 10) - c \sin(x_1 - 10) - d(x_3 - 10) - e_2 \\ u_3 = -x_4 + 10 - e_3 \\ u_4 = f(x_3 - 10) - g((x_3 - 10)^2 - 1)(x_4 - 10) + h(x_1 - 10) - e_4 \end{cases} \quad (3.12)$$

We obtain

$$\dot{V} = -e_1 - e_2 - e_3 - e_4 < 0 \quad (3.13)$$

which is negative definite function in first quadrant. The numerical results are shown in Fig. 3.3. After 30 sec, the motion trajectories approach the origin.

CASE II. Control the chaotic motion to a sine function.

In this case we will control the chaotic motion of the new Froude-van der Pol system (3.8) to sine function of time where $k = 20$. The goal is $y_i = m \sin \omega_i t$, ($i = 1, 2, 3, 4$). The error states are

$$e_i = x_i - y_i = x_i - m \sin \omega_i t \quad (3.14)$$

$$\lim_{t \rightarrow \infty} e_i = \lim_{t \rightarrow \infty} (x_i - m \sin \omega_i t) = 0, \quad i = 1, 2, 3, 4$$

and $\dot{e}_i = \dot{x}_i - m\omega_i \cos \omega_i t$ ($i = 1, 2, 3, 4$) and $m = 3$, $\omega_1 = 0.5$, $\omega_2 = 1$, $\omega_3 = 1.5$,

$\omega_4 = 0.8$. The error dynamics is

$$\begin{cases} \dot{e}_1 = \dot{x}_1 - m\omega_1 \cos \omega_1 t = (x_2 - 20 - m\omega_1 \cos \omega_1 t + u_1) - m\omega_1 \cos \omega_1 t \\ \dot{e}_2 = \dot{x}_2 - m\omega_2 \cos \omega_2 t = [(a - b(x_2 - 20)^2)(x_2 - 20) + c \sin(x_1 - 20) + d(x_3 - 20) \\ \quad - m\omega_2 \cos \omega_2 t + u_2] - m\omega_2 \cos \omega_2 t \\ \dot{e}_3 = \dot{x}_3 - m\omega_3 \cos \omega_3 t = (x_4 - 20 - m\omega_3 \cos \omega_3 t + u_3) - m\omega_3 \cos \omega_3 t \\ \dot{e}_4 = \dot{x}_4 - m\omega_4 \cos \omega_4 t = [-f(x_3 - 20) + g((x_3 - 20)^2 - 1)(x_4 - 20) - h(x_1 - 20) \\ \quad - m\omega_4 \cos \omega_4 t + u_4] - m\omega_4 \cos \omega_4 t \end{cases} \quad (3.15)$$

In Figs. 3.4-5, the error dynamics always exists in first quadrant.

By GYC partial region stability, one can easily choose a Lyapunov function in the form of a positive definite function in first quadrant as:

$$V = e_1 + e_2 + e_3 + e_4 \quad (3.16)$$

By Eq. (3.14), its time derivative is

$$\begin{aligned} \dot{V} &= \dot{e}_1 + \dot{e}_2 + \dot{e}_3 + \dot{e}_4 \\ &= (x_2 - 20 - m\omega_1 \cos \omega_1 t + u_1) + [(a - b(x_2 - 20)^2)(x_2 - 20) + c \sin(x_1 - 20) \\ &\quad + d(x_3 - 20) - m\omega_2 \cos \omega_2 t + u_2] + (x_4 - 20 - m\omega_3 \cos \omega_3 t + u_3) \\ &\quad + [-f(x_3 - 20) + g((x_3 - 20)^2 - 1)(x_4 - 20) - h(x_1 - 20) - m\omega_4 \cos \omega_4 t + u_4] \end{aligned} \quad (3.17)$$

Choose

$$\begin{cases} u_1 = -[(x_2 - 20) - m\omega_1 \cos \omega_1 t] - e_1 \\ u_2 = -[(a - b(x_2 - 20)^2)(x_2 - 20) + c \sin(x_1 - 20) \\ \quad + d(x_3 - 20)(x_4 - 20) - m\omega_2 \cos \omega_2 t] - e_2 \\ u_3 = -[(x_4 - 20) - m\omega_3 \cos \omega_3 t] - e_3 \\ u_4 = -[-f(x_3 - 20) + g((x_3 - 20)^2 - 1)(x_4 - k) \\ \quad - h(x_1 - 20) - m\omega_4 \cos \omega_4 t] - e_4 \end{cases} \quad (3.18)$$

We obtain

$$\dot{V} = -e_1 - e_2 - e_3 - e_4 < 0 \quad (3.19)$$

which is negative definite function in first quadrant. The numerical results are shown in Figs. 3.6-7. After 30 sec., the errors approach zero and the motion trajectories approach to sine function.

CASE III. Control the chaotic motion to the difference of chaotic motions of a delay chaotic system and that of hyperchaotic Lü system [44].

In this case we will control chaotic motion of the new Froude-Van der Pol system (3.8) to the difference of chaotic motions of a delay chaotic system and that of hyperchaotic Lü system. The goal systems are

delay chaotic system:

$$\begin{cases} \frac{dy_1(t-\tau)}{dt} = y_2(t-\tau) \\ \frac{dy_2(t-\tau)}{dt} = (a - by_2^2(t-\tau))y_2(t-\tau) + c \sin y_1(t-\tau) + dy_3(t-\tau) \\ \frac{dy_3(t-\tau)}{dt} = y_4(t-\tau) \\ \frac{dy_4(t-\tau)}{dt} = -fy_3(t-\tau) + g(y_3^2(t-\tau) - 1)y_4(t-\tau) - hy_1(t-\tau) \end{cases} \quad (3.20)$$

and hyperchaotic Lü system:

$$\begin{cases} \frac{d}{dt} z_1 = a_1(z_2 - z_1) + z_4 \\ \frac{d}{dt} z_2 = -z_1 z_3 + c_1 z_2 \\ \frac{d}{dt} z_3 = z_1 z_2 - b_1 z_3 \\ \frac{d}{dt} z_4 = z_1 z_3 + r_1 z_4 \end{cases} \quad (3.21)$$

The error function is $e_i = x_i + y_i(t-\tau) - z_i$, $y_i(t-\tau)$ is the delay state of a new Froude-van der Pol system, and z_i is the state of hyperchaotic Lü system. The goal system for controlling are delay chaotic system and hyperchaotic Lü system, where

initial states are (80.2, 80.35, 80.2, 80.35), (5, 8, -1, -3), respectively, delay time $\tau = 5$,

system parameters $a_1 = 36$, $b_1 = 3$, $c_1 = 20$, $r_1 = -0.35$. We have

$$\lim_{t \rightarrow \infty} e_i = \lim_{t \rightarrow \infty} (x_i + y_i(t - \tau) - z_i) = 0, \quad (i = 1, 2, 3, 4), \text{ where } k = 80 \text{ in Eq.(3.8).}$$

The error dynamics becomes

$$\begin{cases} \dot{e}_1 = \dot{x}_1 + \dot{y}_1(t - \tau) - \dot{z}_1 \\ = (x_2 - 80 + u_1) + y_2(t - \tau) - (a_1(z_2 - z_1) + z_4) \\ \dot{e}_2 = \dot{x}_2 + \dot{y}_2(t - \tau) - \dot{z}_2 \\ = [(a - b(x_2 - 80)^2)(x_2 - 80) + c \sin(x_1 - 80) + d(x_3 - 80) + u_2] \\ + [(a - by_2^2(t - \tau))y_2(t - \tau) + c \sin y_1(t - \tau) + dy_3(t - \tau)] - (-z_1z_3 + c_1z_2) \\ \dot{e}_3 = \dot{x}_3 + \dot{y}_3(t - \tau) - \dot{z}_3 \\ = (x_4 - 80 + u_3) + y_4(t - \tau) - (z_1z_2 - b_1z_3) \\ \dot{e}_4 = \dot{x}_4 + \dot{y}_4(t - \tau) - \dot{z}_4 \\ = [-f(x_3 - 80) + g((x_3 - 80)^2 - 1)(x_4 - 80) - h(x_1 - 80) + u_4] \\ + [-fy_3(t - \tau) + g(y_3^2(t - \tau) - 1)y_4(t - \tau) - hy_1(t - \tau)] - (z_1z_3 + r_1z_4) \end{cases} \quad (3.22)$$

By Figs. 3.8-9, we know the error dynamics always exists in first quadrant.

By GYC partial region stability, one can easily choose a Lyapunov function in the form of a positive definite function in first quadrant as:

$$V = e_1 + e_2 + e_3 + e_4 \quad (3.23)$$

Its time derivative is

$$\begin{aligned} \dot{V} &= \dot{e}_1 + \dot{e}_2 + \dot{e}_3 + \dot{e}_4 \\ &= [(x_2 - 80 + u_1) + y_2(t - \tau) - (a_1(z_2 - z_1) + z_4)] \\ &\quad + \{[(a - b(x_2 - 80)^2)(x_2 - 80) + c \sin(x_1 - 80) + d(x_3 - 80) + u_2] \\ &\quad + [(a - by_2^2(t - \tau))y_2(t - \tau) + c \sin y_1(t - \tau) + dy_3(t - \tau)] - (-z_1z_3 + c_1z_2)\} \\ &\quad + [(x_4 - 80 + u_3) + y_4(t - \tau) - (z_1z_2 - b_1z_3)] \\ &\quad + \{[-f(x_3 - 80) + g((x_3 - 80)^2 - 1)(x_4 - 80) - h(x_1 - 80) + u_4] \\ &\quad + [-fy_3(t - \tau) + g(y_3^2(t - \tau) - 1)y_4(t - \tau) - hy_1(t - \tau)] - (z_1z_3 + r_1z_4)\} \end{aligned} \quad (3.24)$$

Choose

$$\begin{cases} u_1 = (a_1(z_2 - z_1) + z_4) - y_2(t - \tau) - (x_2 - 80) - e_1 \\ u_2 = (-z_1 z_3 + c_1 z_2) - [(a - b y_2^2(t - \tau)) y_2(t - \tau) + c \sin y_1(t - \tau) + d y_3(t - \tau)] \\ \quad - [(a - b(x_2 - 80)^2)(x_2 - 80) + c \sin(x_1 - 80) + d(x_3 - 80)] - e_2 \\ u_3 = (z_1 z_2 - b_1 z_3) - y_4(t - \tau) - (x_4 - 80) - e_3 \\ u_4 = (z_1 z_3 + r_1 z_4) - [-f y_3(t - \tau) + g(y_3^2(t - \tau) - 1) y_4(t - \tau) - h y_1(t - \tau)] \\ \quad - [-f(x_3 - 80) + g((x_3 - 80)^2 - 1)(x_4 - 80) - h(x_1 - 80)] - e_4 \end{cases} \quad (3.25)$$

We obtain

$$\dot{V} = -e_1 - e_2 - e_3 - e_4 < 0 \quad (3.26)$$

which is negative definite function in first quadrant. The numerical results are shown in Figs. 3.10-11. After 30 sec., the errors approach zero and the chaotic trajectories of the new Froude-Van der Pol system approach to delay chaotic system and that of hyperchaotic Lü system.

3.5 Summary

In this Chapter, a new chaos control method by GYC partial region stability theory is proposed. By using the GYC partial region stability theory, the controllers are of lower order than that of controllers by using traditional Lyapunov asymptotical stability theorem. The new Lyapunov function used is a simple linear homogeneous function of states and the lower order controllers are simpler and introduce less simulation error. The new Froude-van der Pol system and hyperchaotic Lü system are used as simulation examples which confirm the effectiveness of the proposed scheme.

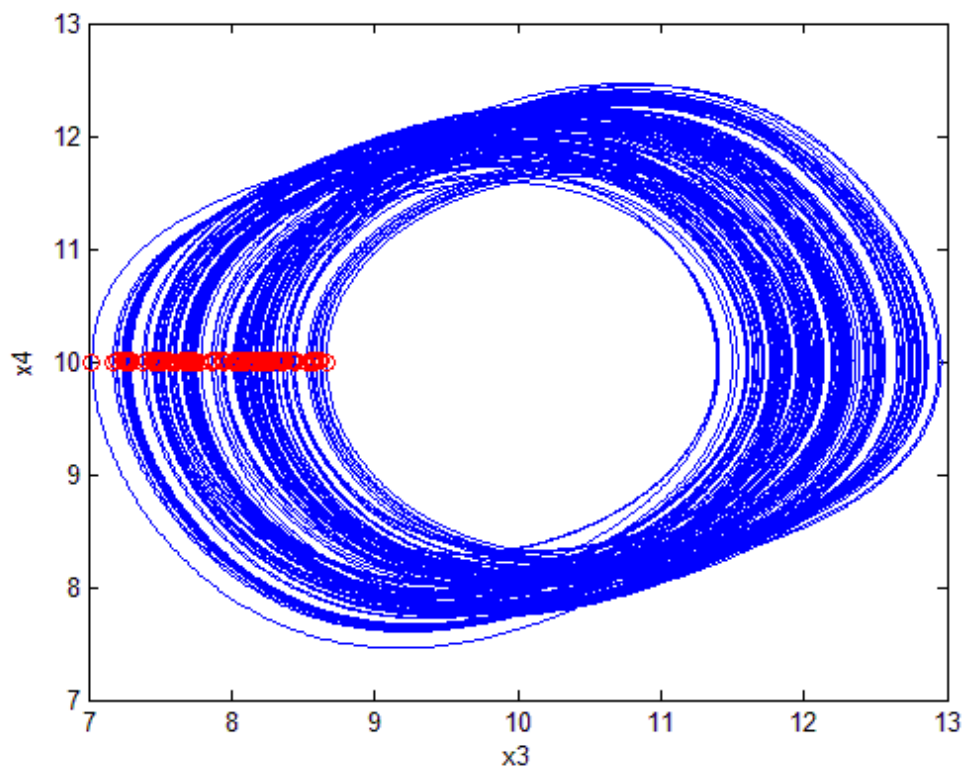
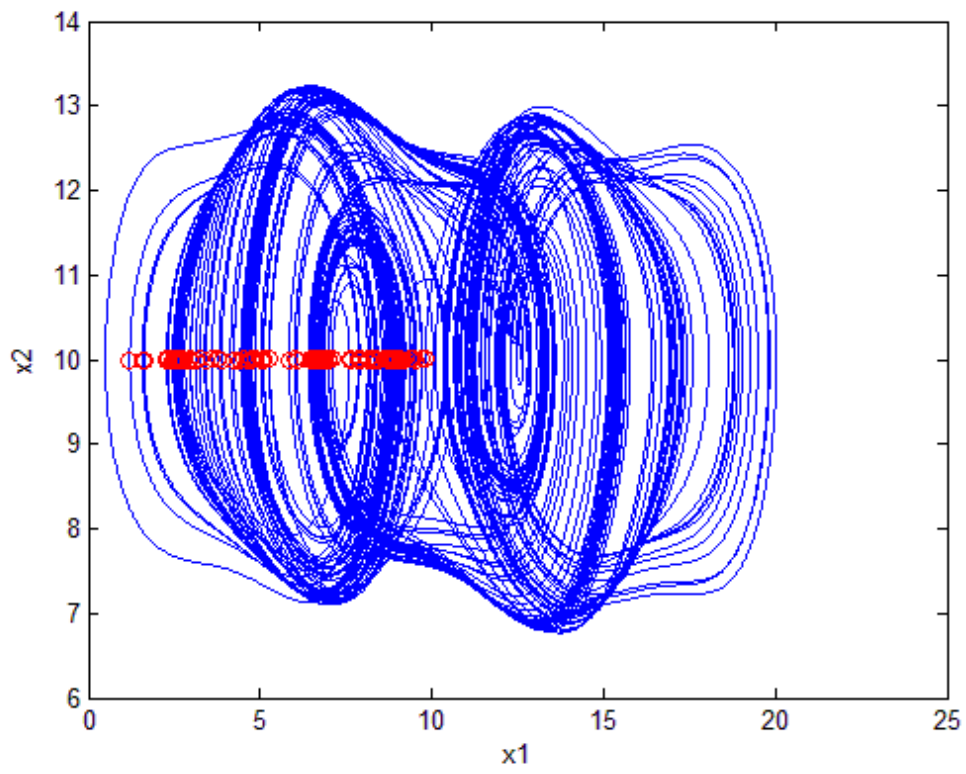


Fig. 3.1 Chaotic phase portraits for new Froude-van der Pol system in the first quadrant.

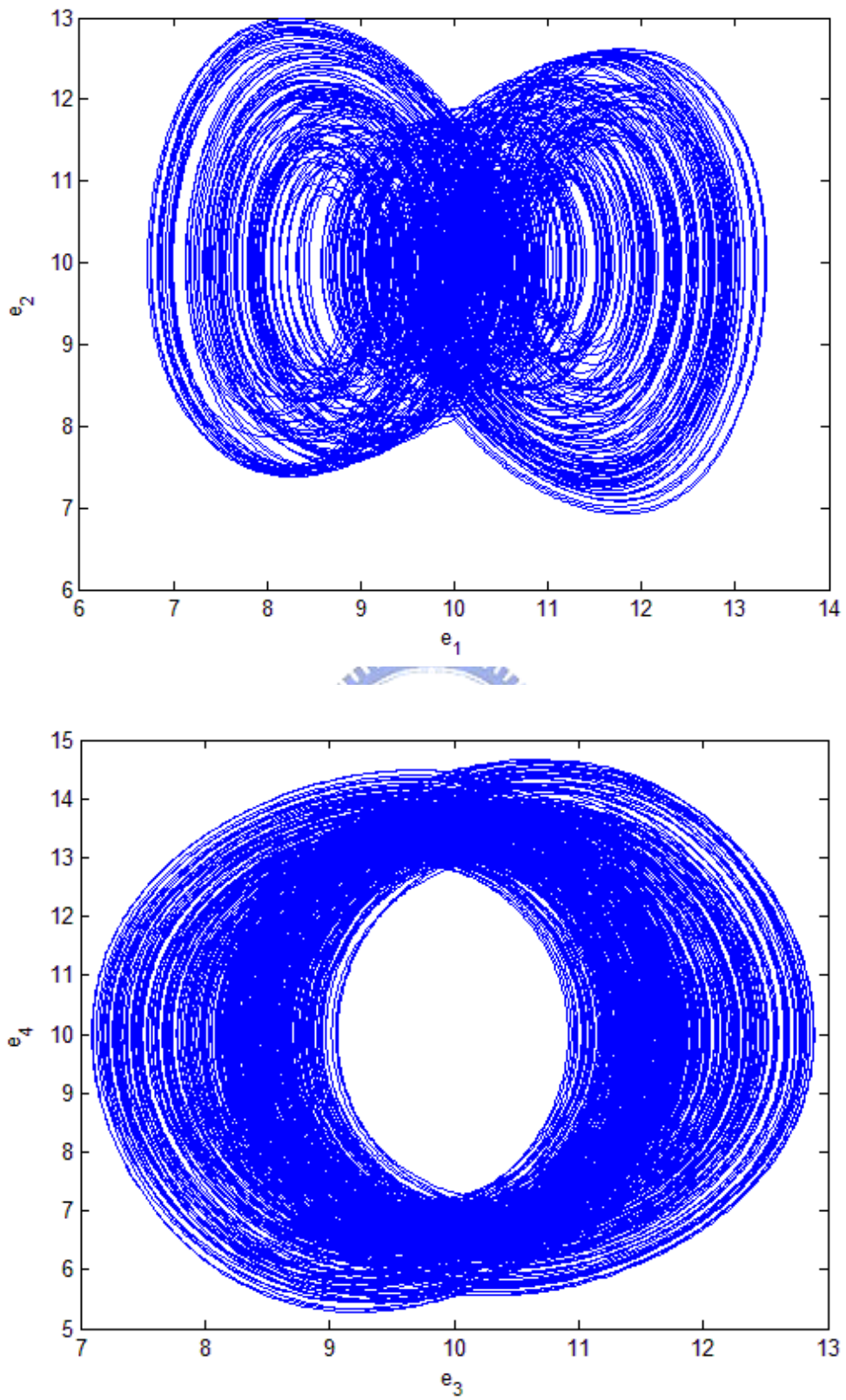


Fig. 3.2 Phase portraits of error dynamics for *Case I*.

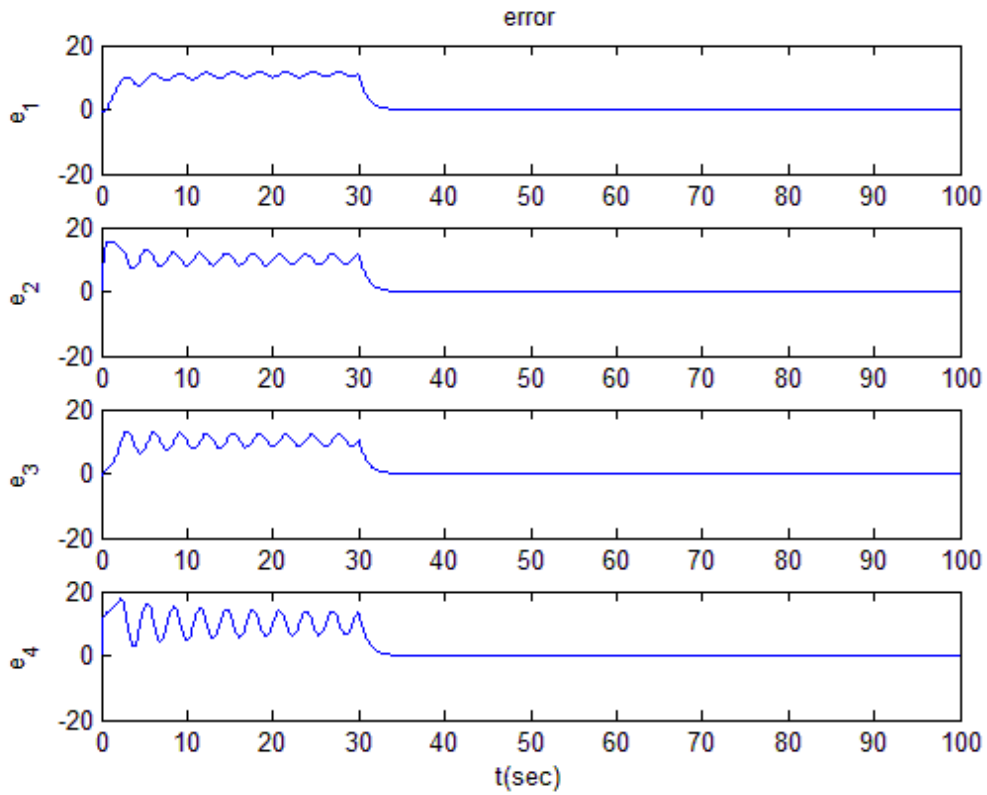


Fig. 3.3 Time histories of errors for *Case I*.

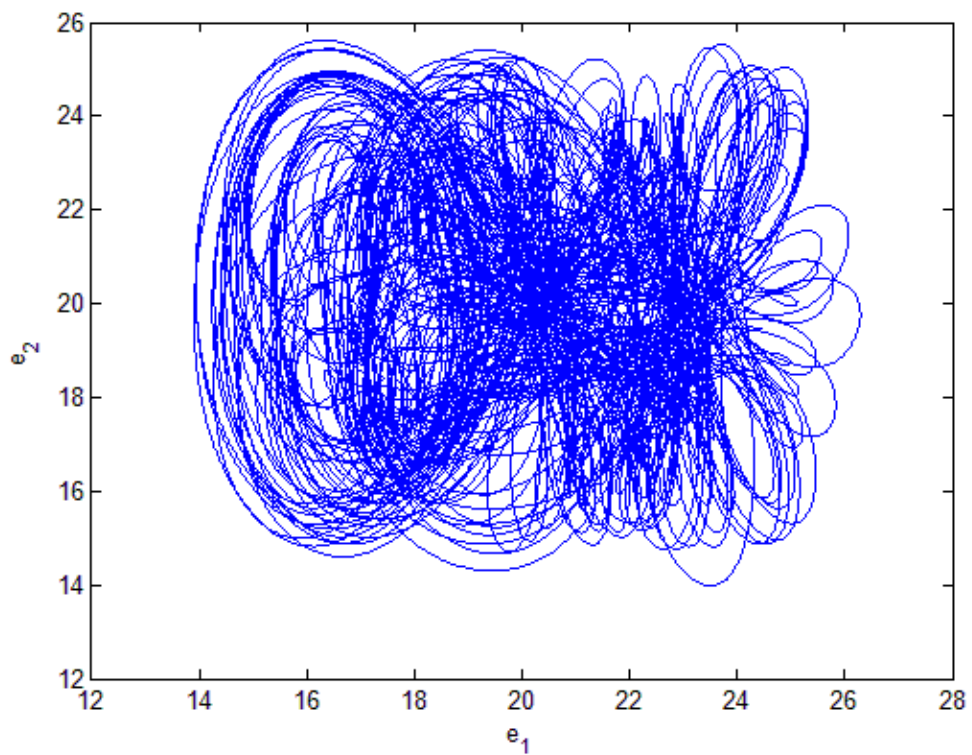


Fig. 3.4 Phase portrait of error dynamics (e_1 & e_2) for *Case II*.

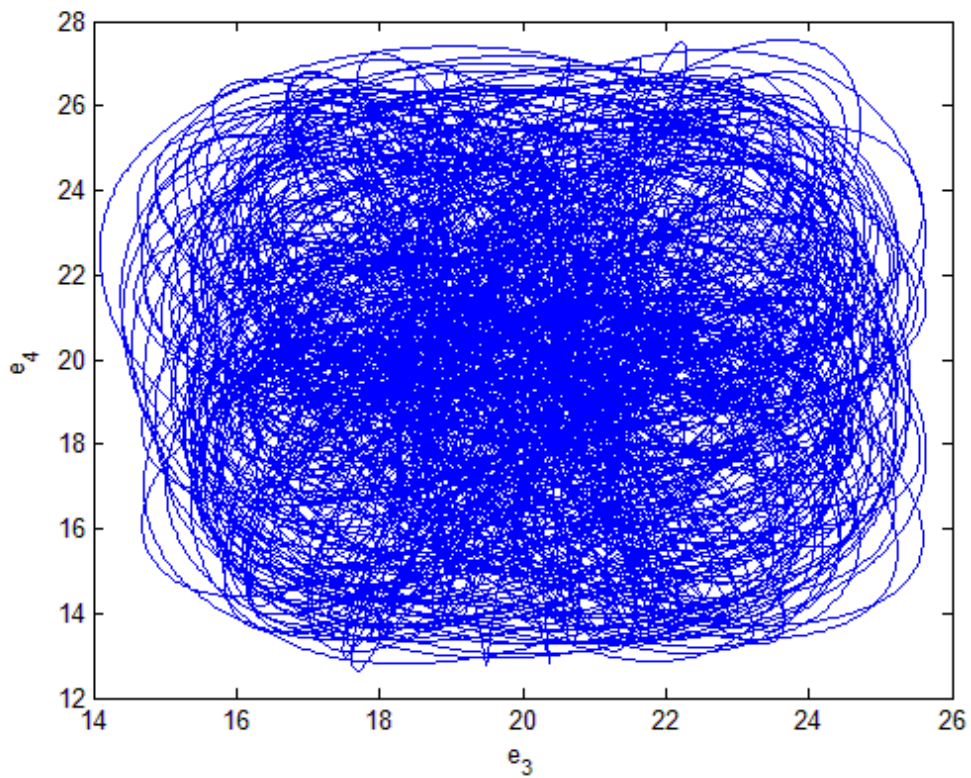


Fig. 3.5 Phase portrait of error dynamics (e_3 & e_4) for *Case II*.

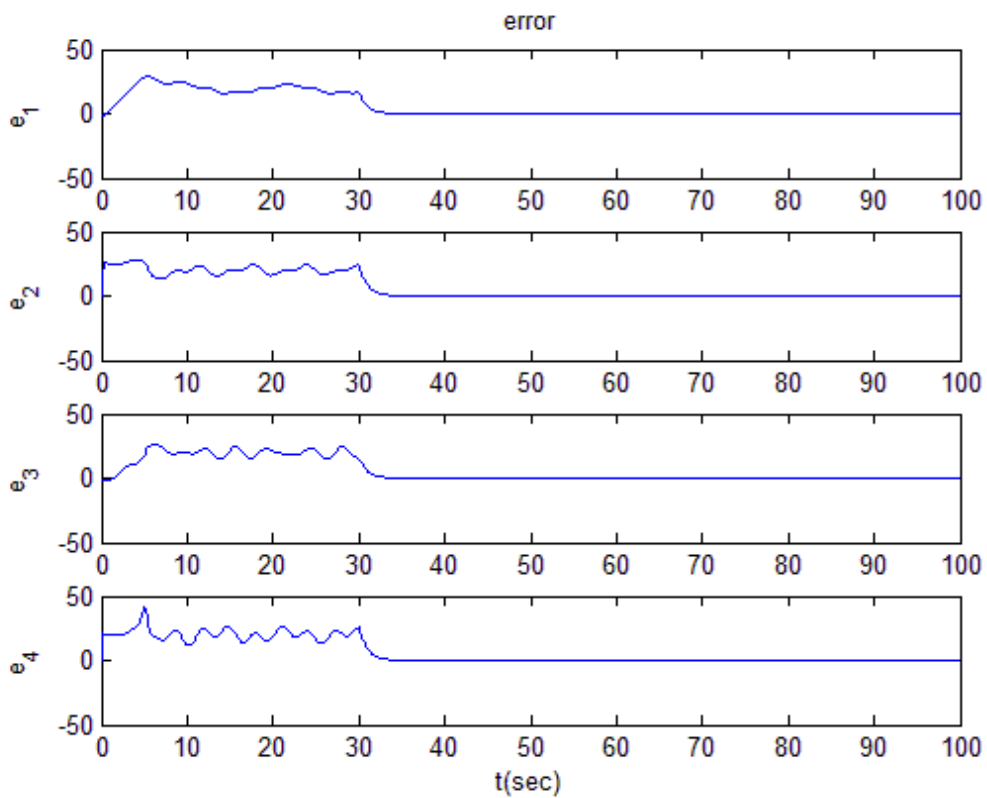


Fig. 3.6 Time histories of errors for *Case II*.

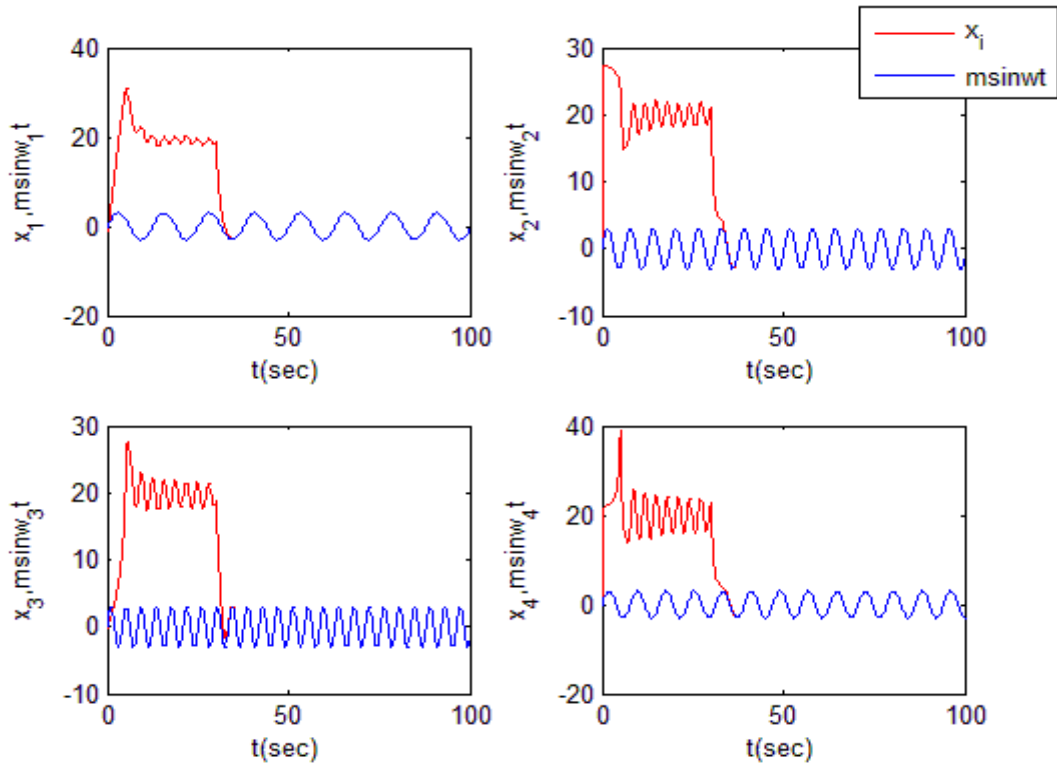


Fig. 3.7 Time histories of x_1, x_2, x_3, x_4 Case II.

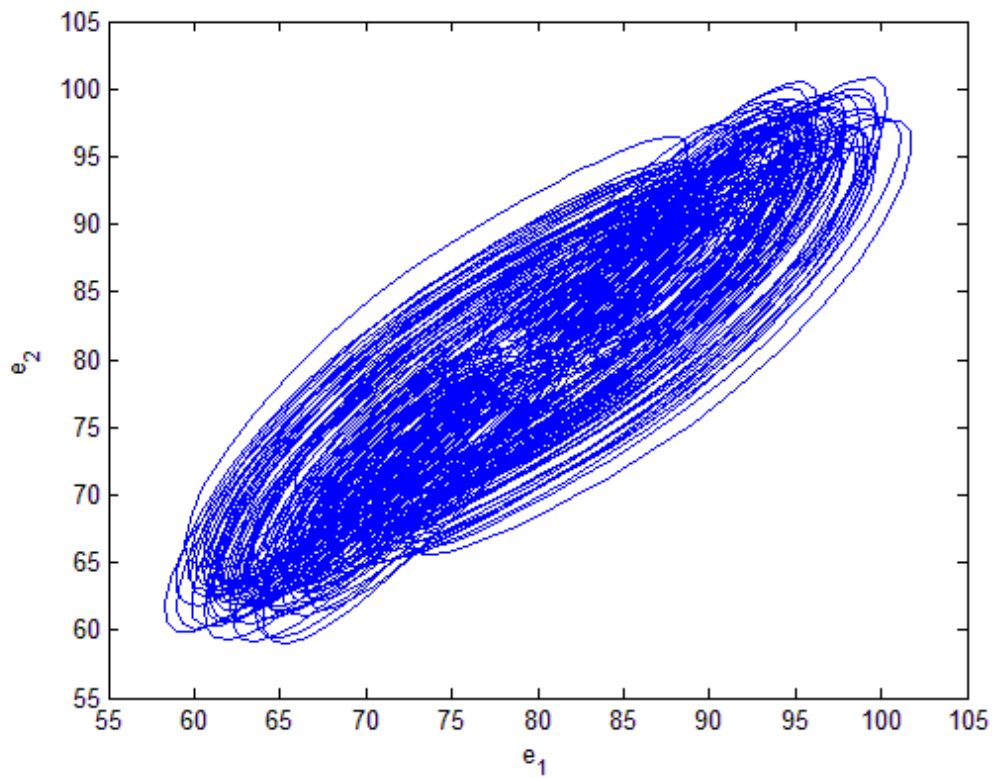


Fig. 3.8 Phase portrait of error dynamics (e_1 & e_2) for Case III.

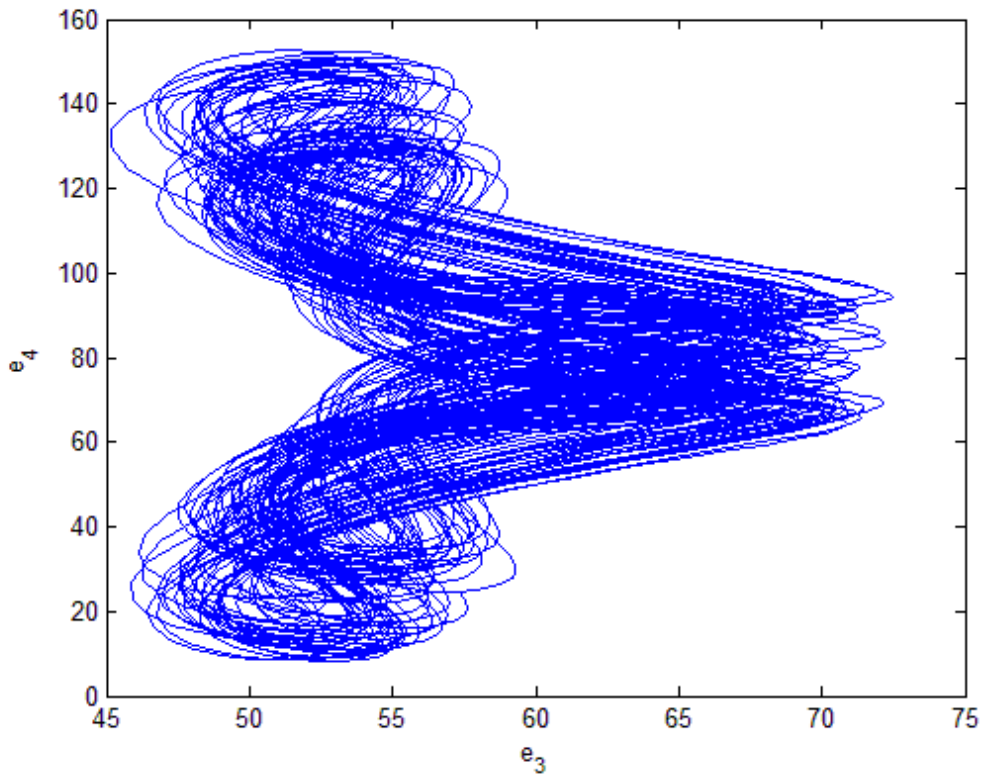


Fig. 3.9 Phase portrait of error dynamics (e_3 & e_4) for *Case III*.

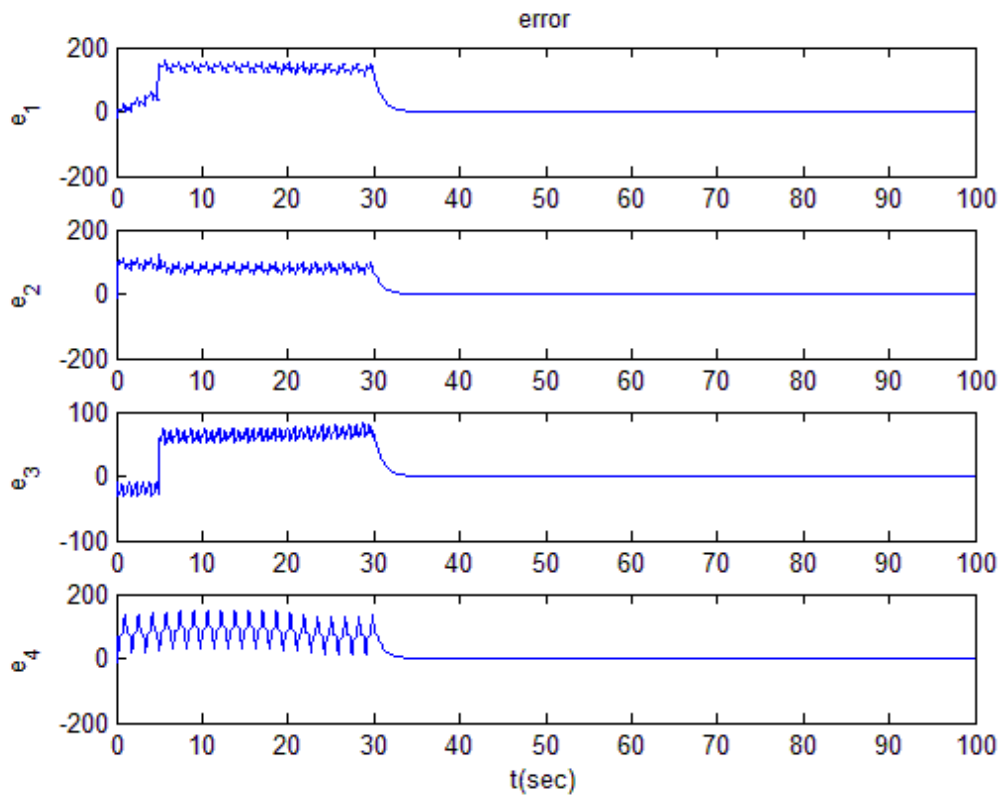


Fig. 3.10 Time histories of errors for *Case III*.

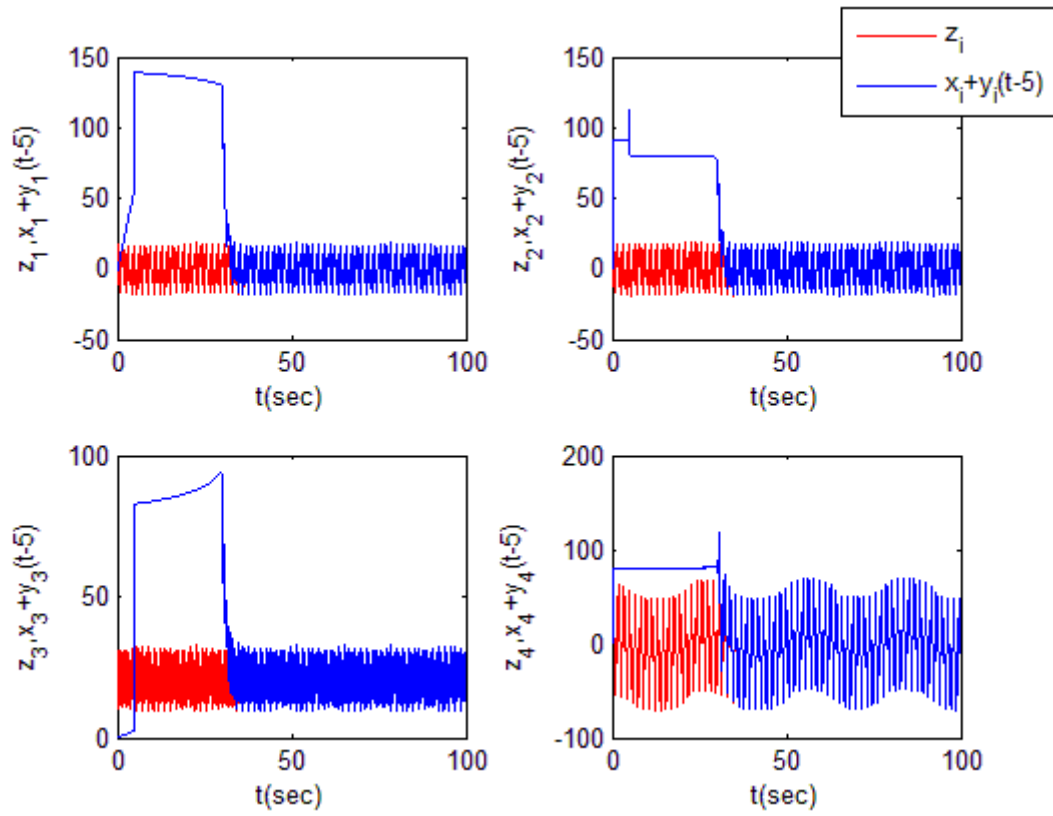


Fig. 3.11 Time histories of x_1, x_2, x_3 for *Case III*.



Chapter 4

Hyperchaos of a Lorenz System with Legendre Function

Parameters

4.1 Preliminaries

The chaotic behaviors of a Lorenz system with Legendre function parameters is firstly studied numerically by time histories of states, phase portraits, Poincaré maps, bifurcation diagram, Lyapunov exponents and parameter diagrams. Abundance of hyperchaos and of chaos is found, which offers the potential for many applications.

4.2 Classical Lorenz System and a Lorenz system with Legendre

Function Parameters

The classical Lorenz system [32] is described as follows:


$$\begin{cases} \frac{dx_1}{dt} = -a(x_1 - x_2) \\ \frac{dx_2}{dt} = -x_1x_3 + cx_1 - x_2 \\ \frac{dx_3}{dt} = x_1x_2 - bx_3 \end{cases} \quad (4.1)$$

where a, b, c are constant parameters. When the parameters of system are $a=10, b=8/3, c=27.43$, and the initial states of system are $x_1(0) = 6, x_2(0) = 5, x_3(0) = 10$, chaos exists in Fig. 4.1. We used Legendre functions as parameters of the system. The Legendre functions are defined by

$$P_n^m(x) = (-1)^m (1-x^2)^{m/2} \frac{d^m}{dx^m} P_n(x) \quad (4.2)$$

where $P_n(x)$ is the Legendre polynomial of degree n .

$$P_n(x) = \frac{1}{2^n n!} \left[\frac{d^n}{dx^n} (x^2 - 1)^n \right] \quad (4.3)$$

Choosing $n=2$, we obtain

$$\begin{cases} L_1(x) = P_2^0(x) = P_2(x) \\ L_2(x) = P_2^1(x) = (-1)(1-x^2)^{1/2} \frac{d}{dx} P_2(x) \\ P_2(x) = \frac{1}{2^2 \cdot 2!} \left[\frac{d^2}{dx^2} (x^2 - 1)^2 \right] \end{cases} \quad (4.4)$$

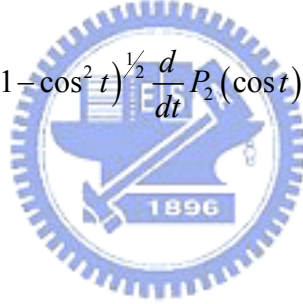
Changing the variable x to time t

$$x = \cos(t), \quad -1 \leq x \leq 1 \quad (4.5)$$

We have two periodic functions of time $L_1(t)$ and $L_2(t)$,

$$\begin{cases} L_1(t) = P_2(\cos t) \\ L_2(t) = P_2^1(\cos t) = (-1)(1-\cos^2 t)^{1/2} \frac{d}{dt} P_2(\cos t) \end{cases} \quad (4.6)$$

as shown in Fig. 4.2.



4.3 Numerical Simulations

In this Section, the parameters of system are given as $a = a_1 + \varepsilon(L_1 + L_2)$,

$b = b_1 + kL_2 + \omega$, $c = c_1 + 0.8L_1$, and $a, b, c, \varepsilon, k, \omega$ are constants:

$a_1 = 10, b_1 = 8/3, c_1 = 27.43, \varepsilon = 1.2, k = 0.24, \omega = 0.8$. The parameters a_1 and b_1 are fixed at 10 and $8/3$, respectively, throughout this Section. Bifurcation diagrams and Lyapunov exponents will be calculated to certify the the existence of hyperchaos.

Let us assume Lyapunov exponents $\lambda_i (i=1,2,3,4)$ satisfying $\lambda_1 > \lambda_2 > \lambda_3$, and $\lambda_4 = 0$. Then the dynamics of the system can be characterized as follows:

- (1) When $\lambda_{1,2,3} < 0$ and $\lambda_4 = 0$, system is periodic.
- (2) When $\lambda_1 > 0, \lambda_{2,3} < 0$ and $\lambda_4 = 0$, system is chaotic.

(3) When $\lambda_{1,2} > 0$, $\lambda_3 < 0$ and $\lambda_4 = 0$, system is hyperchaotic.

We consider three cases described as follows:

(1) Let $\varepsilon = 1.2, \omega = 0.8$ and c_1 and k are varied. Firstly, $c_1 = 27.43$, $k = 2.25$ are fixed, the chaotic phase portrait with Poincaré map of x_1, x_2 states, and chaotic time histories of three states are shown in Figs. 4.3-4, respectively. The chaotic bifurcation diagram by changing constant parameter k and enlarged diagram are shown in Figs. 4.5-6 with $c_1 = 27.43$. Its corresponding Lyapunov exponents are shown in Fig. 4.7.

When $0.001 \leq k \leq 0.636$ two positive Lyapunov exponents are obtained, i.e. hyperchaos is obtained. It can be seen that when $0.685 \leq k \leq 1.909$, $2.1 \leq k \leq 2.604$, $2.658 \leq k \leq 3$, the system is chaotic, and when $1.915 \leq k \leq 1.921$, 1.975 , $1.999 \leq k \leq 2.017$, $2.082 \leq k \leq 2.094$, $2.61 \leq k \leq 2.634$, the system is periodic. In order to investigate the dynamics of the system in detail, the parameter diagrams of c_1 against k are plotted in Figs. 4.8-10. Just like Monet's picture, they give beautiful scenes. White area is the bank of a river, blue area is the water of the river and green area is the duckweed in the river. When $0.001 \leq k \leq 0.636$, both λ_1 and λ_2 are positive, hence, the system is hyperchaotic within this region. Some typical values of parameter k generate hyperchaos, and the range of k for different system behaviors, are listed in Tables 1a and 1b, respectively.

Table 1a Typical values of parameter k generate hyperchaos for $c_1 = 27.43$, $\varepsilon = 1.2$ and $\omega = 0.8$

k	λ_1	λ_2	λ_3	λ_4
0.246	0.779	0.001	-14.08	0
0.294	0.764	0.003	-14.06	0
0.312	0.753	0.007	-14.06	0
0.324	0.756	0.009	-14.06	0
0.456	0.684	0.012	-13.99	0
0.624	0.604	0.013	-13.91	0

Table 1b The ranges of k for different system dynamics for $c_1 = 27.43$, $\varepsilon = 1.2$ and $\omega = 0.8$

System dynamics	Ranges of k
Periodic	$1.915 \leq k \leq 1.921$, 1.975 , $1.999 \leq k \leq 2.017$, $2.082 \leq k \leq 2.094$, $2.61 \leq k \leq 2.634$
Chaotic	$0.685 \leq k \leq 1.909$, $2.1 \leq k \leq 2.604$, $2.658 \leq k \leq 3$
Hyperchaotic	$0.001 \leq k \leq 0.636$

A typical periodic phase portrait and time histories for system at $k = 2.1$ are shown in Figs. 4.11-14. The system was observed that hyperchaos can be generated when $0.001 \leq k \leq 0.636$, and the generation of a hyperchaotic attractor for $k = 0.35$ in Figs. 4.15-16 when $c_1 = 27.43$, $\varepsilon = 1.2$ and $\omega = 0.8$.

(2) Fix $c_1 = 27.43$, $k = 0.24$, $\omega = 0.8$ and let ε is varied. System demonstrates hyperchaotic behavior when $0.001 \leq \varepsilon \leq 5.079$. Fig. 4.17 shows the calculated Lyapunov exponent as a function of ε to classify the chaotic or periodic motions. With changing ε , system becomes periodic when $5.819 \leq \varepsilon \leq 9.439$, and chaotic motions occur with $5.099 \leq \varepsilon \leq 5.799$, $9.459 < \varepsilon \leq 9.979$. Some typical values of ε that generate hyperchaos, and the ranges of ε for different system dynamics, are listed in Tables 2a and 2b.

Table 2a Typical values of parameter ε generate hyperchaos for $c_1 = 27.43$, $k = 0.24$ and $\omega = 0.8$

ε	λ_1	λ_2	λ_3	λ_4
3.22	0.755	0.002	-14.56	0
3.32	0.746	0.005	-14.58	0
3.38	0.742	0.008	-14.59	0
3.60	0.743	0.010	-14.65	0
4.15	0.698	0.013	-14.75	0
4.67	0.639	0.016	-14.82	0

Table 2b The ranges of ε for different system dynamics for $c_1 = 27.43$, $k = 0.24$ and $\omega = 0.8$

System dynamics	Ranges of ε
Periodic	$5.819 \leq \varepsilon \leq 9.439$
Chaotic	$5.099 \leq \varepsilon \leq 5.799$, $9.459 < \varepsilon \leq 9.979$
Hyperchaotic	$0.001 \leq \varepsilon \leq 5.079$

(3) Fix $c_1 = 27.43$, $\varepsilon = 1.2$ and $k = 0.24$ and let ω is varied. The hyperchaos is identified by the existence of two positive Lyapunov exponents, as clearly shown in Fig. 4.18 and enlarged figure for observing in Fig. 4.19, and it shows the Lyapunov exponents as a function of varying ω . This case is based on studying Fig. 4.13a, in which hyperchaotic motion can be hardly observed when $0.001 \leq \omega \leq 0.56$, $0.6 \leq \omega \leq 0.82$, or $0.86 \leq \omega \leq 0.98$, because its values are not extremely obvious. In addition, periodic motion is clearly presented after $\omega \geq 1.46$. Some typical values of ω that generate hyperchaos, and the ranges of ω for different system dynamics, are listed in Tables 3a and 3b, respectively.

Table 3a Typical values of parameter ω generate hyperchaos for $c_1 = 27.43$, $\varepsilon = 1.2$ and $k = 0.24$

ω	λ_1	λ_2	λ_3	λ_4
0.12	0.778	0.001	-14.20	0
0.20	0.792	0.002	-14.29	0
0.54	0.845	0.003	-14.68	0
0.76	0.849	0.004	-14.91	0
0.92	0.877	0.005	-15.10	0

Table 3b The ranges of ω for different system dynamics for $c_1 = 27.43$, $\varepsilon = 1.2$ and $k = 0.24$

System dynamics	Ranges of ω
Periodic	$1.46 \leq \omega \leq 9.979$
Chaotic	$0.58, 0.84, 1.26 \leq \omega \leq 1.3$
Hyperchaotic	$0.001 \leq \omega \leq 0.56, 0.6 \leq \omega \leq 0.82, 0.86 \leq \omega \leq 0.98$

4.4 Summary

Lorenz system with Legendre function parameters is studied firstly. The results are verified by time histories of states, phase portraits, Poincaré maps, bifurcation diagram, Lyapunov exponents and parameter diagrams. Abundant hyperchaos is found for this system, which gives potential in various applications, particularly in secret communication.

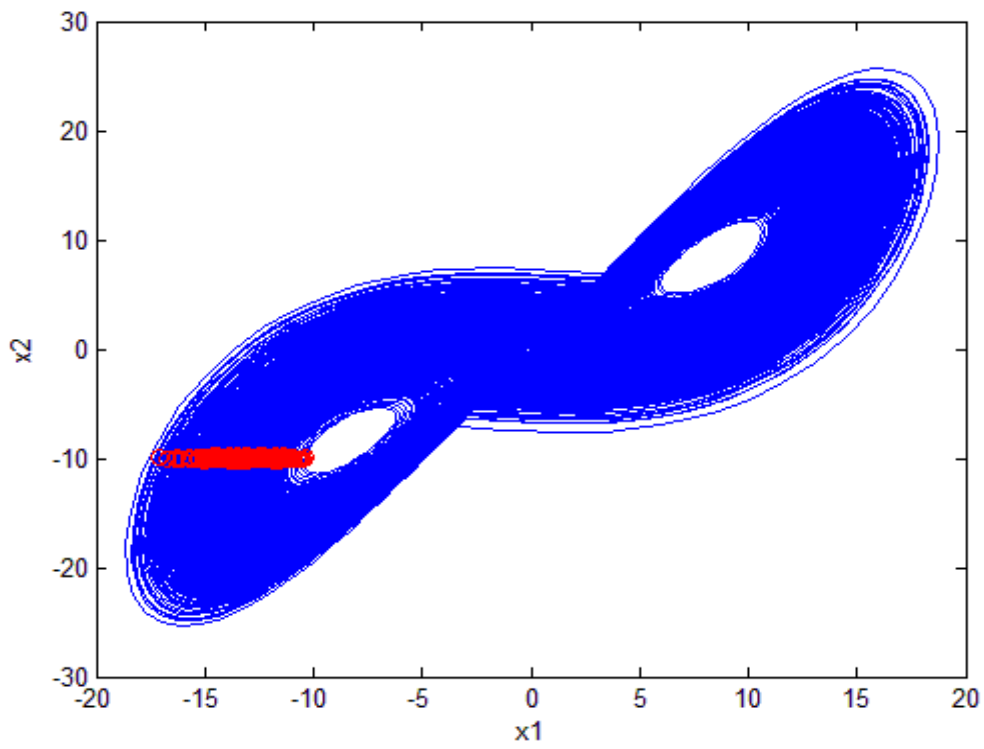


Fig. 4.1 Phase portrait, Poincaré maps of x_1, x_2 states for classical Lorenz system.

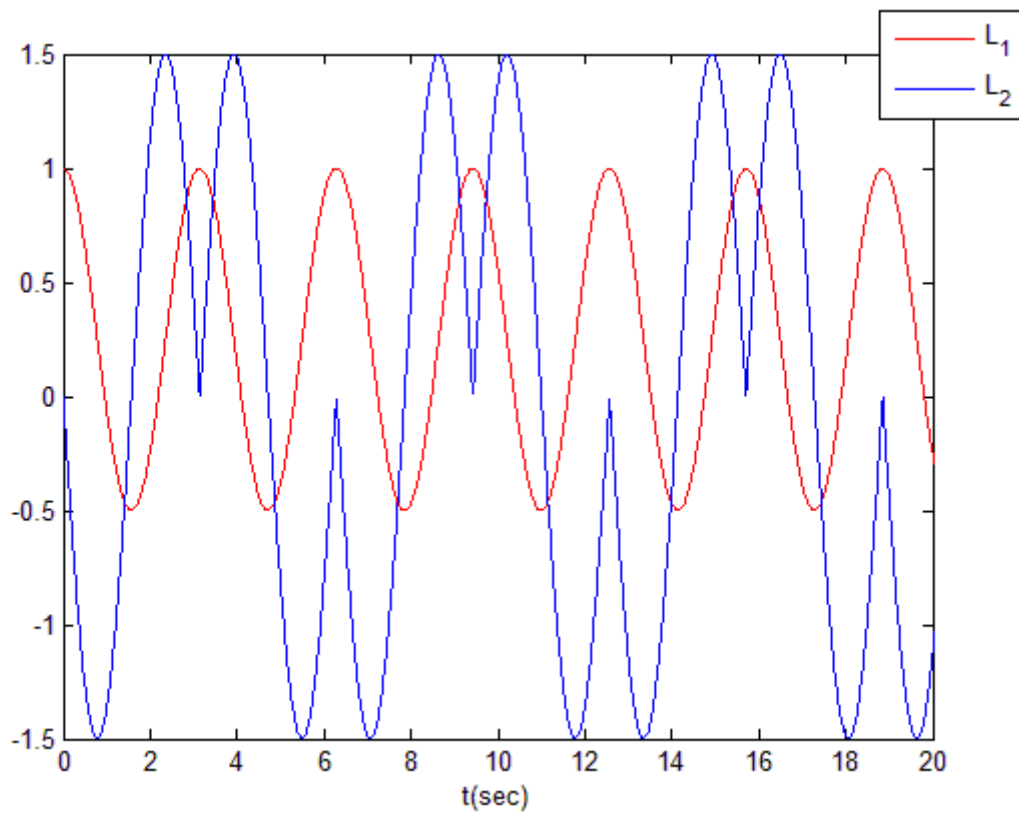


Fig. 4.2 Time histories of L_1 and L_2 .

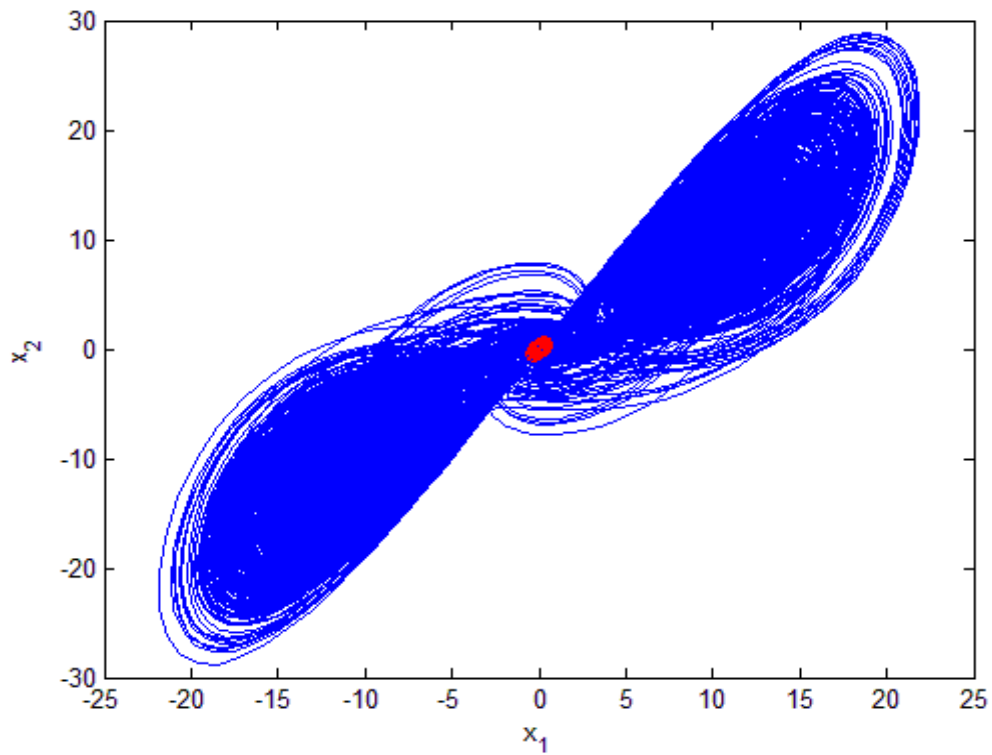


Fig. 4.3 Phase portrait and Poincaré maps for Lorenz system with Legendre function parameters when $c_1 = 27.43$, $k=2.25$.

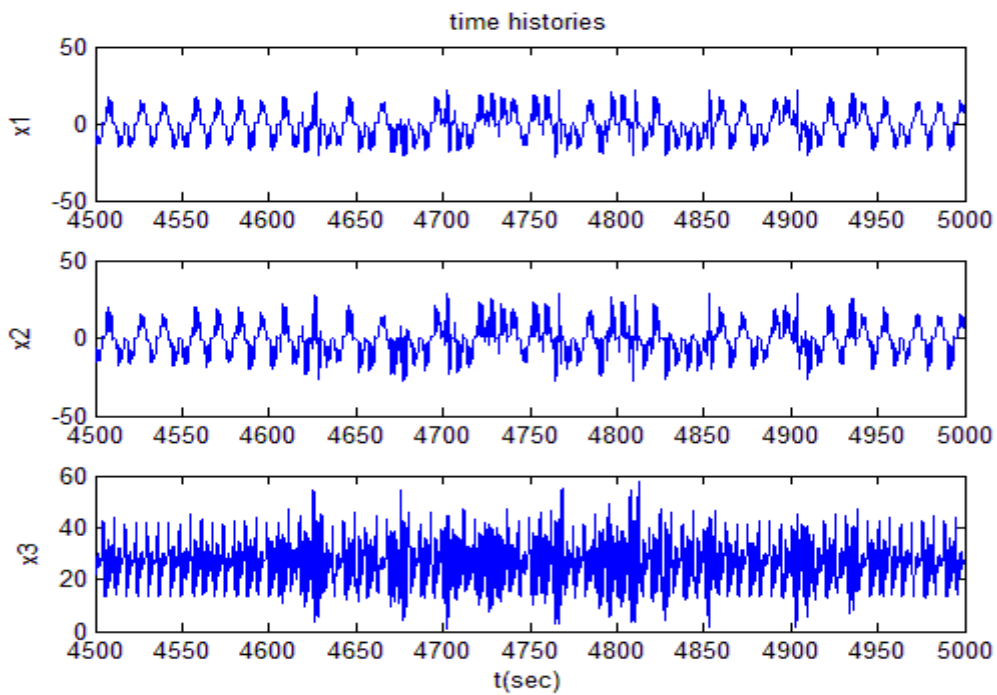


Fig. 4.4 Time histories of three states for Lorenz system with Legendre function parameters when $c_1 = 27.43$, $k=2.25$.

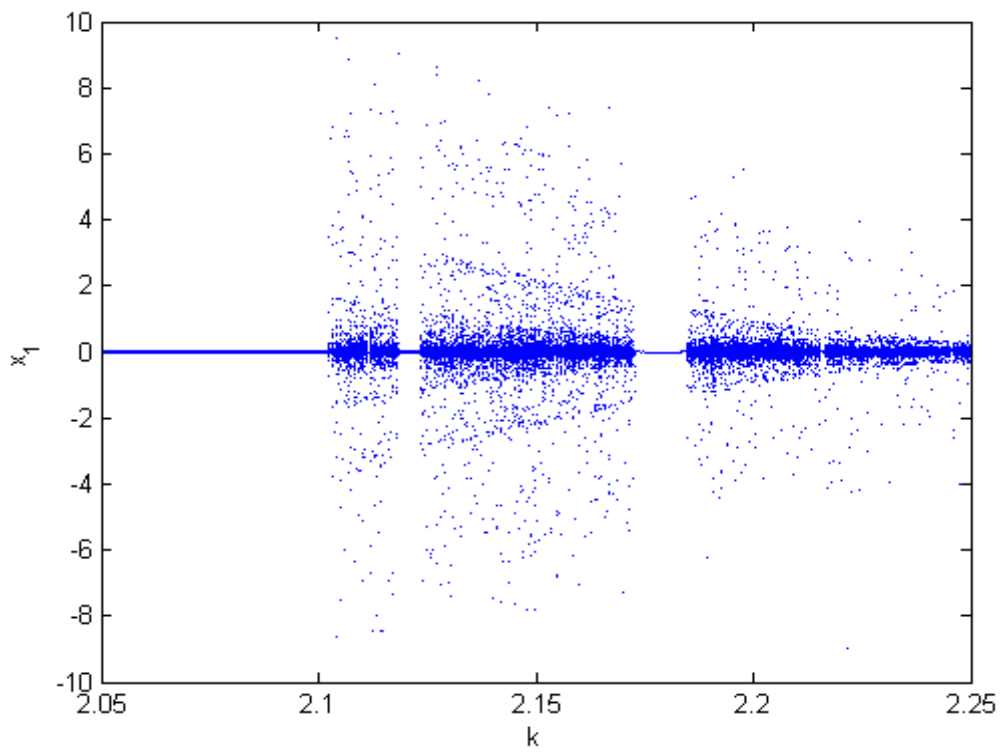


Fig. 4.5 The bifurcation diagram for Lorenz system with Legendre function parameters,

where $c_1 = 27.43$.

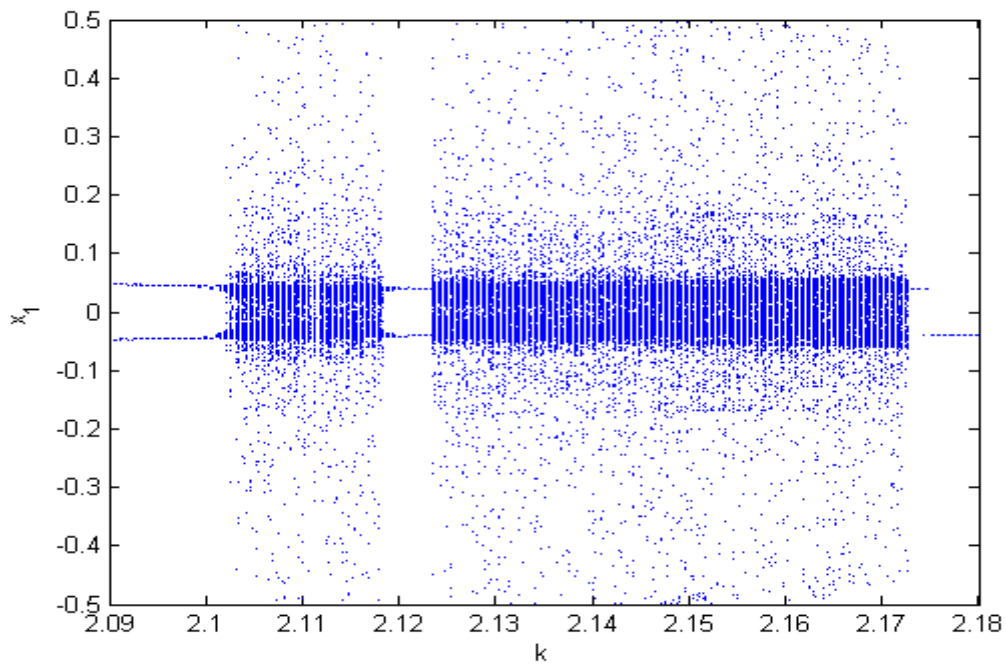


Fig. 4.6 The enlarged bifurcation diagram for Lorenz system with Legendre function

parameters, where $c_1 = 27.43$.

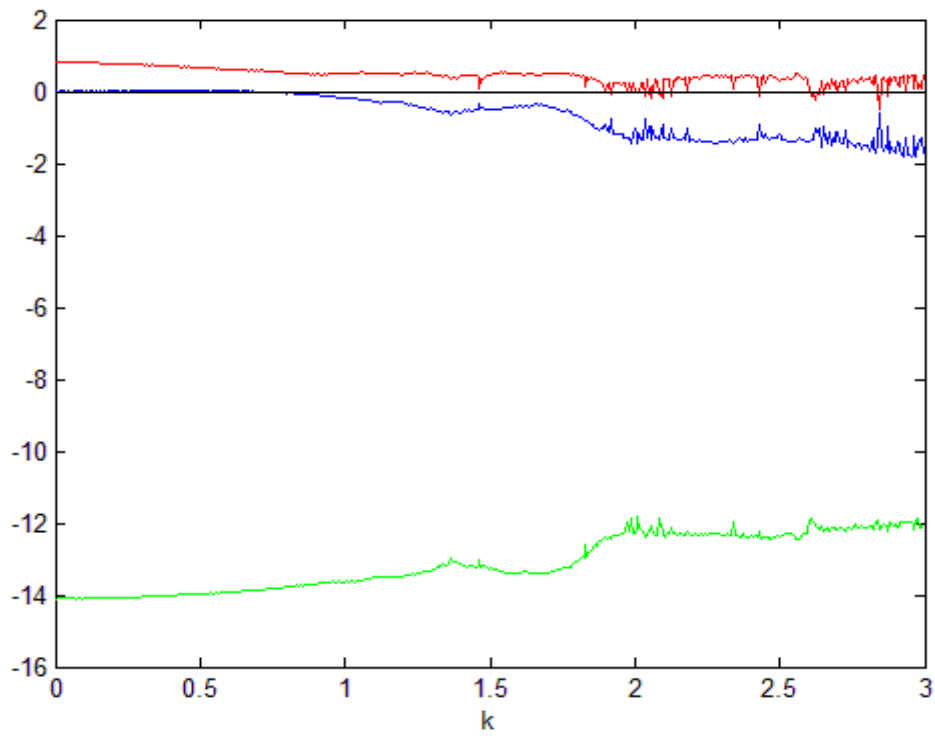


Fig. 4.7 The Lyapunov exponent for Lorenz system with Legendre function parameters.

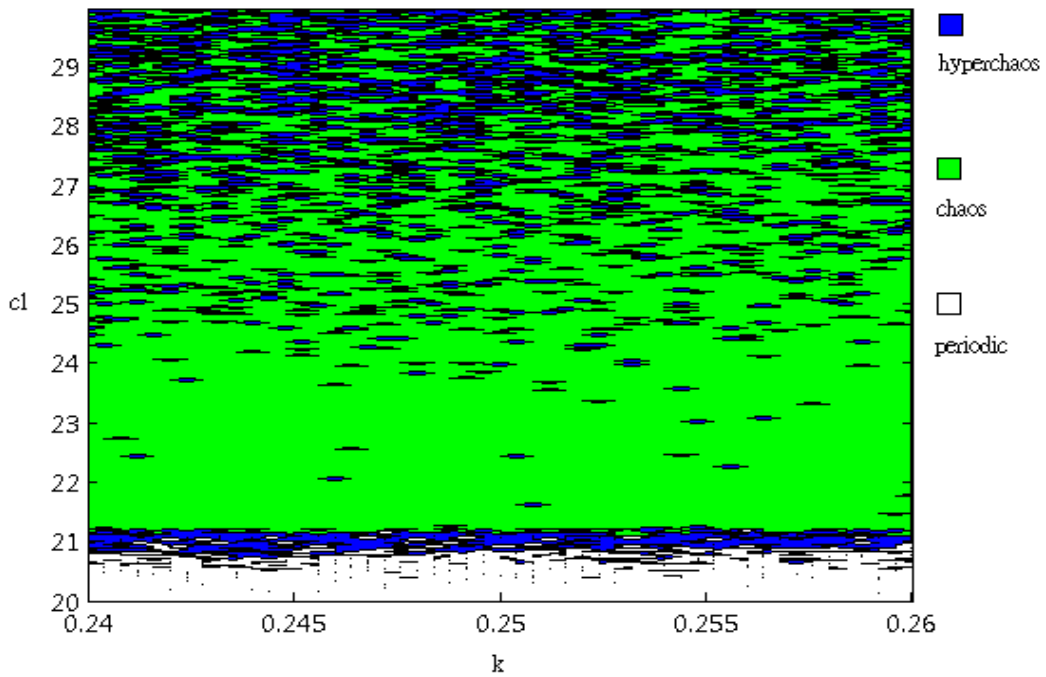


Fig. 4.8 The parameter diagram for Lorenz system with Legendre function parameters.

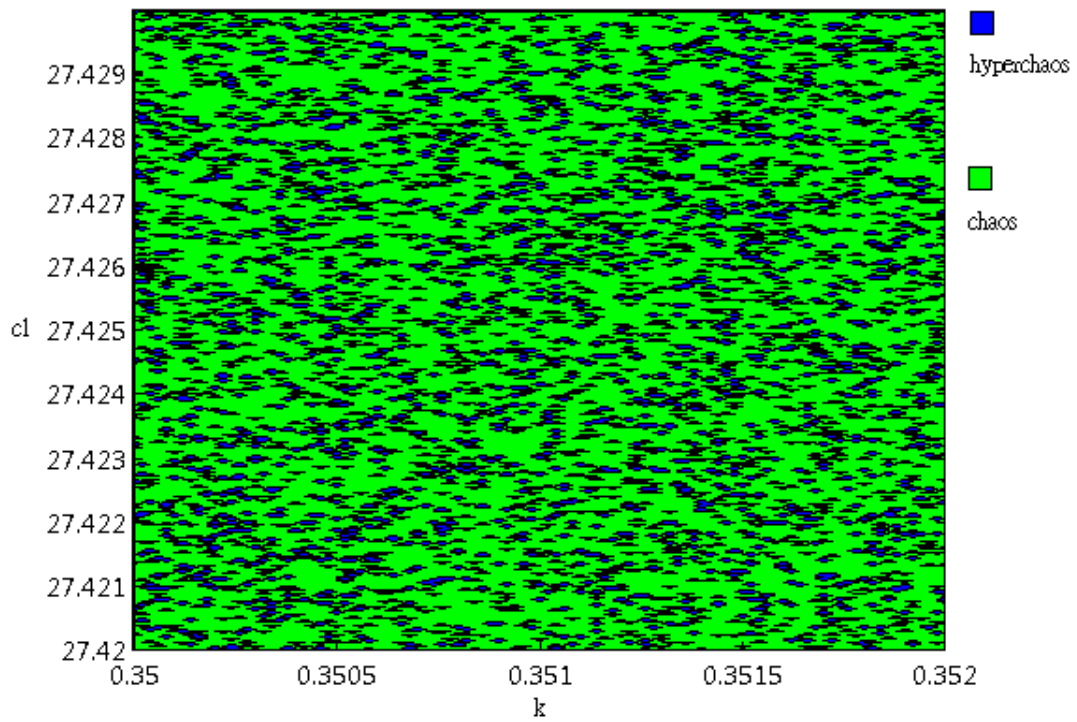


Fig. 4.9 The parameter diagram for modified Lorenz system between $k=0.35\sim 0.352$.

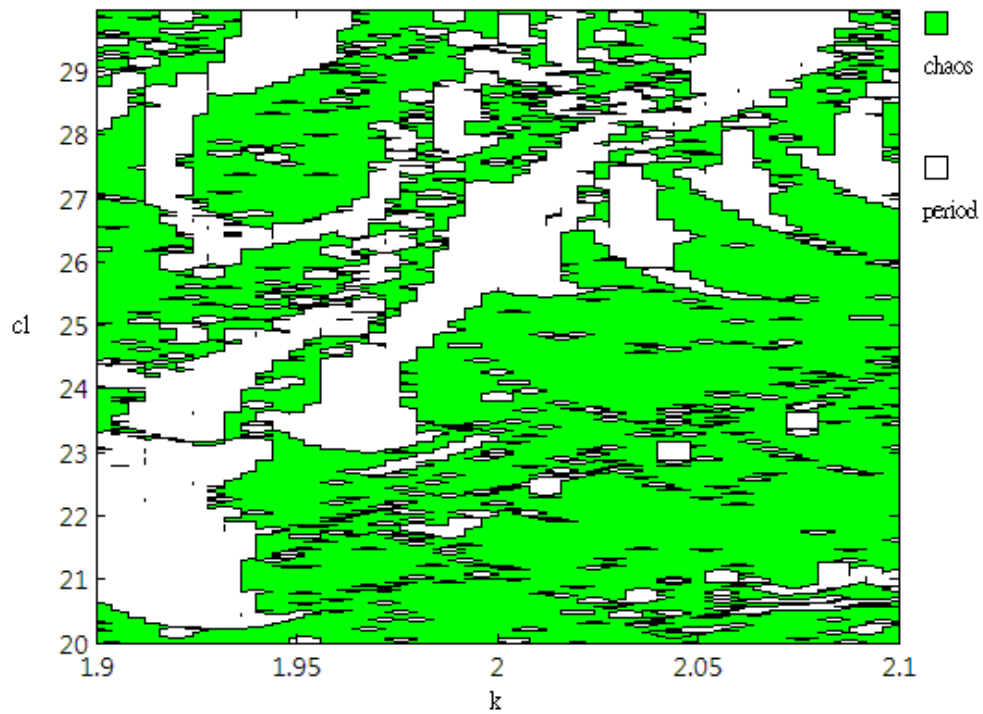


Fig. 4.10 The parameter diagram for modified Lorenz system between $k=2.05\sim 2.35$.

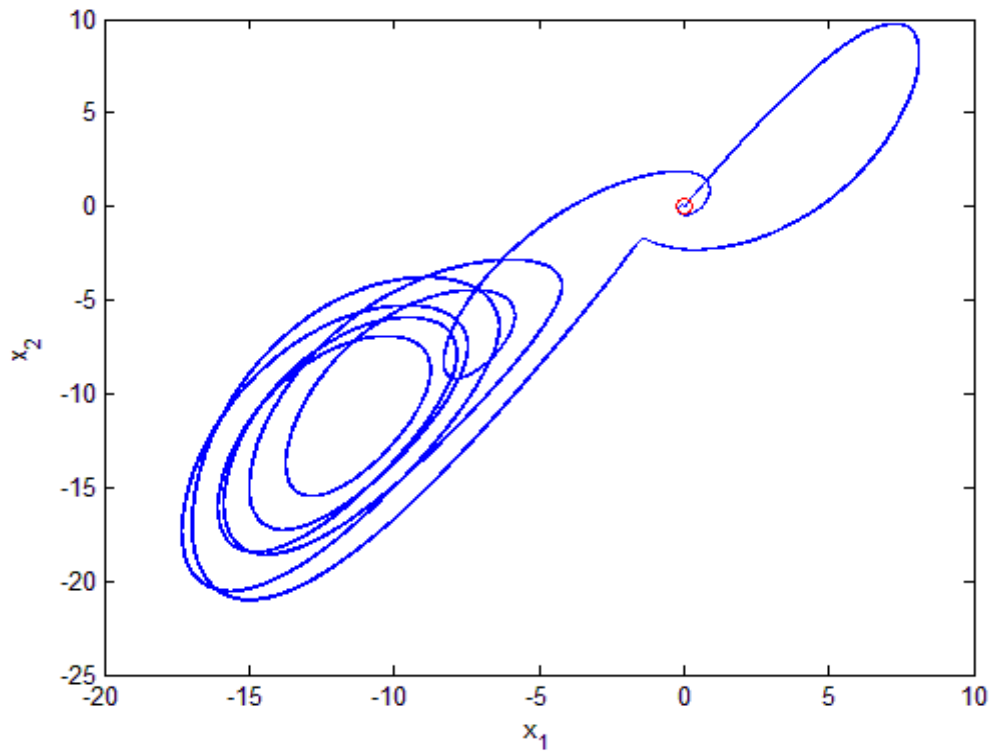


Fig. 4.11 Phase portrait for Lorenz system with Legendre function parameters when

$$c_1 = 27.43, \quad \varepsilon = 1.2, \quad \omega = 0.8 \text{ and } k=2.175(\text{period}1).$$

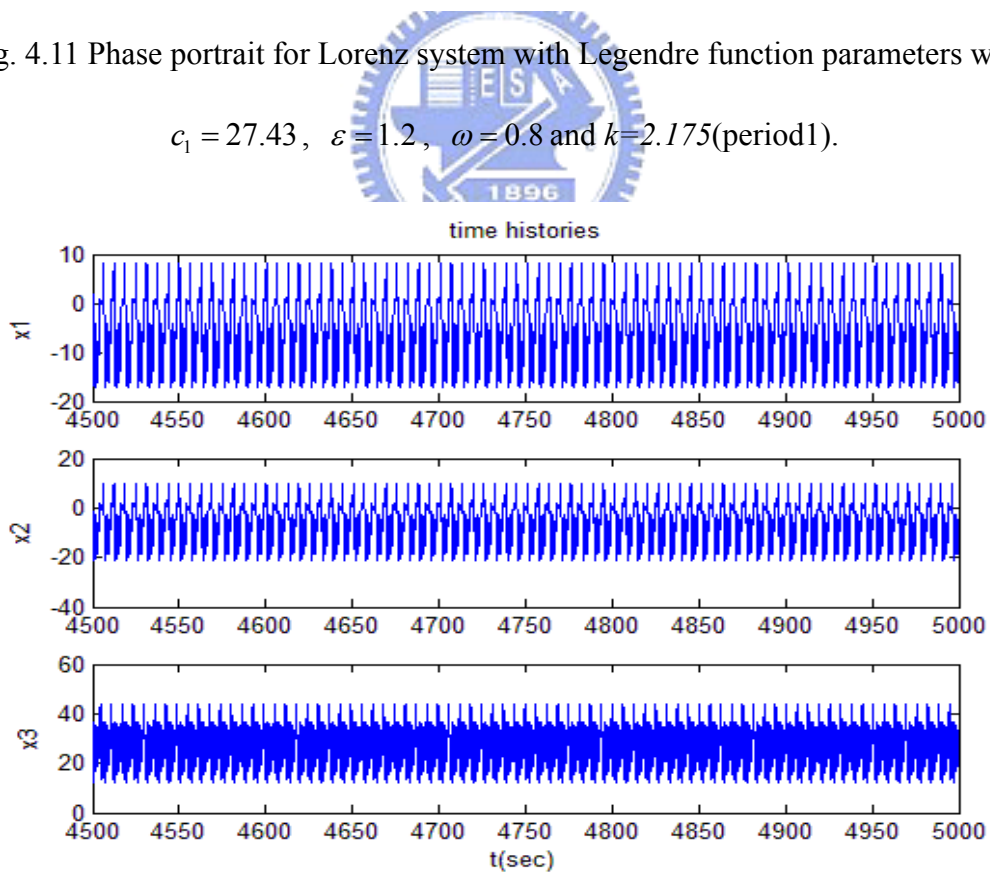


Fig. 4.12 Time histories for Lorenz system with Legendre function parameters when

$$c_1 = 27.43, \quad \varepsilon = 1.2, \quad \omega = 0.8 \text{ and } k=2.175(\text{period}1).$$

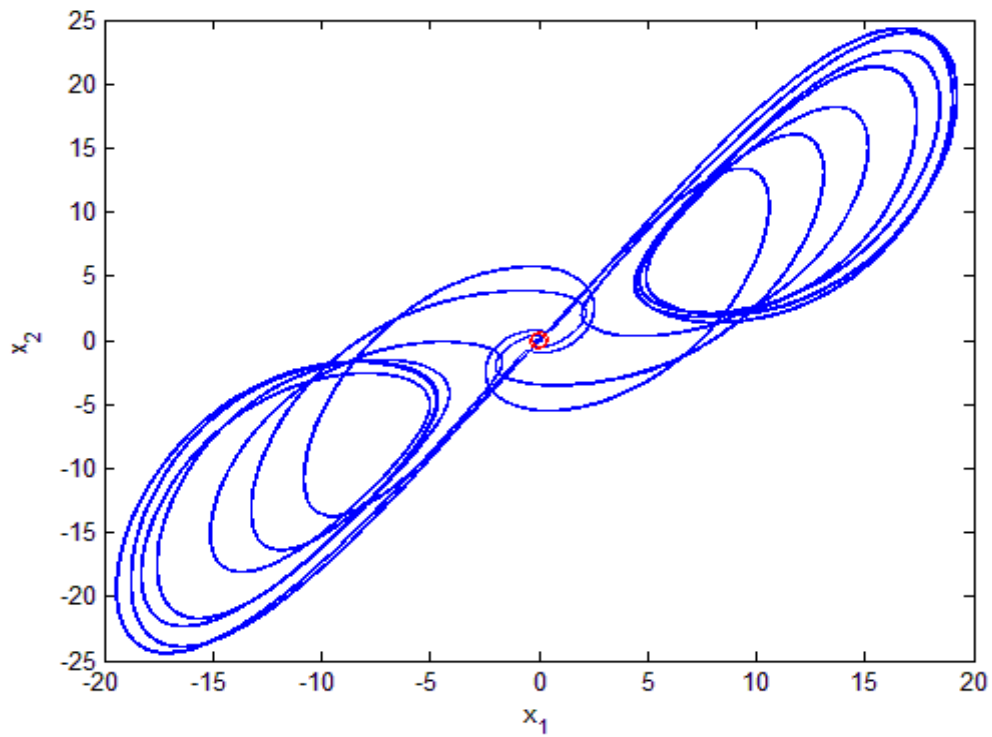


Fig. 4.13 Phase portrait for Lorenz system with Legendre function parameters when

$$c_1 = 27.43, \quad \varepsilon = 1.2, \quad \omega = 0.8 \text{ and } k=2.1(\text{period}2).$$

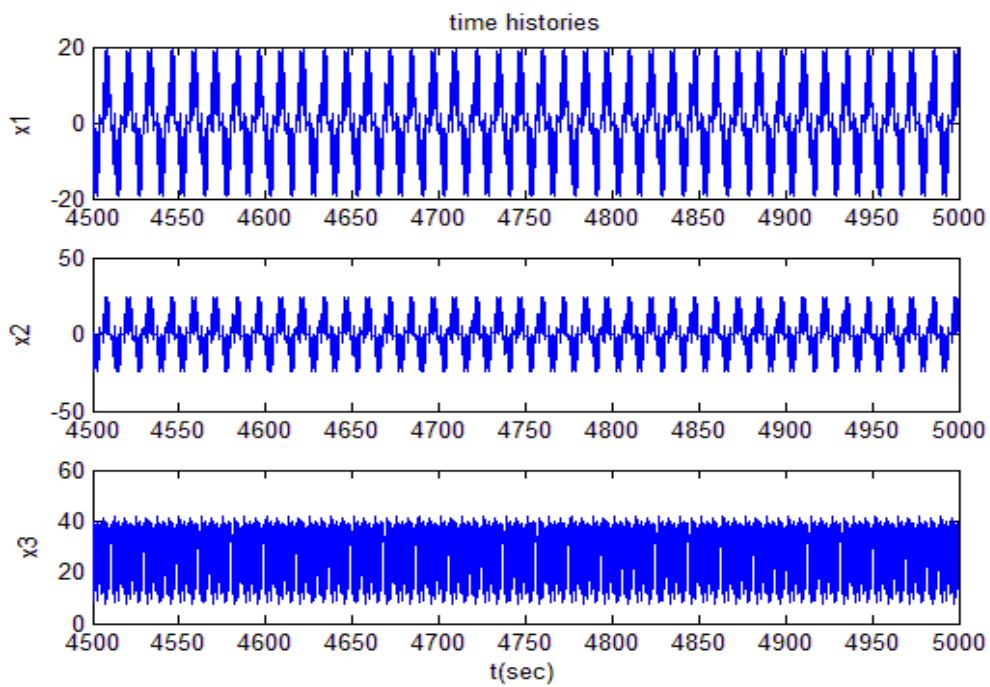


Fig. 4.14 Time histories for Lorenz system with Legendre function parameters when

$$c_1 = 27.43, \quad \varepsilon = 1.2, \quad \omega = 0.8 \text{ and } k=2.1(\text{period}2).$$

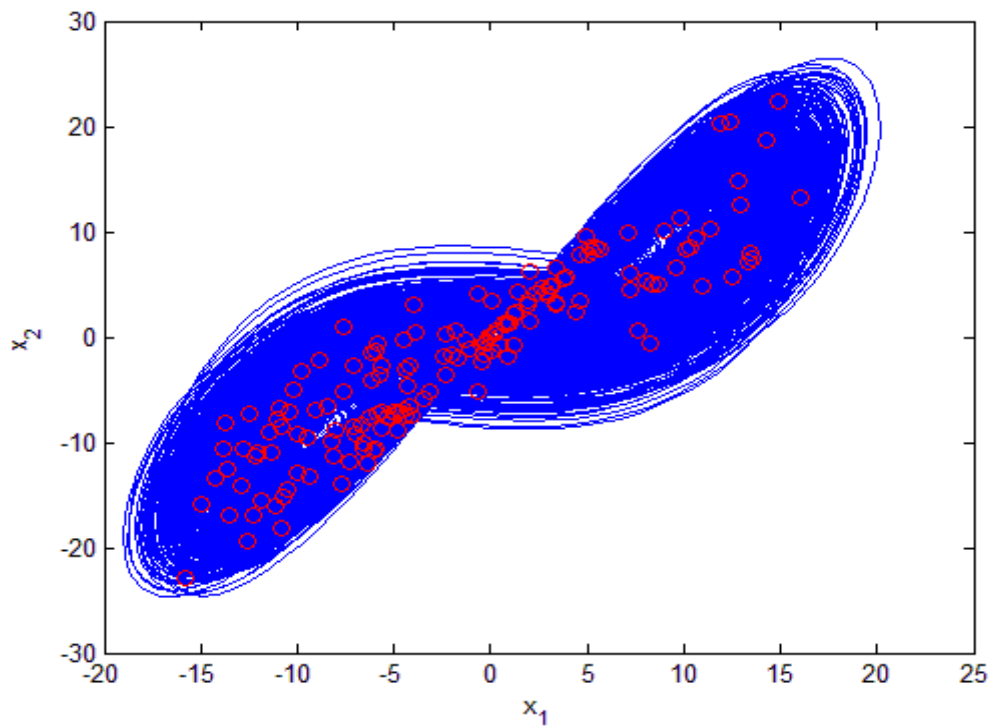


Fig. 4.15 Phase portraits for Lorenz system with Legendre function parameters when $k=0.35$ (hyperchaos)

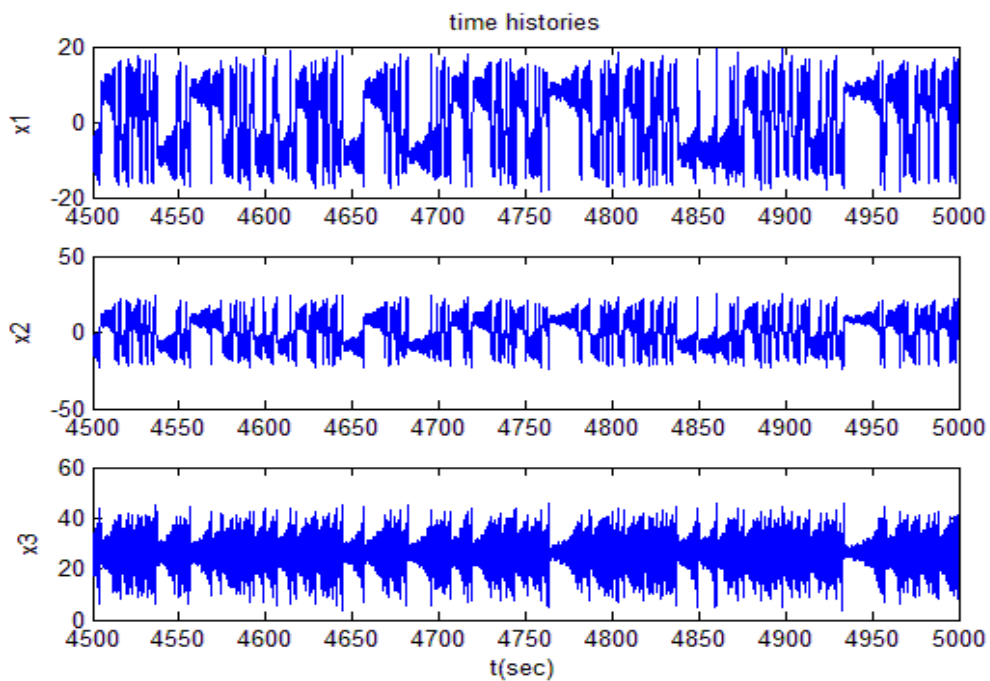


Fig. 4.16 Time histories for Lorenz system with Legendre function parameters when $k=0.35$ (hyperchaos).

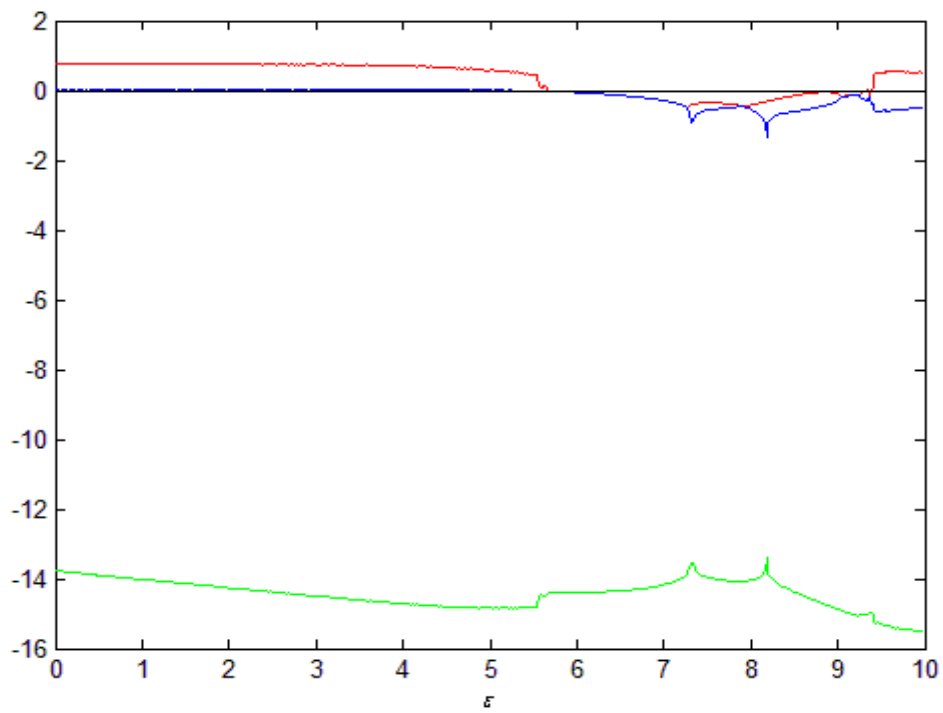


Fig. 4.17 The Lyapunov exponent for Lorenz system with Legendre function parameters
when $\varepsilon = 0 \sim 10$.

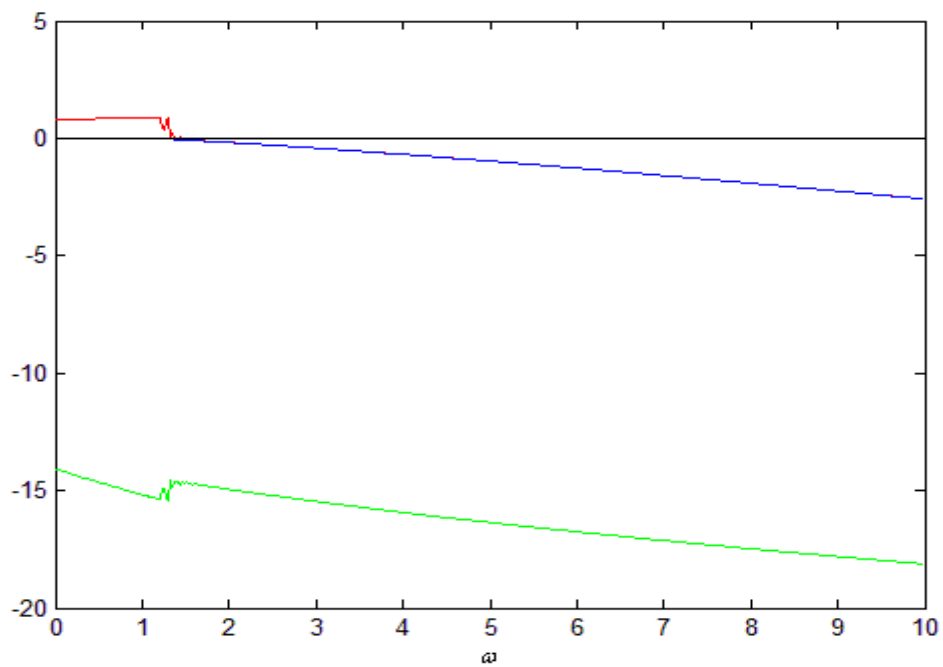


Fig. 4.18 The Lyapunov exponent for Lorenz system with Legendre function parameters
when $\omega = 0 \sim 10$.

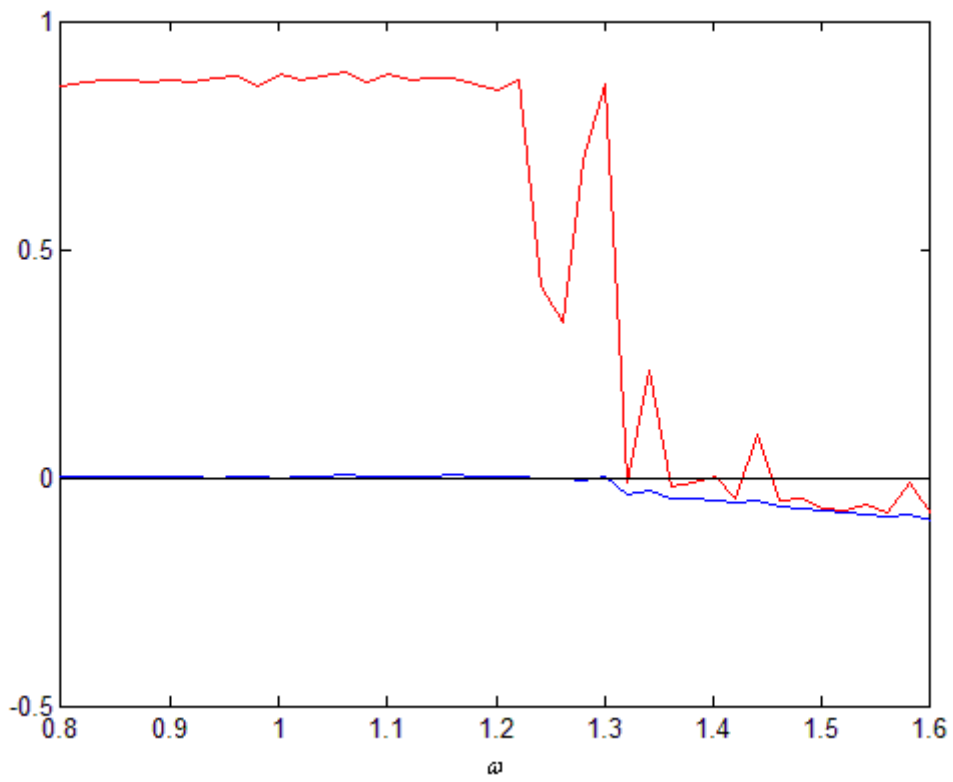


Fig. 4.19 Enlarged figure for Lorenz system with Legendre function parameters when $\omega = 0 \sim 10$.



Chapter 5

Historical Chaos for Chen System

5.1 Preliminaries

In this Chapter, the behavior of historical Chen system is firstly studied. To our best knowledge, most of contemporary Chen system are researched in detail, but there are no articles investigating a thorough inquiry about the history of Chen system so far. Therefore, the historical chaos of Chen system with “*Yin* parameters” is introduced and simulation results are shown by phase portraits, Poincaré maps, bifurcation diagram, Lyapunov exponents in this Chapter.

5.2 Yang Chen system

The *Yang* Chen system [37] is described as follows:

$$\begin{cases} \frac{dx_1(t)}{dt} = a(x_2(t) - x_1(t)) \\ \frac{dx_2(t)}{dt} = (c - a)x_1(t) - x_1(t)x_3(t) + cx_2(t) \\ \frac{dx_3(t)}{dt} = x_1(t)x_2(t) - bx_3(t) \end{cases} \quad (5.1)$$

where initial condition $(x_1, x_2, x_3) = (0.5, 0.26, 0.35)$ and parameters $a=35$, $b=3$ and $c=27.2$, chaos of the *Yang* Chen system is appeared. The chaotic behavior of Eq. (5.1) as phase portraits, Poincaré maps, time histories, periods are shown in Figs. 5.1-6.

5.3 Yin Chen system

In this section, *Yin* Chen equations are:

$$\begin{cases} \frac{dx_1(-t)}{d(-t)} = a(x_2(-t) - x_1(-t)) \\ \frac{dx_2(-t)}{d(-t)} = (c - a)x_1(-t) - x_1(-t)x_3(-t) + cx_2(-t) \\ \frac{dx_3(-t)}{d(-t)} = x_1(-t)x_2(-t) - bx_3(-t) \end{cases} \quad (5.2)$$

It is clear that the derivative are taken with the negative time through left parts of Eq. (5.2). It means that find out the historical behavior of the Chen system and to compare the relation between history and presence. The simulation results are shown in Table 1:

Table 1 Dynamic behaviors of *Yin* Chen system for different signs of parameters

a	b	c	States
+	-	+	Approach to infinity
-	+	+	Approach to infinity
+	+	-	Approach to infinity
-	+	-	Approach to infinity
-	-	+	Approach to infinity
-	-	-	Chaos and periodic

Table 1 shows the dynamic behaviors of *Yin* Chen system for different signs of parameters. An strange and interesting phenomenon is discovered. When initial condition $(x_1, x_2, x_3) = (0.5, 0.26, 0.35)$ and parameters $a = -35$, $b = -3$ and $c = -27.2$, chaos of the *Yin* Chen system is found. Therefore, we call these parameters as *Yin* parameters. In conventional Chinese philosophy, *Yin* is the negative, past or feminine principle in nature, while *Yang* is the positive, present or masculine principle in nature. *Yin* and *Yang* are two fundamental opposites in Chinese philosophy. For this reason, historical Chen system with negative value of parameters, $a = -10$, $b = -8/3$ and $c = -27.2$, can be called *Yin* Chen system with *Yin* parameters. The chaotic behaviors of Eq. (5.2) are shown in Figs. 5.7-13.

5.4 Numerical Simulations

To study the difference and similarity between *Yang* and *Yin* Chen system, the bifurcation diagram and Lyapunov exponents are used. We consider three cases described as follows:

Case1: parameter c is varied and a, b are fixed:

The simulation results are shown in Tables 2-3.

Table 2 Range of parameter c of *Yang* Chen system

0.1~20.1	Converge to a fixed point
20.1~28.2	Chaos
28.2~34.2	Periodic

Table 3 Range of parameter c of *Yin* Chen system

-0.1~-20.0	Converge to a fixed point
-20.0~-28.1	Chaos
-28.1~-34.2	Periodic

Table 2 and 3 show different dynamics in the different ranges of parameter c of *Yang* and *Yin* Chen system, respectively. In Table 2, the behaviors of *Yang* Chen system vary with parameter c , and become chaos, periodic or converging to a fixed point. When $0.1 \leq c \leq 20.1$, *Yang* Chen system will converge to a fixed point. When $20.1 \leq c \leq 28.2$, chaos appears. When $28.2 \leq c \leq 34.2$, periodic motion is found. Table 3 shows that when parameter c is $-34.2 \sim -28.1$, the behaviors of *Yin* Chen system are periodic trajectories. When parameter c is $-28.1 \sim -20$, the chaotic behaviors are shown in *Yin* Chen system. When parameter c is $-20 \sim -0.1$, it will converge to a fixed point. Comparing Table 2 and 3, it can be found that both there are chaos, periodic and fixed point in *Yang* and *Yin* Chen system for parameter c , respectively. Bifurcation diagram and Lyapunov exponents are shown in Figs. 5.14-17.

Case2: parameter b is varied and a, c are fixed:

The simulation results are shown in Tables 4-5.

Table 4 Range of parameter b of *Yang* Chen system

2.80~3.51	Chaos
3.51~3.55	Periodic
3.55~4.40	Chaos
4.40~4.48	Periodic
4.48~4.50	Chaos
4.50~10.00	Periodic

Table 5 Range of parameter b of *Yin* Chen system

-2.80~-3.51	Chaos
-3.51~-3.56	Periodic
-3.56~-4.40	Chaos
-4.40~-10.00	Periodic

Table 4 and 5 show that the behaviors of *Yang* and *Yin* Lorenz system are similar but not the same. Comparing Table 4 and 5, it can be found an obvious difference that when

parameter b is 4.48~4.50, the chaotic behaviors are shown in *Yang* Chen system, but none of *Yin* ones. Bifurcation diagram and Lyapunov exponents are shown in Figs. 5.18-21.

Case3: parameter a is varied and b, c are fixed:

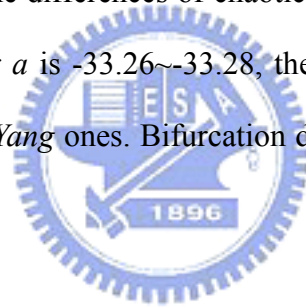
Table 6 Range of parameter a of *Yang* Chen system

30.0~34.0	Periodic
34.0~42.0	Chaos
42.0~44.7	Periodic
44.7~48.0	Chaos
after-48.0	Converge to a fixed point

Table 7 Range of parameter a of *Yin* Chen system

-30.00~-33.26	Periodic
-33.26~-33.28	Chaos
-33.28~-33.43	Periodic
-33.43~-41.80	Chaos
-41.80~-44.70	Periodic
-44.70~-47.80	Chaos
after-47.80	Converge to a fixed point

In Table 6 and 7, there are some differences of chaotic behaviors between *Yang* and *Yin* Chen system. When parameter a is -33.26~-33.28, the chaotic behaviors are shown in *Yin* Chen system, but none of *Yang* ones. Bifurcation diagram and Lyapunov exponents are shown in Figs. 5.22-25.



5.5 Summary

In this Chapter, the *Yin* Chen system is firstly introduced. Compared with the *Yang* and *Yin* Chen system via numerical simulation, we can be found out some similarity and difference between history and presence. If the *Yang* parameter is one of the chaotic parameters for contemporary Chen system, then the chaotic behavior of the historical Chen system can be shown by using the corresponding *Yin* parameters. Table A and B give the similarity and difference between the *Yang* and *Yin* Chen system from bifurcation diagram and Lyapunov exponents. This Chapter explores the another half scope of study for chaos interestingly, which would be proved as epoch-making significance in future.

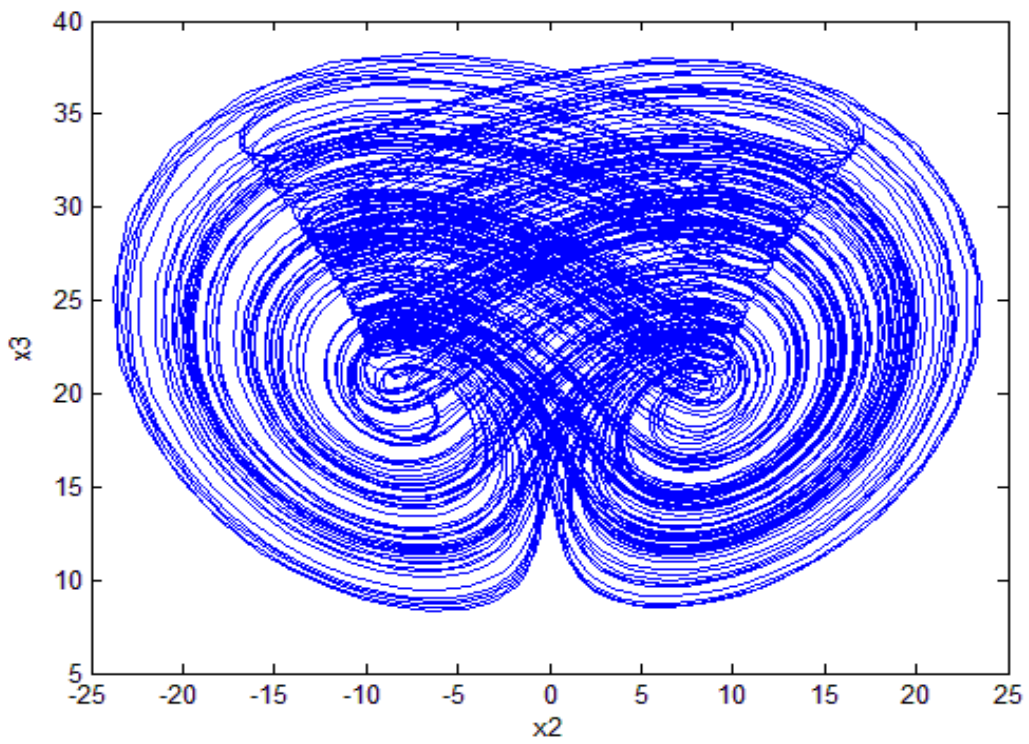
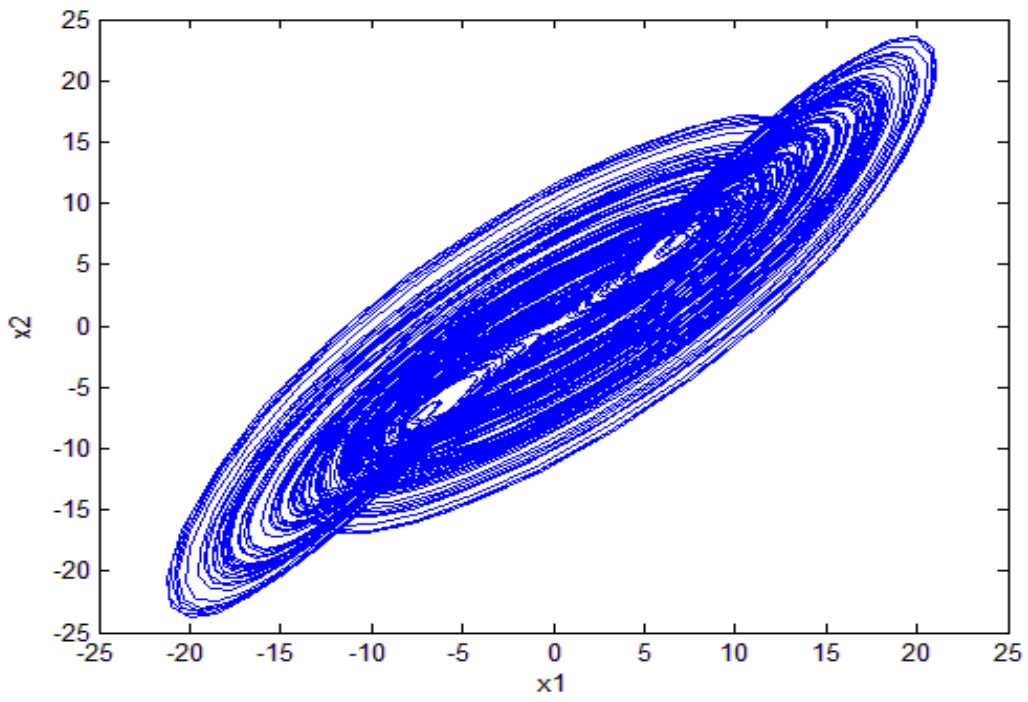


Fig. 5.1 Phase portraits of *Yang Chen* system with $a = 35$, $b = 3$ and $c = 27.2$.

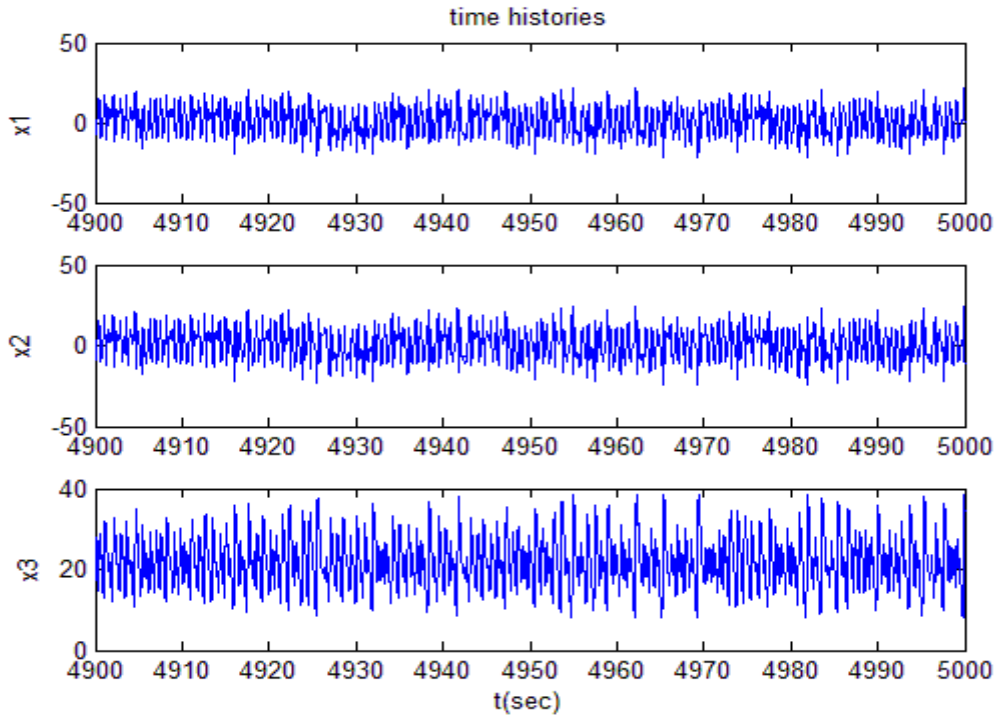


Fig. 5.2 Time histories of three states for *Yang Chen* system with parameters $a = 35$,

$$b = 3 \text{ and } c = 27.2$$

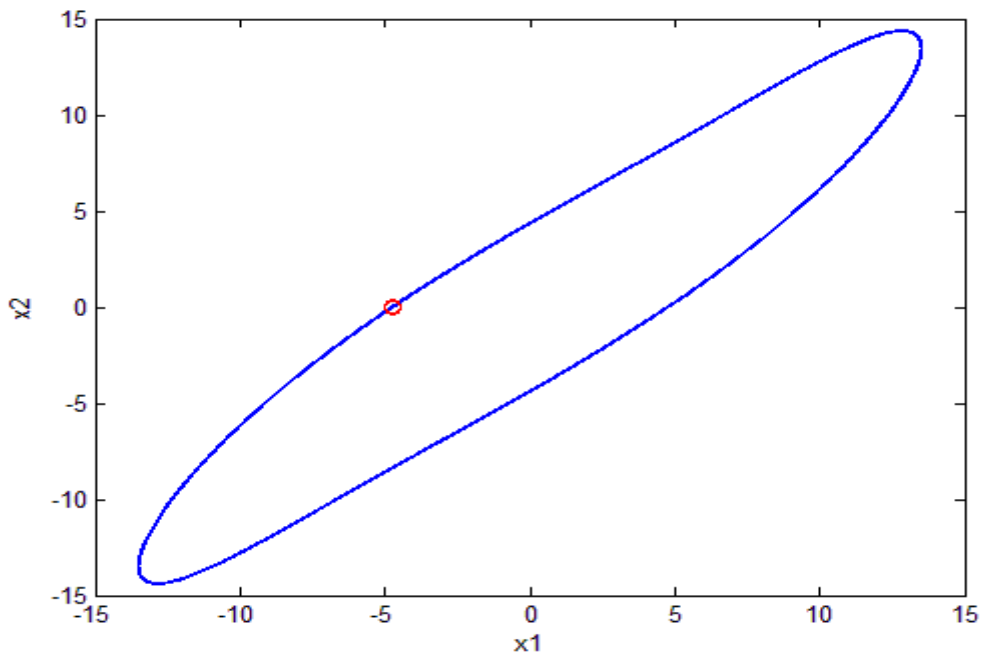


Fig. 5.3 Period1 of phase portraits for *Yang Chen* system with parameters $a = 35$,

$$b = 3 \text{ and } c = 30.$$

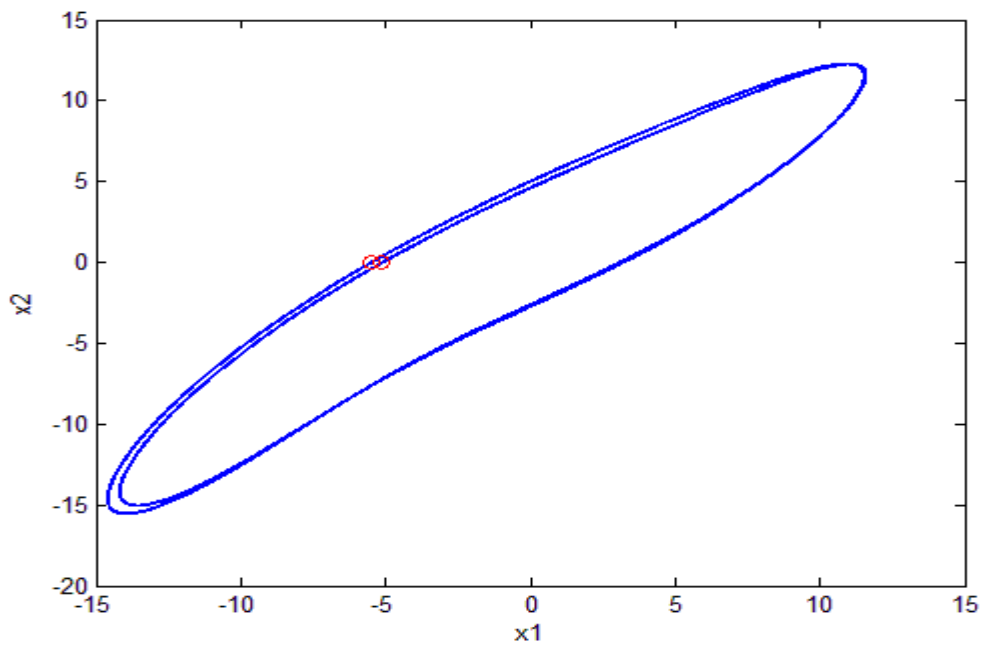


Fig. 5.4 Period2 of phase portraits for *Yang Chen* system with parameters $a = 35$,

$b = 3$ and $c = 28.8$.

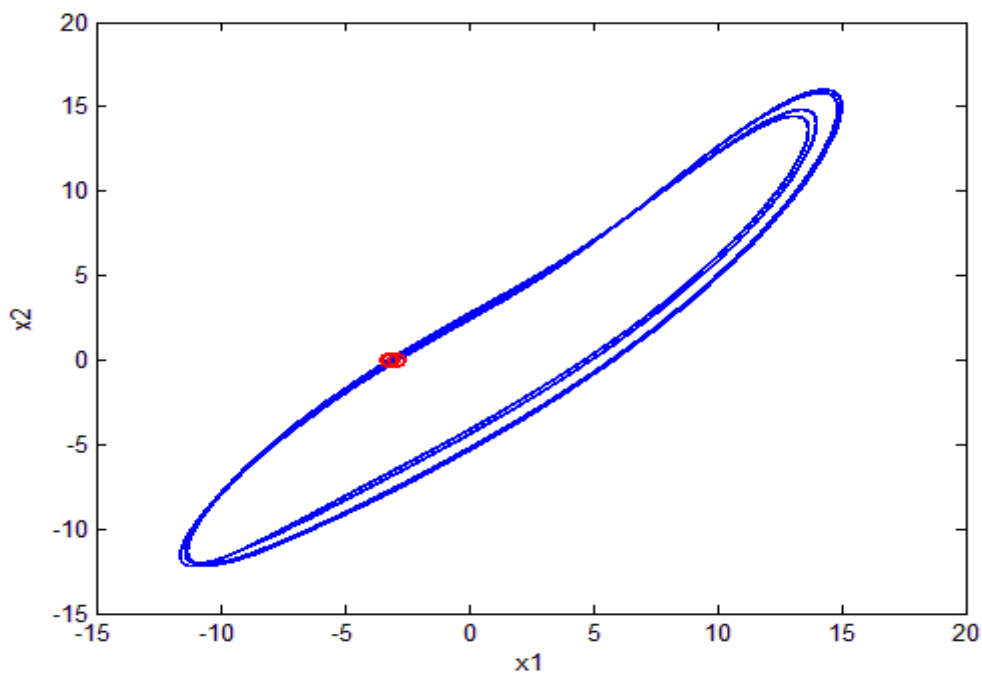
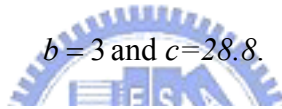


Fig. 5.5 Period4 of phase portraits for *Yang Chen* system with parameters $a = 35$,

$b = 3$ and $c = 28.63$.

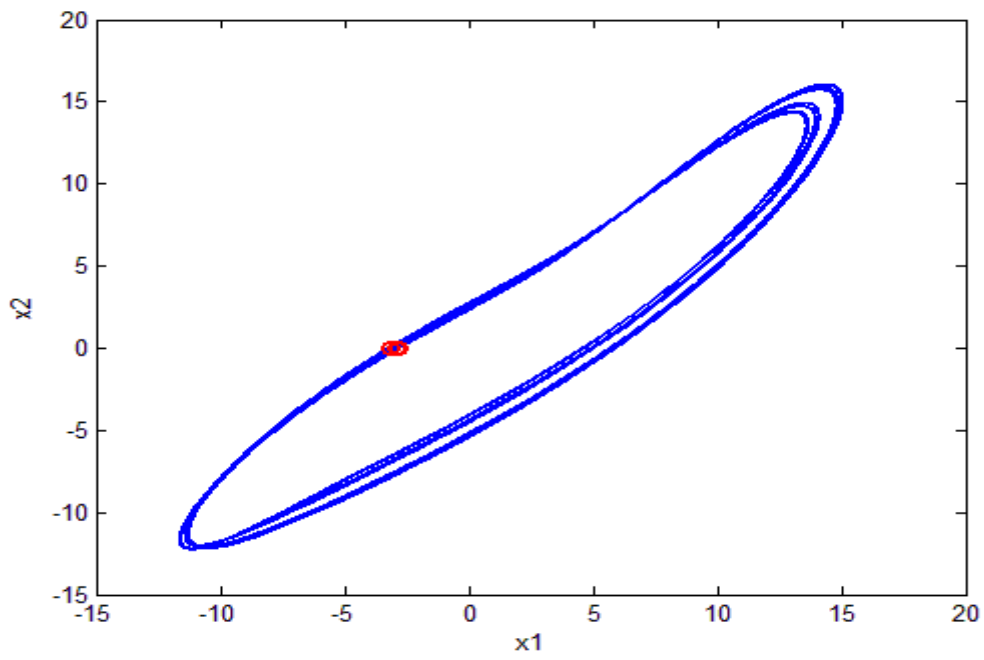


Fig. 5.6 Period8 of phase portraits for *Yang Chen* system with parameters $a = 35$,

$b = 3$ and $c = 28.609$.

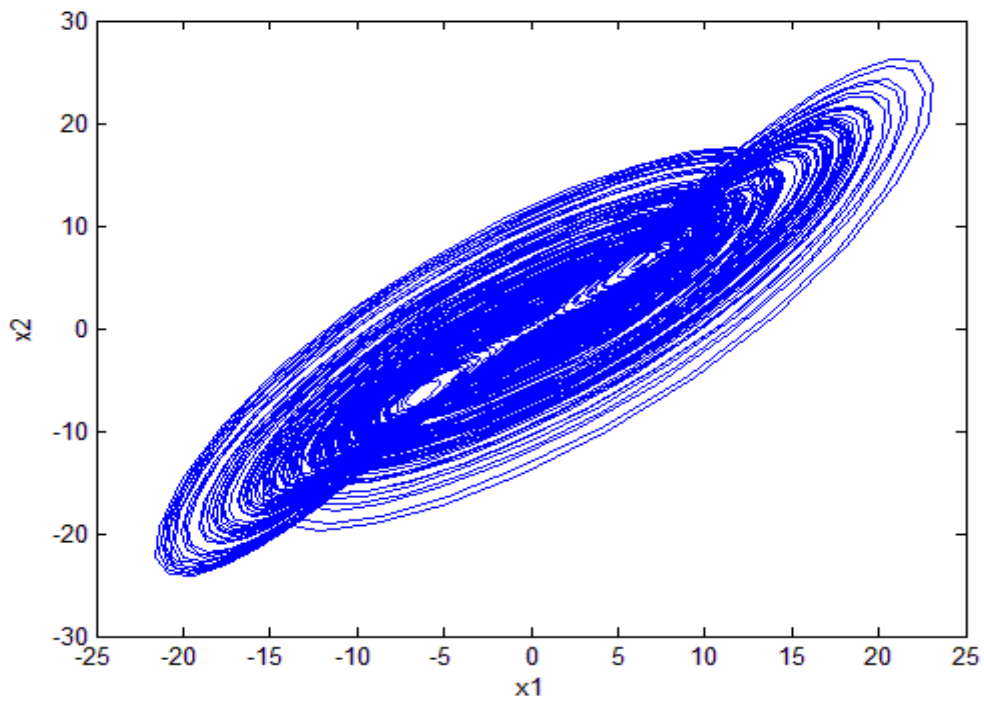
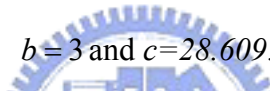


Fig. 5.7 Phase portrait of *Yin Chen* system with $a = -35$, $b = -3$ and $c = -27.2$.

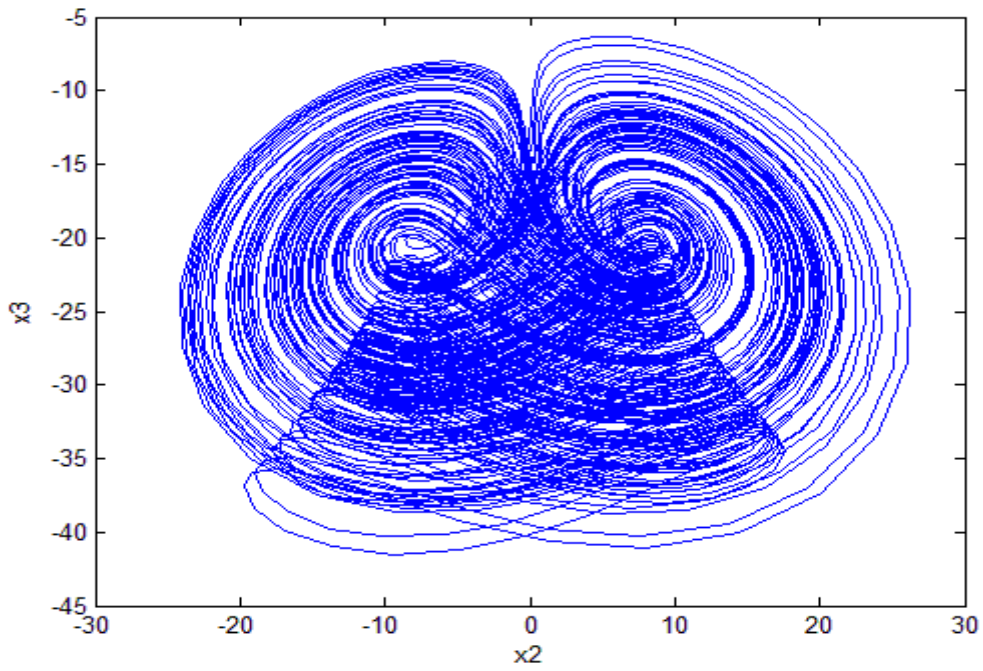


Fig. 5.8 Phase portrait of *Yin Chen* system with $a = -35$, $b = -3$ and $c = -27.2$.

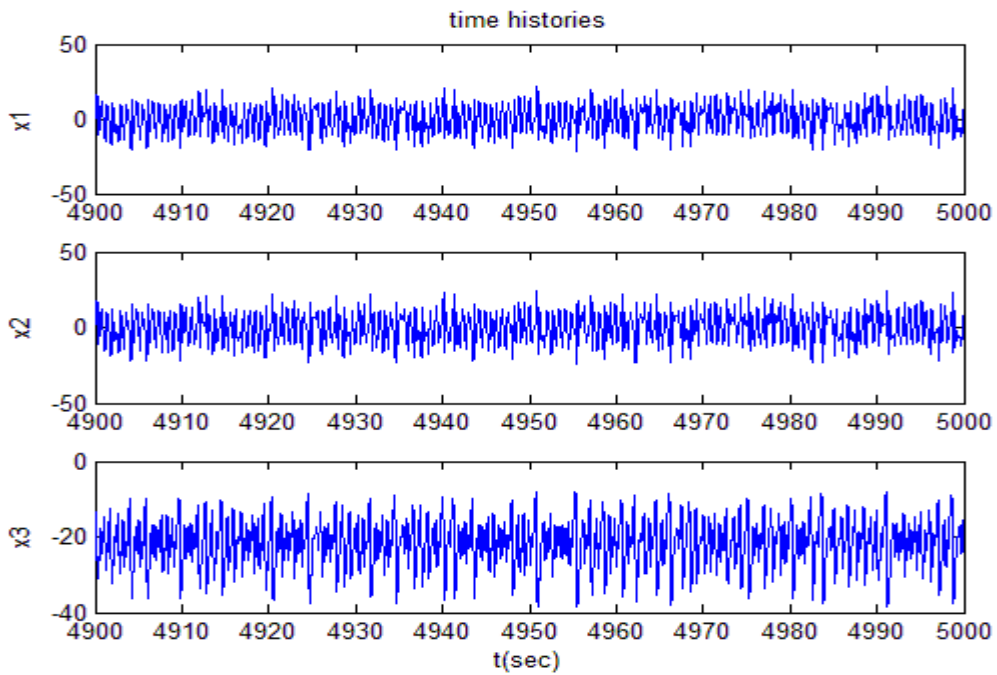


Fig. 5.9 Time histories of three states for *Yin Chen* system with $a = -35$, $b = -3$ and $c = -27.2$.

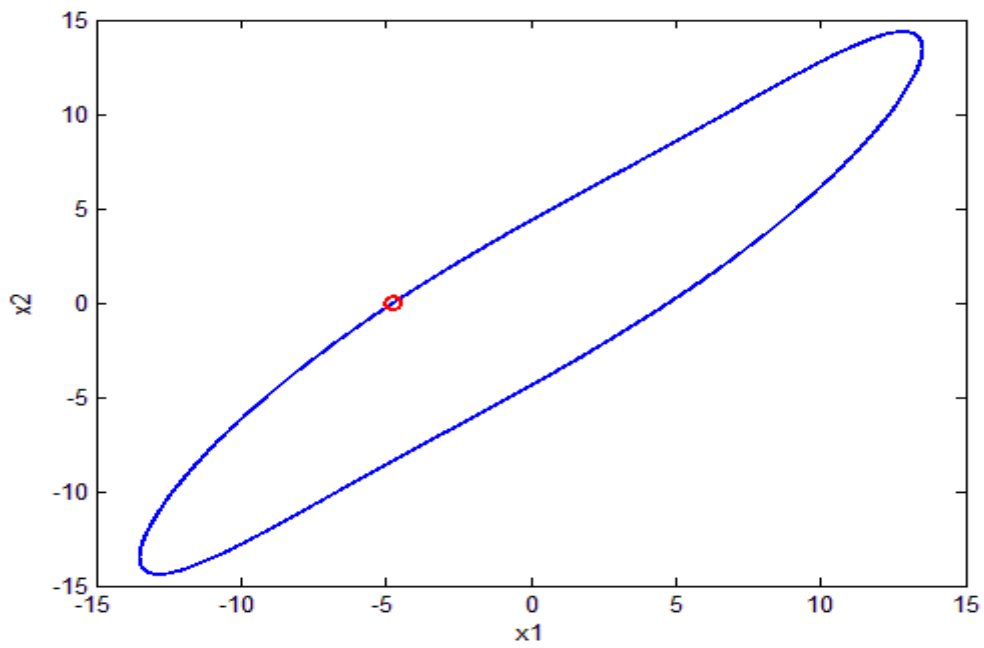


Fig. 5.10 Period1 of phase portraits for *Yin Chen* system with parameters $a = -35$,

$$b = -3 \text{ and } c = -30.$$

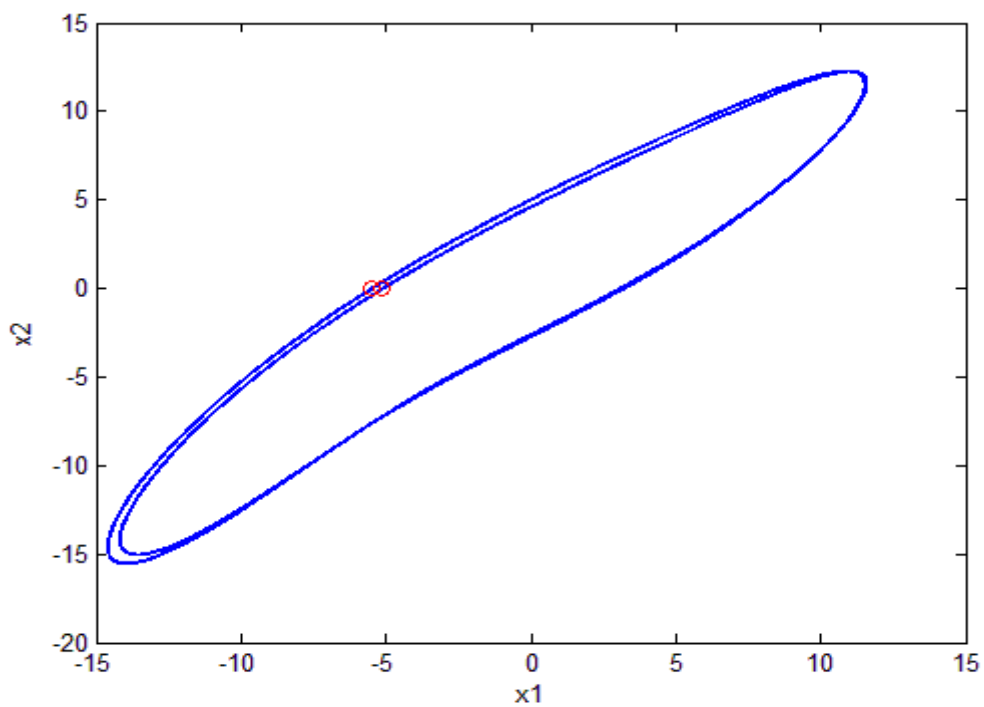


Fig. 5.11 Period2 of phase portraits for *Yin Chen* system with parameters $a = -35$,

$$b = -3 \text{ and } c = -28.8.$$

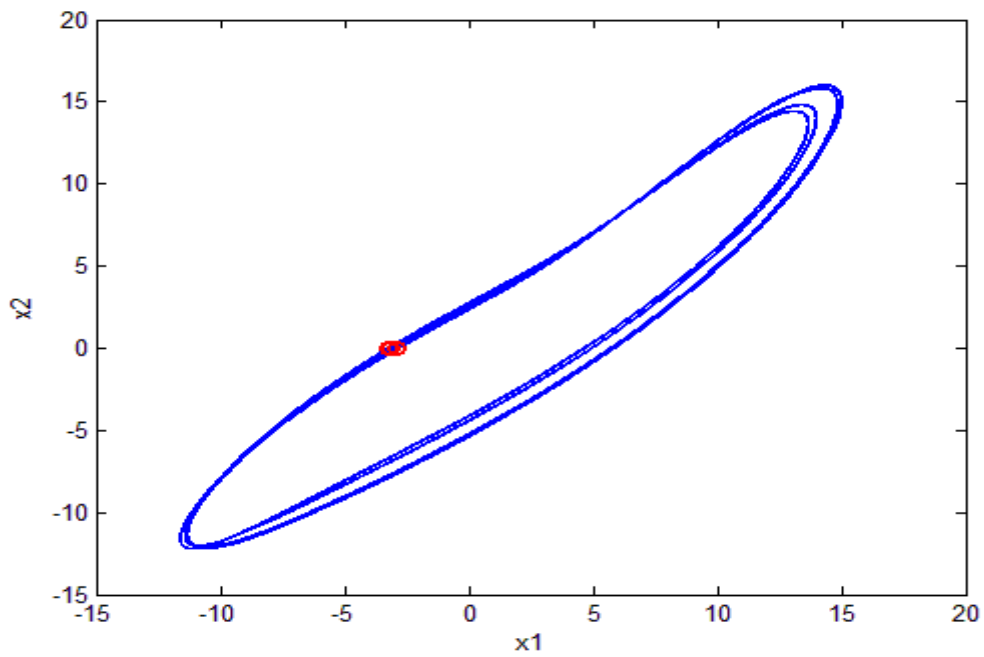


Fig. 5.12 Period4 of phase portraits for *Yin Chen* system with parameters $a = -35$,

$$b = -3 \text{ and } c = -28.63.$$

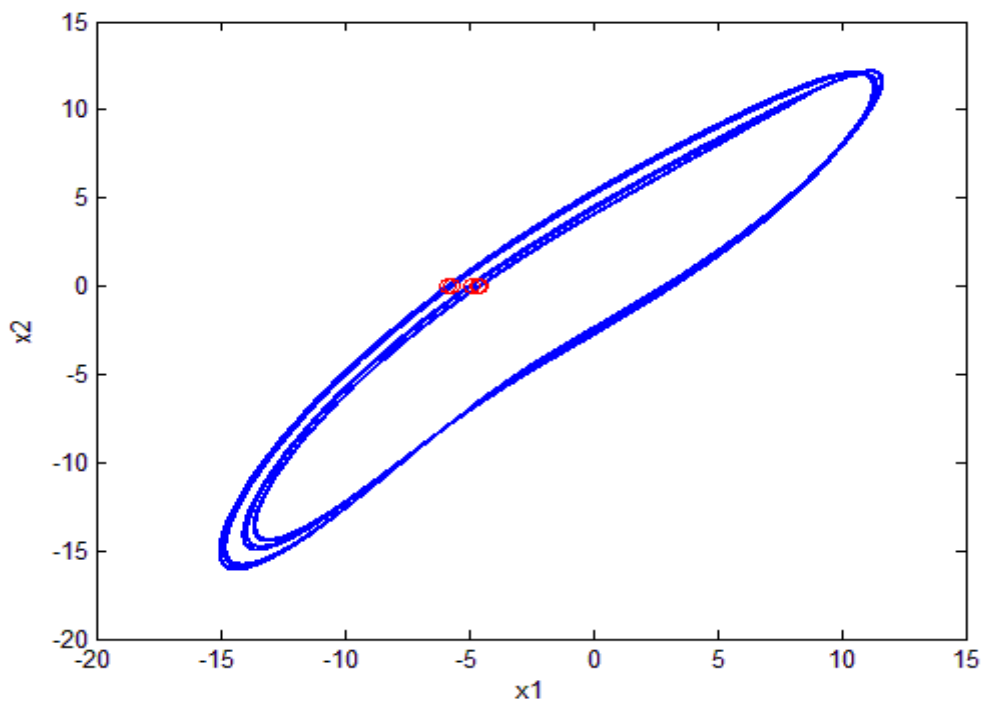


Fig. 5.13 Period8 of phase portraits for *Yin Chen* system with parameters $a = -35$,

$$b = -3 \text{ and } c = -28.609.$$

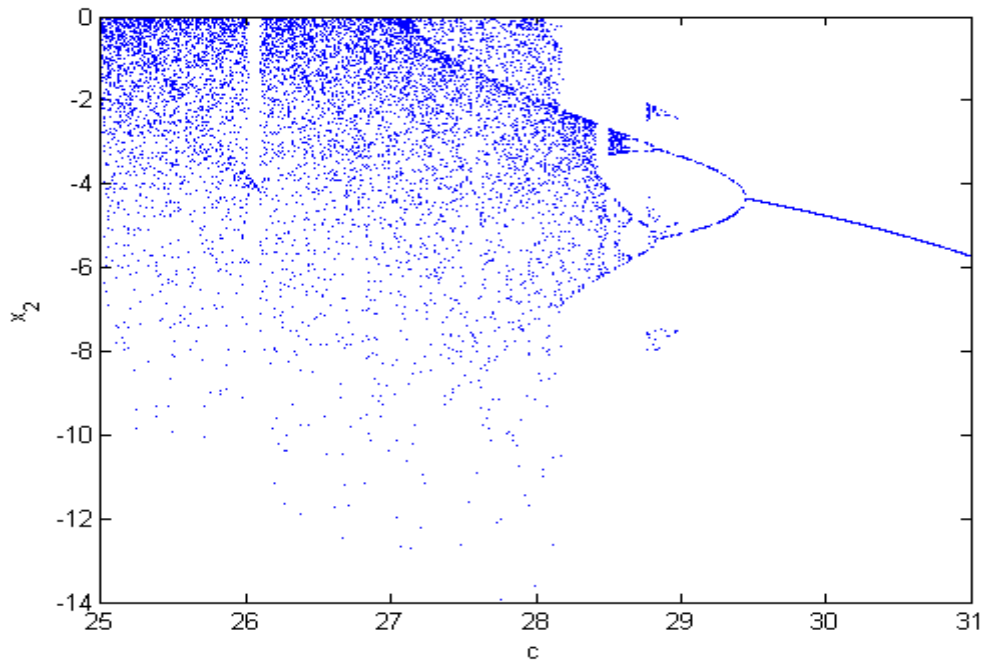


Fig. 5.14 Bifurcation diagram of chaotic *Yang Chen* system with $a = 35$ and $b = 3$.

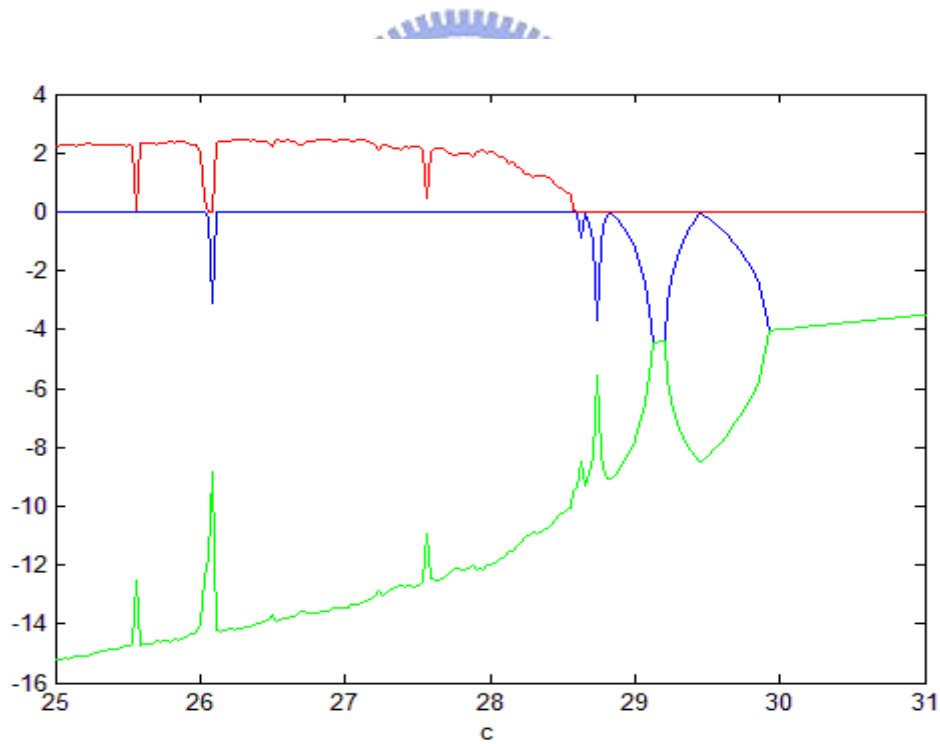


Fig. 5.15 Lyapunov exponents of chaotic *Yang Chen* system with $a = 35$ and $b = 3$.

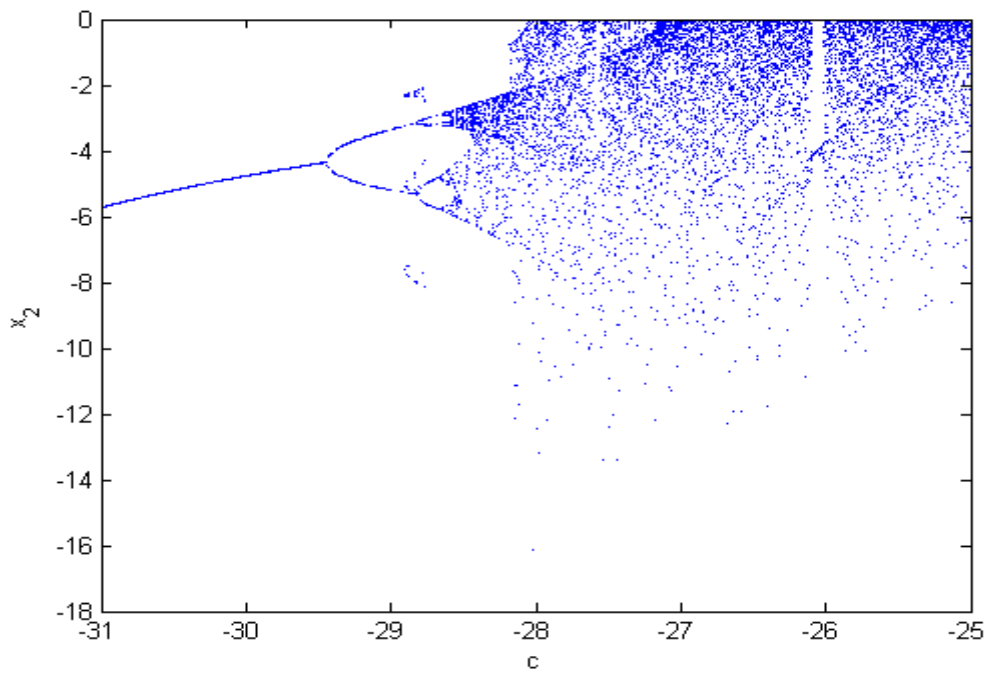


Fig. 5.16 Bifurcation diagram of chaotic *Yin Chen* system with $a = -35$ and $b = -3$.

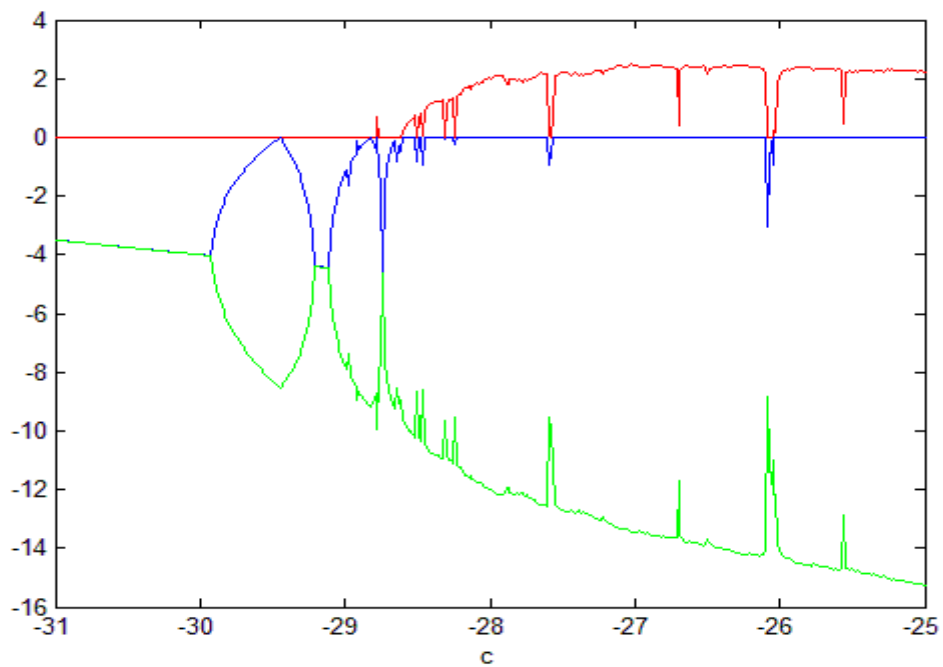


Fig. 5.17 Lyapunov exponents of chaotic *Yin Chen* system with $a = -35$ and $b = -3$.

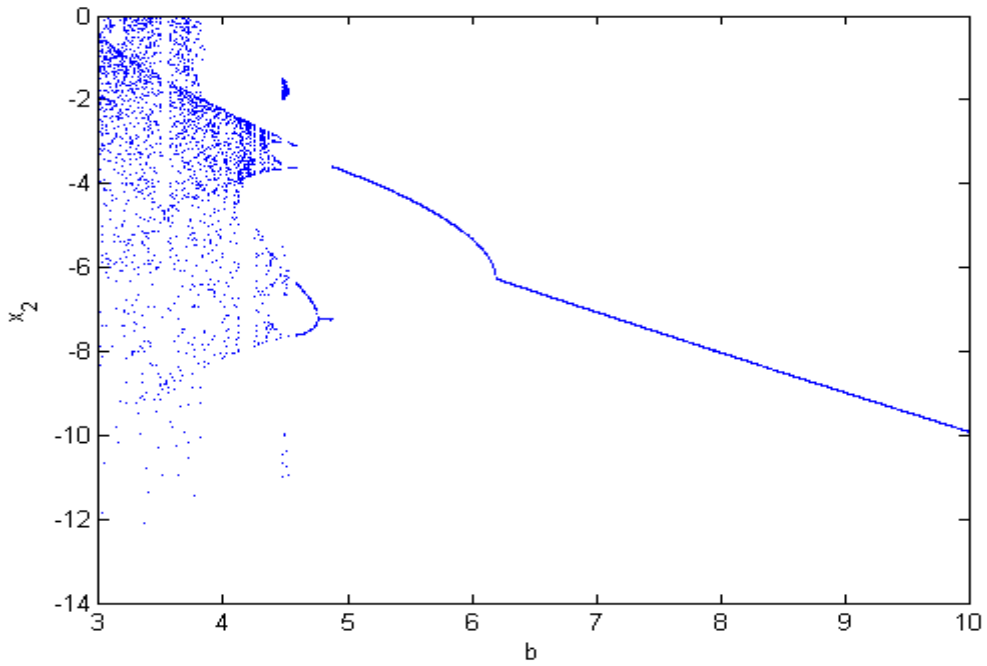


Fig. 5.18 Bifurcation diagram of chaotic *Yang Chen* system with $a = 35$ and $c = 27.2$.

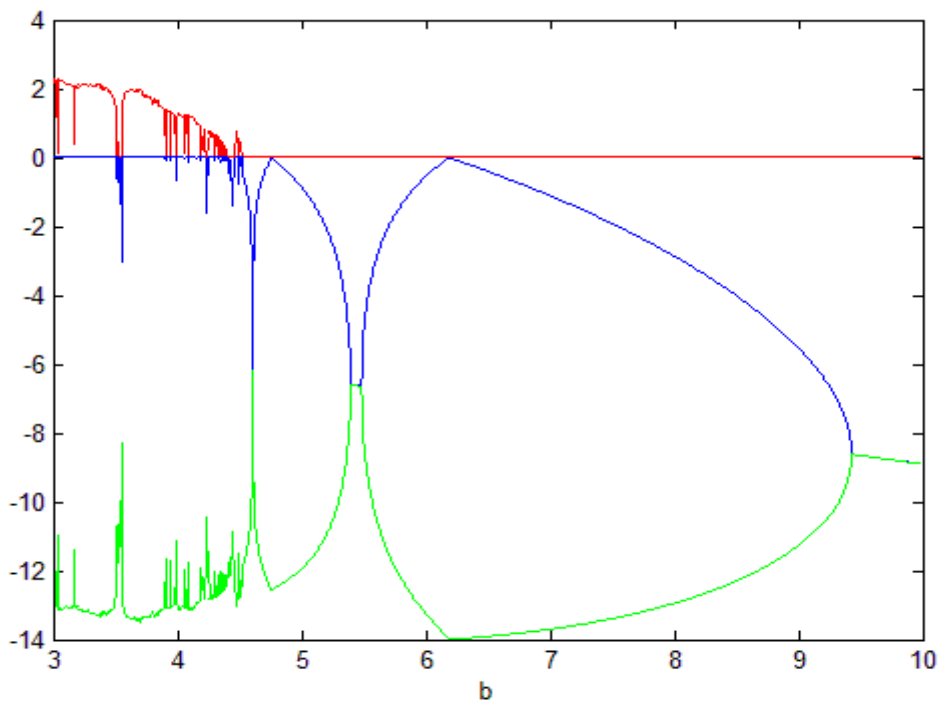


Fig. 5.19 Lyapunov exponents of chaotic *Yang Chen* system with $a = 35$ and $c = 27.2$.

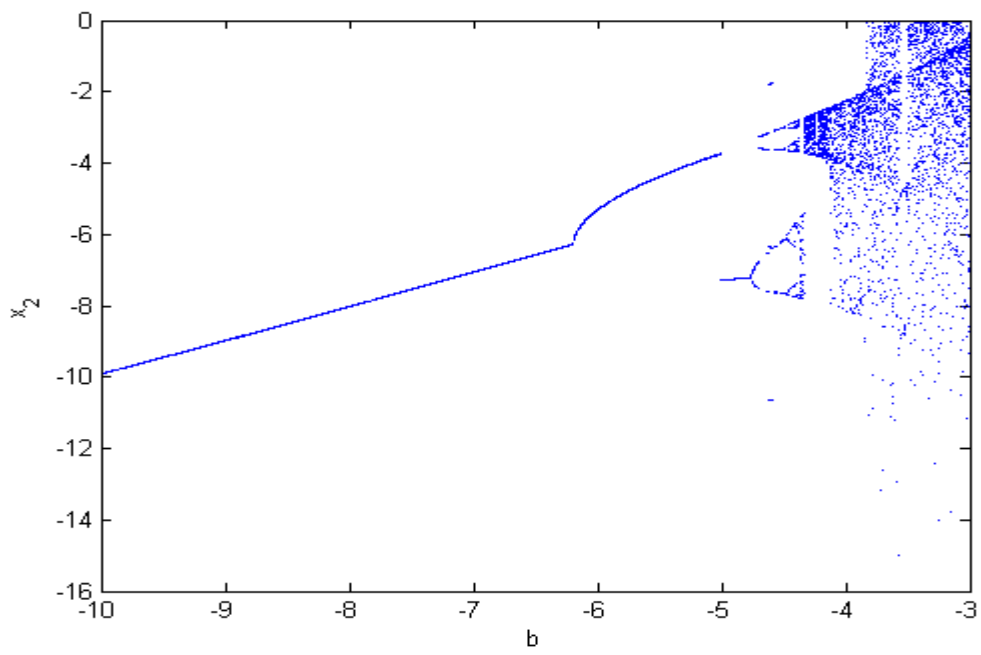


Fig. 5.20 Bifurcation diagram of chaotic *Yin Chen* system with $a = -35$ and $c = -27.2$.

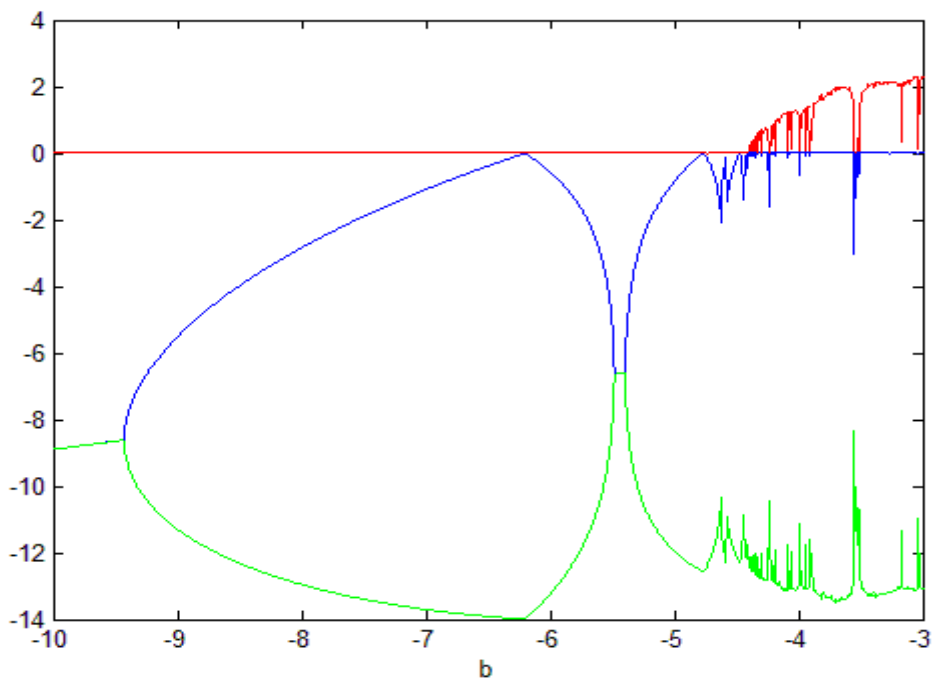


Fig. 5.21 Lyapunov exponents of chaotic *Yin Chen* system with $a = -35$ and $c = -27.2$.

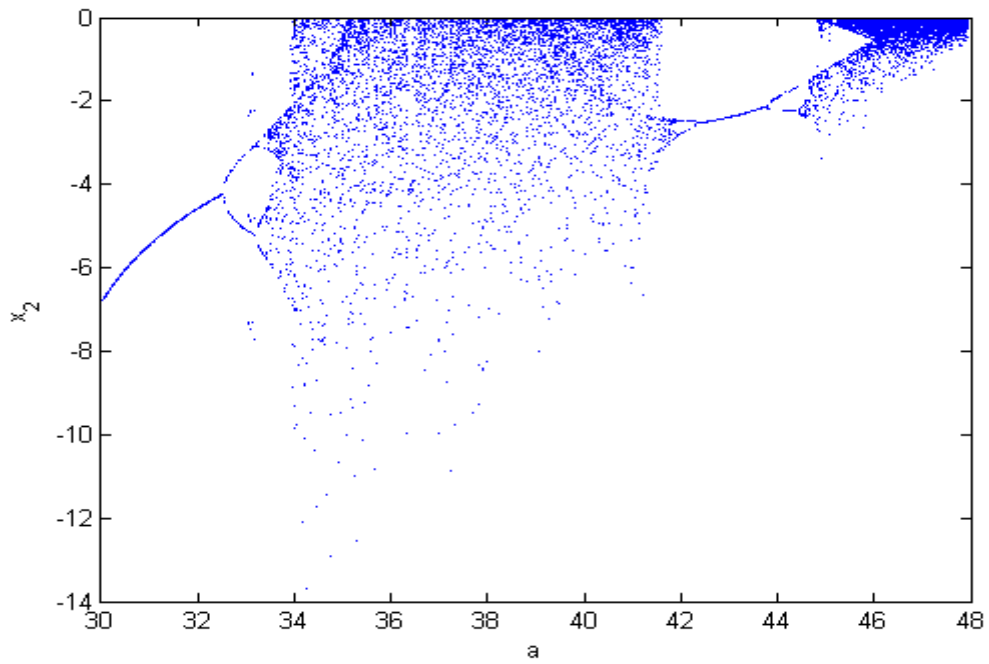


Fig. 5.22 Bifurcation diagram of chaotic *Yang Chen* system with $b = 3$ and $c = 27.2$.

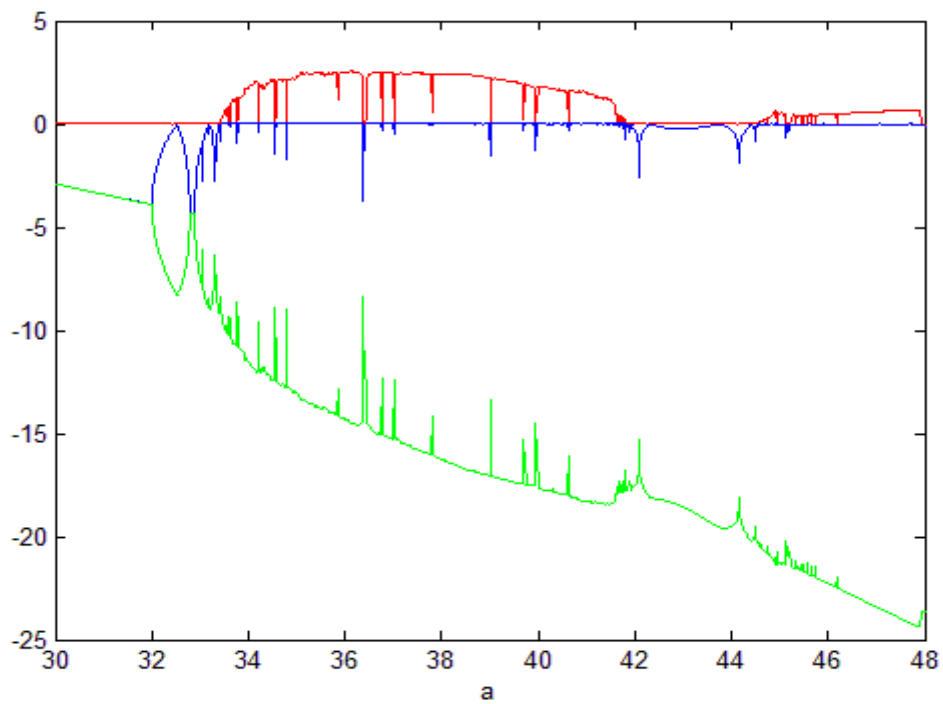


Fig. 5.23 Lyapunov exponents of chaotic *Yang Chen* system with $b = 3$ and $c = 27.2$.

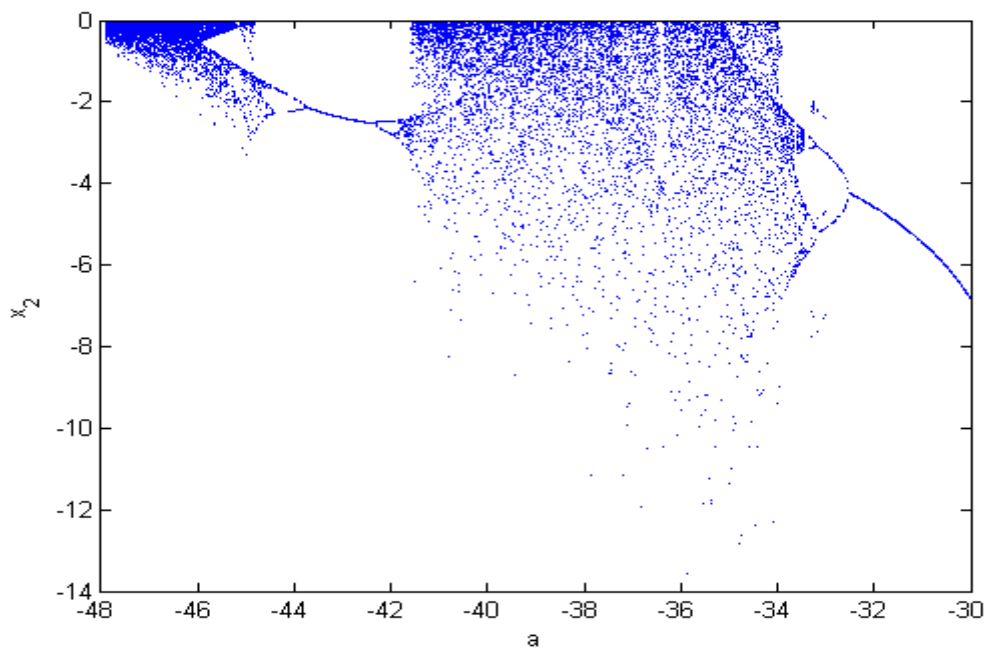


Fig. 5.24 Bifurcation diagram of chaotic *Yin Chen* system with $b = -3$ and $c = -27.2$.

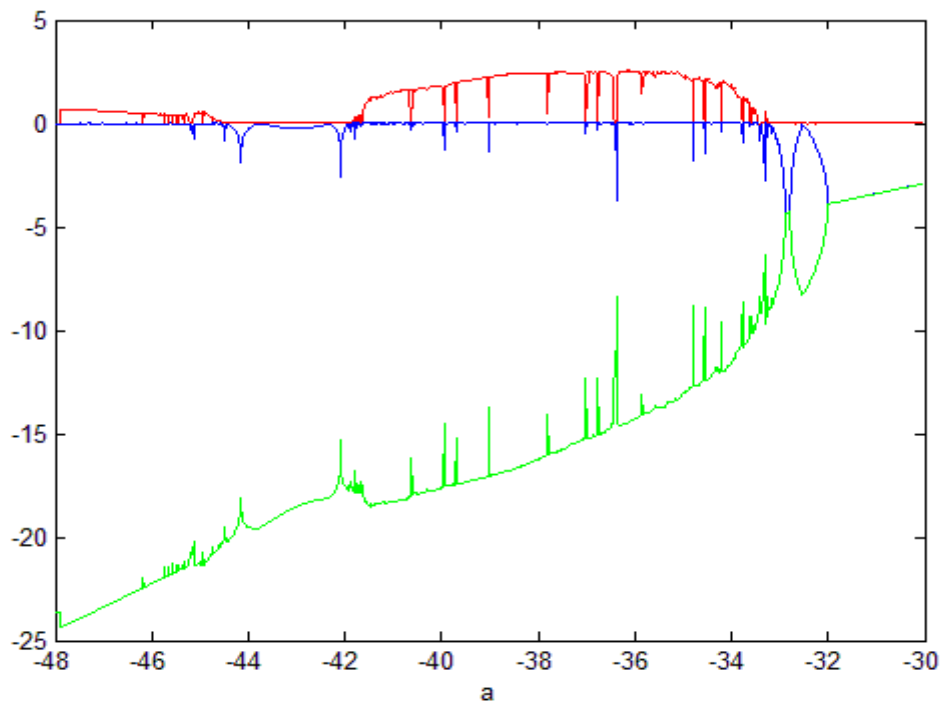


Fig. 5.25 Lyapunov exponents of chaotic *Yin Chen* system with $b = -3$ and $c = -27.2$.

Table A. Comparison with the *Yang* and *Yin* Chen system from bifurcation diagrams.

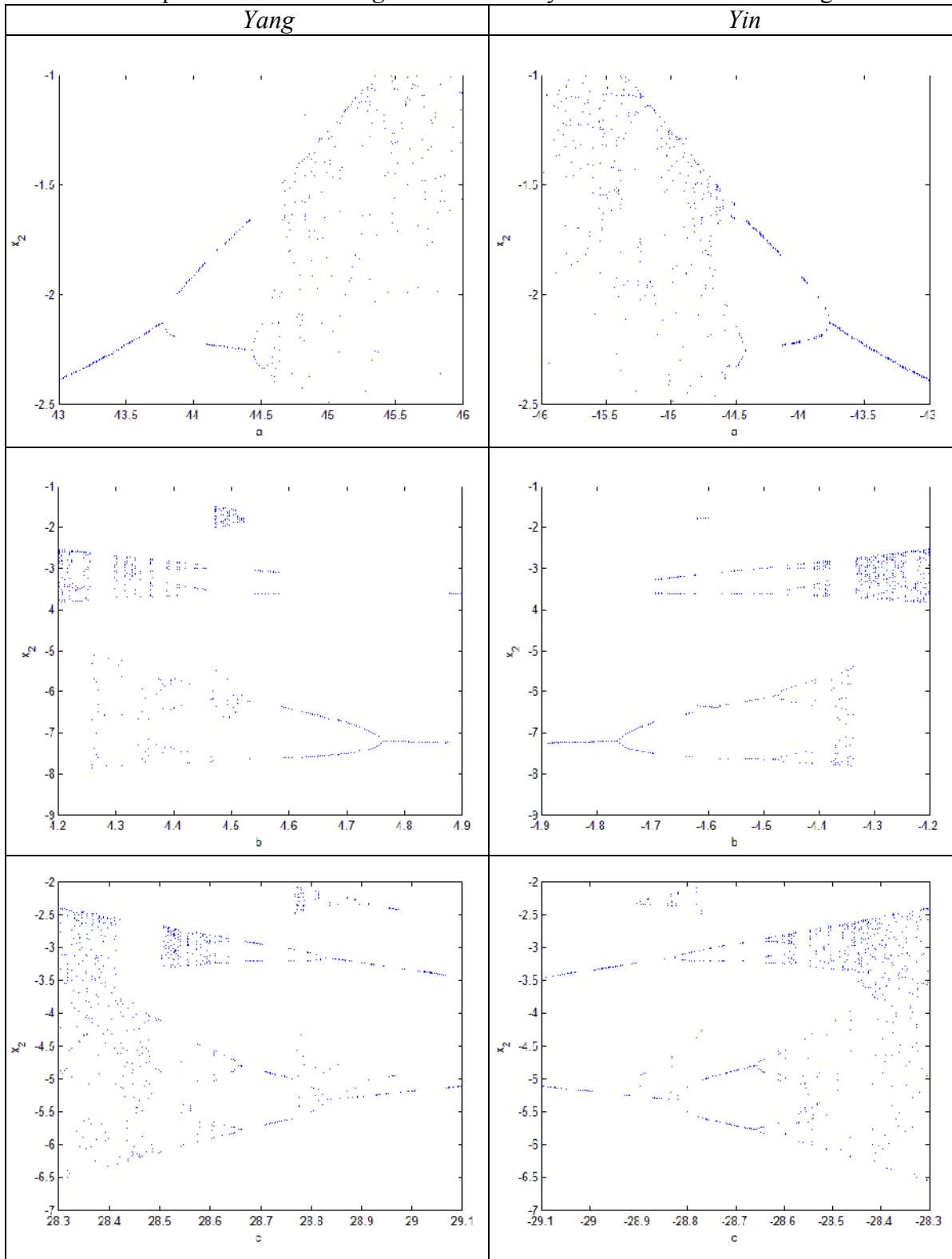
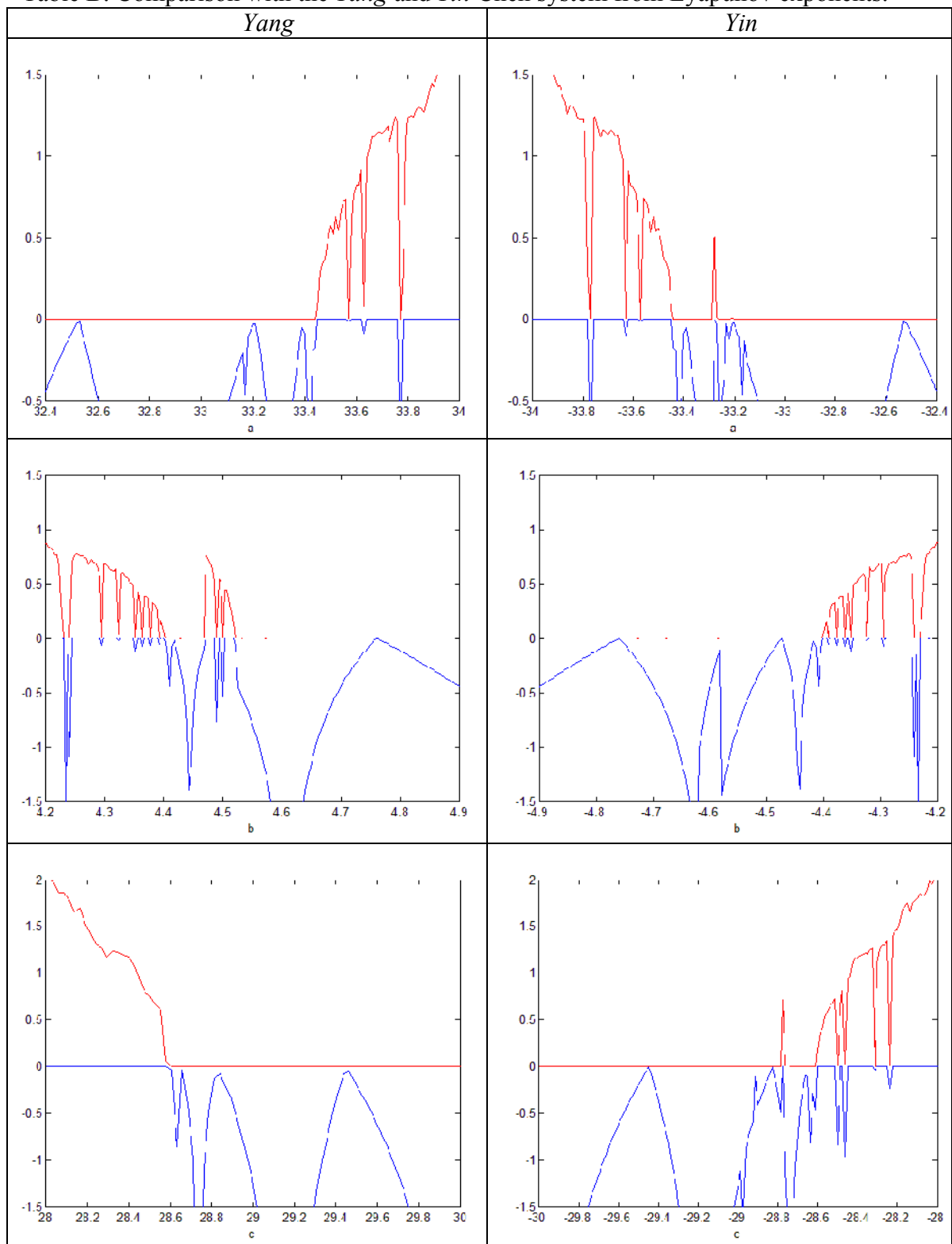


Table B. Comparison with the *Yang* and *Yin* Chen system from Lyapunov exponents.



Chapter 6

Historical Chaos and Yin-Yang Synchronization for Chaotic Chen Systems with Well Designed Active Control

6.1 Preliminaries

In this Chapter, the dynamic behaviors of *Yin* Chen systems is firstly studied. According to Chinese philosophy[40-42], the historical chaos of Chen system with “*Yin*” parameters is illustrated and compared with the contemporary Chen system with “*Yang*” parameters. We employ applicable coupling parameters by linear coupling strategy to complete the goal of generalized synchronization of *Yin* and *Yang* Chen systems. Simulation results are shown by phase portraits, time histories of states and Lyapunov exponents.



6.2 Generalized Yin-Yang Synchronization Strategy

Consider the following unidirectional coupled chaotic systems

$$\begin{cases} \frac{d\mathbf{x}(t)}{dt} = \mathbf{A}\mathbf{x}(t) + \mathbf{f}(t, \mathbf{x}(t)) \\ \frac{d\mathbf{y}(-t)}{d(-t)} = -\mathbf{A}\mathbf{y}(-t) + \mathbf{h}(t, \mathbf{y}(-t)) \end{cases} \quad (6.1)$$

where $\mathbf{x} = [x_1(t), x_2(t), \dots, x_n(t)]^T \in R^n$, $\mathbf{y} = [y_1(-t), y_2(-t), \dots, y_n(-t)]^T \in R^n$, and denote the master state vector and slave state vector respectively, $\mathbf{A} \in R^{n \times n}$ is constant matrix, \mathbf{f} and \mathbf{h} are nonlinear vector functions.

By means of the unidirectional linear coupling method, the slave system in Eq. (6.1) is described as follows:

$$\frac{d\mathbf{y}(-t)}{d(-t)} = -\mathbf{A}\mathbf{y}(-t) + \mathbf{h}(t, \mathbf{y}(-t)) + \mathbf{u}(t, \mathbf{x}(t), \mathbf{y}(-t)) \quad (6.2)$$

where $\mathbf{u}(t, \mathbf{x}(t), \mathbf{y}(-t))$ is a control term, and which is designed on next part subsequently.

The generalized synchronization can be accomplished when $t \rightarrow \pm\infty$, the limit of the error vector $\mathbf{e} = [e_1, e_2, \dots, e_n]^T$, where $e_i = y_i(-t) - x_i(t)$ approaches zero:

$$\lim_{t \rightarrow \pm\infty} \mathbf{e} = 0 \quad (6.3)$$

From (6.1) and (6.2), error equation of system can be acquired:

$$\begin{aligned} \dot{\mathbf{e}} &= -(-\mathbf{A}\mathbf{y}(-t) + \mathbf{h}(t, \mathbf{y}(-t)) + \mathbf{u}(t, \mathbf{x}(t), \mathbf{y}(-t))) - \mathbf{A}\mathbf{x}(t) - \mathbf{f}(t, \mathbf{x}(t)) \\ &= \mathbf{A}\mathbf{e} - \mathbf{h}(t, \mathbf{y}(-t)) - \mathbf{f}(t, \mathbf{x}(t)) - \mathbf{u}(t, \mathbf{x}(t), \mathbf{y}(-t)) \end{aligned} \quad (6.4)$$

where $\mathbf{e} = \mathbf{y}(-t) - \mathbf{x}(t)$

6.3 The Yang and Yin Chen systems

The *Yang* Chen system is described as follows:

$$\begin{cases} \frac{dx_1(t)}{dt} = a(x_2(t) - x_1(t)) \\ \frac{dx_2(t)}{dt} = (c - a)x_1(t) - x_1(t)x_3(t) + cx_2(t) \\ \frac{dx_3(t)}{dt} = x_1(t)x_2(t) - bx_3(t) \end{cases} \quad (6.5)$$

where initial condition $(x_1, x_2, x_3) = (2, 3.2, 1.5)$ and parameters $a = 35$, $b = 3$ and $c = 28$, can be called *Yang* parameters, and chaos of the *Yang* Chen system is appeared. The chaotic behavior of Eq. (6.5) and Lyapunov exponents are shown in Fig. 6.1.

Yin Chen equations are:

$$\begin{cases} \frac{dy_1(-t)}{d(-t)} = a_1(y_2(-t) - y_1(-t)) \\ \frac{dy_2(-t)}{d(-t)} = (c_1 - a_1)y_1(-t) - y_1(-t)y_3(-t) + c_1y_2(-t) \\ \frac{dy_3(-t)}{d(-t)} = y_1(-t)y_2(-t) - b_1y_3(-t) \end{cases} \quad (6.6)$$

where initial condition $(y_1, y_2, y_3) = (20, 120, 18)$ and parameters $a_1 = -35$, $b_1 = -3$ and

$c_1 = -28$, chaos of the *Yin* Chen system is found. Consequently, we can describe these parameters as *Yin* parameters. *Yin* and *Yang* are two fundamental opposites in Chinese philosophy. The phase portrait and Lyapunov exponent of historical Chen system are revealed in Fig. 6.2.

6.4 Numerical Simulations

In this Section, to study the difference between *Yang* and *Yin* Chen systems, we used following four cases:

CASE I. Based on unidirectional linear coupling method, the slave system of Eq. (6.6) is reconstructed as follows:

$$\begin{cases} \frac{dy_1(-t)}{d(-t)} = a_1(y_2(-t) - y_1(-t)) + k(y_1(-t) - x_1(t)) \\ \frac{dy_2(-t)}{d(-t)} = (c_1 - a_1)y_1(-t) - y_1(-t)y_3(-t) + c_1y_2(-t) + k(y_2(-t) - x_2(t)) \\ \frac{dy_3(-t)}{d(-t)} = y_1(-t)y_2(-t) - b_1y_3(-t) + k(y_3(-t) - x_3(t)) \end{cases} \quad (6.7)$$

where k is gain of controllers.

The generalized synchronization error function is $e_i = y_i(-t) - x_i(t)$, $i = 1, 2, 3$.

$$\begin{cases} e_1 = y_1(-t) - x_1(t) \\ e_2 = y_2(-t) - x_2(t) \\ e_3 = y_3(-t) - x_3(t) \end{cases} \quad (6.8)$$

And then

$$\lim_{t \rightarrow \infty} e_i = \lim_{t \rightarrow \infty} (y_i(-t) - x_i(t)) = 0, \quad i = 1, 2, 3 \quad (6.9)$$

The error dynamics becomes

$$\left\{ \begin{aligned}
\dot{e}_1 &= \frac{dy_1(-t)}{dt} - \frac{dx_1(t)}{dt} = -\frac{dy_1(-t)}{d(-t)} - \frac{dx_1(t)}{dt} = -(a_1(y_2(-t) - y_1(-t)) \\
&\quad + k(y_1(-t) - x_1(t))) \\
&\quad - a(x_2(t) - x_1(t)) \\
\dot{e}_2 &= \frac{dy_2(-t)}{dt} - \frac{dx_2(t)}{dt} = -\frac{dy_2(-t)}{d(-t)} - \frac{dx_2(t)}{dt} = -((c_1 - a_1)y_1(-t) - y_1(-t)y_3(-t) \\
&\quad + c_1y_2(-t) + k(y_2(-t) - x_2(t))) \\
&\quad - ((c - a)x_1(t) - x_1(t)x_3(t) + cx_2(t)) \\
\dot{e}_3 &= \frac{dy_3(-t)}{dt} - \frac{dx_3(t)}{dt} = -\frac{dy_3(-t)}{d(-t)} - \frac{dx_3(t)}{dt} = -(y_1(-t)y_2(-t) - b_1y_3(-t) \\
&\quad + k(y_3(-t) - x_3(t))) \\
&\quad - (x_1(t)x_2(t) - bx_3(t))
\end{aligned} \right. \quad (6.10)$$

Let initial condition $(x_1, x_2, x_3) = (2, 3.2, 1.5)$, $(y_1, y_2, y_3) = (20, 120, 18)$, parameters

$a = 35, b = 3, c = 28, a_1 = -35, b_1 = -3, c_1 = -28$, gain $k = 3200$, and we can find out

that the error dynamics behaviors as shown in Figs. 6.3-5. Three error states versus time and time histories of states are shown in Figs. 6.6-7.

CASE II. The slave system of Eq. (6.6) is described as follows:

$$\left\{ \begin{aligned}
\frac{dy_1(-t)}{d(-t)} &= a_1(y_2(-t) - y_1(-t)) + k(y_1(-t) - x_1(t)) + y_3^2(-t) \\
\frac{dy_2(-t)}{d(-t)} &= (c_1 - a_1)y_1(-t) - y_1(-t)y_3(-t) + c_1y_2(-t) + k(y_2(-t) - x_2(t)) + \sin^2 x_1(t) \\
\frac{dy_3(-t)}{d(-t)} &= y_1(-t)y_2(-t) - b_1y_3(-t) + k(y_3(-t) - x_3(t)) + y_3^2(-t)
\end{aligned} \right. \quad (6.11)$$

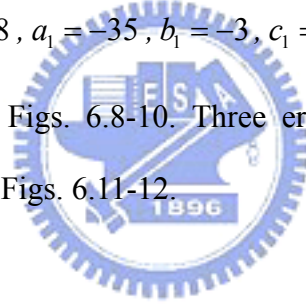
The error dynamics becomes

$$\left\{ \begin{aligned}
\dot{e}_1 &= \frac{dy_1(-t)}{dt} - \frac{dx_1(t)}{dt} = -\frac{dy_1(-t)}{d(-t)} - \frac{dx_1(t)}{dt} = -(a_1(y_2(-t) - y_1(-t))) \\
&\quad + k(y_1(-t) - x_1(t)) + x_3^2(t) \\
&\quad - a(x_2(t) - x_1(t)) \\
\dot{e}_2 &= \frac{dy_2(-t)}{dt} - \frac{dx_2(t)}{dt} = -\frac{dy_2(-t)}{d(-t)} - \frac{dx_2(t)}{dt} = -((c_1 - a_1)y_1(-t) - y_1(-t)y_3(-t)) \\
&\quad + c_1y_2(-t) + k(y_2(-t) - x_2(t)) \\
&\quad + \sin^2 x_1(t) \\
&\quad - ((c - a)x_1(t) - x_1(t)x_3(t) + cx_2(t)) \\
\dot{e}_3 &= \frac{dy_3(-t)}{dt} - \frac{dx_3(t)}{dt} = -\frac{dy_3(-t)}{d(-t)} - \frac{dx_3(t)}{dt} = -(y_1(-t)y_2(-t) - b_1y_3(-t)) \\
&\quad + k(y_3(-t) - x_3(t)) + x_1^2(t) \\
&\quad - (x_1(t)x_2(t) - bx_3(t))
\end{aligned} \right. \quad (6.12)$$

where initial condition $(x_1, x_2, x_3) = (2, 3.2, 1.5)$, $(y_1, y_2, y_3) = (20, 120, 18)$,

parameters $a = 35$, $b = 3$, $c = 28$, $a_1 = -35$, $b_1 = -3$, $c_1 = -28$, gain $k = 3100$, and the

error dynamics are shown in Figs. 6.8-10. Three error states versus time and time histories of states are shown in Figs. 6.11-12.



CASE III. The slave system of Eq. (6.6) is defined by following equations:

$$\left\{ \begin{aligned}
\frac{dy_1(-t)}{d(-t)} &= a_1(y_2(-t) - y_1(-t)) + k(y_1(-t) - x_1(t)) + \delta(x_3(t) - 2y_3(-t)) \\
\frac{dy_2(-t)}{d(-t)} &= (c_1 - a_1)y_1(-t) - y_1(-t)y_3(-t) + c_1y_2(-t) + k(y_2(-t) - x_2(t)) \\
&\quad + \delta \cos^2 y_1(-t) \\
\frac{dy_3(-t)}{d(-t)} &= y_1(-t)y_2(-t) - b_1y_3(-t) + k(y_3(-t) - x_3(t)) + \delta(x_3(t) - 2y_3(-t))
\end{aligned} \right. \quad (6.13)$$

The error dynamics becomes

$$\left\{ \begin{aligned}
\dot{e}_1 &= \frac{dy_1(-t)}{dt} - \frac{dx_1(t)}{dt} = -\frac{dy_1(-t)}{d(-t)} - \frac{dx_1(t)}{dt} = -(a_1(y_2(-t) - y_1(-t)) \\
&\quad + k(y_1(-t) - x_1(t)) \\
&\quad + \delta(x_3(t) - 2y_3(-t))) \\
&\quad - a(x_2(t) - x_1(t)) \\
\dot{e}_2 &= \frac{dy_2(-t)}{dt} - \frac{dx_2(t)}{dt} = -\frac{dy_2(-t)}{d(-t)} - \frac{dx_2(t)}{dt} = -((c_1 - a_1)y_1(-t) - y_1(-t)y_3(-t) \\
&\quad + c_1y_2(-t) + k(y_2(-t) - x_2(t)) \\
&\quad + \delta \cos^2 y_1(-t)) \\
&\quad - ((c - a)x_1(t) - x_1(t)x_3(t) + cx_2(t)) \\
\dot{e}_3 &= \frac{dy_3(-t)}{dt} - \frac{dx_3(t)}{dt} = -\frac{dy_3(-t)}{d(-t)} - \frac{dx_3(t)}{dt} = -(y_1(-t)y_2(-t) - b_1y_3(-t) \\
&\quad + k(y_3(-t) - x_3(t))) \\
&\quad + \delta(x_3(t) - 2y_3(-t)) \\
&\quad - (x_1(t)x_2(t) - bx_3(t))
\end{aligned} \right. \quad (6.14)$$

where initial condition $(x_1, x_2, x_3) = (2, 3.2, 1.5)$, $(y_1, y_2, y_3) = (20, 120, 18)$, parameters $a = 35$, $b = 3$, $c = 28$, $a_1 = -35$, $b_1 = -3$, $c_1 = -28$, gain $k = 2700$, control gain $\delta = 1.8$, and phase portraits of the error dynamics are shown in Figs. 6.13-15. Three error states versus time and time histories of states are exhibited in Figs. 6.16-17.

CASE IV. According to unidirectional linear coupling, the slave system of Eq. (6.6) is described as follows:

$$\left\{ \begin{aligned}
\frac{dy_1(-t)}{d(-t)} &= a_1(y_2(-t) - y_1(-t)) + k \sin(y_1(-t) - x_1(t)) \\
\frac{dy_2(-t)}{d(-t)} &= (c_1 - a_1)y_1(-t) - y_1(-t)y_3(-t) + c_1y_2(-t) + k \sin(y_2(-t) - x_2(t)) \\
\frac{dy_3(-t)}{d(-t)} &= y_1(-t)y_2(-t) - b_1y_3(-t) + k \sin(y_3(-t) - x_3(t))
\end{aligned} \right. \quad (6.15)$$

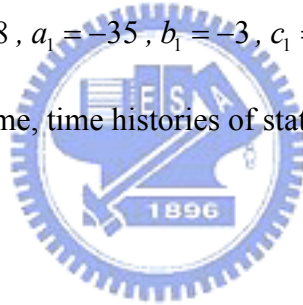
The error dynamics becomes

$$\left\{ \begin{aligned}
\dot{e}_1 &= \frac{dy_1(-t)}{dt} - \frac{dx_1(t)}{dt} = -\frac{dy_1(-t)}{d(-t)} - \frac{dx_1(t)}{dt} = -(a_1(y_2(-t) - y_1(-t))) \\
&\quad + k \sin(y_1(-t) - x_1(t)) \\
&\quad - a(x_2(t) - x_1(t)) \\
\dot{e}_2 &= \frac{dy_2(-t)}{dt} - \frac{dx_2(t)}{dt} = -\frac{dy_2(-t)}{d(-t)} - \frac{dx_2(t)}{dt} = -((c_1 - a_1)y_1(-t) - y_1(-t)y_3(-t)) \\
&\quad + c_1 y_2(-t) + k \sin(y_2(-t) - x_2(t)) \\
&\quad - ((c - a)x_1(t) - x_1(t)x_3(t) + cx_2(t)) \\
\dot{e}_3 &= \frac{dy_3(-t)}{dt} - \frac{dx_3(t)}{dt} = -\frac{dy_3(-t)}{d(-t)} - \frac{dx_3(t)}{dt} = -(y_1(-t)y_2(-t) - b_1 y_3(-t)) \\
&\quad + k \sin(y_3(-t) - x_3(t)) \\
&\quad - (x_1(t)x_2(t) - bx_3(t))
\end{aligned} \right. \quad (6.16)$$

where initial condition $(x_1, x_2, x_3) = (2, 3.2, 1.5)$, $(y_1, y_2, y_3) = (20, 120, 18)$,

parameters $a = 35$, $b = 3$, $c = 28$, $a_1 = -35$, $b_1 = -3$, $c_1 = -28$, $k = 2900$, and the error

dynamics, error states versus time, time histories of states are shown in Figs. 6.18-20.



6.5 Summary

In this Chapter, *Yin* chaos and *Yin-Yang* generalized synchronization are investigated for Chen system via four numerical simulation examples. The synchronization is researched by two coupled chaotic systems with a unidirectional linear error coupling. To choose an applicable gain parameters by linear coupling method achieves the goal of generalized synchronization is the key note. We found that coupled chaotic systems with constant coupling parameters in *Case I-III* can achieve synchronized, and with function coupling in *Case IV* can only complete the target of generalized synchronization. This papers explores the relationship between the past and present scopes for chaos study, and investigates its error dynamics behaviors for generalized synchronization .

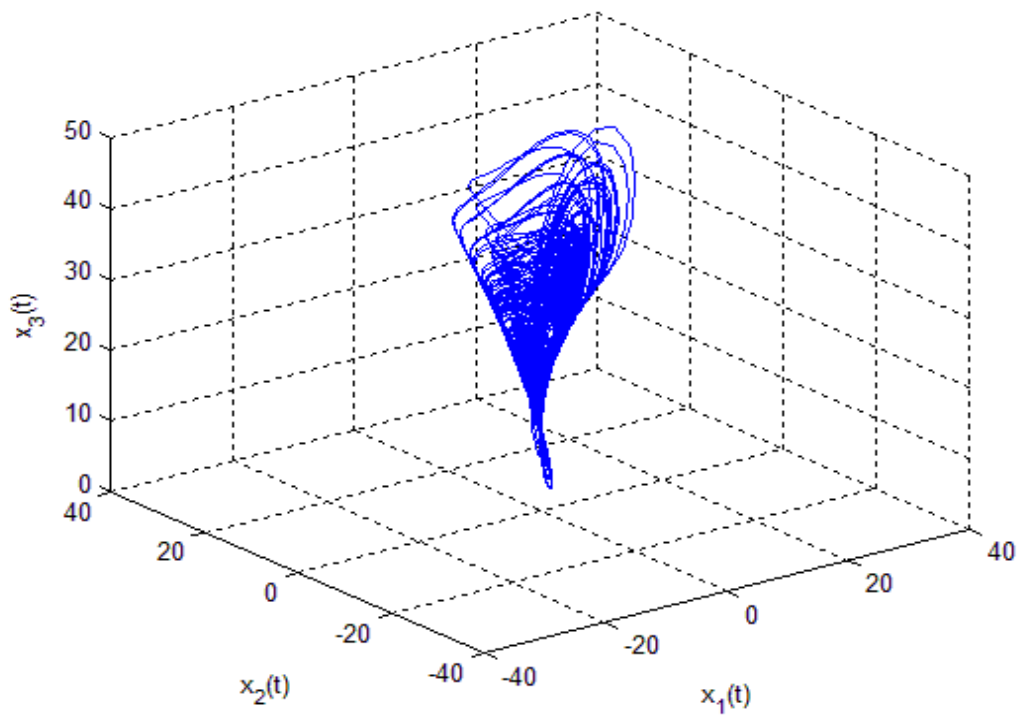


Fig. 6.1 Phase portrait of *Yang* Chen system with $a=35$, $b=3$, and $c=28$.

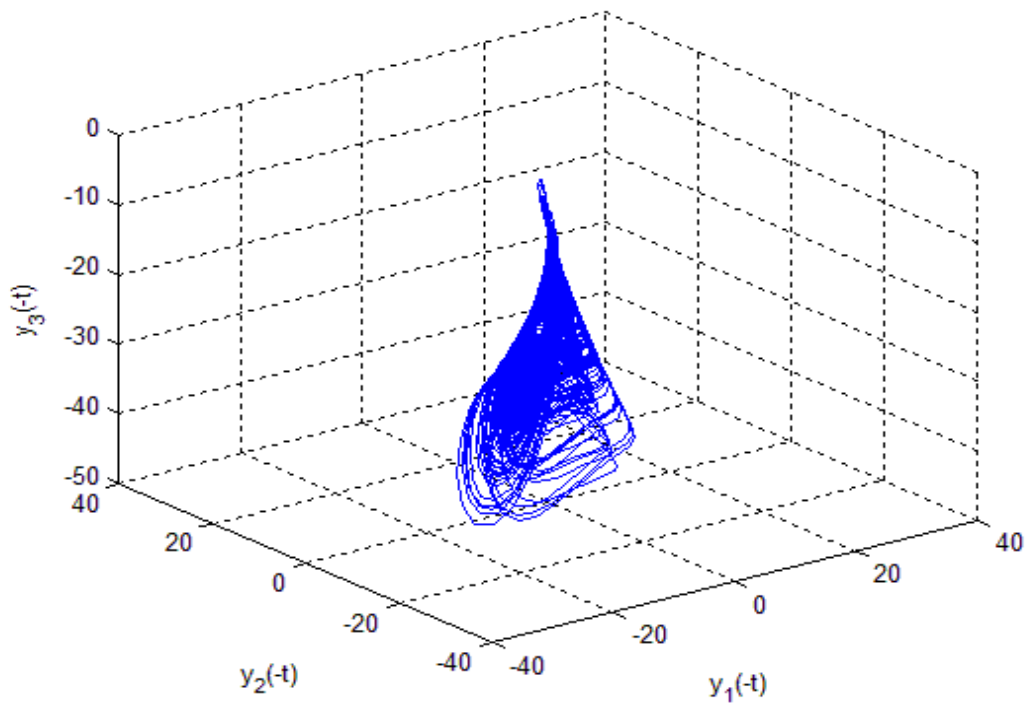


Fig. 6.2 Phase portrait of *Yin* Chen system with $a_1 = -35$, $b_1 = -3$ and $c_1 = -28$.

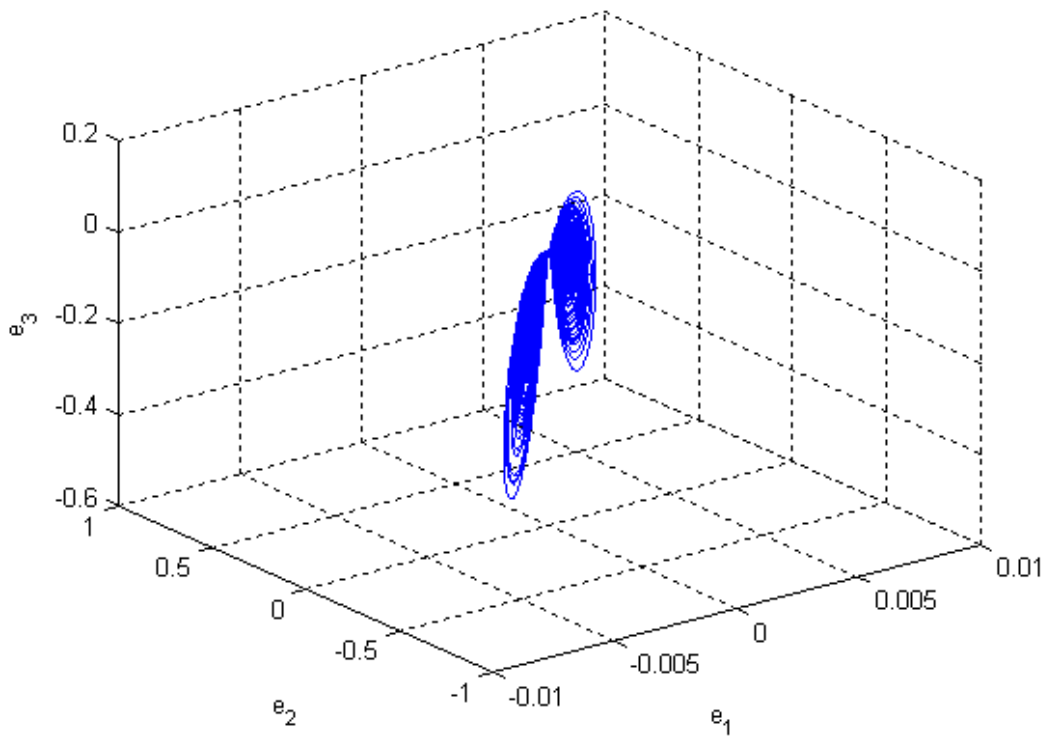


Fig. 6.3 Phase portrait of three errors dynamics with $k = 3200$ for *Case I*.

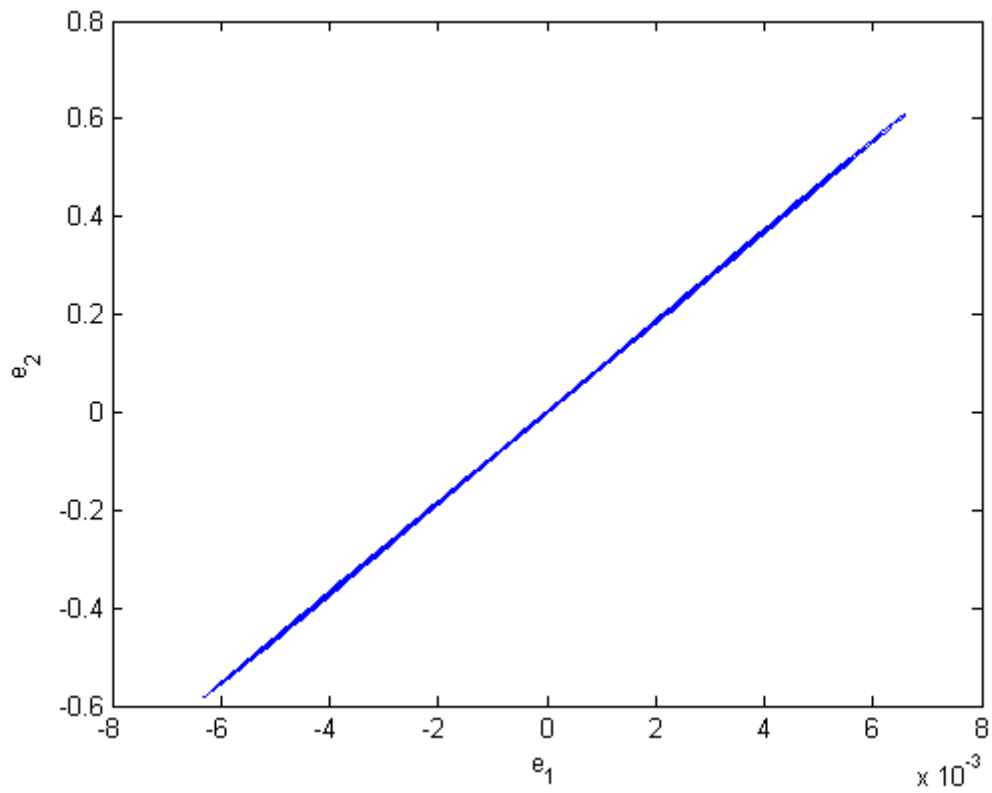


Fig. 6.4 Phase portrait of errors dynamics (e_1 & e_2) with $k = 3200$ for *Case I*.

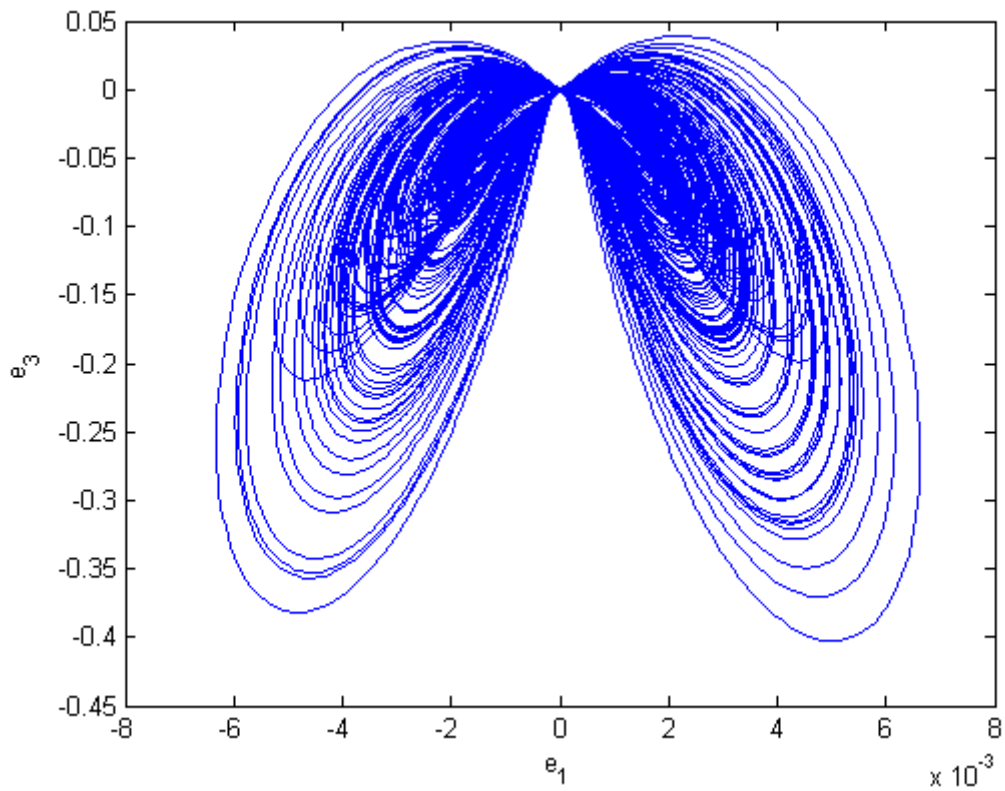


Fig. 6.5 Phase portrait of errors dynamics (e_1 & e_3) with $k = 3200$ for *Case I*.

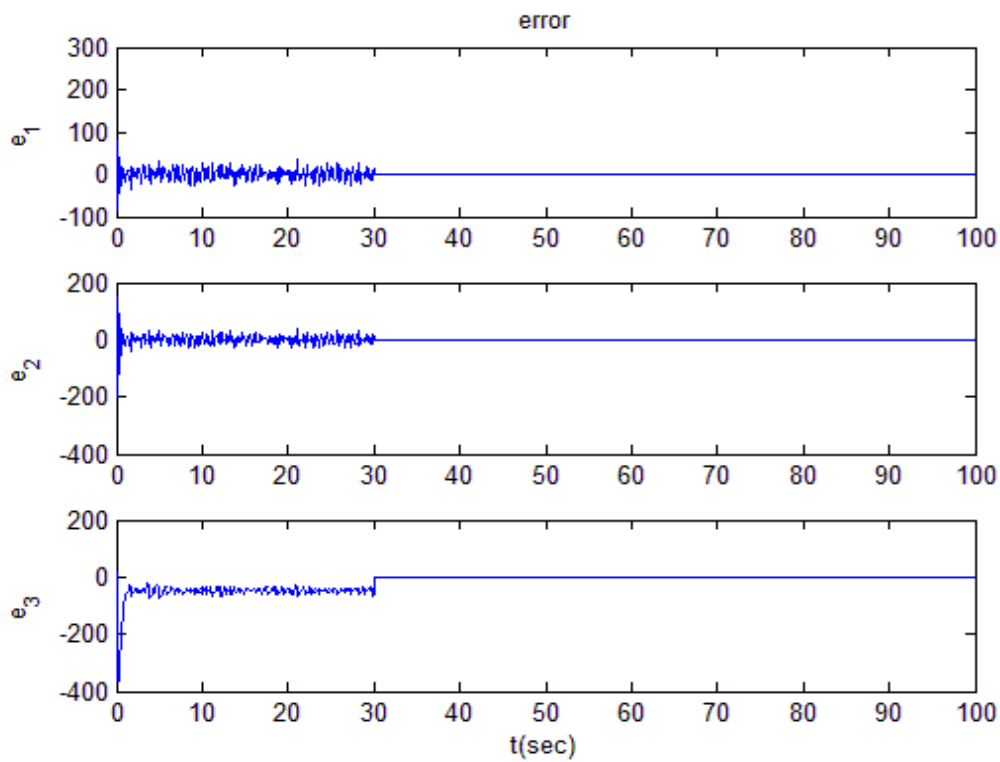


Fig. 6.6 Time histories of errors with $k = 3200$ for *Case I*.

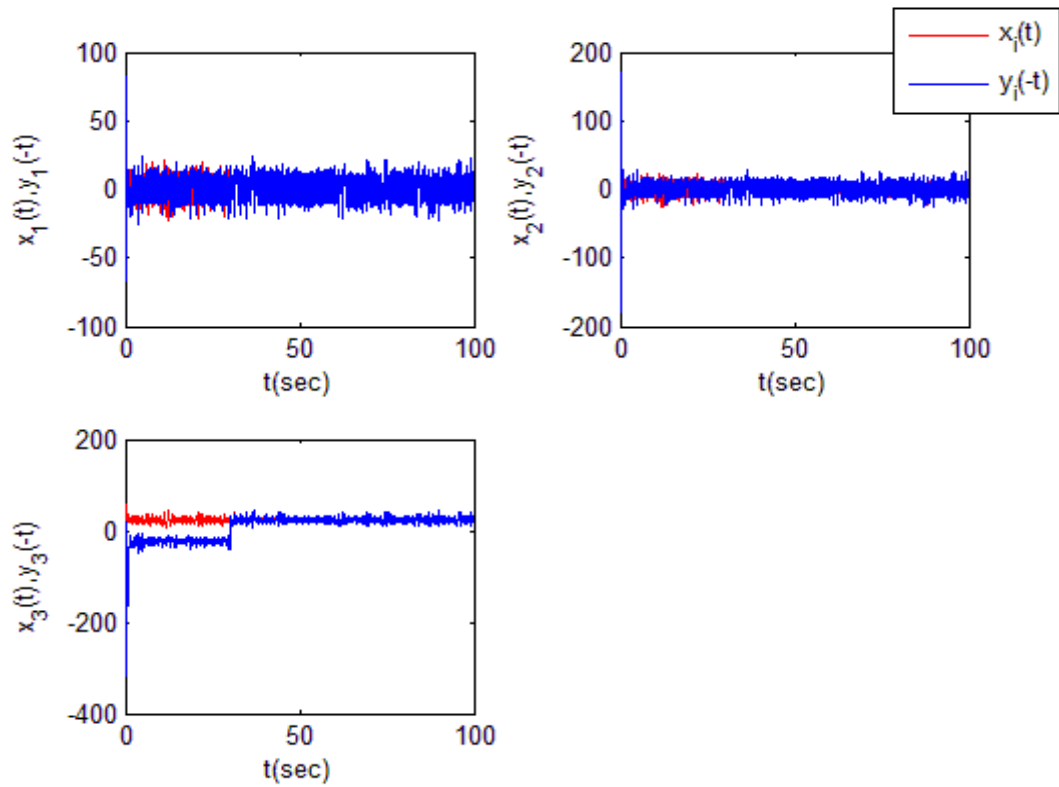


Fig. 6.7 Time histories of x_i versus y_i with $k = 3200$ for *Case I*.

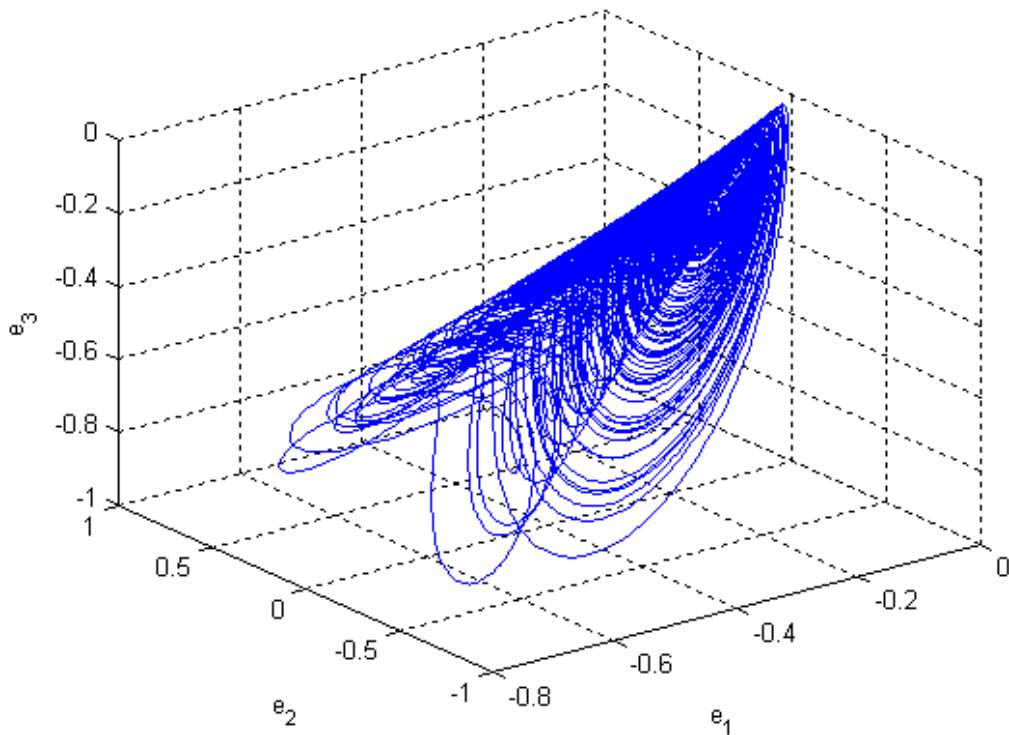


Fig. 6.8 Phase portrait of three errors dynamics with $k = 3100$ for *Case II*.

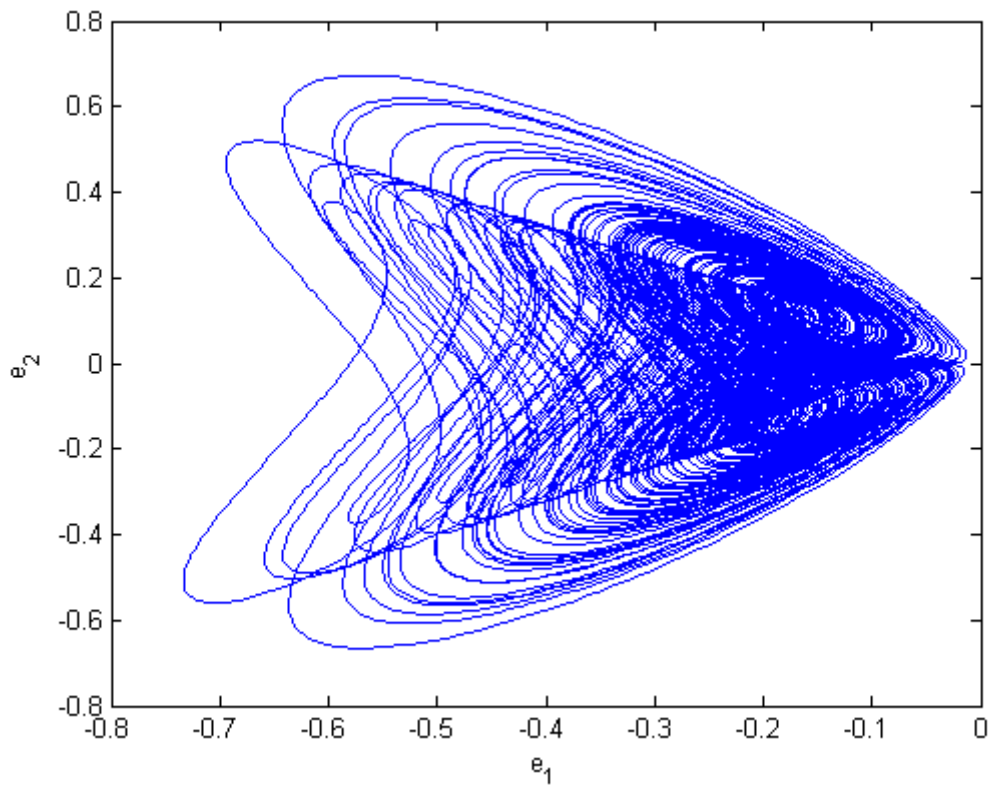


Fig. 6.9 Phase portrait of errors dynamics (e_1 & e_2) with $k = 3100$ for *Case II*.

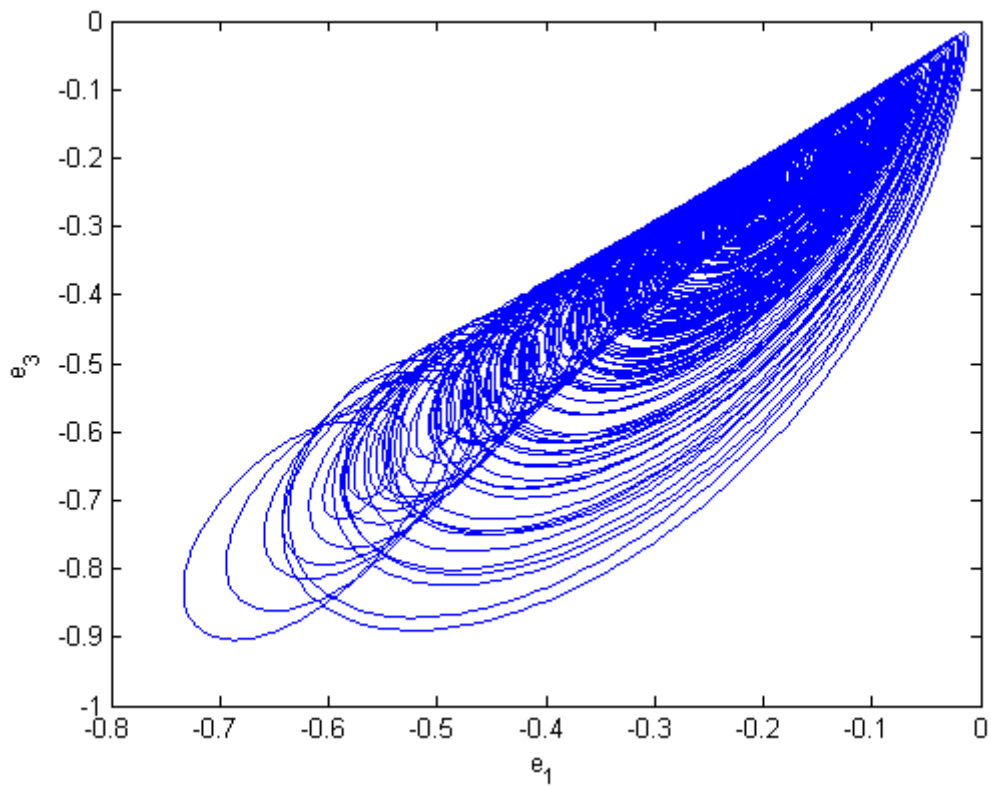


Fig. 6.10 Phase portrait of errors dynamics (e_1 & e_3) with $k = 3100$ for *Case II*.

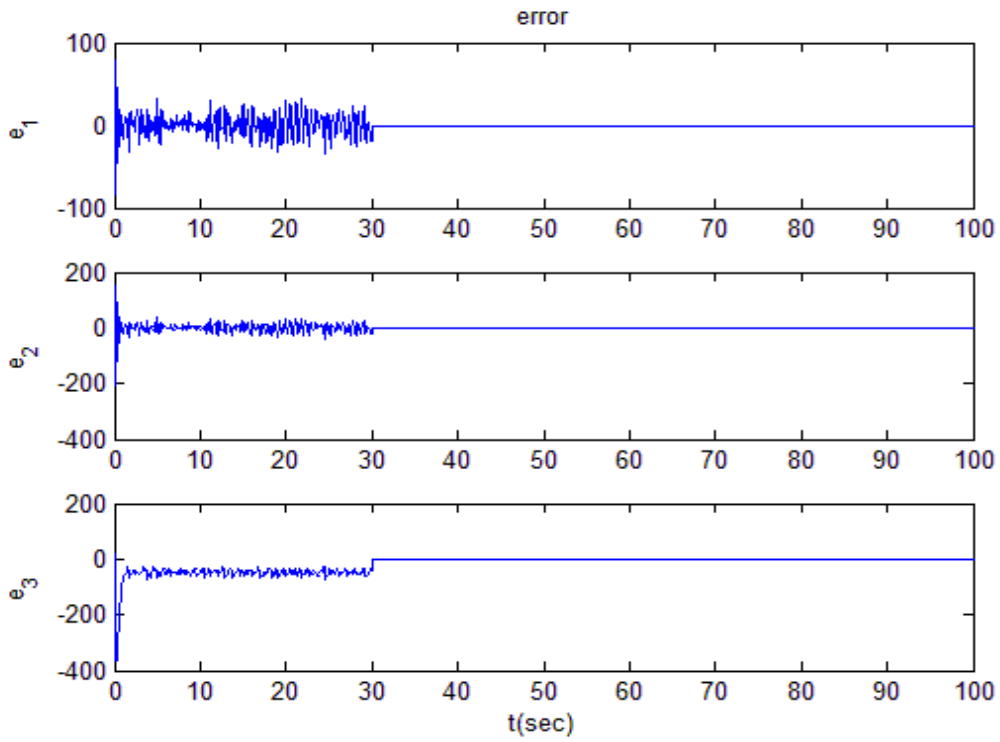


Fig. 6.11 Time histories of errors with $k = 3100$ for *Case II*.

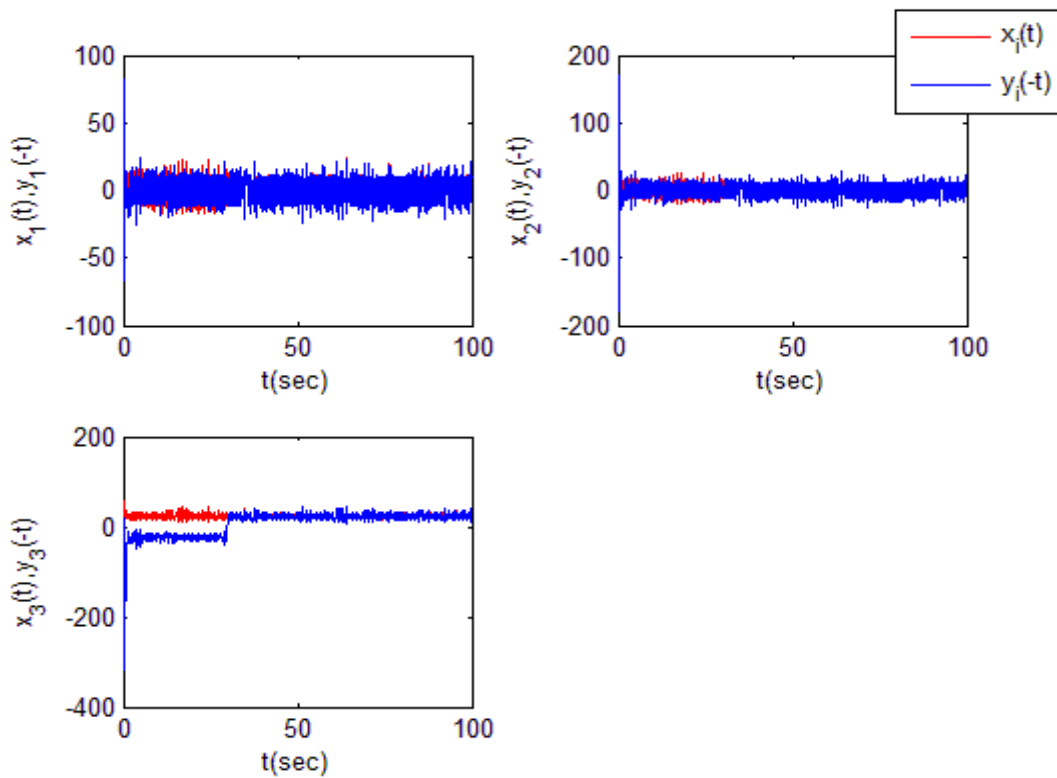


Fig. 6.12 Time histories of x_i versus y_i with $k = 3100$ for *Case II*.

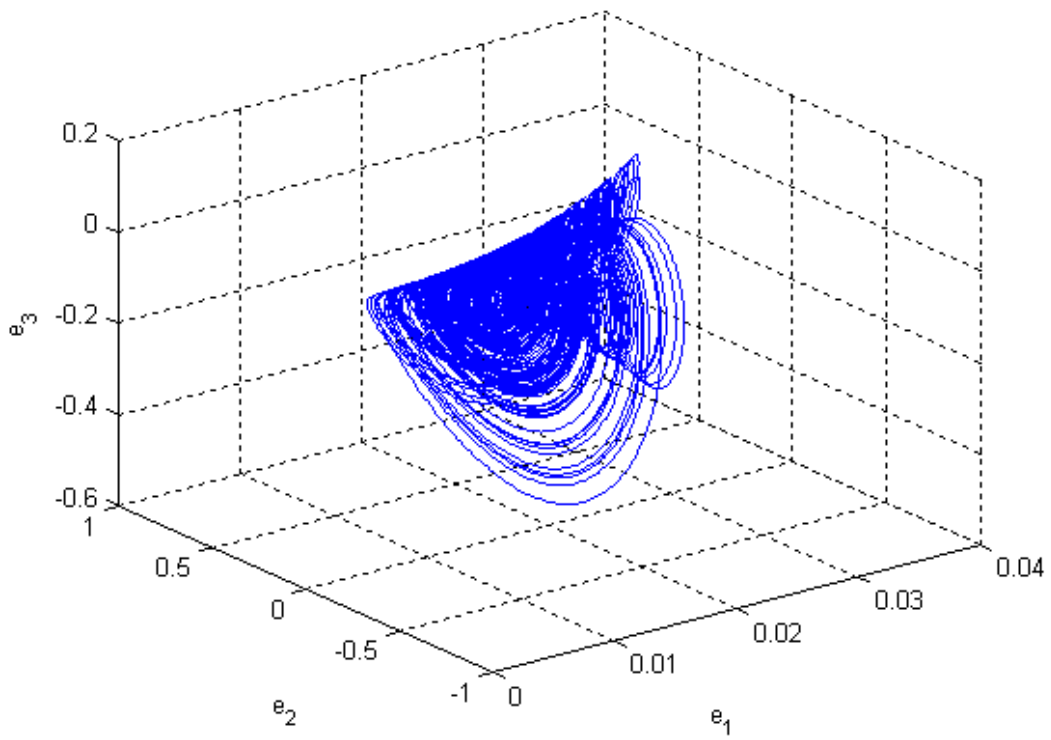


Fig. 6.13 Phase portrait of three errors dynamics with $k = 2700$ for *Case III*.

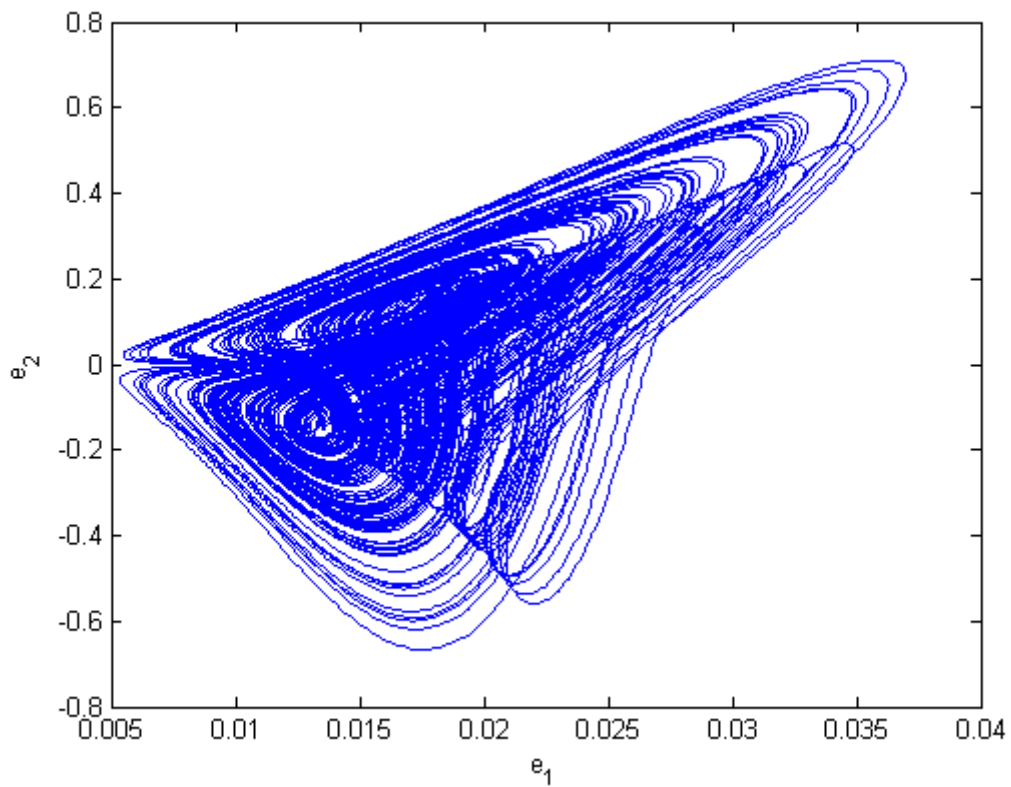


Fig. 6.14 Phase portraits of errors dynamics (e_1 & e_2) with $k = 2700$ for *Case III*.

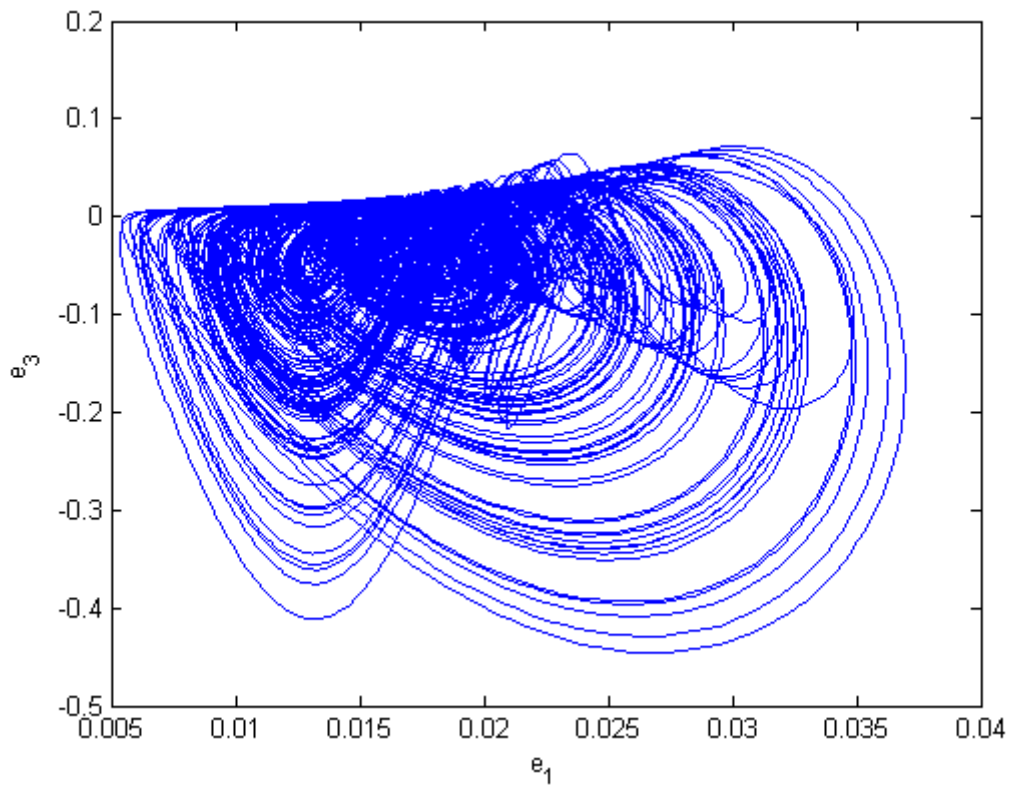


Fig. 6.15 Phase portraits of errors dynamics (e_1 & e_3) with $k = 2700$ for *Case III*.

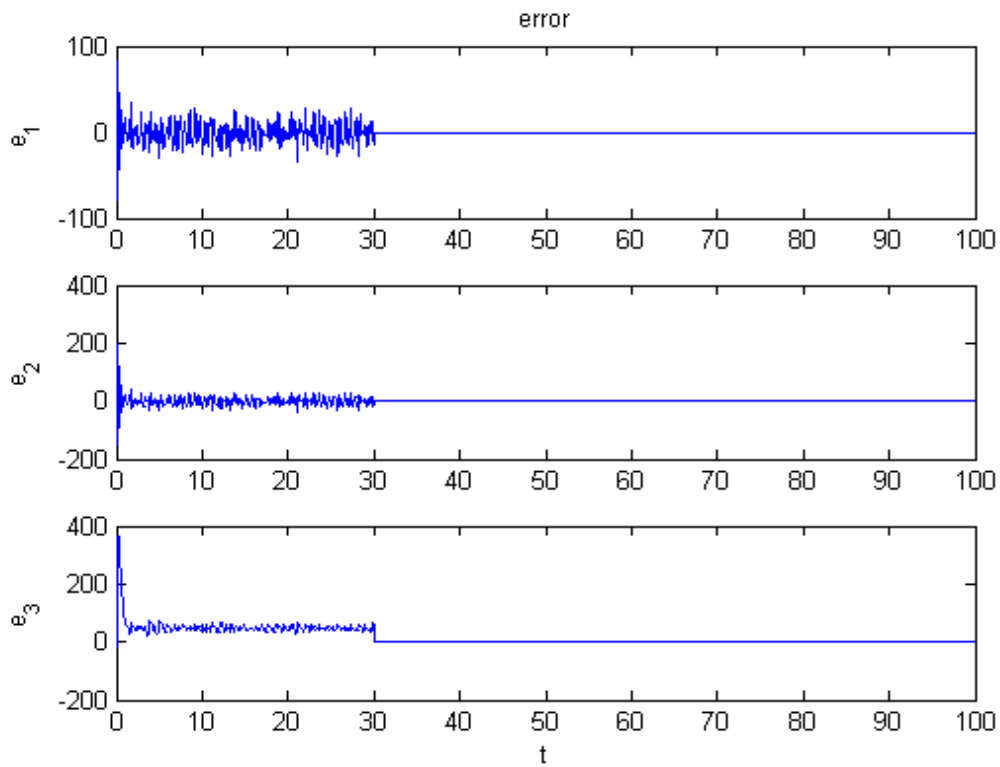


Fig. 6.16 Time histories of errors with $k = 2700$ for *Case III*.

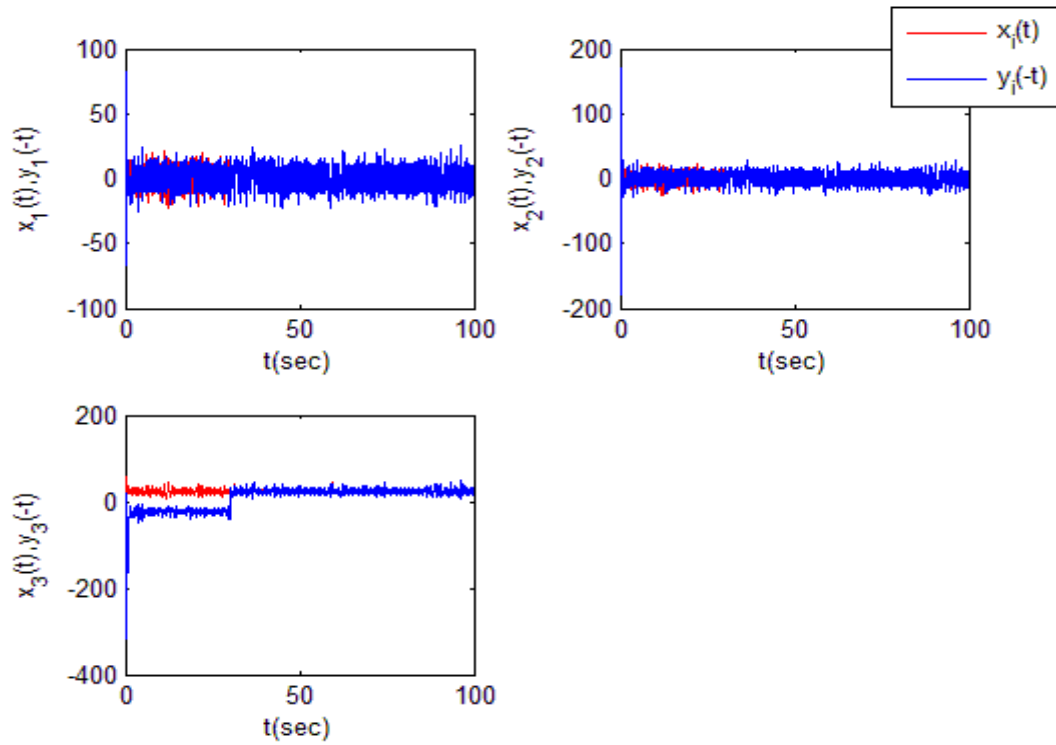


Fig. 6.17 Time histories of x_i versus y_i with $k = 2700$ for *Case III*.

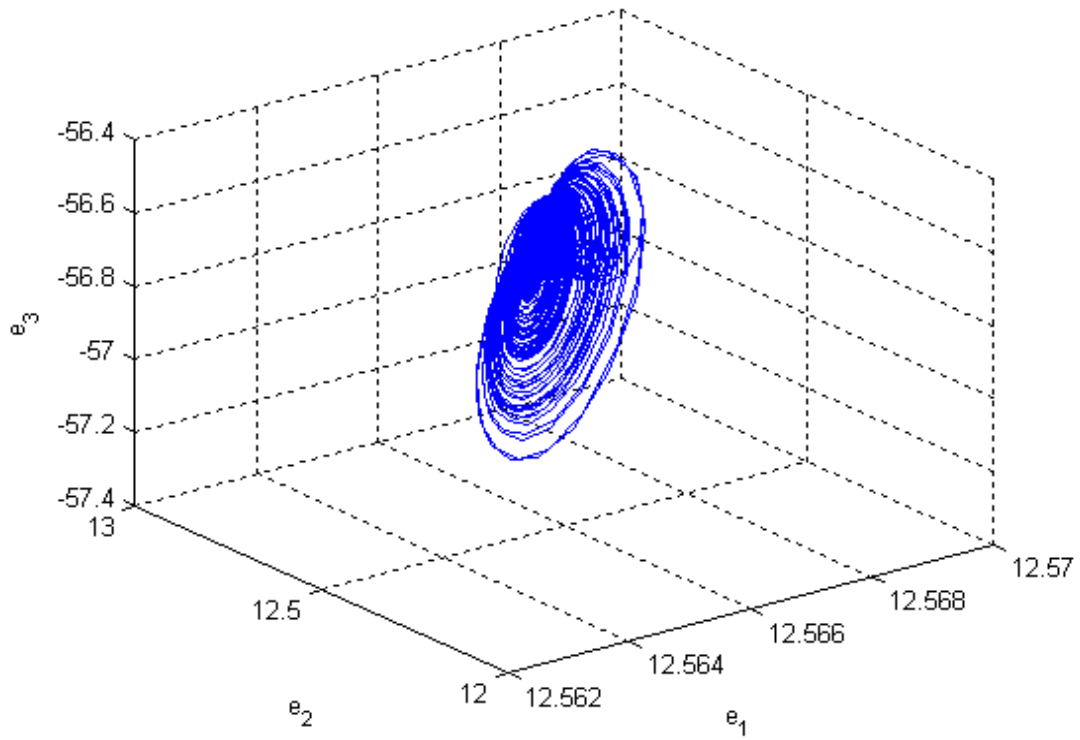


Fig. 6.18 Phase portraits of three errors dynamics with $k = 2900$ for *Case IV*.

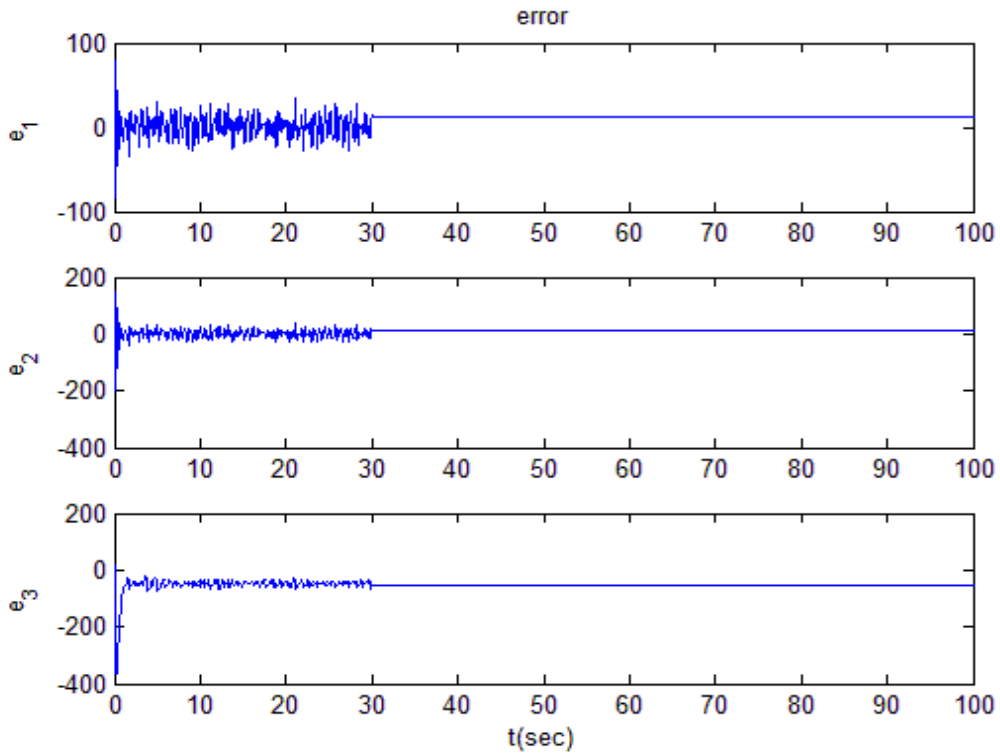


Fig. 6.19 Time histories of errors with $k = 2900$ for *Case IV*.

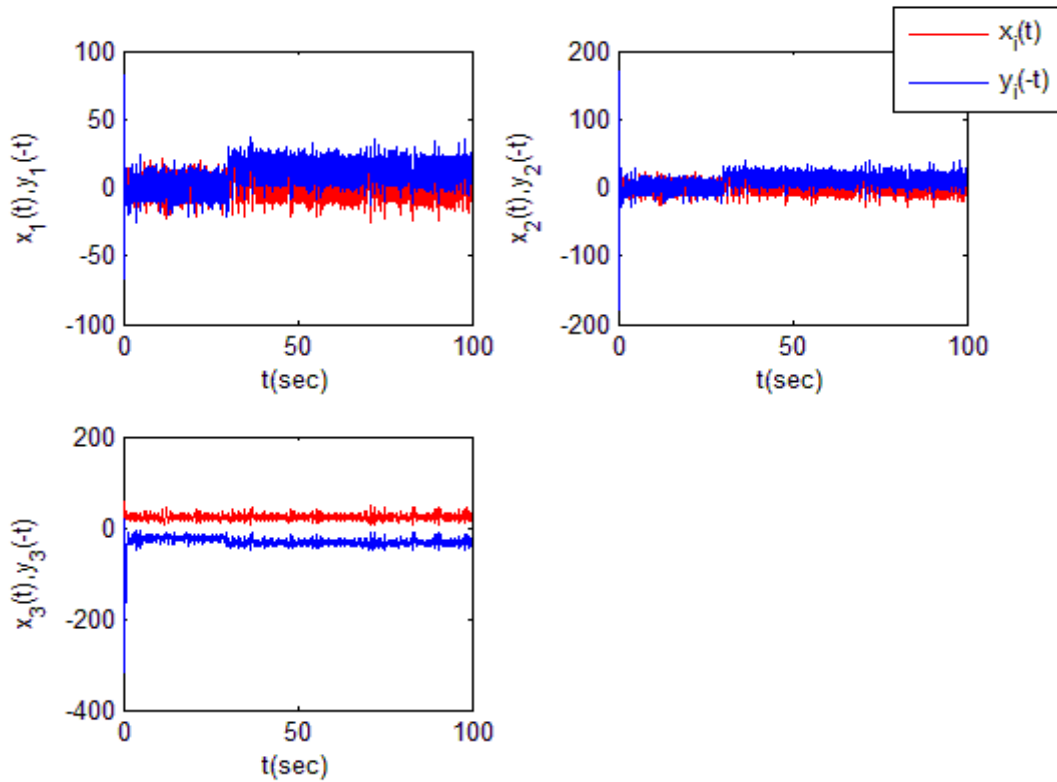


Fig. 6.20 Time histories of x_i versus y_i with $k = 2900$ for *Case IV*.

Chapter 7

Pragmatical Generalized Yin-Yang Synchronization for Chaotic Chen System by Adaptive Control

7.1 Preliminaries

In this Chapter, we study chaos synchronization of historical and contemporary Chen systems. In ancient Chinese philosophy, the historical chaos of Chen system with “*Yin*”, i.e. negative, parameters may be explained and compared with the chaos of the contemporary Chen system with “*Yang*”, i.e. positive, parameters. For simplicity, the former is termed as *Yin* Chen system and the later as *Yang* Chen system. We take advantage of using an adaptive *Yin-Yang* chaos synchronization of *Yin* and *Yang* Chen systems by pragmatical asymptotically stability theorem. This pragmatical adaptive synchronization of two chaotic systems of which one has uncertain parameters the another has estimated parameters, is achieved by pragmatical asymptotically stability theorem. In conclusion, three numerical cases are shown.

7.2 Pragmatical generalized Yin-Yang synchronization scheme by adaptive control

Consider the following two nonlinear chaotic systems,

$$\begin{cases} \frac{d\mathbf{x}(t)}{dt} = \mathbf{A}\mathbf{x}(t) + \mathbf{f}(\mathbf{x}(t), \mathbf{B}) \\ \frac{d\mathbf{y}(-t)}{d(-t)} = \mathbf{A}_1\mathbf{y}(-t) + \mathbf{g}(\mathbf{y}(-t), \mathbf{B}_1) + u(t) \end{cases} \quad (7.1)$$

where $\mathbf{x}(t) = [x_1(t), x_2(t), \dots, x_n(t)]^T \in R^n$, $\mathbf{y}(-t) = [y_1(-t), y_2(-t), \dots, y_n(-t)]^T \in R^n$, and denote the master state vector and slave state vector respectively, $\mathbf{A}, \mathbf{A}_1 \in R^{n \times n}$ are

uncertain and estimated coefficient matrices, f and g are nonlinear vector functions, \mathbf{B}, \mathbf{B}_1 are uncertain and estimated coefficient vectors in f and g , and $\mathbf{u}(t) = [u_1, u_2, \dots, u_n]^T \in R^n$ is a control input vector.

Our goal is to design a controller $\mathbf{u}(t)$ so that the state vector of slave system asymptotically approaches the state vector of the master system plus a given chaotic vector function $\mathbf{F}(t) = [F_1(t), F_2(t), \dots, F_n(t)]^T$. This is a special kind of generalized synchronization called generalized *Yin-Yang* synchronization:

$$\mathbf{y}(-t) = \mathbf{G}(\mathbf{x}(t), t) = \mathbf{x}(t) + \mathbf{F}(t) \quad (7.2)$$

The chaotic system which affords $\mathbf{F}(t)$ is called a given system. The synchronization is accomplished when $t \rightarrow \infty$, the limit of the error vector $\mathbf{e}(t) = [e_1, e_2, \dots, e_n]^T$

approaches zero:

$$\lim_{t \rightarrow \infty} \mathbf{e}(t) = 0 \quad (7.3)$$

where

$$\mathbf{e}(t) = \mathbf{x}(t) - \mathbf{y}(-t) + \mathbf{F}(t) \quad (7.4)$$

From Eq. (7.4) we have

$$\begin{aligned} \frac{d\mathbf{e}(t)}{dt} &= \frac{d\mathbf{x}(t)}{dt} - \frac{d\mathbf{y}(-t)}{dt} + \frac{d\mathbf{F}(t)}{dt} \\ &= \frac{d\mathbf{x}(t)}{dt} + \frac{d\mathbf{y}(-t)}{d(-t)} + \frac{d\mathbf{F}(t)}{dt} \end{aligned} \quad (7.5)$$

$$\dot{\mathbf{e}}(t) = \mathbf{A}\mathbf{x}(t) + \mathbf{f}(\mathbf{x}(t), \mathbf{B}) + (\mathbf{A}_1\mathbf{y}(-t) + \mathbf{g}(\mathbf{y}(-t), \mathbf{B}_1) + \mathbf{u}(t)) + \dot{\mathbf{F}}(t) \quad (7.6)$$

A Lyapunov function $V(\mathbf{e}, \tilde{\mathbf{A}}, \tilde{\mathbf{B}})$ is chosen as a positive definite function

$$V(\mathbf{e}, \tilde{\mathbf{A}}, \tilde{\mathbf{B}}) = \frac{1}{2} \mathbf{e}^T \mathbf{e} + \frac{1}{2} \tilde{\mathbf{A}}^T \tilde{\mathbf{A}} + \frac{1}{2} \tilde{\mathbf{B}}^T \tilde{\mathbf{B}} \quad (7.7)$$

where $\tilde{\mathbf{A}} = \mathbf{A} - \mathbf{A}_1$, $\tilde{\mathbf{B}} = \mathbf{B} - \mathbf{B}_1$.

Its derivative along any solution of the differential equation system consisting of

Eq. (7.5) and update parameter differential equations for $\tilde{\mathbf{A}}$ and $\tilde{\mathbf{B}}$ is

$$\begin{aligned} \dot{\mathbf{V}}(\mathbf{e}, \tilde{\mathbf{A}}, \tilde{\mathbf{B}}) = & \mathbf{e}^T [\mathbf{A}\mathbf{x}(t) + \mathbf{f}(\mathbf{x}(t), \mathbf{B}) + (\mathbf{A}_1\mathbf{y}(-t) + \mathbf{g}(\mathbf{y}(-t), \mathbf{B}_1) + \mathbf{u}(t)) + \dot{\mathbf{F}}(t)] \\ & + \tilde{\mathbf{A}}\dot{\mathbf{A}} + \tilde{\mathbf{B}}\dot{\mathbf{B}} \end{aligned} \quad (7.8)$$

where $\mathbf{u}(t)$, $\dot{\tilde{\mathbf{A}}}$, and $\dot{\tilde{\mathbf{B}}}$ are chosen so that $\dot{\mathbf{V}} = \mathbf{e}^T \mathbf{C} \mathbf{e}$, \mathbf{C} is a diagonal negative definite matrix, and $\dot{\mathbf{V}}$ is a negative semi-definite function of \mathbf{e} and parameter differences $\tilde{\mathbf{A}}$ and $\tilde{\mathbf{B}}$. In current scheme [3-7] of adaptive control of chaotic motion, traditional Lyapunov stability theorem and Babalat lemma are used to prove the error vector approaches zero, as time approaches infinity. But the question, why the estimated or given parameters also approach to the uncertain parameters, remains no answer. By pragmatismal asymptotical stability theorem, the question can be answered strictly.



7.3 The chaotic behavior of Yang and Yin Chen systems

The *Yang* Chen system is described as follows:

$$\begin{cases} \frac{dx_1(t)}{dt} = a(x_2(t) - x_1(t)) \\ \frac{dx_2(t)}{dt} = (c - a)x_1(t) - x_1(t)x_3(t) + cx_2(t) \\ \frac{dx_3(t)}{dt} = x_1(t)x_2(t) - bx_3(t) \end{cases} \quad (7.9)$$

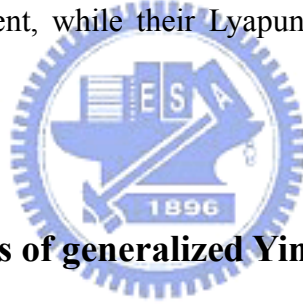
where initial condition $x_1(0) = 2, x_2(0) = 3.2, x_3(0) = 1.5$ and parameters $a = 35, b = 3$ and $c = 28$, can be called *Yang* parameters, and chaos of the *Yang* Chen system is called *Yang* chaos. The chaotic behaviors of Eq. (7.9) are shown in Fig. 6.1.

The *Yin* Chen equations are:

$$\begin{cases} \frac{dy_1(-t)}{d(-t)} = a_1(y_2(-t) - y_1(-t)) \\ \frac{dy_2(-t)}{d(-t)} = (c_1 - a_1)y_1(-t) - y_1(-t)y_3(-t) + c_1y_2(-t) \\ \frac{dy_3(-t)}{d(-t)} = y_1(-t)y_2(-t) - b_1y_3(-t) \end{cases} \quad (7.10)$$

where initial condition $y_1(0) = 20, y_2(0) = 120, y_3(0) = 18$ and parameters $a_1 = -35,$

$b_1 = -3$ and $c_1 = -28$, can be called *Yin* parameters, and chaos of the *Yin* Chen system is called *Yin* chaos. Obviously, the derivative are taken with the back-time in the left hand sides of Eq. (7.10). It means Eq. (7.10) aims to find out the historical behavior of the Chen system and to figure out the difference between history and presence. The phase portrait of *Yin* Chen system are revealed in Fig. 6.2. The phase portraits of *Yin* and *Yang* Chen systems are quite different, while their Lyapunov exponents are approximately symmetric but small different.



7.4 Numerical simulations of generalized Yin-Yang synchronization

In this Section, adaptive synchronization from *Yin* Chen system to *Yang* Chen system is proposed. The *Yang* Chen system as master system and the *Yin* Chen system as slave system are given below:

Yang Chen system is master:

$$\begin{cases} \frac{dx_1(t)}{dt} = a(x_2(t) - x_1(t)) \\ \frac{dx_2(t)}{dt} = (c - a)x_1(t) - x_1(t)x_3(t) + cx_2(t) \\ \frac{dx_3(t)}{dt} = x_1(t)x_2(t) - bx_3(t) \end{cases} \quad (7.11)$$

Yin Chen system is slave:

$y_1(0) = 0.7, y_2(0) = 0.5, y_3(0) = 0.8$. The two systems will approach synchronization for any initial conditions by appropriate controllers and update laws for the differences between uncertain and estimated parameters. As a result, the following controllers and update laws are designed by using pragmatistical asymptotical stability theorem as follows:

Choosing Lyapunov function as:

$$V = \frac{1}{2}(e_1^2 + e_2^2 + e_3^2 + \tilde{a}^2 + \tilde{b}^2 + \tilde{c}^2) \quad (7.16)$$

where $\tilde{a} = a - a_1$, $\tilde{b} = b - b_1$ and $\tilde{c} = c - c_1$.

Its time derivative is:

$$\begin{aligned} \dot{V} &= e_1 \dot{e}_1 + e_2 \dot{e}_2 + e_3 \dot{e}_3 + \tilde{a} \dot{\tilde{a}} + \tilde{b} \dot{\tilde{b}} + \tilde{c} \dot{\tilde{c}} \\ &= e_1 [a(x_2(t) - x_1(t)) + a_1(y_2(-t) - y_1(-t)) + u_1] \\ &\quad + e_2 [(c - a)x_1(t) - x_1(t)x_3(t) + cx_2(t) \\ &\quad + (c_1 - a_1)y_1(-t) - y_1(-t)y_3(-t) + c_1 y_2(-t) + u_2] \\ &\quad + e_3 [x_1(t)x_2(t) - bx_3(t) + y_1(-t)y_2(-t) - b_1 y_3(-t) + u_3] \\ &\quad + \tilde{a}(-\dot{a}_1) + \tilde{b}(-\dot{b}_1) + \tilde{c}(-\dot{c}_1) \end{aligned} \quad (7.17)$$

We choose the update laws for those uncertain parameters are:

$$\begin{cases} \dot{\tilde{a}} = -\dot{a}_1 = \tilde{a}e_1 \\ \dot{\tilde{b}} = -\dot{b}_1 = \tilde{b}e_3 \\ \dot{\tilde{c}} = -\dot{c}_1 = \tilde{c}e_2 \end{cases} \quad (7.18)$$

through Eq. (7.17) and (7.18), the appropriate controllers can be designed as:

$$\begin{cases} u_1 = -a(x_2(t) - x_1(t)) - a_1(y_2(-t) - y_1(-t)) - e_1 - \tilde{a}^2 \\ u_2 = -((c - a)x_1(t) - x_1(t)x_3(t) + cx_2(t)) \\ \quad - ((c_1 - a_1)y_1(-t) - y_1(-t)y_3(-t) + c_1 y_2(-t)) - e_2 - \tilde{c}^2 \\ u_3 = -(x_1(t)x_2(t) - bx_3(t)) - (y_1(-t)y_2(-t) - b_1 y_3(-t)) - e_3 - \tilde{b}^2 \end{cases} \quad (7.19)$$

We obtain

$$\dot{V} = -e_1^2 - e_2^2 - e_3^2 < 0 \quad (7.20)$$

which is negative semi-definite function of e_1, e_2, e_3, a_1, b_1 and c_1 . The Lyapunov asymptotical stability theorem is not satisfied. We cannot obtain that common origin of error dynamics (7.15) and parameter dynamics (7.18) is asymptotically stable. By pragmatistical asymptotically stability theorem (see Appendix B), D is a 6-manifold, $n = 6$ and the number of error state variables $p = 3$. When $e_1 = e_2 = e_3 = 0$ and a_1, b_1, c_1 take arbitrary values, $\dot{V} = 0$, so X is of 3 dimensions, $m = n - p = 6 - 3 = 3$, $m + 1 < n$ is satisfied. According to the pragmatistical asymptotically stability theorem, error vector e approaches zero and the estimated parameters also approach the uncertain parameters. The equilibrium point is pragmatically asymptotically stable. Under the assumption of equal probability, it is actually asymptotically stable. The simulation results are shown in Figs. 7.1-4.

CASE II. The given system for generalized synchronization is a Ikeda-Lorenz system[45] which affords $F(t)$, is described as follows:

$$\begin{cases} \frac{dz_1(t)}{dt} = -d_1 z_1(t) - e_1 \sin z_1(t) + f(z_2(t) - z_1(t)) \\ \frac{dz_2(t)}{dt} = -d_2 z_1(t) - e_2 \sin z_2(t) + h z_1(t) - z_1(t) z_3(t) - z_2(t) \\ \frac{dz_3(t)}{dt} = -d_3 z_1(t) - e_3 \sin z_3(t) + z_1(t) z_2(t) - g z_3(t) \end{cases} \quad (7.21)$$

where $d_1 = 0.1, d_2 = 0.2, d_3 = 0.05, e_1 = 1, e_2 = 0.3, e_3 = 1.8, f = 16, h = 45.92, g = 4$, and initial condition $z_1(0) = 1, z_2(0) = 2, z_3(0) = 3$. Phase portrait is shown in Fig. 7.5.

By Eq. (7.4)

$$e_i = x_i(t) - y_i(-t) + F_i(t) \quad (i = 1, 2, 3) \quad (7.22)$$

where $F_i(t) = \frac{1}{2} z_i(t)$

For generalized synchronization, we have

$$\lim_{t \rightarrow \infty} e_i = \lim_{t \rightarrow \infty} [(x_i(t) + \frac{1}{2} z_i(t)) - y_i(-t)] = 0 \quad (i=1,2,3) \quad (7.23)$$

Where Eq. (7.22) is rewritten as

$$\begin{cases} e_1 = [x_1(t) + \frac{1}{2} z_1(t)] - y_1(-t) \\ e_2 = [x_2(t) + \frac{1}{2} z_2(t)] - y_2(-t) \\ e_3 = [x_3(t) + \frac{1}{2} z_3(t)] - y_3(-t) \end{cases} \quad (7.24)$$

from Eq. (7.24), the following error dynamics:

$$\begin{cases} \dot{e}_1 = \frac{dx_1(t)}{dt} + \frac{1}{2} \frac{dz_1(t)}{dt} - \frac{dy_1(-t)}{dt} = \frac{dx_1(t)}{dt} + \frac{1}{2} \frac{dz_1(t)}{dt} + \frac{dy_1(-t)}{d(-t)} \\ = a(x_2(t) - x_1(t)) + \frac{1}{2} (-d_1 z_1(t) - e_1 \sin z_1(t) + f(z_2(t) - z_1(t))) \\ + a_1(y_2(-t) - y_1(-t)) + u_1 \\ \dot{e}_2 = \frac{dx_2(t)}{dt} + \frac{1}{2} \frac{dz_2(t)}{dt} - \frac{dy_2(-t)}{dt} = \frac{dx_2(t)}{dt} + \frac{1}{2} \frac{dz_2(t)}{dt} + \frac{dy_2(-t)}{d(-t)} \\ = (c - a)x_1(t) - x_1(t)x_3(t) + cx_2(t) + \frac{1}{2} (-d_2 z_1(t) - e_2 \sin z_2(t) + hz_1(t) - z_1(t)z_3(t) - z_2(t)) \\ + (c_1 - a_1)y_1(-t) - y_1(-t)y_3(-t) + c_1 y_2(-t) + u_2 \\ \dot{e}_3 = \frac{dx_3(t)}{dt} + \frac{1}{2} \frac{dz_3(t)}{dt} - \frac{dy_3(-t)}{dt} = \frac{dx_3(t)}{dt} + \frac{1}{2} \frac{dz_3(t)}{dt} + \frac{dy_3(-t)}{d(-t)} \\ = x_1(t)x_2(t) - bx_3(t) + \frac{1}{2} (-d_3 z_1(t) - e_3 \sin z_3(t) + z_1(t)z_2(t) - gz_3(t)) \\ + y_1(-t)y_2(-t) - b_1 y_3(-t) + u_3 \end{cases} \quad (7.25)$$

Choose a Lyapunov function in the form of a positive definite function:

$$V(e_1, e_2, e_3, \tilde{a}, \tilde{b}, \tilde{c}) = \frac{1}{2} (e_1^2 + e_2^2 + e_3^2 + \tilde{a}^2 + \tilde{b}^2 + \tilde{c}^2) \quad (7.26)$$

where $\tilde{a} = a - a_1$, $\tilde{b} = b - b_1$, $\tilde{c} = c - c_1$, and a_1, b_1, c_1 are estimates of uncertain parameters

a, b , and c , respectively.

Its time derivative is

$$\begin{aligned}
\dot{V} &= e_1 \dot{e}_1 + e_2 \dot{e}_2 + e_3 \dot{e}_3 + \tilde{a} \dot{\tilde{a}} + \tilde{b} \dot{\tilde{b}} + \tilde{c} \dot{\tilde{c}} \\
&= e_1 [a(x_2(t) - x_1(t)) + \frac{1}{2}(-d_1 z_1(t) - e_1 \sin z_1(t) + f(z_2(t) - z_1(t)))] \\
&\quad + a_1(y_2(-t) - y_1(-t)) + u_1] + e_2 [(c - a)x_1(t) - x_1(t)x_3(t) + cx_2(t) \\
&\quad + \frac{1}{2}(-d_2 z_1(t) - e_2 \sin z_2(t) + h z_1(t) - z_1(t)z_3(t) - z_2(t)) \\
&\quad + (c_1 - a_1)y_1(-t) - y_1(-t)y_3(-t) + c_1 y_2(-t) + u_2] + e_3 [x_1(t)x_2(t) - b x_3(t) \\
&\quad + \frac{1}{2}(-d_3 z_1(t) - e_3 \sin z_3(t) + z_1(t)z_2(t) - g z_3(t)) + y_1(-t)y_2(-t) - b_1 y_3(-t) + u_3] \\
&\quad + \tilde{a}(-\dot{a}_1) + \tilde{b}(-\dot{b}_1) + \tilde{c}(-\dot{c}_1) \tag{7.27}
\end{aligned}$$

We choose the update laws for \tilde{a} , \tilde{b} and \tilde{c} as:

$$\begin{cases} \dot{\tilde{a}} = -\dot{a}_1 = \tilde{a}e_1 \\ \dot{\tilde{b}} = -\dot{b}_1 = \tilde{b}e_3 \\ \dot{\tilde{c}} = -\dot{c}_1 = \tilde{c}e_2 \end{cases} \tag{7.28}$$

Choose

$$\begin{cases} u_1 = -a(x_2(t) - x_1(t)) - a_1(y_2(-t) - y_1(-t)) \\ \quad - \frac{1}{2}(-d_1 z_1(t) - e_1 \sin z_1(t) + f(z_2(t) - z_1(t))) - e_1 - \tilde{a}^2 \\ u_2 = -(c - a)x_1(t) + x_1(t)x_3(t) - cx_2(t) - (c_1 - a_1)y_1(-t) \\ \quad + y_1(-t)y_3(-t) - c_1 y_2(-t) \\ \quad - \frac{1}{2}(-d_2 z_1(t) - e_2 \sin z_2(t) + h z_1(t) - z_1(t)z_3(t) - z_2(t)) - e_2 - \tilde{c}^2 \\ u_3 = -x_1(t)x_2(t) + b x_3(t) - y_1(-t)y_2(-t) + b_1 y_3(-t) \\ \quad - \frac{1}{2}(-d_3 z_1(t) - e_3 \sin z_3(t) + z_1(t)z_2(t) - g z_3(t)) - e_3 - \tilde{b}^2 \end{cases} \tag{7.29}$$

We obtain

$$\dot{V} = -e_1^2 - e_2^2 - e_3^2 < 0 \tag{7.30}$$

which is negative semi-definite function of e_1, e_2, e_3, a_1, b_1 and c_1 . The Lyapunov asymptotical stability theorem is not satisfied. We cannot obtain that common origin of error dynamics (7.25) and parameter dynamics (7.28) is asymptotically stable. In this case, according to pragmatcal asymptotically stability theorem (see Appendix B), D is a

6-manifold, $n = 6$ and the number of error state variables $p = 3$. When $e_1 = e_2 = e_3 = 0$ and a_1, b_1, c_1 take arbitrary values, $\dot{V} = 0$, so X is of 3 dimensions, $m = n - p = 6 - 3 = 3$, $m + 1 < n$ is satisfied. Based on the pragmatical asymptotically stability theorem, error vector e approaches zero and the estimated parameters also approach the uncertain parameters. The equilibrium point is pragmatically asymptotically stable. Under the assumption of equal probability, it is actually asymptotically stable. The simulation results are shown in Figs. 7.6-9.

CASE III. The goal system for generalized synchronization is a Rössler system as $F(t)$ described as follows:

$$\begin{cases} \frac{dz_1(t)}{dt} = -(z_2(t) + z_3(t)) \\ \frac{dz_2(t)}{dt} = z_1(t) + f_1 z_2(t) \\ \frac{dz_3(t)}{dt} = g_1 + z_3(t)(z_1(t) - h_1) \end{cases} \quad (7.31)$$

where $f_1 = 0.2, g_1 = 0.4, h_1 = 5.7$, and initial condition $z_1(0) = 0.8, z_2(0) = 0.3, z_3(0) = 0.6$. Phase portrait is shown in Fig. 7.10.

We have

$$\lim_{t \rightarrow \infty} e_i = \lim_{t \rightarrow \infty} ((x_i(t) + z_i^2(t)) - y_i(-t)) = 0 \quad (i = 1, 2, 3) \quad (7.32)$$

where

$$\begin{cases} e_1 = [x_1(t) + z_1^2(t)] - y_1(-t) \\ e_2 = [x_2(t) + z_2^2(t)] - y_2(-t) \\ e_3 = [x_3(t) + z_3^2(t)] - y_3(-t) \end{cases} \quad (7.33)$$

from (7.32), the following error dynamics:

$$\begin{cases}
\dot{e}_1 = \frac{dx_1(t)}{dt} + 2z_1(t)\left(\frac{dz_1(t)}{dt}\right) - \frac{dy_1(-t)}{dt} = \frac{dx_1(t)}{dt} + 2z_1(t)\left(\frac{dz_1(t)}{dt}\right) + \frac{dy_1(-t)}{d(-t)} \\
= a(x_2(t) - x_1(t)) + 2z_1(-z_2(t) + z_3(t)) + a_1(y_2(-t) - y_1(-t)) + u_1 \\
\dot{e}_2 = \frac{dx_2(t)}{dt} + 2z_2(t)\left(\frac{dz_1(t)}{dt}\right) - \frac{dy_2(-t)}{dt} = \frac{dx_2(t)}{dt} + 2z_2(t)\left(\frac{dz_1(t)}{dt}\right) + \frac{dy_2(-t)}{d(-t)} \\
= (c - a)x_1(t) - x_1(t)x_3(t) + cx_2(t) + 2z_2(t)(z_1(t) + f_1z_2(t)) \\
+ (c_1 - a_1)y_1(-t) - y_1(-t)y_3(-t) + c_1y_2(-t) + u_2 \\
\dot{e}_3 = \frac{dx_3(t)}{dt} + 2z_3(t)\left(\frac{dz_1(t)}{dt}\right) - \frac{dy_3(-t)}{dt} = \frac{dx_3(t)}{dt} + 2z_3(t)\left(\frac{dz_1(t)}{dt}\right) + \frac{dy_3(-t)}{d(-t)} \\
= x_1(t)x_2(t) - bx_3(t) + y_1(-t)y_2(-t) - b_1y_3(-t) + 2z_3(t)(g_1 + z_3(t)(z_1(t) - h_1)) + u_3
\end{cases} \quad (7.34)$$

Choose a Lyapunov function in the form of a positive definite function:

$$V(e_1, e_2, e_3, \tilde{a}, \tilde{b}, \tilde{c}) = \frac{1}{2}(e_1^2 + e_2^2 + e_3^2 + \tilde{a}^2 + \tilde{b}^2 + \tilde{c}^2) \quad (7.35)$$

where $\tilde{a} = a - a_1, \tilde{b} = b - b_1, \tilde{c} = c - c_1$, and a_1, b_1, c_1 are estimates of uncertain parameters

a, b , and c , respectively.

Its time derivative is

$$\begin{aligned}
\dot{V} &= e_1\dot{e}_1 + e_2\dot{e}_2 + e_3\dot{e}_3 + \tilde{a}\dot{\tilde{a}} + \tilde{b}\dot{\tilde{b}} + \tilde{c}\dot{\tilde{c}} \\
&= e_1[a(x_2(t) - x_1(t)) + 2z_1(-z_2(t) + z_3(t)) + a_1(y_2(-t) - y_1(-t)) + u_1] \\
&+ e_2[(c - a)x_1(t) - x_1(t)x_3(t) + cx_2(t) + 2z_2(t)(z_1(t) + f_1z_2(t)) \\
&+ (c_1 - a_1)y_1(-t) - y_1(-t)y_3(-t) + c_1y_2(-t) + u_2] \\
&+ e_3[x_1(t)x_2(t) - bx_3(t) + y_1(-t)y_2(-t) - b_1y_3(-t) \\
&+ 2z_3(t)(g_1 + z_3(t)(z_1(t) - h_1)) + u_3] + \tilde{a}(-\dot{a}_1) + \tilde{b}(-\dot{b}_1) + \tilde{c}(-\dot{c}_1) \quad (7.36)
\end{aligned}$$

We choose the update laws for those uncertain parameters are:

$$\begin{cases}
\dot{\tilde{a}} = -\dot{a}_1 = \tilde{a}e_1 \\
\dot{\tilde{b}} = -\dot{b}_1 = \tilde{b}e_3 \\
\dot{\tilde{c}} = -\dot{c}_1 = \tilde{c}e_2
\end{cases} \quad (7.37)$$

Choose

$$\begin{cases} u_1 = -a(x_2(t) - x_1(t)) - a_1(y_2(-t) - y_1(-t)) \\ \quad - 2z_1(t)(-(z_2(t) + z_3(t))) - e_1 - \tilde{a}^2 \\ u_2 = -(c - a)x_1(t) + x_1(t)x_3(t) - cx_2(t) - (c_1 - a_1)y_1(-t) \\ \quad + y_1(-t)y_3(-t) - c_1y_2(-t) - 2z_2(z_1 + f_1z_2) - e_2 - \tilde{c}^2 \\ u_3 = -x_1(t)x_2(t) + bx_3(t) - y_1(-t)y_2(-t) + b_1y_3(-t) \\ \quad - 2z_3(t)(g_1 + z_3(t)(z_1(t) - h_1)) - e_3 - \tilde{b}^2 \end{cases} \quad (7.38)$$

We obtain

$$\dot{V} = -e_1^2 - e_2^2 - e_3^2 < 0 \quad (7.39)$$

which is negative semi-definite function of e_1, e_2, e_3, a_1, b_1 and c_1 . The Lyapunov asymptotical stability theorem is not satisfied. We cannot obtain that common origin of error dynamics (7.34) and parameter dynamics (7.37) is asymptotically stable. In this case, according to pragmatical asymptotically stability theorem (see Appendix B), D is a 6-manifold, $n = 6$ and the number of error state variables $p = 3$. When $e_1 = e_2 = e_3 = 0$ and a_1, b_1, c_1 take arbitrary values, $\dot{V} = 0$, so X is of 3 dimensions, $m = n - p = 6 - 3 = 3$, $m + 1 < n$ is satisfied. Based on the pragmatical asymptotically stability theorem, error vector e approaches zero and the estimated parameters also approach the uncertain parameters. The equilibrium point is pragmatically asymptotically stable. Under the assumption of equal probability, it is actually asymptotically stable. The simulation results are shown in Figs. 7.11-14.

7.5 Summary

In this Chapter, pragmatical generalized *Yin-Yang* synchronization of chaotic Chen system is investigated. The *Yang* Chen system and *Yin* Chen systems are used in three simulation examples which exhibit its effectiveness of the proposed method. By using pragmatical asymptotical stability theorem, with the same conditions for the Lyapunov

function, $V > 0$, $\dot{V} \leq 0$, as in the current scheme of adaptive synchronization, we not only obtain the generalized synchronization of chaotic systems but also prove that the estimated parameters approach the uncertain values. This Chapter explores the conjunction from the history to presence, and researches pragmatical synchronization by adaptive control. The nonlinear *Yin* dynamics gives a vast new field for nonlinear dynamics.



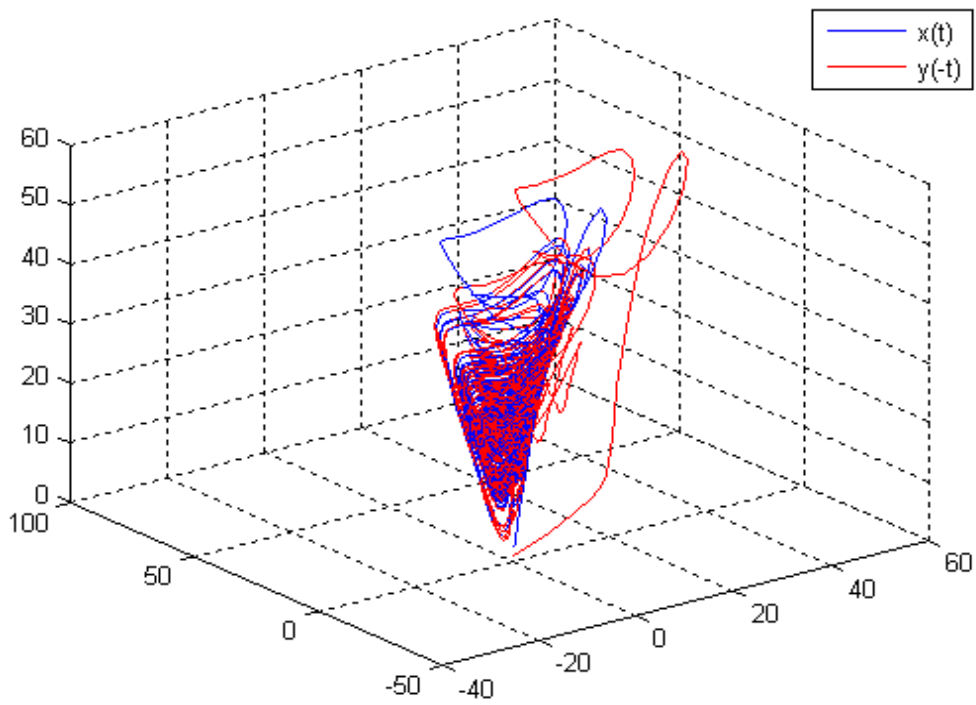


Fig. 7.1 Phase portrait of *Yin* and *Yang* chaotic systems for *Case I*.

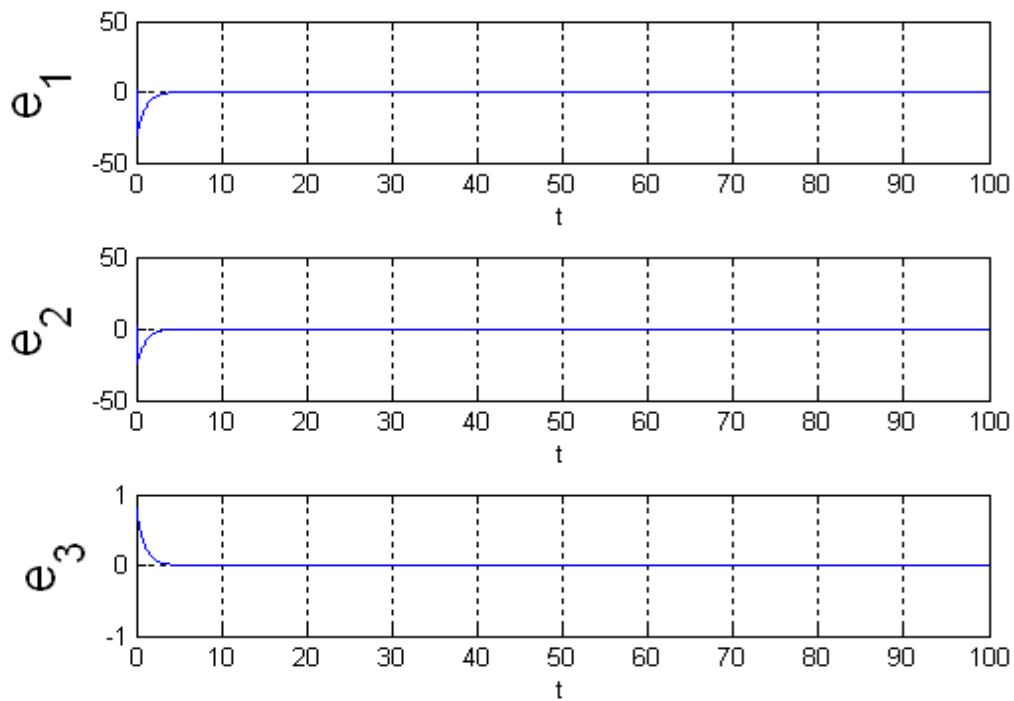


Fig. 7.2 Time histories of errors for *Yin* and *Yang* Chen chaotic systems for *Case I*.

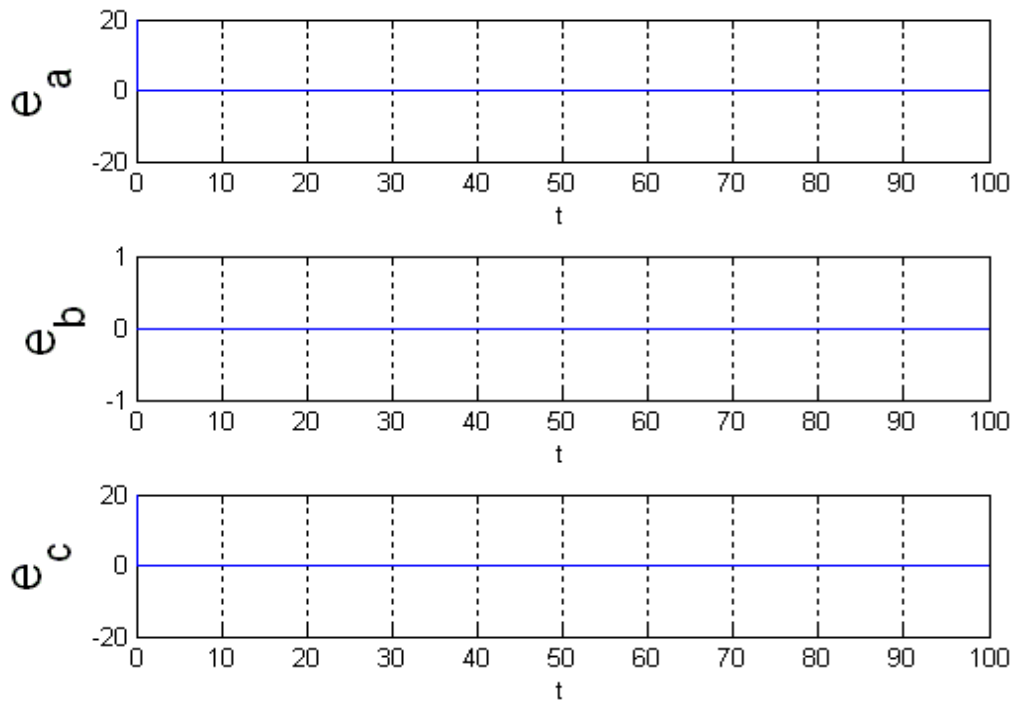


Fig. 7.3 Time histories of parametric errors for *Yin* and *Yang* Chen chaotic systems for

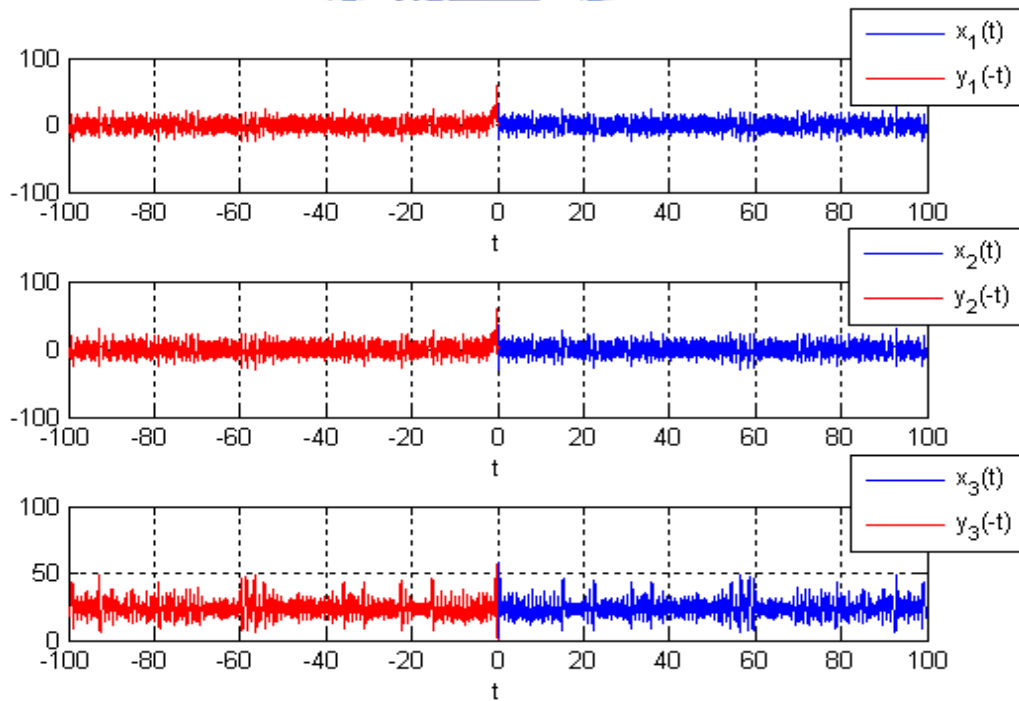
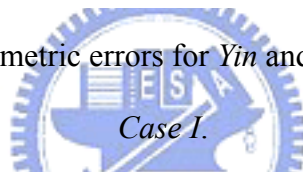


Fig. 7.4 Time histories of states of *Yin* and *Yang* Chen chaotic systems for *Case I*.

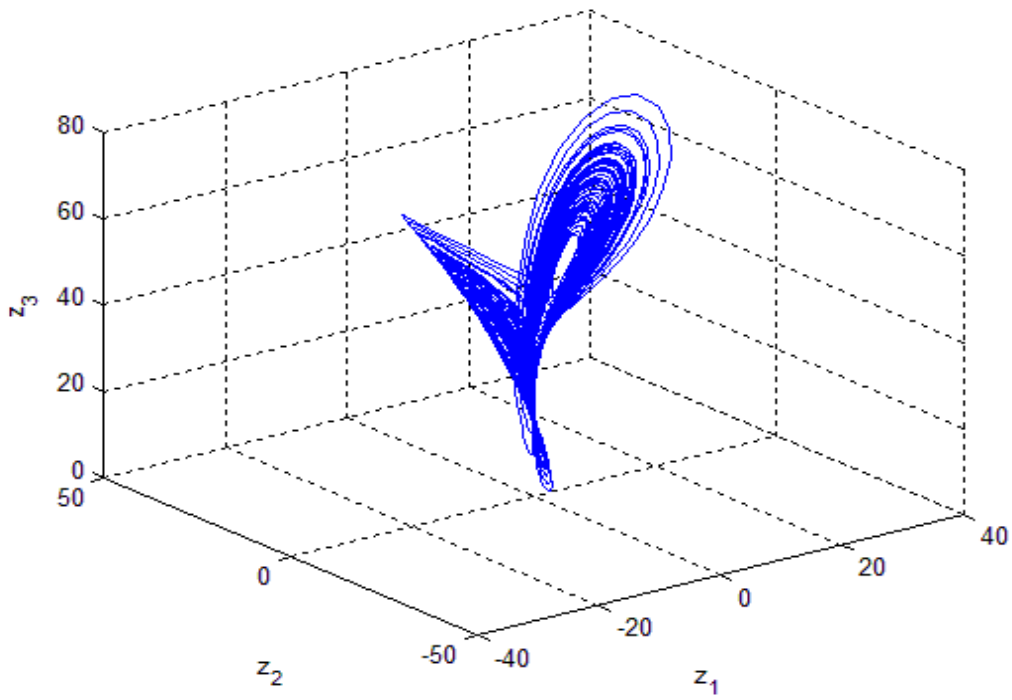


Fig. 7.5 Phase portrait of Ikeda-Lorenz system.

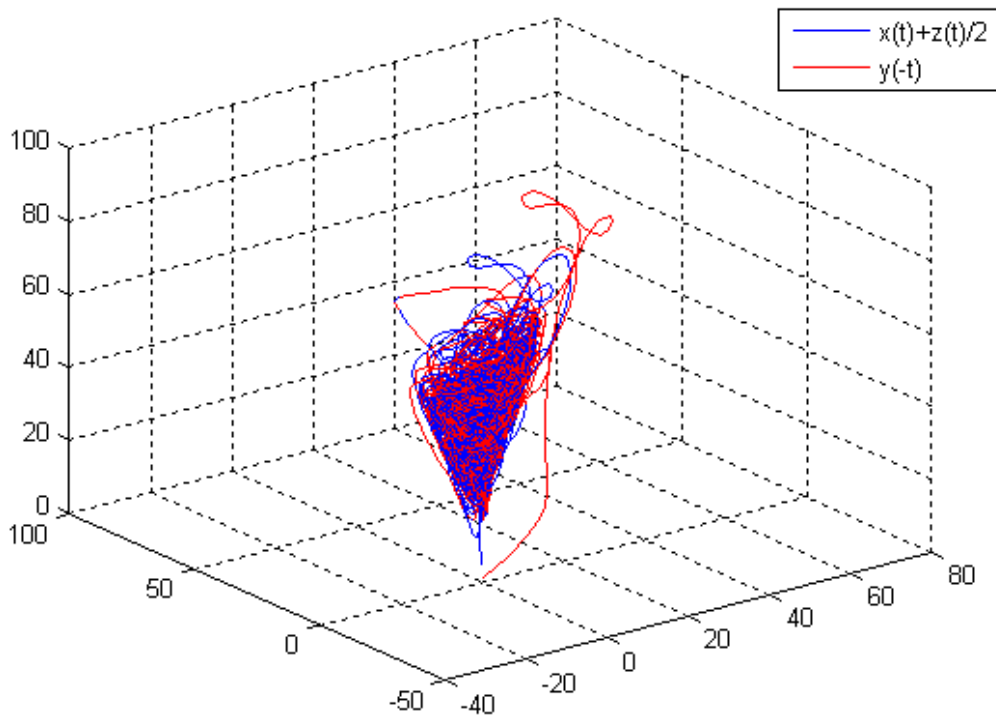


Fig. 7.6 Phase portrait of Yin and Yang chaotic systems with Ikeda-Lorenz system as goal system for Case II.

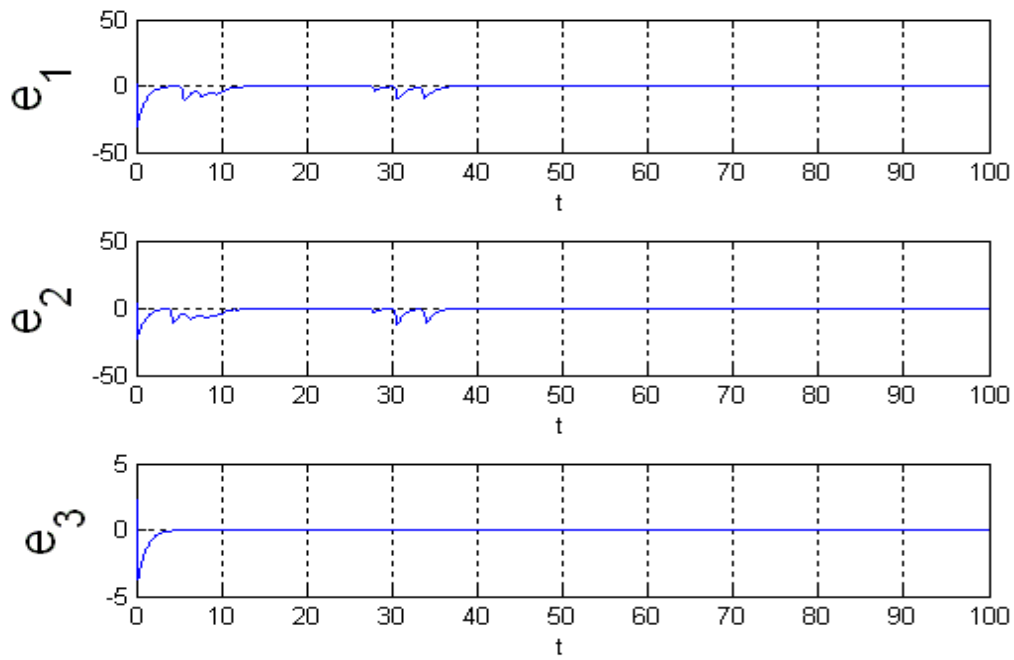


Fig. 7.7 Time histories of errors for *Yin* and *Yang* Chen chaotic systems for *Case II*.

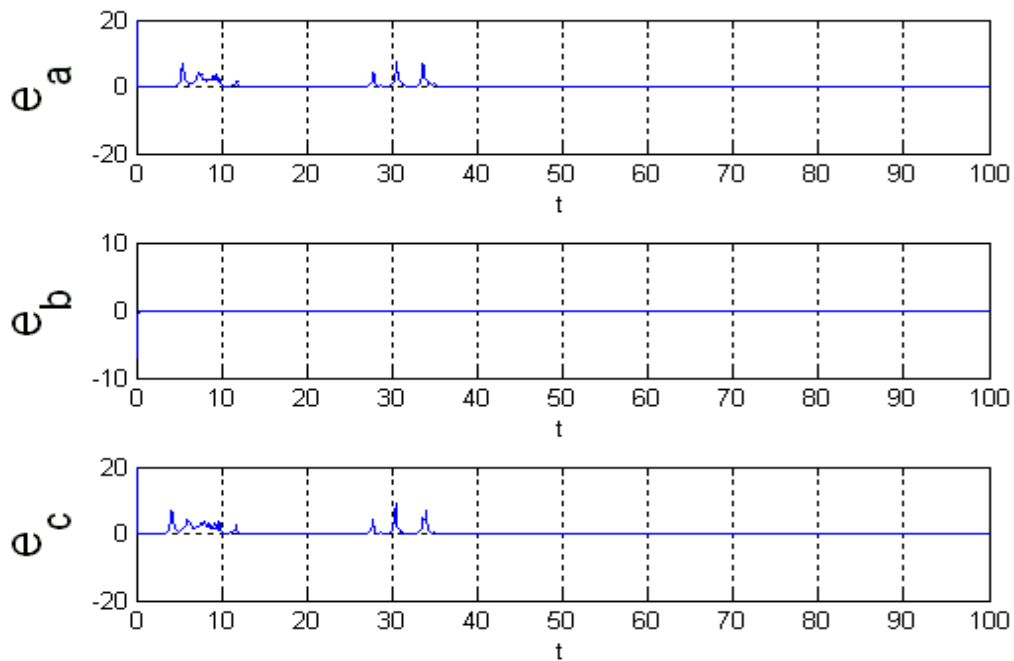


Fig. 7.8 Time histories of parametric errors for *Yin* and *Yang* Chen chaotic systems for *Case II*.

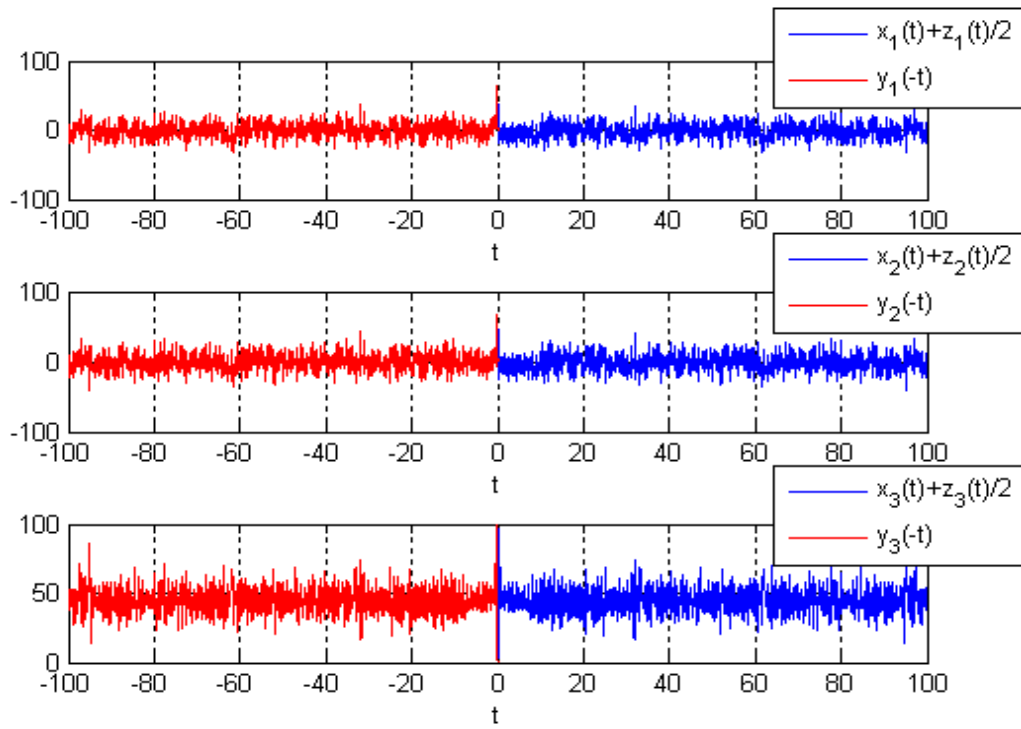


Fig. 7.9 Time histories of states of *Yin* and *Yang* Chen chaotic systems for *Case II*.

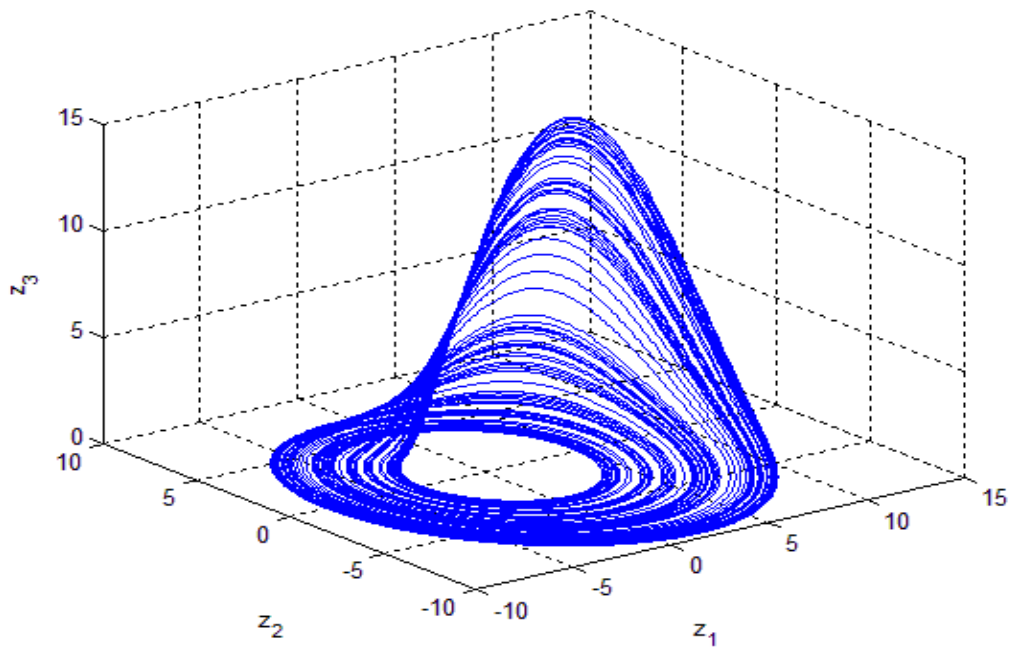


Fig. 7.10 Phase portrait of Rössler system.

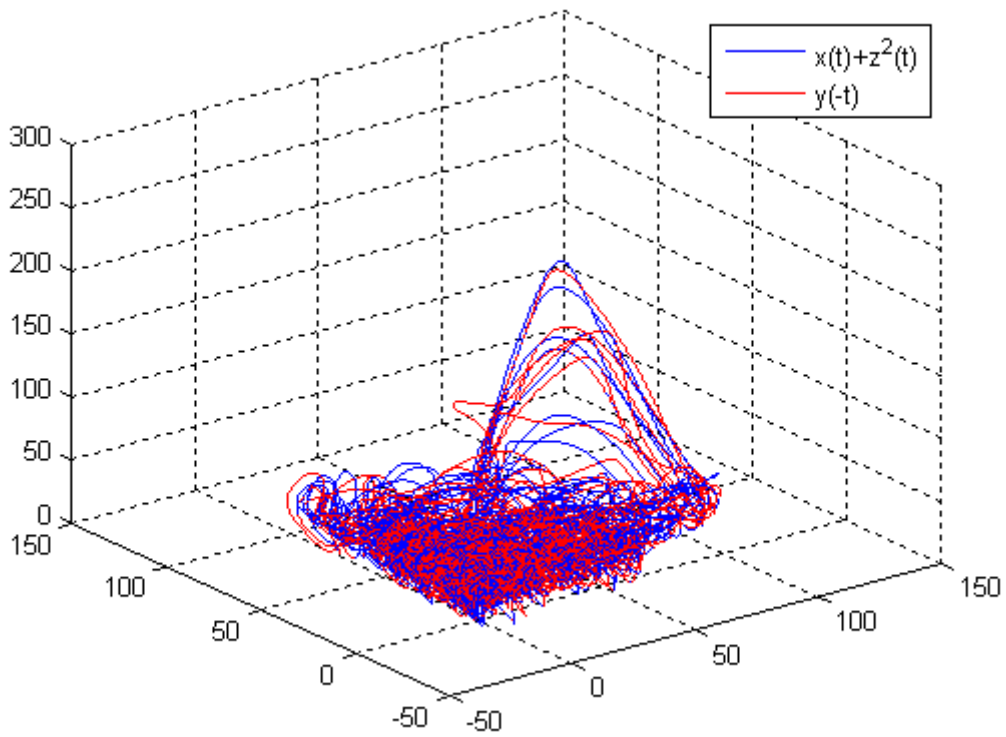


Fig. 7.11 Phase portrait of *Yin* and *Yang* chaotic systems with Rössler system as goal system for *Case III*.

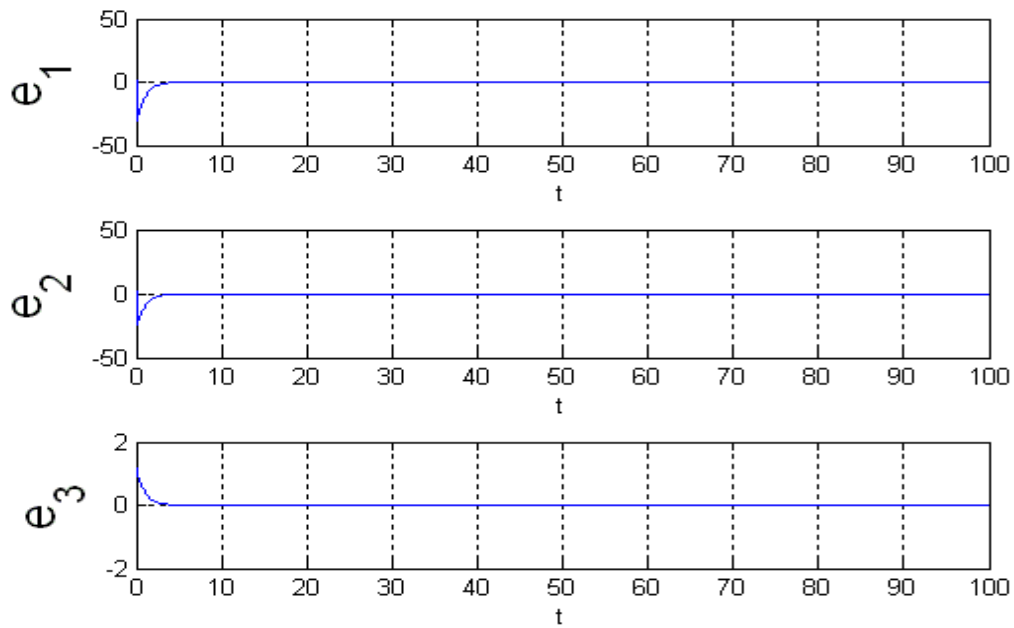


Fig. 7.12 Time histories of errors for *Yin* and *Yang* Chen chaotic systems for *Case III*.

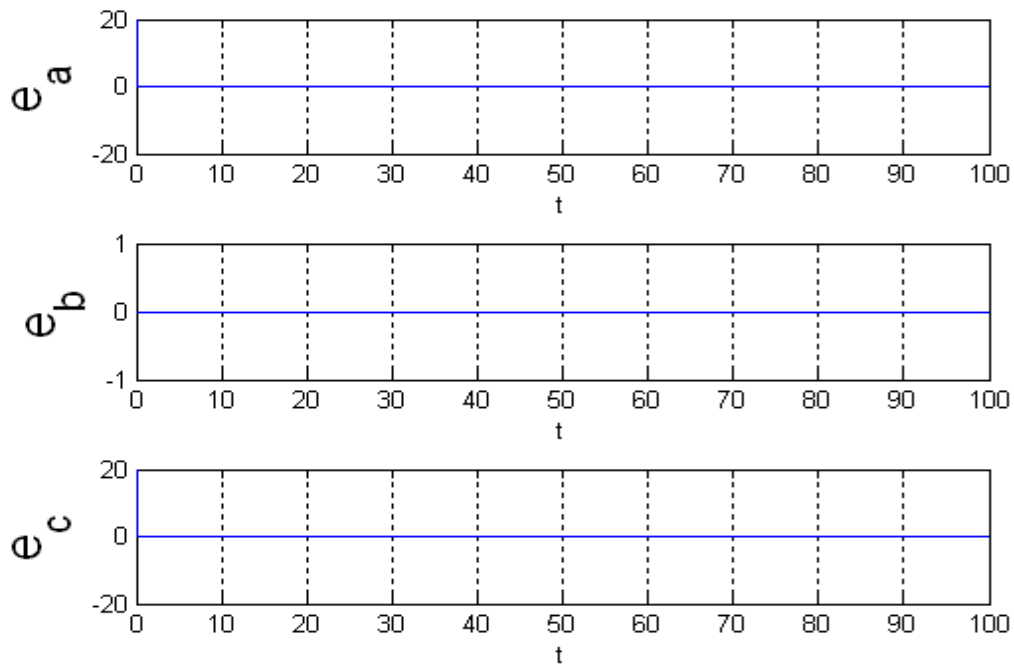


Fig. 7.13 Time histories of parametric errors for *Yin* and *Yang* Chen chaotic systems for

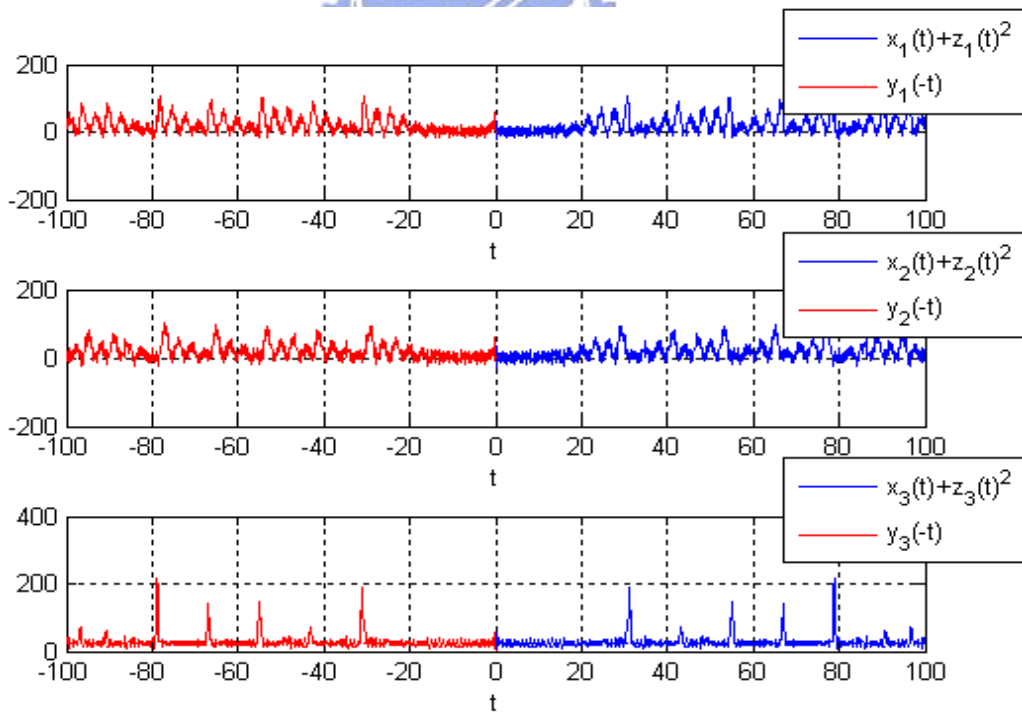
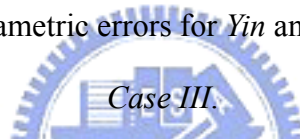


Fig. 7.14 Time histories of states of *Yin* & *Yang* Chen chaotic systems for *Case III*.

Chapter 8

Conclusions

In this thesis, a new chaos generalized synchronization method by GYC partial region stability theory is proposed. By using the GYC partial region stability the Lyapunov function is a simple linear homogeneous function of error states and the controllers are simpler. Lorenz system with Legendre function parameters is studied firstly. The results are verified by time histories of states, phase portraits, Poincaré maps, bifurcation diagram, Lyapunov exponents and parameter diagrams. Abundant hyperchaos is found for this system, which gives potential in various applications, particularly in secret communication. The *Yin* Chen system is firstly introduced. Comparing the *Yang* and *Yin* Chen system via numerical simulation, we find out some similarity and difference between history and presence. This thesis explores the historical space for chaos study interestingly, it would be proved epoch-making significance in future. The synchronization is researched by two coupled chaotic systems with a unidirectional linear error coupling. To choose an applicable gain parameters skillfully by linear coupling method achieves the goal of generalized synchronization. By using pragmatical asymptotical stability theorem, with the same conditions for the Lyapunov function, $V > 0$, $\dot{V} \leq 0$, as in the current scheme of adaptive synchronization, we not only obtain the generalized synchronization of chaotic systems but also prove that the estimated parameters approach the uncertain values. This thesis explores the conjunction from the history to presence, and studies pragmatical synchronization by adaptive control. The nonlinear Yin dynamics gives a vast new field for nonlinear dynamics.

Appendix A

GYC Partial Region Stability Theory [24-26]

A.1 Definition of the Stability on Partial Region

Consider the differential equations of disturbed motion of a nonautonomous system in the normal form

$$\frac{dx_s}{dt} = X_s(t, x_1, \dots, x_n), \quad (s = 1, \dots, n) \quad (\text{A.1})$$

where the function X_s is defined on the intersection of the partial region Ω (shown in Fig. A1) and

$$\sum_s x_s^2 \leq H \quad (\text{A.2})$$

and $t > t_0$, where t_0 and H are certain positive constants. X_s which vanishes when the variables x_s are all zero, is a real valued function of t, x_1, \dots, x_n . It is assumed that X_s is smooth enough to ensure the existence, uniqueness of the solution of the initial value problem. When X_s does not contain t explicitly, the system is autonomous.

Obviously, $x_s = 0$ ($s = 1, \dots, n$) is a solution of Eq.(A.1). We are interested to the asymptotical stability of this zero solution on partial region Ω (including the boundary) of the neighborhood of the origin which in general may consist of several subregions (Fig. A1).

Definition 1:

For any given number $\varepsilon > 0$, if there exists a $\delta > 0$, such that on the closed given partial region Ω when

$$\sum_s x_{s0}^2 \leq \delta, \quad (s = 1, \dots, n) \quad (\text{A.3})$$

for all $t \geq t_0$, the inequality

$$\sum_s x_s^2 < \varepsilon, \quad (s = 1, \dots, n) \quad (\text{A.4})$$

is satisfied for the solutions of Eq.(A.1) on Ω , then the disturbed motion $x_s = 0$ ($s = 1, \dots, n$) is stable on the partial region Ω .

Definition 2:

If the undisturbed motion is stable on the partial region Ω , and there exists a $\delta' > 0$, so that on the given partial region Ω when

$$\sum_s x_{s0}^2 \leq \delta', \quad (s = 1, \dots, n) \quad (\text{A.5})$$

The equality

$$\lim_{t \rightarrow \infty} \left(\sum_s x_s^2 \right) = 0 \quad (\text{A.6})$$

is satisfied for the solutions of Eq.(A.1) on Ω , then the undisturbed motion $x_s = 0$ ($s = 1, \dots, n$) is asymptotically stable on the partial region Ω .

The intersection of Ω and region defined by Eq.(A.5) is called the region of attraction.

Definition of Functions $V(t, x_1, \dots, x_n)$:

Let us consider the functions $V(t, x_1, \dots, x_n)$ given on the intersection Ω_1 of the partial region Ω and the region

$$\sum_s x_s^2 \leq h, \quad (s = 1, \dots, n) \quad (\text{A.7})$$

for $t \geq t_0 > 0$, where t_0 and h are positive constants. We suppose that the functions are single-valued and have continuous partial derivatives and become zero when $x_1 = \dots = x_n = 0$.

Definition 3:

If there exists $t_0 > 0$ and a sufficiently small $h > 0$, so that on partial region Ω_1 and $t \geq t_0$, $V \geq 0$ (or ≤ 0), then V is a positive (or negative) semidefinite, in general semidefinite, function on the Ω_1 and $t \geq t_0$.

Definition 4:

If there exists a positive (negative) definitive function $W(x_1 \dots x_n)$ on Ω_1 , so that on the partial region Ω_1 and $t \geq t_0$

$$V - W \geq 0 \text{ (or } -V - W \geq 0), \quad (\text{A.8})$$

then $V(t, x_1, \dots, x_n)$ is a positive definite function on the partial region Ω_1 and $t \geq t_0$.

Definition 5:

If $V(t, x_1, \dots, x_n)$ is neither definite nor semidefinite on Ω_1 and $t \geq t_0$, then $V(t, x_1, \dots, x_n)$ is an indefinite function on partial region Ω_1 and $t \geq t_0$. That is, for any small $h > 0$ and any large $t_0 > 0$, $V(t, x_1, \dots, x_n)$ can take either positive or negative value on the partial region Ω_1 and $t \geq t_0$.

Definition 6: Bounded function V

If there exist $t_0 > 0$, $h > 0$, so that on the partial region Ω_1 , we have

$$|V(t, x_1, \dots, x_n)| < L$$

where L is a positive constant, then V is said to be bounded on Ω_1 .

Definition 7: Function with infinitesimal upper bound

If V is bounded, and for any $\lambda > 0$, there exists $\mu > 0$, so that on Ω_1 when

$$\sum_s x_s^2 \leq \mu, \text{ and } t \geq t_0, \text{ we have}$$

$$|V(t, x_1, \dots, x_n)| \leq \lambda$$

then V admits an infinitesimal upper bound on Ω_1 .

A.2 GYC Theorem of Stability and of Asymptotical Stability on Partial Region

Theorem 1

If there can be found a definite function $V(t, x_1, \dots, x_n)$ on the partial region for Eq. (A.1), and the derivative with respect to time based on these equations are:

$$\frac{dV}{dt} = \frac{\partial V}{\partial t} + \sum_{s=1}^n \frac{\partial V}{\partial x_s} X_s \quad (\text{A.9})$$

Then, it is a semidefinite function on the partial region whose sense is opposite to that of V , or if it becomes zero identically, then the undisturbed motion is stable on the partial region.

Proof:

Let us assume for the sake of definiteness that V is a positive definite function. Consequently, there exists a sufficiently large number t_0 and a sufficiently small number $h < H$, such that on the intersection Ω_1 of partial region Ω and

$$\sum_s x_s^2 \leq h, \quad (s = 1, \dots, n)$$

and $t \geq t_0$, the following inequality is satisfied

$$V(t, x_1, \dots, x_n) \geq W(x_1, \dots, x_n),$$

where W is a certain positive definite function which does not depend on t . Besides that, Eq. (A.9) may assume only negative or zero value in this region.

Let ε be an arbitrarily small positive number. We shall suppose that in any case $\varepsilon < h$. Let us consider the aggregation of all possible values of the quantities x_1, \dots, x_n , which are on the intersection ω_2 of Ω_1 and

$$\sum_s x_s^2 = \varepsilon, \quad (\text{A.10})$$

and let us designate by $l > 0$ the precise lower limit of the function W under this condition. By virtue of Eq. (A.8), we shall have

$$V(t, x_1, \dots, x_n) \geq l \quad \text{for } (x_1, \dots, x_n) \text{ on } \omega_2. \quad (\text{A.11})$$

We shall now consider the quantities x_s as functions of time which satisfy the differential equations of disturbed motion. We shall assume that the initial values x_{s0} of these functions for $t = t_0$ lie on the intersection Ω_2 of Ω_1 and the region

$$\sum_s x_s^2 \leq \delta, \quad (\text{A.12})$$

where δ is so small that

$$V(t_0, x_{10}, \dots, x_{n0}) < l \quad (\text{A.13})$$

By virtue of the fact that $V(t_0, 0, \dots, 0) = 0$, such a selection of the number δ is obviously possible. We shall suppose that in any case the number δ is smaller than ε . Then the inequality

$$\sum_s x_s^2 < \varepsilon, \quad (\text{A.14})$$

being satisfied at the initial instant will be satisfied, in the very least, for a sufficiently small $t - t_0$, since the functions $x_s(t)$ vary continuously with time. We shall show that these inequalities will be satisfied for all values $t > t_0$. Indeed, if these inequalities were not satisfied at some time, there would have to exist such an instant $t = T$ for which this inequality would become an equality. In other words, we would have

$$\sum_s x_s^2(T) = \varepsilon,$$

and consequently, on the basis of Eq. (A.11)

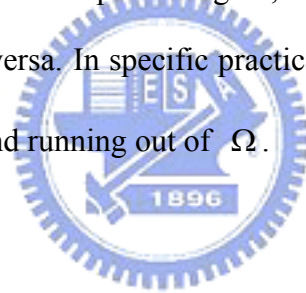
$$V(T, x_1(T), \dots, x_n(T)) \geq l \tag{A.15}$$

On the other hand, since $\varepsilon < h$, the inequality (Eq.(A.7)) is satisfied in the entire interval of time $[t_0, T]$, and consequently, in this entire time interval $\frac{dV}{dt} \leq 0$. This yields

$$V(T, x_1(T), \dots, x_n(T)) \leq V(t_0, x_{10}, \dots, x_{n0}),$$

which contradicts Eq. (A.14) on the basis of Eq. (A.13). Thus, the inequality (Eq.(A.4)) must be satisfied for all values of $t > t_0$, hence follows that the motion is stable.

Finally, we must point out that from the view-point of mathematics, the stability on partial region in general does not be related logically to the stability on whole region. If an undisturbed solution is stable on a partial region, it may be either stable or unstable on the whole region and vice versa. In specific practical problems, we do not study the solution starting within Ω_2 and running out of Ω .



Theorem 2

If in satisfying the conditions of Theorem 1, the derivative $\frac{dV}{dt}$ is a definite function on the partial region with opposite sign to that of V and the function V itself permits an infinitesimal upper limit, then the undisturbed motion is asymptotically stable on the partial region.

Proof:

Let us suppose that V is a positive definite function on the partial region and that consequently, $\frac{dV}{dt}$ is negative definite. Thus on the intersection Ω_1 of Ω and the region defined by Eq. (A.7) and $t \geq t_0$ there will be satisfied not only the inequality (Eq.(A.8)), but the following inequality as well:

$$\frac{dV}{dt} \leq -W_1(x_1, \dots, x_n), \tag{A.16}$$

where W_1 is a positive definite function on the partial region independent of t .

Let us consider the quantities x_s as functions of time which satisfy the differential equations of disturbed motion assuming that the initial values $x_{s0} = x_s(t_0)$ of these quantities satisfy the inequalities (Eq. (A.12)). Since the undisturbed motion is stable in any case, the magnitude δ may be selected so small that for all values of $t \geq t_0$ the quantities x_s remain within Ω_1 . Then, on the basis of Eq. (A.16) the derivative of function $V(t, x_1(t), \dots, x_n(t))$ will be negative at all times and, consequently, this function will approach a certain limit, as t increases without limit, remaining larger than this limit at all times. We shall show that this limit is equal to some positive quantity different from zero. Then for all values of $t \geq t_0$ the following inequality will be satisfied:

$$V(t, x_1(t), \dots, x_n(t)) > \alpha \quad (\text{A.17})$$

where $\alpha > 0$.

Since V permits an infinitesimal upper limit, it follows from this inequality that

$$\sum_s x_s^2(t) \geq \lambda, \quad (s = 1, \dots, n), \quad (\text{A.18})$$

where λ is a certain sufficiently small positive number. Indeed, if such a number λ did not exist, that is, if the quantity $\sum_s x_s^2(t)$ were smaller than any preassigned number no matter how small, then the magnitude $V(t, x_1(t), \dots, x_n(t))$, as follows from the definition of an infinitesimal upper limit, would also be arbitrarily small, which contradicts Eq. (A.17).

If for all values of $t \geq t_0$ the inequality (Eq. (A.18)) is satisfied, then Eq. (A.16) shows that the following inequality will be satisfied at all times:

$$\frac{dV}{dt} \leq -l_1,$$

where l_1 is positive number different from zero which constitutes the precise lower limit of the function $W_1(t, x_1(t), \dots, x_n(t))$ under condition (Eq. (A.18)). Consequently, for all values of $t \geq t_0$ we shall have:

$$V(t, x_1(t), \dots, x_n(t)) = V(t_0, x_{10}, \dots, x_{n0}) + \int_{t_0}^t \frac{dV}{dt} dt \leq V(t_0, x_{10}, \dots, x_{n0}) - l_1(t - t_0),$$

which is, obviously, in contradiction with Eq.(A.17). The contradiction thus obtained shows that the function $V(t, x_1(t), \dots, x_n(t))$ approached zero as t increase without limit. Consequently, the same will be true for the function $W(x_1(t), \dots, x_n(t))$ as well, from which it follows directly that

$$\lim_{t \rightarrow \infty} x_s(t) = 0, \quad (s = 1, \dots, n),$$

which proves the theorem.

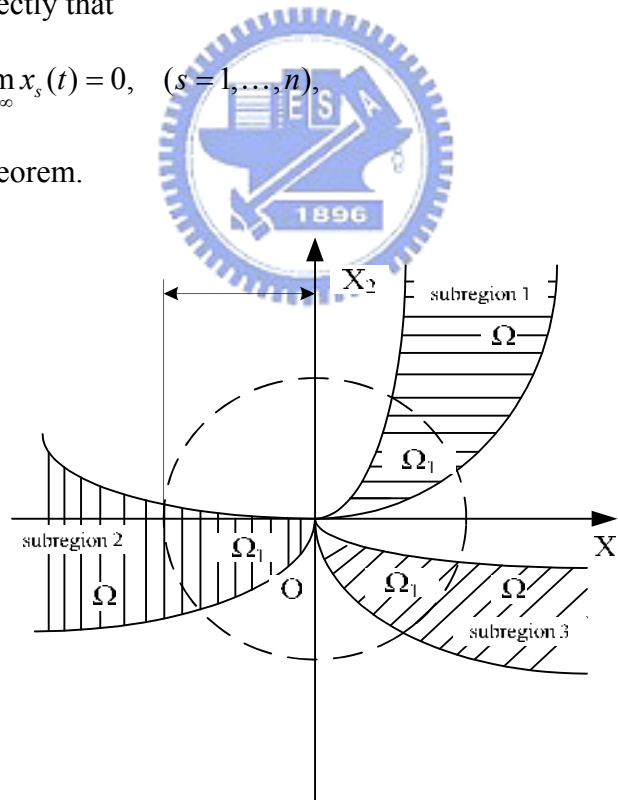


Fig. A1 Partial regions Ω and Ω_1 .

Appendix B

Systems of Positive States [52-55]

B.1 Three species prey-predator system

The three species prey-predator system which consists of two competing preys and one predator can be described by the following set of nonlinear differential equations:

$$\begin{cases} \frac{dx}{dt} = r_1(1 - k_1^{-1}x - k_1^{-1}c_2y) - \Phi_1(x, y)z \\ \frac{dy}{dt} = r_2(1 - k_2^{-1}c_1x - k_2^{-1}y) - \Phi_2(x, y)z \\ \frac{dz}{dt} = e_1\Phi_1(x, y)z + e_2\Phi_2(x, y)z - \alpha z \end{cases} \quad (\text{B.1})$$

where α, r_i, k_i, e_i and $c_i, i=1,2$ are the model parameters assuming only positive values, and the functions $\Phi_i(x, y), i=1,2$ represent the densities of the two prey species and z represents the density of the predator species. The predator z consumes the preys x, y according to the response functions [52]:

$$\Phi_1(x, y) = \frac{a_1x}{1 + b_1x + b_2y}, \quad \Phi_2(x, y) = \frac{a_2y}{1 + b_1x + b_2y} \quad (\text{B.2})$$

where $a_i, i=1,2$ are the search rates of a predator for the preys x, y respectively, while $b_i = h_i a_i, i=1,2$ where $h_i, i=1,2$ are the expected handling times spent with the preys x, y respectively. The parameters e_1 and e_2 represent, the conversion rates of the preys x, y to predator z . Obviously, when b_1 and b_2 are very small the functional of response $\Phi_i, (i=1,2)$ become linear response see Voltterra functional response [53]. In the other hand as one of both b_1 and b_2 tends to zero the system approaches to hyperbolic Holling type II [54]. The prescribed model characterized by nonlinear response since amount of food consumed by predator per unit time depends upon the available food sources from the two preys x and y .

B.2 Double Mackey-Glass systems

We consider two double Mackey-Glass systems which consist of two coupled Mackey-Glass equations [55]:

$$\begin{cases} \dot{x}_1 = \frac{bx_{1\tau}}{1+x_{1\tau}^n} - rx_1 \\ \dot{x}_2 = \frac{bx_{2\tau}}{1+x_{2\tau}^n} - rx_2 - x_1 \end{cases} \quad (\text{B.3})$$

The system is a model of blood production of patients with leukemia. The variables x_1 , x_2 are the concentration of the mature blood cells in the blood, and $x_{1\tau}$, $x_{2\tau}$ are presented the request of the cells which is made after τ seconds, i.e. $x_{i\tau} = x_i(t-\tau)$, ($i=1,2$). The time delay τ indicates the difference between the time of cellular production in the bone marrow and of the release of mature cells into the blood. According to the observations, the time τ is large in the patients with leukemia and the concentration of the blood cells becomes oscillatory. In this study, the delay time fixed in 20 second ($\tau = 20$) and the parameters are shown as follow: $b = 0.2$, $r = 0.1$, and $n = 10$.

B.3 Energy communication system in biological research

The so-call static state in life sciences means that the system of life is approach to a stable condition. Moreover, the relation of energy communication among the elements in a system of life is called arrangement of static state. The energy communication of elements in a system of life in static state can be divided into two forms:

(1) Independent form:

All the elements in a system of life can communicate energy individually with other energy systems out of theirs. The mathematics form is as follow:

$$\begin{cases} \frac{du_1}{dt} = -A_1u_1^2 + B_1u_1 + (C_{12} - D_{12}u_1)u_2 - \varphi_1 \\ \frac{du_2}{dt} = -A_2u_2^2 + B_2u_2 + (C_{21} - D_{21}u_2)u_1 - \varphi_2 \end{cases} \quad (\text{B.5})$$

where A_i, B_i, C_{ij} and D_{ij} ($i, j=1, 2, \dots, n$) are parameters, u_1 and u_2 are two different elements in a system of life and ϕ_1, ϕ_2 are modified terms. The term $(-A_i u_i^2 + B_i u_i)$ represents the energy communicated with other energy systems, and the term $(C_{ij} - D_{ij} u_i) u_j$ represents the energy communicated with the elements in the system of themselves. As a result, independent form can be $(-A_i u_i^2 + B_i u_i) \neq 0, (i=1, 2, \dots, n)$ and $(C_{ij} - D_{ij} u_i) u_j, (i, j=1, 2, \dots, n)$ are very small in general. If the natural medium is change, such as the lack of food or the limit of living space, $(C_{ij} - D_{ij} u_i) u_j$ may be rising.

(2) Dependent form:

There are two different parts of elements in these systems of life. The first part of elements can communicate energy individually with other energy systems out of theirs. The mathematics form is the same to (Eq. (B.5)). The second part of elements can not communicate energy individually with other energy systems out of theirs, they have to be provided the energy by the first part of elements. The mathematics form is as follow:

$$\begin{cases} \frac{du_i}{dt} = -A_i u_i^2 + B_i u_i + \sum_{j=k+1}^n (C_{ij} - D_{ij} u_i) u_j - \phi_i \\ \frac{du_j}{dt} = \sum_{h=1}^{m_j} (C_{jh} - D_{jh} u_j) u_h - \phi_j \end{cases} \quad (B.6)$$

$(i \in k, j \in n - k)$

where k represents the number of the first part elements and m_j represents the number of the second part elements.

In further studies, the system of food chain with three states can be described by the mathematical model as follow:

$$\begin{cases} \frac{du_1}{dt} = A_1u_1^2 + B_1u_1 + (C_{12} - D_{12}u_1)u_2 - \varphi_1 \\ \frac{du_2}{dt} = (C_{21} - D_{21}u_2)u_1 + (C_{23} - D_{23}u_2)u_3 - \varphi_2 \\ \frac{du_3}{dt} = (C_{32} - D_{32}u_3)u_2 - \varphi_3 \end{cases} \quad (\text{B.7})$$

B.4 Virus-immune system

A mathematical model of the virus-immune system consisting of the following three nonlinear differential equations is considered in this study:

$$\begin{cases} \frac{dT}{dt} = s - \mu_1T + rT \left[1 - \frac{T+I}{\Gamma} \right] - kVT \\ \frac{dI}{dt} = kVT - \mu_2I \\ \frac{dV}{dt} = \mu_3NI - kVT - \mu_4V \end{cases} \quad (\text{B.5})$$

where T , I and V represent the population concentrations of uninfected, infected target cells and virus respectively. We denote by the s constant supply of target cells from its precursor. These cells have a finite life time and μ_1 represents the average death rates of these cells. These target cells are assumed to grow logistically with specific growth rate r and carrying capacity Γ . In the presence of virus, the target cells become infected. Since virus must meet the cells in order to infect them, a mass action term is used to model infection with k as the infection rate. μ_2 denote the natural death rate of infected cells. All infected cells are assumed to be capable of producing virus. It is assumed that N virion are released by each infected cell during its lifetime. μ_3 represents the death rate of infected cells due to lysis. μ_4 is the death rate of free virus.

Appendix C

Pragmatical Asymptotical Stability Theory [56-58]

The stability for many problems in real dynamical systems is actual asymptotical stability, although may not be mathematical asymptotical stability. The mathematical asymptotical stability demands that trajectories from all initial states in the neighborhood of zero solution must approach the origin as $t \rightarrow \infty$. If there are only a small part or even a few of the initial states from which the trajectories do not approach the origin as $t \rightarrow \infty$, the zero solution is not mathematically asymptotically stable. However, when the probability of occurrence of an event is zero, it means the event does not occur actually. If the probability of occurrence of the event that the trajectories from the initial states are that they do not approach zero when $t \rightarrow \infty$, is zero, the stability of zero solution is actual asymptotical stability though it is not mathematical asymptotical stability. In order to analyze the asymptotical stability of the equilibrium point of such systems, the pragmatical asymptotical stability theorem is used.

Let X and Y be two manifolds of dimensions m and n ($m < n$), respectively, and φ be a differentiable map from X to Y , then $\varphi(X)$ is subset of Lebesgue measure 0 of Y [56]. For an autonomous system

$$\frac{dx}{dt} = f(x_1, \dots, x_n) \quad (\text{C-1})$$

where $x = [x_1, \dots, x_n]^T$ is a state vector, the function $f = [f_1, \dots, f_n]^T$ is defined on

$D \subset R^n$ and $\|x\| \leq H > 0$. Let $x=0$ be an equilibrium point for the system (C-1). Then

$$f(0) = 0 \quad (\text{C-2})$$

For a nonautonomous systems,

$$\dot{x} = f(x_1, \dots, x_{n+1}) \quad (C-3)$$

where $x = [x_1, \dots, x_{n+1}]^T$, the function $f = [f_1, \dots, f_n]^T$ is define on $D \subset R^n \times R_+$, here $t = x_{n+1} \in R_+$. The equilibrium point is

$$f(0, x_{n+1}) = 0. \quad (C-4)$$

Definition The equilibrium point for the system (C-1) is pragmatically asymptotically stable provided that with initial points on C which is a subset of Lebesque measure 0 of D , the behaviors of the corresponding trajectories cannot be determined, while with initial points on $D - C$, the corresponding trajectories behave as that agree with traditional asymptotical stability [57-58].

Theorem Let $V = [x_1, \dots, x_n]^T : D \rightarrow R_+$ be positive definite and analytic on D , where x_1, x_2, \dots, x_n are all space coordinates such that the derivative of V through Eq. (C-1) or (C-3), \dot{V} , is negative semi-definite of $[x_1, x_2, \dots, x_n]^T$.

For autonomous system, Let X be the m -manifold consisted of point set for which $\forall x \neq 0, \dot{V}(x) = 0$ and D is a n -manifold. If $m+1 < n$, then the equilibrium point of the system is pragmatically asymptotically stable.

For nonautonomous system, let X be the $m+1$ -manifold consisting of point set of which $\forall x \neq 0, \dot{V}(x_1, x_2, \dots, x_n) = 0$ and D is $n+1$ -manifold. If $m+1+1 < n+1$, i.e. $m+1 < n$ then the equilibrium point of the system is pragmatically asymptotically stable. Therefore, for both autonomous and nonautonomous system the formula $m+1 < n$ is universal. So the following proof is only for autonomous system. The proof for nonautonomous system is similar.

Proof Since every point of X can be passed by a trajectory of Eq. (C-1), which is one-dimensional, the collection of these trajectories, A , is a $(m+1)$ -manifold [57-58].

If $m+1 < n$, then the collection C is a subset of Lebesgue measure 0 of D . By the above definition, the equilibrium point of the system is pragmatically asymptotically stable.

If an initial point is ergodically chosen in D , the probability of that the initial point falls on the collection C is zero. Here, equal probability is assumed for every point chosen as an initial point in the neighborhood of the equilibrium point. Hence, the event that the initial point is chosen from collection C does not occur actually. Therefore, under the equal probability assumption, pragmatical asymptotical stability becomes actual asymptotical stability. When the initial point falls on $D - C$, $\dot{V}(x) < 0$, the corresponding trajectories behave as that agree with traditional asymptotical stability because by the existence and uniqueness of the solution of initial-value problem, these trajectories never meet C .

In Eq. (7.7) V is a positive definite function of n variables, i.e. p error state variables and $n-p=m$ differences between unknown and estimated parameters, while $\dot{V} = e^T C e$ is a negative semi-definite function of n variables. Since the number of error state variables is always more than one, $p > 1$, $m+1 < n$ is always satisfied, by pragmatical asymptotical stability theorem we have

$$\lim_{t \rightarrow \infty} e = 0 \quad (C-5)$$

and the estimated parameters approach the uncertain parameters. The pragmatical adaptive control theorem is obtained. Therefore, the equilibrium point of the system is pragmatically asymptotically stable. Under the equal probability assumption, it is actually asymptotically stable for both error state variables and parameter variables.

References

- [1] L.M. Pecora, T.L. Carroll, "Synchronization in chaotic systems", *Phys Rev Lett*, 64 (2005) 821-824.
- [2] S.H. Chen, J.H. Lü, "Synchronization of an uncertain unified chaotic system via adaptive control", *Chaos, Solitons & Fractals*, 26 (2005) 913-920.
- [3] L. Shen, M. Wang, "Adaptive control of chaotic systems based on a single layer neural network", *Physics Letters A*, 368(5) (2007) 379-382.
- [4] M. Sun, L. Tian, S. Jiang and J. Xu, "Feedback control and adaptive control of the energy resource chaotic system", *Chaos, Solitons&Fractals*, 32(5) (2007) 1725-1734.
- [5] F. Moez, "An adaptive feedback control of linearizable chaotic systems", *Chaos, Solitons & Fractals*, 15 (2003) 883.
- [6] T. Fang, W. Ling, "An adaptive active control for the modified Chua's circuit", *Physics Letters A*, 346 (2005) 342-346.
- [7] M.T. Yassen, "Adaptive control and synchronization of a modified Chua's circuit system", *Appl Math Comput*, 135 (2001) 113.
- [8] M.T. Yassen, "Chaos synchronization between two different chaotic system using active control", *Chaos, Solitons & Fractals*, 23 (2005) 131-140.
- [9] J.H. Park, "Adaptive synchronization of Rössler system with uncertain parameters", *Chaos, Solitons and Fractals*, 25 (2005) 333-338.
- [10] R. Femat, J.A. Ramirez, and G.F. Anaya, "Adaptive synchronization of high-order chaotic systems: A feedback with low-order parameterization", *Physica D*, 139 (2000) 231-246.
- [11] C. Wang, S.S. Ge, "Adaptive synchronization for uncertain chaotic via backstepping design", *Chaos, Solitons & Fractals*, 12 (2001) 1199-1206.

- [12] E.M. Elabbasy, H. N. Agiza and M. M. El-Desoky, “Adaptive synchronization of a hyperchaotic system with uncertain parameter”, *Chaos, Solitons and Fractals*, 30 (2006) 1133-1142.
- [13] A. Krawiecki, A. Sukiennicki, “Generalizations of the concept of marginal synchronization of chaos”, *Chaos, Solitons and Fractals*, 11(9)(2000) 1445–1458.
- [14] M.Y. Chen, Z.Z. Han, and Y. Shang, “General synchronization of Genesio-Tesi system”, *International J. of Bifurcation and Chaos*, 14(1) (2004) 347-354.
- [15] E. Ott, C. Grebogi and J.A. Yorke, “Controlling chaos”, *Phys Rev Lett*, 64 (1990) 1196-1199.
- [16] T. Yang, L.B. Yang and C.M. Yang, “Theory of control of chaos using sample data”, *Physics Letters A*, 246 (1998) 284-288.
- [17] G. Chen, X. Dong, “On feedback control of chaotic continuous time systems”, *IEEE Trans Circ Syst I*, (1993) 591.
- [18] T. Yang, C.M. Yang and L.B. Yang, “Control of Rossler system to periodic motions using impulsive control method”, *Physics Letters A*, 232 (1997) 356-361.
- [19] Y. Yu, S. Zhang, “Controlling uncertain Lu system using backstepping design”, *Chaos, Solitons and Fractals*, 15 (2003) 897.
- [20] C.C. Wang, J.P. Su, “A new adaptive variable structure control for chaotic synchronization and secure communication”, *Chaos, Solitons & Fractals*, 20 (2004) 967-977.
- [21] M. Rafikov, J. Balthazar, “On control and synchronization in chaotic and hyperchaotic systems via linear feedback control”, *Communications in Nonlinear Science and Numerical Simulation*, 13 (2008) 1246-1255.
- [22] K. Keiji, H. Michio and K. Hideki, “Sliding mode control for a class of chaotic systems”, *Phys Lett A*, 245 (1998) 511.
- [23] E.N. Sanchez, J.P. Perez, M. Martinez M and G. Chen, “Chaos stabilization: an

- inverse optimal control approach”, *Latin Am Appl Res: Int J*, 32 (2002) 111.
- [24] Z.M. Ge, C.W. Yao and H.K. Chen, “Stability on partial region in dynamics”, *Journal of Chinese Society of Mechanical Engineer*, Vol.15, No.2, (1994) 140-151.
- [25] Z.M. Ge, H.K. Chen, “Three asymptotical stability theorems on partial region with applications”, *Japanese Journal of Applied Physics*, Vol. 37 (1998) 2762-2773.
- [26] Z.M. Ge, “Necessary and sufficient conditions for the stability of a sleeping top described by three forms of dynamic equations”, *Physical Review E*, 77, 046606, (2008).
- [27] O.E. Rössler, “An equation for hyperchaos”, *Phys Lett A*, 71 (1979) 155-157.
- [28] J.Y. Hsieh, C.C. Hwang, A.P. Wang and W.J. Li, “Controlling hyperchaos of the Rössler system”, *Int J Control*, 72 (1999) 882-886.
- [29] K. Thamilmaran, M. Lakshmanan and A. Venkatesan, “Hyperchaos in a modified canonical Chua’s circuit”, *Int J Bifurcat Chaos*, 14 (2004) 221-243.
- [30] C. Barbara, C. Silvano, “Hyperchaotic behaviour of two bi-directionally Chua’s circuits”, *Int J Circ Theory Appl*, 30 (2002) 625-637.
- [31] G. Grassi, S.A. Mascolo, “A systematic procedure for synchronizing hyperchaos via observer design”, *J Circ Syst Comput*, 11 (2002) 1-16.
- [32] E.N. Lorenz, “Deterministic non-periodic flows”, *J. Atmos*, 20 (1963) 130.
- [33] J.Y. Chen, K.W. Wong, L.M. Cheng and J.W. Shuai, “A secure communication scheme based on the phase synchronization of chaotic systems”, *Chaos*, 13 (2003) 508-514.
- [34] T. Plienpanich, P. Niamsup and Y. Lenbury, “Controllability and stability of the perturbed Chen chaotic dynamical system”, *Appl. Math. Comput.*, 171 (2005) 927-947.
- [35] T. Ueta, G. Chen, “Bifurcation analysis of Chen’s equation”, *Int. J. Bifurcat. Chaos*,

8 (2000) 1917-1931.

- [36] M.T. Yassen, "The optimal control of Chen chaotic dynamical system", *Appl. Math. Comput.*, 131 (2002) 171-180.
- [37] M.T. Yassen, "Chaos control of Chen chaotic dynamical system", *Chaos, Solitons and Fractals*, 15 (2003) 271-283.
- [38] T. Ueta, G. Chen, "Bifurcation analysis of Chen's attractor", *Int. J. Bifurcation and Chaos*, 10 (2000) 1917-1931.
- [39] X. Yu, Y. Xia, "Detecting unstable periodic orbits in Chen's chaotic attractor", *Int. J. Bifurcation and Chaos*, 10 (2001) 1987-1991.
- [40] Smith, J. Richard, *Fathoming the Cosmos and Ordering the World: The Yijing (I Ching or Classic of Changes) and Its Evolution in China*. University of Virginia Press. (2008) [ISBN 978-0813927053](#).
- [41] Karcher, Stephen, *I Ching: The Classic Chinese Oracle of Change: The First Complete Translation with Concordance*. London: Vega Books. (2002) [ISBN 1-84333-003-2](#).
- [42] S.J. Marshall, *The Mandate of Heaven: Hidden History in the I Ching*. Columbia University Press. (2001) [ISBN 0-231-12299-3](#).
- [43] A. Buonomo, "The periodic solution of Van der Pol's equation", *SIAM J. Appl. Math.*, 59 (1999) 1156-1171.
- [44] M.T. Yassen, "Synchronization hyperchaos of hyperchaotic systems", *Chaos, Solitons and Fractals*, 37 (2008) 465-475.
- [45] Z.M. Ge, C.Y. Ho, S.Y. Li and C.M. Chang, "Chaos control of new Ikeda-Lorenz system by GYC partial region stability theory", *Math. Meth. Appl. Sci.* (2008).
- [46] Z. Li, C.Z. Han and S.J. Shi, "Modification for synchronization of Rössler and Chen chaotic systems", *Phys Lett A*, 301 (2002) 224-230.
- [47] X. Yu, Y. Song, "Chaos synchronization via controlling partial state of chaotic

- systems”, *Int J Bifurcat Chaos*, 11 (2001) 1737-1741.
- [48] L. Fortuna, D. Porto, “Quantum-CNN to generate nanscale chaotic oscillator”, *International Journal of Bifurcation and Chaos*, 14(3) (2004) 1085-1089.
- [49] Z.M. Ge, Y.S. Chen, “Synchronization of unidirectional coupled chaotic systems via partial stability”, *Chaos, Solitons and Fractals*, 21 (2004) 101-111.
- [50] Z.M. Ge, C.C. Chen, “Phase synchronization of coupled chaotic multiple time scales systems”, *Chaos, Solitons and Fractals*, 20 (2004) 639-647.
- [51] Z.M. Ge, C.M. Chang, “Chaos synchronization and parameters identification of single time scale brushless DC motors”, *Chaos, Solitons and Fractals*, 20 (2004) 883-903.
- [52] Y. Kuang, “Basic properties of mathematical population models”, *Biomathematics*, 17 (2002) 129-142.
- [53] A. El-Gohary, M. Yassen, “Optimal control and synchronization of Lotka-Volterra model”, *Chaos, Solitons & Fractals*, 12 (2001) 2087-2093.
- [54] J. Sugie, M. Katayama, “Global asymptotic stability of a predator-prey system of Holling type”, *Nonlinear Analysis*, 160 (1999) 105-121.
- [55] M.C. Mackey, L. Glass, “Oscillation and chaos in physiological control systems”, *Science*, 197(4300) (1977) 287-289.
- [56] Y. Matsushima, *Differentiable Manifolds*, Marcel Dekker, City, (1972).
- [57] Z.M. Ge, J.K. Yu, “Pragmatical asymptotical stability theorems on partial region and for partial variable with applications to gyroscopic systems”, *The Chinses Journal of Mechanics*, 16(4) (2000) 179-187.
- [58] Z.M. Ge, J.K. Yu and Y.T. Chen, “Pragmatical asymptotical stability theorem with application to satellite system”, *Jpn. J. Appl. Phys.*, 38 (1999) 6178.